236-p $3.50

U. S. ARMY
TRANSPORTATION RESEARCH COMMAND
FORT EUSTIS, VIRGINIA

TRECOM TECHNICAL REPORT 64-9

COMPILATION AND ANALYSIS OF TEST DATA ON FIBERGLASS-REINFORCED PLASTICS

Task 1D121401A14203
Contract DA 44-177-AMC-90(T)

March 1964

prepared by:

KAMAN AIRCRAFT CORPORATION
Bloomfield, Connecticut

DISCLAIMER NOTICE

DDC AVAILABILITY NOTICE

HEADQUARTERS
U S ARMY TRANSPORTATION RESEARCH COMMAND
FORT EUSTIS VIRGINIA

This work was performed under Contract DA 44-177-AMC-90(T) with the Kaman Aircraft Corporation during the period 15 June 1963 to 15 November 1963.

The information contained in this report is a compilation and analysis of test data on fiberglass-reinforced plastics from tests conducted by the Kaman Aircraft Corporation during previous years. The report is offered in hopes of providing useful information on fiberglass-reinforced plastics with application to advanced aircraft design studies being conducted by this Command and other Government agencies.

Publication of this report by this Command does not necessarily imply endorsement of the test data and results contained herein; the report is published only to make the information available.

James P. Waller
JAMES P. WALLER
Project Engineer

Robert L. Echols
ROBERT L. ECHOLS
Group Leader
Physical Sciences Group

APPROVED.

FOR THE COMMANDER:

Larry M. Hewin
LARRY M. HEWIN
Technical Director

Task 1D121401A14203
Contract DA 44-177-AMC-90(T)
TRECOM Technical Report 64-9
March 1964

COMPILATION AND ANALYSIS OF TEST DATA ON FIBERGLASS-REINFORCED PLASTICS

Kaman Aircraft Corporation Report No. R-479

Prepared by
Kaman Aircraft Corporation
Bloomfield, Connecticut

for
U. S. ARMY TRANSPORTATION RESEARCH COMMAND
FORT EUSTIS, VIRGINIA

CONTENTS

			Page
LIST OF ILLUSTRATIONS			v
LIST OF TABLES			ix
SUMMARY			1
CONCLUSIONS			2
RECOMMENDATIONS			3
INTRODUCTION			5
SECTION	I	MATERIALS LABORATORY INVESTIGATIONS	6
	II	COMPOSITE BLADE DEVELOPMENT	40
	III	ALL FIBERGLASS-REINFORCED PLASTIC BLADE DEVELOPMENT	110
	IV	EVALUATION OF THE EFFECT OF WEATHERING AND PROTECTIVE COATING SYSTEMS ON A FIBERGLASS-REINFORCED PLASTIC HELICOPTER ROTOR BLADE SPECIMEN	167
	V	EVALUATION OF A ONE-PIECE, TWO-BLADED TAIL ROTOR SPAR OF DIRECTED FIBERGLASS-REINFORCED PLASTIC	173
	VI	V/STOL ROTOPROP DEVELOPMENT	187
DISTRIBUTION			227

BLANK PAGE

LIST OF ILLUSTRATIONS

Figure		Page
I- A1	Suggested Control Tube Design	8
I- A2	Brand "Z" Control Tube	8
I- A3	Brand "Y" Control Tube	9
I- D1	3 M Suggested Unidirectional Test Specimen	35
I- D2	$\pm$ 5° Oriented Unidirectional Test Specimen	38
II- 1	Sketch of Basic Helicopter Blade	43
II- 2	Typical Hub, Grip, and Blade Root-End Test Setup	45
II- 3	Close-up of Rotor Hub Blade Grip and Blade Root-End Installation	45
II- 4	View Showing Centrifugal Force Application Beam	46
II- 5	Instrumentation and Bolt Hole Locations, Blade and Grip Root-End Specimen	47
II- 6	Configurations of Blade Root-End Development with Fiberglass-Reinforced Plastic	49
II- 7	Original Stub Configuration Showing General Failure	50
II- 8	Close-up View of Stub Failure	51
II- 9	View Showing Failure of Fiberglass Channel Reinforced Stub	53
II-10	View Showing Failure of Static Test Stubs	54
II-11	Flatwise Bending Moment Distributions	55
II-12	Flatwise Bending Moment Distributions	56
II-13	Flatwise Bending Moment Distributions	57
II-14	Flatwise Bending Moment Distributions	58
II-15	Flatwise Bending Moment Distributions	59
II-16	Flatwise Bending Moment Distributions	60
II-17	Root-End Strain Distribution	61
II-18	Root-End Strain Distribution	62
II-19	Root-End Strain Distribution	63
II-20	Root-End Strain Distribution	64
II-21	Root-End Strain Distribution	65
II-22	Root-End Strain Distribution	66
II-23	Root-End Strain Distribution	67
II-24	Root-End Strain Distribution	68
II-25	Root-End Strain Distribution	69
II-26	Root-End Strain Distribution	70
II-27	Root-End Strain Distribution	71
II-28	Root-End Strain Distribution	72
II-29	Root-End Strain Distribution	73
II-30	Root-End Strain Distribution	74
II-31	Root-End Strain Distribution	75
II-32	Root-End Strain Distribution	76

Figure		Page
II-33	Root-End Strain Distribution.	77
II-34	Section View of Original Fiberglass Cheek Plate	79
II-35	Fatigue Specimen Load Setup	82
II-36	General Arrangement of Hub and Grip Fatigue Jig Viewed rom Movable Retention End	83
II-37	General Arrangement of Hub and Grip Fatigue Jig Viewed from Fixed Retention End	83
II-38	General View Showing Centrifugal Force Application Load Beam	84
II-39	Close-up of Typical Blade Root-End and Blade Grip Installed Into Rotor Hub	84
II-40	General View Showing Mechanical Shaker and Torque Application System	85
II-41	View Showing Vari-Drive System and its Attachment to Mechanical Shaker	85
II-42	Blade Root-End S-N Curve.	88
II-43	Spanwise Cracks in Upper and Lower Grip Facings	89
II-44	Blade Root-End Crack Propagation.	90
II-45	Blade Root-End Specimen Damage.	91
II-46	Blade Root-End Lower Surface.	92
II-47	Blade Root-End Upper Surface.	93
II-48	Blade Root-End Spanwise Cracks.	94
II-49	Blade Root-End Spanwise Cracks.	95
II-50	Epoxy Filled Spanwise Cracks.	96
II-51	Evolution of the Use of Fiberglass in Kaman Rotor Blade	98
II-52	Overall View of Test Setup.	100
II-53	View of Exciter Attachment.	101
II-54	Test Setup for Steady Plus Vibratory Flatwise Bending	113
II-55	Summary of 7500 IN.LB. Steady Flatwise Bending Moment.	116
II-56	Blade Test Results - Cycles vs. Probability of Failure.	117
III- 1	Spar Tip Section.	121
III- 2	Original Fiberglass Blade Root-End Construction.	122
III- 3	Evolution of the Use of Fiberglass in Kaman Rotor Blades.	123
III- 4	Original Fiberglass Blade Completed	124
III- 5	Fiberglass Blade Whirl Test Rig	127
III- 6	Translucent Structure of Fiberglass Blade . . .	128
III- 7	Fiberglass Blade Skin Construction.	129
III- 8	Fiberglass Blades with Stringers Visible. . . .	131
III- 9	Fiberglass Blades (with Stringers) Mounted on Jet Powered HH-43B Helicopter	132

Figure		Page
III-10	Fiberglass Blades (with Stringers) Installed on Helicopter for Flight Test Evaluation.	133
III-11	Collective Stick Position vs. Rotor Speed (Hover).	136
III-12	Steady Flatwise Bending Moment Distribution. . .	137
III-13	Steady Flatwise Bending Moment Distribution. . .	138
III-14	Steady Flatwise Bending Moment Distribution. . .	139
III-15	Steady Flatwise Bending Moment vs. Airspeed. . .	140
III-16	Vibratory Flatwise Bending Moment vs. Airspeed .	141
III-17	Vibratory Flatwise Bending Moment vs. Airspeed .	142
III-18	Vibratory Flatwise Bending Moment vs. Airspeed .	143
III-19	Vibratory Flatwise Bending Moment vs. Airspeed .	144
III-20	Total Vibratory Flatwise Bending Moment vs. Airspeed	145
III-21	Total Vibratory Flatwise Bending Moment vs. Airspeed	146
III-22	Total Vibratory Flatwise Bending Moment vs. Airspeed	147
III-23	Vibratory Flap ℄ Bending Moment vs. Airspeed . .	148
III-24	Steady Flap ℄ Bending Moment vs. Airspeed. . . .	149
III-25	Vibratory Torsional Moment vs. Airspeed.	150
III-26	Steady Torsional Moment vs. Airspeed	151
III-27	Controllability and Power.	152
III-28	Pilot Seat Vertical Accelerations vs. Airspeed .	153
III-29	Cyclic and Collective Pullout.	154
III-30	Rotor Head Fatigue Tests	159
III-31	Rotor Blade Torsional Fatigue Tests.	160
III-32	Rotor Blade Flap Area Fatigue Tests.	161
III-33	Applications of Glass Fiber Reinforced Plastic Construction	164
III-34	Fatigue Test of Blade Section Damaged by Rifle Fire	165
III-35	Fatigue Test of Blade Section Damaged by Rifle Fire	165
IV- 1	Glass Blade Exposure Test Setup.	169
IV- 2	Evaluation of Weathering Effects on Glass Blade Specimen	170
IV- 3	Effects of Weathering on Coated and Uncoated Surfaces	171
V- 1	Elastic Hinged Tail-Rotor	175
V- 2	Elastic Hinged Tail-Rotor	176
V- 3	Tail-Rotor Torsional Section Static Test	182
V- 4	Tail-Rotor Torsional Section Fatigue Test. . . .	183
V- 5	SCOTCHPLY Torsional Evaluation	184
V- 6	Tail-Rotor Spar Endurance Test	185

Figure		Page
VI- 1	K-16B Experimental V/STOL Aircraft.	188
VI- 2	K-16B Rotoprop Control Flap	191
VI- 3	Rotoprop Whirl Stand.	193
VI- 4	Sketch of K-16 Flap Fatigue Jig	199
VI- 5	Flap Fatigue Test Drive System.	200
VI- 6	Flap Fatigue Test Clamp and Gage Positions.	201
VI- 7	Flap Fatigue Test Apparatus	202
VI- 8	Flap Fatigue Test Apparatus	203
VI- 9	Close-up of Rotoprop on Whirl Stand	204
VI-10	View of Flap Retention Failure.	205
VI-11	View of Flap Cable Failure.	206
VI-12	View of Flap Failure.	207
VI-13	View of Flap Failure.	207
VI-14	Flap Endurance.	208
VI-15	Flap Endurance.	209
VI-16	Flap Endurance.	210
VI-17	Flap Endurance.	211
VI-18	Flap Endurance.	212
VI-19	Flap Endurance.	213
VI-20	Flap Endurance.	214
VI-21	Flap Endurance.	215
VI-22	Flap Endurance.	216
VI-23	Flap Endurance.	217
VI-24	Flap Endurance.	218
VI-25	Flap Endurance.	219
VI-26	Flap Endurance.	220
VI-27	Flap Endurance.	221
VI-28	Flap Endurance.	222
VI-29	Flap Endurance.	223
VI-30	Flap Endurance.	224
VI-31	Tie-Down Test of K-16B Aircraft	225

LIST OF TABLES

Table		Page
I-A	Table of Tube and Rod Properties.	10
I-B1	Physical Properties of Polyester Fiberglass-Reinforced Plastic Laminates.	14
I-B2	Postcure Effect on Polyester Laminates.	15
I-B3	Block Shear Strength of Secondary Bonded Polyester Joints.	17
I-C1	Physical Properties of FRP Laminates (Phenolic)	21
I-C2	Physical Properties of FRP Laminates (Phenolic)	23
I-C3	Physical Properties of FRP Laminates (Phenolic)	24
I-D1	Physical Properties of FRP Laminates (Epoxy). .	27
I-D2	Physical Properties of FRP Laminates (Epoxy) Environmental Exposure.	29
I-D3	Room Temperature Physical Properties of Epon 820 and Epon 828 Combined with Versamid 125 and Versamid 140	33
I-D4	Physical Properties of FRP Laminates (Epoxy) .	36
I-D5	$\pm$ 5° Oriented Scotchply	39
II-A	Chronological Summary of Fatigue Testing. . . .	102
II-B	Summary of Rotor Blade Skin Fatigue Testing . .	115
III-A	Summary of Blade Moments in Flight Maneuvers. .	155
III-B	Summary of Blade Moments in Flight Maneuvers. .	156
III-C	Load Oriented Glass Fiber Construction in Kaman Rotor Blades.	162
VI-A	Test History of Flaps	196

BLANK PAGE

SUMMARY

Fiberglass-reinforced plastic was first used as a laminated wood reinforcement for a primary structural rotor blade application in a helicopter development program in 1953. Since that time, the use of fiberglass cloth and oriented glass fibers for primary structures has increased at a rapid rate and has culminated in the development of an all-fiberglass rotor blade of superior performance.

This report is a compilation and analysis of significant test data obtained in the evaluation of the all-glass rotor blade. Included are the associated areas of the development of glass fiber control tubing, the use of glass reinforcement for the "Roto-prop" (rotor-propeller) on a V/STOL aircraft, the elastic hinge study suggesting a maintenance-free tail rotor, and the effects of weathering upon glass blade properties and structure.

CONCLUSIONS

Results of the developments and tests reported herein offer conclusive evidence as to the superior structural integrity and fatigue resistance of a properly designed and fabricated all-glass fiber helicopter main rotor blade.

Limited investigations indicate:

1. achievement of all-weather, all-climate capability and the complete elimination of serious moisture effects such as corrosion.
2. significantly greater number of flight hours between overhaul periods because of improved blade life.
3. outstanding structural integrity after damage from small-arms fire.
4. elimination of defective finish problem by the nature of the all-fiberglass construction.
5. substantial reduction of manufacturing costs.
6. reproducibility of dimension and physical property offering individually interchangeable blades.
7. greater resistance to handling damage, and simplicity of repair, if required.
8. greater ease of inspection, suggesting optimum field maintainability.

Concluded, from the associated test programs, is the feasibility of achieving glass fiber control tubes with strength and fatigue properties equal to or greater than standard aircraft specification steel tubing, and appreciating a weight reduction with corresponding dynamic load improvements.

Obvious from these efforts is the expansion to include larger shafts where weight and corrosion factors are important, as well as basic strength.

From limited testing and stress analysis, it is concluded that an elastic hinged structure (no bearings), such as a two-bladed, one-piece tail rotor, can be developed which will give maintenance-free service.

It is interesting that the torsional shear strength (perpendicular to the strands) of oriented unidirectional fibers in this configuration was found by test to be at least six times greater than the published interlaminar shear data used in the original design criteria for the same material. It can be expected, therefore, that higher torsional shear allowables can be conservatively used to predict substantial gains in life expectancy for this type of application.

RECOMMENDATIONS

In view of the outstanding developments accomplished through the use of fiberglass-reinforced plastics, it is recommended that the advancement of the state of the art with respect to helicopter dynamic components be continued.

This is deemed paramount not only because of the properties, strength and fatigue qualities of the material and the ultimate economic savings to be realized through reduced manufacturing costs, longer service life, and availability of [illegible] noncritical material; but also because of the material knowledge to be derived from structures that are subjected to combinations of stress loadings.

Acquisition of such knowledge would find application in many other major design fields.

Continuance of the all-glass blade program is recommended to gather quantities of flight strain and fatigue data to substantiate completely and statistically the strength improvements here reported and to support the benefits perceived by limited investigations.

The present state of the art will now support full-scale exploratory development needed for high-strength, low-weight, maintenance-free aircraft landing-gear systems. The elastic oriented unidirectional members of an all-glass-fiber monolithic-constructed landing gear would reduce the shock transmissibility into the fuselage without the need for added shock absorbers. The resilient and durable material can be readily shaped, can house electronic antennae, and can eliminate protruding joint weldments, rivets or bolts, thereby economically reducing the common drag effects of metallic gear. It is recommended that this type of system be developed for meeting the needed landing gear requirements.

Further, it is recommended that a program of study on glass-fiber-oriented control tubes and shafts be encouraged. Here, again, the strength and fatigue qualities are outstanding, but other properties such as noncorrosiveness, nonmagnetism, lightness of weight, and notch insensitivity are not to be overlooked. Such properties would manifest themselves logistically, particularly in weight-sensitive airborne applications.

Recommended, also, is a complete study of the elastic properties of unidirectional laminates as indicated by the solution of the hinged tail rotor. Along with the fundamental practical concept of a maintenance-free, long-service-life system, is the contribution of filling in the void now found concerning torsional shear data for directed glass fibers. As pointed out in this report, the torsional shear strength can exceed the published interlaminar shear strength by at least six to one. Quantitative testing is required to substantiate these results, which can then be utilized by creative designers and stress analysts.

INTRODUCTION

In 1953, Kaman Aircraft Corporation was experiencing a structural problem with the rotor blade for a newer more powerful model helicopter. This blade was basically of wood construction and, due to the heavy forces acting upon it, was subject to limited fatigue life. At this time the attractive properties and characteristics of fiberglass-reinforced plastics appeared to lend a solution to the rotor blade problem, and structures made from such materials were tested as compatible bonded reinforcements to the wood structure.

The results were excellent, and since then fiberglass has been incorporated in many of Kaman designs requiring high-strength-to-weight ratios and adequate fatigue life.

In addition to the demanding structural requirements and because of the basic simplicity of fabrication, fiberglass is used in many nonstructural areas such as engine nacelle fairings, air inlet ducts, drive shaft and pylon fairings, instrument panel shield, cabin heater ducts, stabilizers, and many others.

On the Kaman Model HH-43B, approximately 2 percent of the helicopter's empty weight is made up of fiberglass. In the later UH-2A model, the usage of fiberglass increased to account for nearly 6 percent of the helicopter's weight.

This report is a compilation and analysis of the most significant test data and results of the usage of fiberglass-reinforced plastics at Kaman Aircraft Corporation as they were developed in time to justify or substantiate the use of the materials for their applications in the aircraft.

SECTION I

MATERIALS LABORATORY INVESTIGATIONS

Parallel with the design studies and the testing of full-scale parts (Test and Development Section), the Materials Engineering Laboratory performs testing of small specimens in accordance with Federal testing standards and company specifications.

Because of the physical property changes of fiberglass-reinforced plastic with various resins, resin content, laminating pressures and temperatures, post curing, fiber orientation, etc., the Material Engineering Laboratory fabricates samples with the various parameters to optimize the part for its intended application.

In addition, the Laboratory analyzes failures of tested parts to determine cause and quality and evaluates parts fabricated by other manufacturers.

This section reports some of the results on topics such as tabulations of a comparison of several FRP tubes and rods; physical properties, post cure effects, and water absorption effects on FRP laminates of polyester, phenolic, and epoxy resin systems; and studies of tensile specimen configurations.

A. CONTROL TUBES OF FIBERGLASS-REINFORCED PLASTIC

Statement of Problem

Kaman Aircraft Corporation, since its inception, has been associated with the use of primary structure reciprocating control components operating in high centrifugal fields. Standard hardware has been steel tubing with welded end-fittings, and this has performed satisfactorily. However, if lighter weight tubing could be realized, the associated load and endurance improvement would be most beneficial.

With the appreciation for the need to develop high-endurance, unidirectional, fiberglass-reinforced plastic tubing, Kaman solicited for the procurement of tubing to test and evaluate. The request stressed such considerations as the importance of smooth alignment of the longitudinal fiber stock, the mandatory external tube wrap for fiber binding and scuff protection, and the option of internal wraps if required by fabrication process. Figure I-A1 is a sketch of the suggested tube cross section.

Description of Specimens

Two companies responded to the solicitation with samples of tubing. Figure I-A2 is a sketch of the sample from, let us say, Brand "Z"; and Figure I-A3 is a sketch and photograph of the cross section of tubing received from the Brand "Y" Company.

Although they were not made to Kaman specifications, two other commercial specimens were tested as side interests. They were a solid rod of wrapped fiberglass cloth and a sample of pressure tubing, that is, tubing possessing strength against bursting from internal pressure.

All four samples were epoxy resin systems. The Brand "Y" tube was fabricated from Minnesota Mining and Manufacturing Company's "Scotchply" with a thin scrim cloth backing.

The results of the tensile testing of the few specimens is tabulated in Table I-A.

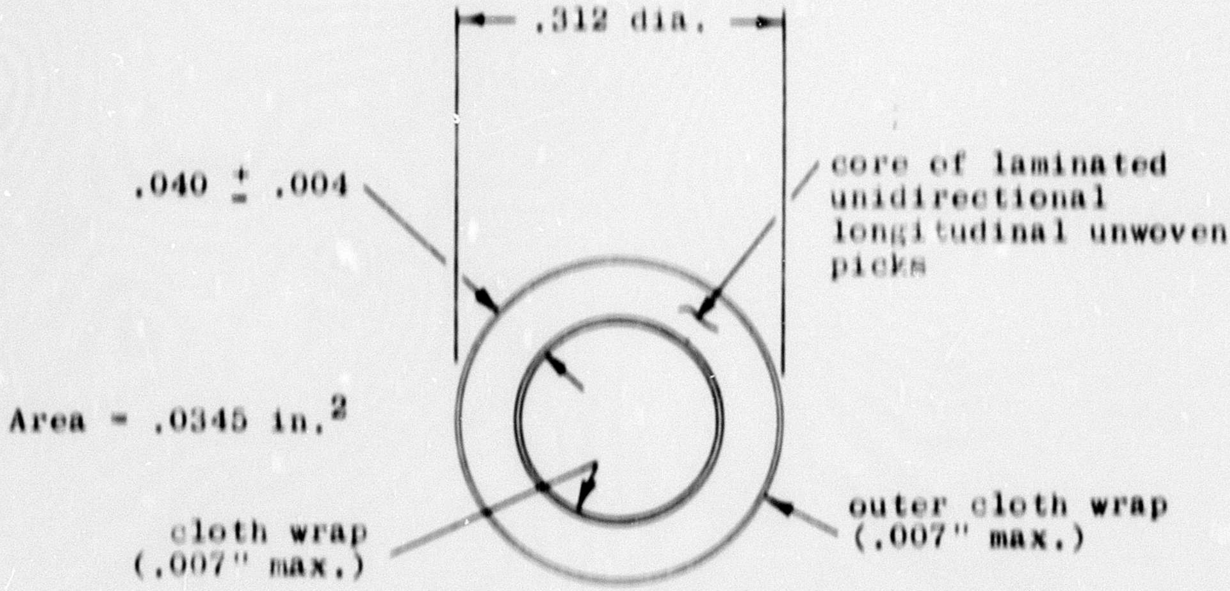

Figure I-A1. Suggested Control Tube Design

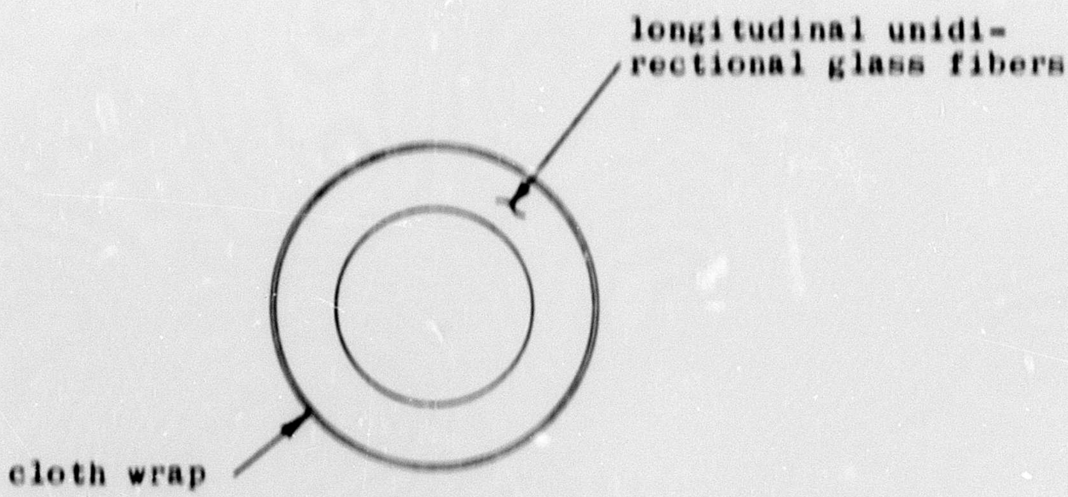

Figure I-A2. Brand "Z" Control Tube

BLANK PAGE

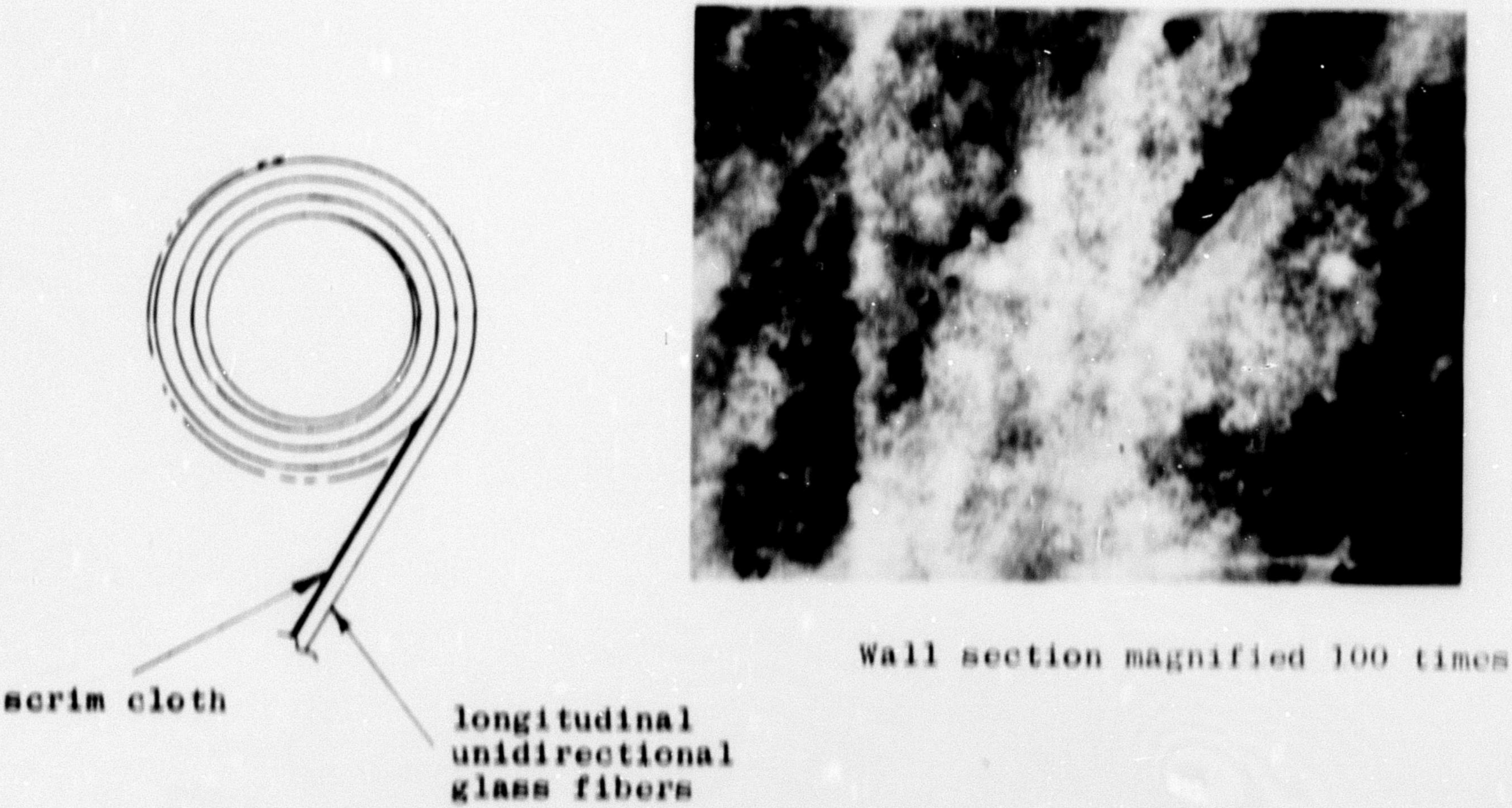

Figure I-A3. Brand "Y" Control Tube

Table I-A
TABLE OF TUBE AND ROD PROPERTIES

	Specimen No.	Comm'l. Rod	Comm'l. Tubing	Brand "Z" Tubing	Brand "Y" Tubing	4130 STL Tubing
Outside Diameter (in.)		.376	.340	.335	.291	.250
Wall (in.)		--	.030	.020	.041	.035
Cross Section Area (in.^{2})		.111	.029	.020	.031	.0236
Unit Weight(lb/ft.)		.072	.024	.024	.027	.0804
Densigy (lbs/cu.in.)		.054	.069	.069	.072	.290
Resin Content (%)		43.8	27.5	37.7	34.7	--
Failing Loads(lbs.)	1	4,440	1,790	1,740	2,620	2,240
	2	4,290	1,670	1,530	2,600	--
	3	4,360	1,900	--	--	--
Tensile Strength (psi)	1	40,000	62,600	60,000	84,500	95,000
	2	38,600	57,600	52,200	83,900	--
	3	39,300	65,700	--	--	--
Specific Strength (psi) (lbs/cu.in.)	1	740,000	898,000	870,000	1,173,000	327,500
	2	716,000	855,000	757,000	1,164,000	--
	3	728,000	951,000	--	--	--

BLANK PAGE

Discussion and Conclusion

Table I-A compares the four fiberglass specimens with aircraft specification steel tubing. From the given section properties and weights, an interesting transformation is made in converting the tensile strength into a specific strength or strength/weight parameter. On a specific strength basis, it is immediately evident that each of the glass fiber products is superior to the steel tubing.

The commercial rod, constructed of high resin content and woven cloth in which one-half of the glass fibers are oriented perpendicular to the axial load, exceeds the steel value by a factor of two.

The commercial tubing was 2½ times stronger than the steel tube. The good tensile characteristics are probably attributed to excellent quality control in fabrication for its intended purpose of burst strength. The lower resin content indicates good use of glass stock for static strength.

The more sophisticated tube, Brand "Y", was fabricated very closely to Kaman recommendations and is shown to exceed the specific strength of the steel tube by nearly 3½ times. It is interesting that this value can be expected to substantially increase in view of the nonclassic failure of the test specimen. The premature failure occurred as longitudinal separations of the fibers. It has been the experience at Kaman that stabilization of the glass fibers within the unit structure will result in a substantial increase in strength.

On the other hand, misuse of glass fibers can result in a substantial reduction of expected strength, as evidenced by the Brand "Z" tube, which had the same material system as Brand "Y". Visible to the naked eye was the ragged construction and disregard for smooth alignment of the fiber stock in this specimen. Although even this poorly fabricated piece was superior to the steel on a strength-to-weight basis, the drastic strength reduction penalty for inefficient use of glass-reinforced plastics shows clearly the importance of design knowledge, quality control, and reliability of those engaged in fabricating primary structures from glass and plastic materials.

Immediate priority demands preclude further development at this time; however, it is concluded that stabilization of tube fiber structure can be achieved with minor modification of the Brand "Y" fabricating technique. The results in strength and fatigue properties superior to the aircraft specification steel tubing and a weight reduction with corresponding dynamic load improvements.

B. POLYESTER LAMINATES

Statement of Problem

Because of the relaxed demand for strength properties in non-structural applications such as certain fairings, ducts, panels, and others, Kaman Aircraft Corporation for the most part uses the lower cost polyester resin systems in such cases. Although not critical prime structures, these parts still demand reliability in environmental usage. In this regard, the Kaman Material Engineering Laboratory carries on tests to evaluate these systems and to determine the effects of resin content, laminating pressures and temperatures, post curing, etc.

Description of Parts

All test methods and specimens described herein are in conformance with Federal and/or military testing standards.

Physical Properties

Table I-B1 compares five different polyester resins.

The resins were:

Laminac 4110	manufactured by American Cyanamid Corp.
Laminac 4116	manufactured by American Cyanamid Corp.
Laminac 4128	manufactured by American Cyanamid Corp.
Selectron 5003	manufactured by Pittsburgh Plate Glass Co.
Polylite 8000	manufactured by Reichold Chemicals Corp.

The specimens were made of 12 plies of No. 181 fiberglass cloth impregnated with the resin, benzoyl peroxide, and Promoter 400 in proportion of 100-2-1 parts by weight respectively. They were cured in a press for one hour at 180° F., and the thickness was controlled by placing shims between the press heads.

It is noted by the tabulation (Table I-B1) that the tensile and flexural strengths of all the specimens are relatively close to each other and substantially above the MIL-R-7575A minimum standards. The significantly controlled thickness and resulting uniformity of resin content in all systems can be noted.

It is concluded that in the manufacture of fiberglass polyester systems when reputable products are used, maximum strength can be achieved by a process of quality control of the resin content through proper pressure application and curing temperature.

Effect of Varying Postcuring Cycles

Table 1-B2 shows the results of four postcuring cycles on 12-ply laminates of No. 181 fiberglass cloth. Since the values obtained are comparable to one another and in all cases exceed the minimum requirements of the military specifications, it is concluded that any of these cycles may be employed in the production of polyester laminations. However, care should be observed in the long-period room temperature postcure to assure an ambient temperature of 70° F.

TABLE 1-B1

PHYSICAL PROPERTIES OF POLYESTER FIBERGLASS-REINFORCED PLASTIC LAMINATES

Polyester	Specimen Number	Rockwell "M" Hardness	Laminate Thickness (Inch)	Resin Content	Resin Density (Grams/ML.)	Tensile Strength (PSI)	Tensile Modulus (10^6 PSI)	Flexural Strength (PSI)	Flexural Modulus (10^6 PSI)
Laminac 4110	1	114	.122	37.2	1.817	55,800	3.45	78,900	3.13
	2					56,100	3.20	80,500	3.10
	3					48,300	2.85	81,400	3.28
	4					51,300	4.12	81,700	3.20
Laminac 4116	1	114	.124	37.2	1.803	50,800	3.16	80,000	3.01
	2					58,400	4.06	75,200	2.88
	3					52,900	2.61	77,600	2.92
	4					51,000	3.17	70,800	2.57
Laminac 4128	1	115	.123	37.3	1.820	55,900	3.60	75,600	2.97
	2					50,800	3.24	77,400	2.95
	3					50,900	3.00	76,400	2.97
	4					47,200	3.59	74,800	2.95
Selectron 5003	1	116	.125	37.3	1.818	57,900	3.45	77,300	3.09
	2					49,600	3.11	74,500	3.00
	3					49,400	3.29	76,900	3.08
	4					52,200	3.32	77,700	3.08
Polylite 8000	1	116	.122	36.8	1.832	53,900	3.34	64,400	2.79
	2					54,100	3.22	68,500	2.89
	3					52,800	3.26	70,200	2.83
	4					52,200	3.24	75,700	2.75
MIL-R-7575A		95			1.800	40,000		50,000	2.50

NOTE: Mix and Cure Cycle - 12-ply No. 181 Fiberglass cloth impregnated with: Resin - 100 (Parts by Wt.), Benzoyl Peroxide - 2, Promoter 400 - 1 -- 1 Hr. at 180° F.

Table 1-12

POSTCURE EFFECT ON POLYESTER LAMINATES

Postcure Cycle	* Specimen No.	Tensile Strength (PSI)	Tensile Modulus (10^6 PSI)	Flexural Strength (PSI)	Flexural Modulus (10^6 PSI)	Barcol Hardness
3 weeks @ room temp.	1	47,100	3.15			
	2	30,900	3.57			
	3			64,300	2.63	58
	4			66,100	2.64	64
2½ hours @ 120° F.	1	50,200	3.69			
	2	42,700	3.50			
	3			70,700	2.74	68
	4			77,000	3.14	68
1½ hours @ 140° F.	1	43,700	3.38			
	2	42,200	3.34			
	3			72,600	2.94	65
	4			62,300	2.65	69
1 hour @ 180° F.	1	48,400	3.35			
	2	51,600	3.39			
	3			66,100	2.90	67
	4			71,100	2.63	64
MIL-R-7575B		40,000		50,000	2.50	55

* Specimens: 12-ply No. 181 Fiberglass Cloth impregnated with:

Laminac 4116 = 100 Parts by Weight
Benzoyl Peroxide = 4 " " "
Promoter 400 = 2 " " "

Basic cure at room temperature

Secondary Bonded Polyester Joints

Many designs of fiberglass laminations, out of necessity, must be fabricated by the secondary bonding of structures. To ensure the integrity of the joint, it is imperative to use compatible materials and proper technique. It has been the experience at Kaman that epoxy systems are stronger and more compatible to most materials than are the polyester systems. Table I-B3 is a tabluation of block shear strength for secondary bonded polyester joints. To ensure compatibility, the same resin system was used in the cured laminate as used in the joint, with the exception of the addition of an inert filler (CAB-O-SIL - a silica flour) to the joint resin mixture. The results show general low-strength shear values. Although the resin supported with a cheesecloth spacer was superior to the joints not using the cheesecloth, the average strength still fell under the 2,400 psi minimum of the Kaman Specification.

BLANK PAGE

Table I-B3

BLOCK SHEAR STRENGTH OF SECONDARY BONDED POLYESTER JOINTS

		Shear Strength Value (PSI)										
		Specimen Number										
Parts by Weight	Note	1	2	3	4	5	6	7	8	9	10	Aver.
Laminac 4116 = 100 Benzoyl Peroxide = 2 Promoter 400 = 2 Cab-O-Sil = 5	1	360	266	266	300	460	386	326	253	200	413	323
Laminac 4116 = 100 Benzoyl Peroxide = 2 Promoter 400 = 2 Cab-O-Sil = 5	2	1713	1883	2273	2410	2880	2293	1853	2213	2660	2160	2234
Laminac 4116 = 100 Benzoyl Peroxide = 2 Promoter 400 = 2 Cab-O-Sil = 5	3	1075	933	1160	1096	670	1066	743	800	810	1096	950
Laminac 4116 = 100 Benzoyl Peroxide = 2 Promoter 400 = 1 Cab-O-Sil = $3\frac{1}{2}$	3	616	510	533	376	840	2083	1680	933	--	--	946
	4	1523	853	573	773	1103	1123	853	613	733	733	888
Laminac 4116 = 100 Mek Peroxide = 2 Promoter 400 = 1 Cab-O-Sil = $3\frac{1}{2}$	3	826	833	766	666	1200	1366	1666	1230	1210	1000	1076
Laminac 4116 = 100 BZ050 Peroxide = 2 Promoter 400 = 1 Cab-O-Sil = $3\frac{1}{2}$	3	1500	1953	1733	1106	1746	1890	853	1800	1360	993	1491

Table I-B3 (Cont'd.)

BLOCK SHEAR STRENGTH OF SECONDARY BONDED POLYESTER JOINTS

Parts by Weight		Note	Shear Strength Value (PSI) — Specimen Number 1	2	3	4	5	6	7	8	9	10	Aver.
Laminac 4116	= 100	3											
Benzoyl Peroxide	= 2		676	650	850	1160	2033	726	1126	966	723	573	948
Promoter 400	= 1												
Glass Flock	= 6												

(10-Ply, No. 181 Fiberglass Cloth - Polyester Laminates Fully Cured)

(Secondary Bond Cured for 1½ Hours at 130° F.)

Note: 1 - Without Cheesecloth spacer - Hand Pressure
2 - With Cheesecloth spacer - Bonding Pressure - 30 PSI
3 - Without Cheesecloth spacer - Bonding Pressure - 30 PSI
4 - Repeated run

BLANK PAGE

C. PHENOLIC LAMINATES

In some applications, it is desirable or necessary to use fiberglass preimpregnated with the resin system. Phenolic resins are found to lend themselves well to this type of application. FM-47 (Bloomingdale Rubber Company, Aberdeen, Maryland) is an approved phenolic used in some Kaman designs. Of particular interest is the Kaman application and its effect upon the design strength of the structure.

Specifically, in the fabrication of thin-skinned structures, such as a single ply of No. 181 fiberglass cloth or a double ply of No. 120 cloth, Federal minimum standards in most instances are greater than the tested values from these specimens. This is probably due to local imperfections in the cloth which are not supported by the surrounding fibers as in multiply laminates. Table I-C1 shows the reduced values of tensile strength for the thin specimens and also the superior values for a 13-ply specimen made by the same personnel using the same equipment.

Table I-C2 indicates the loss of tensile and flexural properties when the part is overcured. This overcuring is visually evident by a darkening of the resin and would be cause for rejection if observed on any manufactured part.

Table I-C3 shows a comparison of the FM-47 phenolic preimpregnated resin system and the wet lay-up epoxy system using a "standard" resin mixture of:

SHELL CHEMICAL CO.	Resin Epon 820	= 100 parts/wgt.
	Versamid 125	= 10 " "
	DTA (Diethylenetriamine)	= 6 " "

It is observed that:

1. The physical properties of the two systems are equal when the resin content of the systems is nearly equal and within the optimum range.

2. With optimum resin content, the thickness of No. 120 glass fabric in a cured laminate is .0035 to .0037 inch per ply.

3. Fabricating pressures over 50 psi have little effect on a laminate of No. 120 glass fabric impregnated with FM-47.

4. Resin content in the FM-47 laminate must be controlled in the preimpregnated state since no "squeeze-out" of resin is experienced during cure up to 100 psi pressure.

5. Tensile properties of the wet lay-up epoxy laminate are more adversely affected by excessive resin content than in the phenolic laminate.

BLANK PAGE

Table I-C1

PHYSICAL PROPERTIES OF F.R.P. LAMINATES (Phenolic)

Description	Cure	Specimen Number	Thickness (Inch)	% Resin Content	Tensile Strength (PSI)	Tensile Modulus (10^6 PSI)	Flexural Strength (PSI)	Flexural Modulus (10^6 PSI)
No. 181 (1-ply) FM-47 Preimpregnated	(Clamped)	1	.013		25,000	1.70		
		2	.0125		10,660			
		3	.0125		24,750			
No. 181 (1-ply) FM-47 Preimpregnated	45 min. at 335° F. (100 PSI)	1	.011		33,000	2.50		
		2	.011		30,150			
No. 120 (2-ply) FM-47 Preimpregnated	45 min. at 335° F. (50 PSI)	1	.007		38,000	3.25		
		2	.007		37,400			
		3	.007		25,000			
No. 120 (2-ply) FM-47 Preimpregnated	45 min. at 335° F. (100 PSI)	1	.007		27,500	3.24		
		2	.007		41,900			
		3	.007		36,000			
No. 120 (2-ply) FM-47 Preimpregnated	45 min. at 335° F. (50 PSI - Fluid Pressure)	1	.009		26,000	3.26		
		2	.009		32,000			
		3	.007		36,300			
No. 181 (13-Ply) FM-47 Preimpregnated (Longitudinal)	1 Hr. at 330° F. (.125" Shimmed Press)	1	.140	37.6	45,000	3.09	67,000	2.62
		2			40,000	3.06	70,300	2.57
		3			45,200	3.12	64,700	2.57
		4			45,800	3.34	65,000	2.67
		5	.140		46,500	3.40		

Table I-C1 (Cont'd.)

PHYSICAL PROPERTIES OF F.R.P. LAMINATES (Phenolic)

Description	Cure	Specimen Number	Thickness (Inch)	% Resin Content	Tensile Strength (PSI)	Tensile Modulus (10^6 PSI)	Flexural Strength (PSI)	Flexural Modulus (10^6 PSI)
No. 181 (13-ply) FM-47 Preimpregnated (Transverse)	1 Hr. at 330° F.	1	.141	38.7	45,700	3.14	67,400	2.70
		2			43,250	2.79	70,300	2.73
		3			47,750	2.70	70,000	2.85
		4			45,500	2.96	71,100	2.77
		5	.141		41,000	2.88		
(Longitudinal)	1 Hr. at 330° F. (100 PSI)	1	.143	38.4	50,600	2.78	69,700	2.54
		2			42,700	2.85	64,500	2.55
		3			46,900	2.97	65,500	2.54
		4	.143		50,300	3.28	73,000	2.62
(Longitudinal)	1 Hr. at 330° F. (70 PSI)	1	.145	39.0	45,600	2.96	69,400	2.46
		2			51,100	2.84	68,500	2.41
		3			47,900	3.18	67,700	2.41
		4			69,900	3.05	68,200	2.41
		5	.145		43,400	2.96		

MIL-R-7575 for both No. 120 and No. 181 Fabric and Phenolic Resin 38,000

Table 1-C2

PHYSICAL PROPERTIES OF F.R.P. LAMINATES (Phenolic)

Description	Cure	Specimen Number	Tensile Strength (PSI)	Tensile Modulus (10^6 PSI)	Flexural Strength (PSI)	Flexural Modulus (10^6 PSI)
No. 120 Glass	300° F. Normal	1	45,800	2.93	73,000	2.49
Fabric FM-47	Cure low Press.	2	49,200	2.97	66,000	2.32
Preimpregnated		3	28,200	3.06		
	300° extended	1	31,600	2.10	40,600	1.82
	Cure low Press.	2	43,600	2.62	41,300	1.89

Table I-C3

PHYSICAL PROPERTIES OF F.R.P. LAMINATES (Phenolic)

Description	Note	Specimen Number	Thickness (Inch)	% Resin Content	Tensile Strength (PSI)	Tensile Modulus (10^6 PSI)	Flexural Strength (PSI)	Flexural Modulus (10^6 PSI)
No. 120 Glass Fabric (18-ply) FM-47 Preimpregnated	1	1	.087	46.4	36,500	2.91	66,100	2.63
		2			40,100	2.86	70,200	2.75
		3			38,700	2.76	68,100	2.66
		4	.087		42,700	2.88	65,100	2.66
	2	5	.085		46,600	3.07	67,000	2.57
		6	.085		47,600	3.28	64,200	2.48
	3	1	.085	46.0	44,800	2.68	61,500	2.45
		2			47,900	3.06	64,900	2.57
		3			41,600	2.73	66,700	2.54
		4	.085		48,100	2.83	65,400	2.63
	2	5	.083		50,400	2.98	61,300	2.34
		6	.083		50,400	2.99	64,100	2.51
	1	1	.067	36.0	55,300	3.42	80,800	3.11
		2			43,600	3.20	74,700	3.14
		3			56,800	3.52	82,200	3.08
		4			52,000	3.50		
		5	.067		58,000	3.59		

Table I-C3 (Cont'd.)

PHYSICAL PROPERTIES OF F.R.P. LAMINATES (Phenolic)

Description	Note	Specimen Number	Thickness (Inch)	% Resin Content	Tensile Strength (PSI)	Tensile Modulus (10^6 PSI)	Flexural Strength (PSI)	Flexural Modulus (10^6 PSI)
No. 120 Glass Fabric (18-ply) Epon 820 - Versamid 125-DTA 100 - 10 - 6 (Parts by Weight) Wet Lay-up	4	1	.083	43.6	43,400	3.06	64,300	2.41
		2			45,300	3.00	66,000	2.62
		3			44,660	3.00		
		4			38,900	2.73		
		5	.083		45,400	2.76		
		1	.066	37.4	51,800	3.28	77,100	3.07
		2			53,600	3.21	80,900	3.27
		3			48,800	3.31		
		4			57,300	3.36		
		5	.066		53,800	3.36		

Note: 1. One Hour at 330° F. - 100 PSI
2. Postcured 20 min. at 330° F.
3. One Hour at 330° F. - 50 PSI
4. $1\frac{1}{2}$ Hour at 180° F. (Heated Platens) (Shims in Press)

D. EPOXY LAMINATES

Where maximum physical properties are desirable with wet lay-up fabrication, epoxy resins are generally used. Kaman's experience with epoxy laminates of greater than 5 plies in thickness has repeatedly shown quality control laboratory examination which yields strength values exceeding the 45,000 psi tensile and 65,000 psi flexural strength minimums of MIL specifications. For laminates of lesser plies, the results are widely scattered, with a general reduction in strength values. It is to be noted that this characteristic is a function of the plies and not the thickness of the fabric.

This ply and strength relationship was used in a Kaman design proposal for a small helicopter fuselage where the body skin was to be made up of a 7-ply lamination of No. 116 fabric. (.005-inch nominal cloth thickness) in preference to a 3-ply lamination of No. 181 fabric (.010 inch nominal cloth thickness). Specimens of both of these lay-ups, with the same resin system, were made and tested for comparison. Strength values were obtained in the longitudinal, transverse, and biased directions. Table I-D1 is a tabulation of the results, where it is seen that the average tension value for the 7-ply No. 116 fabric laminate is approximately 26 percent higher than that for the 3-ply No. 181 fabric laminate; yet the 7-ply No. 116 laminate is .008 inch thinner and approximately 22 percent lighter than the 3-ply No. 181 laminate.

In addition to the above specimens which were laminated with the warp in the same direction, a 3-ply No. 116 laminate was made with the warp in the same direction and one was made with the warp in three directions (isotropic). From each laminate, tensile specimens were cut longitudinally, transversely, and at a bias with the warp and were tested for comparison. Typical thin laminate scatter was observed, with the only definite indication of improved strength shown in the isotropic biased-cut specimen.

As with other resin systems, the epoxies are subject to environmental exposure effects. To get some idea as to the severity of reduction in tensile properties, laminate specimens were placed in Kaman's environmental chamber and subjected to exposure at 120° F. and 97 percent relative humidity. Table I-D2 shows a tabulation of average strength values taken from test lots of five and compares samples of unexposed specimens to those under exposure for 7 days and 30 days. Although based upon a relatively small number of specimens, the data obtained reveal an 18 percent to 36 percent reduction in tensile strength after 7 days exposure and a 35 percent to 57 percent reduction after 30 days under the same conditions.

BLANK PAGE

Table I-D1

PHYSICAL PROPERTIES OF F.R.P. LAMINATES (Epoxy)

Description Woven Fiberglass Cloth		Specimen Number	Average Thickness (Inch)	Weight (grams/ft.^{2})	Tensile Strength (PSI)	Tensile Modulus (10^6 PSI)
No. 181 Cloth						
(Epon 820 = 100 parts by wt.)	3-ply -	1	.034	144	37,400	2.89
(Versamid 125 = 10 parts by wt.)	longitudinal	2			40,300	2.34
(DTA = 6 parts by wt.)		3			43,750	0.85
	3-ply -	1			40,000	2.00
	transverse	2			43,700	2.02
		3			42,300	2.60
	3-ply -	1			9,660	0.76
	biased	2			10,570	0.81
		3	.034	144	10,180	0.90
No. 116 Cloth						
(Epon 820 = 100 parts by wt.)	7-ply -	1	.026	112	51,400	3.48
(Versamid 125 = 10 parts by wt.)	longitudinal	2			52,250	3.33
(DTA = 6 parts by wt.)		3			50,000	3.33
	7-ply -	1			50,800	2.73
	transverse	2			51,900	2.24
		3			50,750	2.98
	7-ply -	1			24,600	1.12
	biased	2			24,400	0.81
		3	.026	112	24,500	1.34

Table I-D1 (Cont'd.)

PHYSICAL PROPERTIES OF F.R.P. LAMINATES (Epoxy)

Description Woven Fiberglass Cloth		Specimen Number	Average Thickness (Inch)	Weight (grams/ft.2)	Tensile Strength (PSI)	Tensile Modulus 10^6 PSI)
No. 116 Cloth	3-ply -	1	.013	48	30,600	2.31
(Epon 820 = 100 parts by wt.)	longitudinal	2			42,700	2.43
(Versamid 125 = 10 parts by wt.)		3			39,500	2.48
(DTA = 6 parts by wt.)						
	3-ply -	1			33,100	2.24
	transverse	2			35,000	2.28
		3			29,000	2.08
	3-ply -	1			19,200	0.83
	biased	2			18,200	0.73
		3			18,900	0.53
	3-ply -	1			37,000	2.16
	longitudinal	2			41,500	1.76
	(isotropic)	3			37,600	1.71
	3-ply -	1			34,100	1.71
	transverse	2			34,700	1.82
	(isotropic)	3			30,000	1.67
	3-ply -	1			28,400	1.50
	biased	2			30,800	1.41
	(isotropic)	3	.013	48	28,000	1.48

Table I-D2

PHYSICAL PROPERTIES OF F.R.P. LAMINATES (Epoxy) - Environmental Exposure

Description	% Resin Content	Tensile Strength (PSI)	Tensile Modulus (10^6 PSI)	
No. 120 (8-ply) Epon 820, Versamid 125, DTA (100-10-6 pts. by wt.) 16 hrs. at Rm. Temp., Postcure 2 hrs. at 180° F. (Vacuum bag)	48.2	43,130	3.23	Unexposed
		30,050	--	7 days at 120° F., 97% R.H.
		24,600	2.61	30 days at 120° F., 97% R.H.
No. 120 (8-ply) Epon 820, Versamid 125, DTA (100-10-6 pts. by wt.) 1 hr. at 180° F. (vacuum bag in press. - air pressure = 30 PSI)	36.5	41,800	2.93	Unexposed
		34,425	--	7 days at 120° F., 97% R.H.
		23,950	2.63	30 days at 120° F., 97% R.H.
No. 120 (8-ply) Epon 820, Versamid 125, DTA (100-10-6 pts. by wt.) 1 hr. at 180° F. (vacuum bag in press. - pressure at 30 PSI)	38.0	47,180	3.11	Unexposed
		39,075	--	7 days at 120° F., 97% R.H.
		27,350	2.84	30 days at 120° F., 97% R.H.
No. 120 (8-ply) Epon 820, Versamid 125, DTA (100-10-6 pts. by wt.) 1 hr. at 180° F. (vacuum bag in press. with .030 shims)	47.8	47,500	3.10	Unexposed
		31,375	--	7 days at 120° F., 97% R.H.
		24,100	2.80	30 days at 120° F., 97% R.H.
No. 120 (8-ply) Epon 820, Versamid 125, DTA (100-25-4 pts. by wt.) 1 hr. at 180° F. (vacuum bag in press. - air pressure = 30 PSI)	50.6	41,500	2.99	Unexposed
		39,050	--	7 days at 120° F., 97% R.H.
		25,050	2.54	30 days at 120° F., 97% R.H.

Table I-D2 (Cont'd.)

PHYSICAL PROPERTIES OF F.R.P. LAMINATES (Epoxy) - Environmental Exposure

Description	% Resin Content	Tensile Strength (PSI)	Tensile Modulus (10^6 PSI)	
No. 116 (8-ply) Epon 820, Versamid 125, DTA (100-10-6 pts. by wt.) 1 hr. at 180° F. (vacuum bag in press. - air pressure = 30 PSI)	33.5	47,725	2.88	Unexposed
		28,575	--	7 days at 120° F., 97% R.H.
		20,400	2.74	30 days at 120° F., 97% R. H.
No. 181 (3-ply) Epon 820, Versamid 125, DTA (100-10-6 pts by wt.) 1 hr. at 180° F. (vacuum bag in press. - air pressure = 30 PSI)	33.0	47,020	3.30	Unexposed
		42,525	--	7 days at 120° F., 97% R.H.
		30, 900	2.93	30 days at 120° F., 97% R.H.

BLANK PAGE

Although the above results show a serious effect of environmental moisture or strength, it must be pointed out that the environmental exposure conditions were selected to be severe so as to accelerate the evaluation. Furthermore, the specimen had milled edges with exposed fibers conducive to "wicking" permeability and had no protective coating. The test does indicate that laminates need environmental exposure protection, as do other aircraft materials. With care to avoid exposed fibers and providing normal aircraft finishes and maintenance, Kaman fiberglass-laminated rotor blade components have experienced service life exposures exceeding 1000 hours of operating time and, in instances, have had intermittent usage for more than eight years without evidence of deterioration. Section IV of this report offers additional data concerning weathering effects upon an all-glass fiber rotor blade.

Whenever possible, Kaman Aircraft evaluates new materials in the interest of fabricating products with improved quality. For example, Shell Chemical Company's "Epon 826" is a new epoxy laminating resin which is being qualified to MIL-A-9300 and was tested for comparison with Shell's "Epon 820", which has been Kaman's standard epoxy laminating resin for room or intermediate temperature cure. The viscosity of Epon 826 is about the same as that of Epon 820; however, it does not contain a reactive diluent as does Epon 820. (The diluent additive lowers the viscosity but also may affect certain physical properties.)

In mixture with the epoxy, "Versamid" polyamide resins (a General Mills product) are generally used to obtain a degree of toughness and flexibility in the cured laminate. Versamid 125 has been the standard polyamide modifier used at Kaman. In the uncured state, it is less susceptible to atmospheric moisture and is faster curing than Versamid 140; however, the latter has a lower viscosity and a higher heat distortion point.

A series of tests were made to evaluate and compare the above resins in the following combinations:

1. Epon 826 with Versamid 125 - compared to
   Epon 820 with Versamid 125

2. Epon 826 with Versamid 140 - compared to
   Epon 820 with Versamid 140

3. Epon 820 with Versamid 125 compared to
   Epon 820 with Versamid 140

4. Epon 826 with Versamid 125 - compared to Epon 826 with Versamid 140

5. Epon 826 compared to Epon 820

All the above test laminates were cured at room temperature using Diethylene Triamine (DTA) as a curing agent.

The test panels from which the specimens were made were of 12 plies of Type VIII A (No. 181 - 150) glass fabric, MIL-C-9084. The warp was in the longitudinal direction, and the resin content ranged from 31.8 to 33.8 percent, with an average of 33.5 percent. All specimens were made and tested in accordance with Federal Test Standard 406. The final thickness in the 12-ply laminates ranged from .0092 to .0095 inch per ply.

Table I-D3 shows the results of this testing, with the average values obtained from 5 specimens. While this small number of specimens is not enough to give unqualified results, it does give an indication of what can be expected with optimum resin content and controlled uniform thickness.

1. Epon 826 with Versamid 125 is 5.25 percent stronger in flexure than Epon 820 with Versamid 125. There is little difference in tensile strength.

2. Epon 826 with Versamid 140 is 9.1 percent stronger in flexure than Epon 820 with Versamid 140. There is little difference in tensile strength.

3. Epon 826 with DTA is 6.7 percent stronger in flexure than Epon 820 with DTA. There is little difference in tensile strength.

4. There are no appreciable differences in room temperature physical properties between Epon 820 with Versamid 125 and Epon 820 with Versamid 140; however, differences would be expected at elevated temperatures.

Elevated temperature, fatigue, and environmental investigations should be conducted for a more complete evaluation of these resin compounds.

With increased demands upon helicopter rotor structures, Kaman Aircraft sought solution to many problems through the use of fiberglass, particularly oriented glass fibers. Materials supplied by several reputable manufacturers have been used quite successfully in Kaman fabrications, and the quality control specimens tested in conjunction with manufacturing

BLANK PAGE

Table 1-D3

ROOM TEMPERATURE PHYSICAL PROPERTIES OF EPON 820 AND EPON 826
COMBINED WITH VERSAMID 125 AND VERSAMID 140

Resin System		Tensile PSI	Tensile Mod, PSI	Flexural PSI	Flexural Mod, PSI	Thick, Inch	Resin %	Hardness Rockwell M
Shell 820	-	Avg.						
100 Pts/Wt.		59,600	3.80×10^6	83,260	3.15×10^6	.1135	33.8	108
DTA	-							
8 Pts/Wt.		High 62,600	4.06	86,300	3.22	.114		
		Low 50,600	3.50	81,800	3.10	.113		
Shell 820	-	Avg.						
100 Pts/Wt.		58,940	3.72	79,140	3.09	.114	33.5	100
DTA	-							
6 Pts/Wt.		High 59,500	3.89	80,400	3.15	.116		
Versamid 125	-	Low 58,000	3.55	77,600	3.02	.112		
10 Pts/Wt.								
Shell 820	-	Avg.						
100 Pts/Wt.		59,720	3.61	80,660	3.14	.112	33.3	107
DTA	-							
6 Pts/Wt.		High 62,500	3.72	82,800	3.27	.114		
Versamid 140	-	Low 57,300	3.49	77,700	3.08	.111		
10 Pts/Wt.								
Shell 826	-	Avg.						
100 Pts/Wt.		60,030	3.61	83,420	2.99	.113	33.5	107
DTA	-							
6 Pts/Wt.		High 63,750	3.65	86,000	3.01	.114		
Versamid 125	-	Low 57,700	3.57	81,300	2.93	.112		
10 Pts/Wt.								

Table I-D3 (Cont'd.)

ROOM TEMPERATURE PHYSICAL PROPERTIES OF EPON 828 AND EPON 826 COMBINED WITH VERSAMID 125 AND VERSAMID 140

Resin System		Tensile PSI	Tensile Mod. PSI	Flexural PSI	Flexural Mod. PSI	Thick. Inch	Resin %	Hardness Rockwell M
Shell 826	-	Avg.						
100 Pts/Wt.		60,420	3.66	88,000	3.28	.114	32.5	108
DTA	-							
6 Pts/Wt.		High 63,700	3.74	90,300	3.36	.115		
Versamid 140	-	Low 55,700	3.53	84,000	3.14	.111		
10 Pts/Wt.								
Shell 826	-	Avg.						
100 Pts/Wt.		61,800	3.86	88,880	3.27	.111	31.8	107
DTA	-							
8 Pts/Wt.		High 65,600	4.03	91,800	3.34	.112		
		Low 57,900	3.69	86,600	3.22	.106		

BLANK PAGE

processes generally exceed, by a substantial margin, the requirements of MIL-P-25421A (minimum tensile strength = 100,000 psi, minimum flexural strength = 125,000 psi). Many, perhaps most, of Kaman's applications deal with structures subject to high fatigue requirements with primary high steady stresses and cyclic combined stresses. In such cases, where the inherent transverse weakness of the pure unidirectional fiber lay-up is inadequate, success has been achieved by incorporating lay-ups of plies alternately oriented at $\pm$ 5^{o} or, where demanded, $\pm$ 15^{o} - the degree orientation being about the primary stress path

One of the areas subject to much discussion, and as yet unresolved in Federal test methods, is the technique for specimen tensile testing. Specifically, when testing unidirectional or $\pm$ 5^{o} oriented specimens, invalid failures invariably occur in the grip area and not in the test section. An excellent example of this is found in Table I-D4, where specimens of directed fiberglass tape (Fiber Glass Division, Ferro Corporation, Nashville, Tenn.) impregnated with epoxy resin (U. S. Polymeric Corporation, Stamford, Conn.) were made and tested in accordance with Federal Test Method 406.

The results show scattered values all substantially above minimum MIL specification, and yet all failed prematurely in the grip area. This characteristic has also been brought out by investigations of the Reinforced Plastic Division of Minnesota Mining and Manufacturing Company, who suggest modifying tensile specimens to incorporate reinforcing aluminum plates as shown in Figure I-D1.

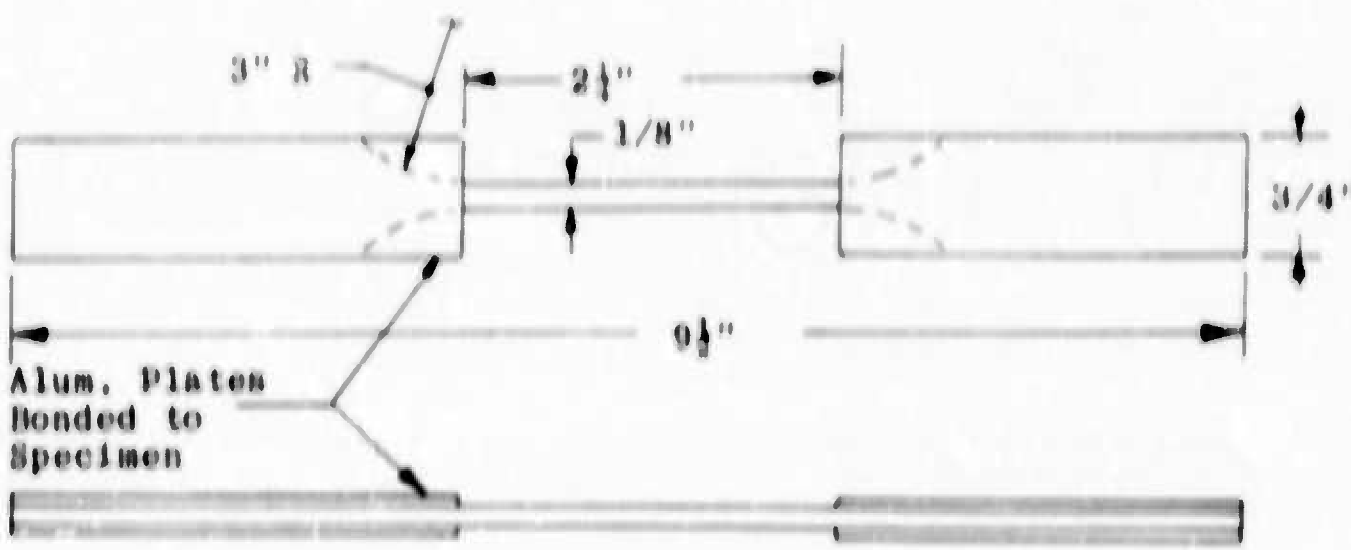

Figure I-D1.
3 M Suggested Unidirectional Test Specimen

Table 1-D4

PHYSICAL PROPERTIES OF F.R.P. LAMINATES (Epoxy)

Description	Specimen Number	% Resin Content	Density, Grams/cc	Tensile Strength	Tensile Modulus (10^6 PSI)	Flexural Strength (PSI)	Flexural Modulus (10^6 PSI)
Directed Fiberglass tape	1	19.8	2.09	166,000	7.40	198,500	7.23
manufactured by Fiber	2	19.8	2.09	187,000	7.10	199,000	6.86
Glass Division, Ferro	3	22.8	1.95	187,500	6.60	182,000	6.18
Corporation, Nashville,	4	22.8	1.95	174,000	6.64	184,500	6.47
Tenn. Impregnated by	5	25.0	1.95	165,000	6.25	169,000	5.86
U. S. Polymeric Corpora-	6	25.0	1.95	150,000	5.94	164,000	5.85
tion, Stamford, Conn.	7	27.0	1.905	150,000	5.35	167,000	5.67
	8	27.0	1.905	149,000	6.17	164,030	5.80

BLANK PAGE

The Kaman Material Engineering Laboratory has been unsuccessful with this method in testing $\pm$ 5° specimens where analysis has shown bonding failures under the aluminum plates. Kaman also has made a limited investigation on $\pm$ 5° tensile specimens. Instead of making pieces with relatively long test sections, the test area was formed by sanding a 2.50-inch radius on each side of the laminate (see Figure 1-D2).

Although limited tests were made, an apparent pattern is observed when the test area width is varied as shown in Figure 1-D2 and Table 1-D5.

With the specimen test width at approximately .25 inch (similar to Type II of Federal Test Method 406), failure occurred in the grip area at relatively low values (still above MIL-P-25421A). When the section was reduced to approximately .20 inch, tensile strength increased slightly but again a grip area failure occurred. However, at a test section width of about .14 inch, the tensile strength again increased and the failure occurred in the test section. When the width was reduced to .09 inch, a valid failure occurred in the order of 140,000 psi. This concurred with 3 M test values for the $\pm$ 5° oriented "Scotchply", which was used in the above test.

The results suggest that for a given symmetrical orientation of unidirectional fibers, there exists an optimum test area width when the test section is constructed as described herein.

Figure I-D2.
± 5° Oriented Unidirectional Test Specimen

Table I-D5

$\pm$ 5° ORIENTED SCOTCHPLY

Specimen	Thickness (Inch)	Width (Inch)	Tensile Strength (PSI)	
A1	.146	.232	107,000	Failed in Grips
A2	.148	.228	108,000	Failed in Grips
A3	.143	.262	122,000	Failed in Grips
B1	.142	.195	108,000	Failed in Grips
B2	.143	.204	113,000	Failed in Grips
B3	.146	.215	123,500	Failed in Grips
C1	.144	.140	123,500	
C2	.147	.143	128,000	
C3	.152	.143	134,000	
D1	.145	.093	137,000	
D2	.144	.096	143,500	
D3	.143	.083	140,000	
D4	.144	.083	146,500	

SECTION II

COMPOSITE BLADE DEVELOPMENT

BACKGROUND

The rotors that support a helicopter are mechanical rotating elements that have to meet most of the special requirements of high-strength rotating machinery plus having their own peculiar type of behavior that makes their design extremely sophisticated.

In particular, the helicopter rotors operate by an oscillating relationship to the air, which induces variable forces and vibratory strains of a continuous nature.

This discussion will concentrate on the rotor blade part of the Kaman helicopter rotor, disregarding the very highly stressed mechanical components of the so-called hub and blade attachment.

The helicopter rotor blades are very slender bodies, which are shaped to closely controlled airfoils and endowed with control systems capable of making them follow the cyclically variable path that is required to maneuver the helicopters in their various modes of performance.

The blades involved in our discussion for the Kaman HH-43B "Huskie" Helicopter represent a further structural problem because the structure itself is used as an elastic twist and bending hinge and the controls are applied to them through the characteristic Kaman servo flaps (Figure II-1). This particular arrangement has permitted simplification of the attaching machinery and requires much lighter control loads for the inboard parts of the ship, but it introduces problems of delicate dynamic and elastic balance for the blade and all its components.

The blade under discussion is a "paddle" about 24 feet long, 17 inches chord, and approximately 2 inches thick at the maximum point with a well-rounded leading edge and a trimly tapered trailing edge.

An idea of the precision requirements for these blades is as follows:

The weight of two blades must be controlled to be balanced within 1 pound in 170 or .59 percent.

The airfoil shapes must be held to a tolerance of plus or minus .010 inch on all contours after all the various operations of fabrication, balancing, coating, etc., are successively performed, and including the basic raw materials stock variations.

The torsional stiffness of the blade is held to approximately 1.5 inch-pounds per degree out of 190, or .79 percent, and the location of the center of gravity of the system is measured repeatedly and kept within a .032-inch-diameter circle.

All these requirements which are necessary for smooth running and proper control response are ensured by a continuous series of in-process controls and check points with a lot of fine hand trimming and rational redistribution of weights to prevent the total assembly from exceeding the very strict limits.

In addition to all this, some dynamic checks are taken on the blades by studying their response to vibration and determining the proper balance in the chordwise direction that will permit uniform control response in flight. Finally, no blade can be installed on an aircraft unless its performance has been checked on a test rig or on an experimental aircraft to ensure that all the previous care has been actually translated into an operable component.

These blades may be subject to hard use and they may be damaged and repaired; also, they usually have an established overhaul interval after which they have to be very closely inspected before they are used again.

On all such occasions, where material is replaced or added to the blades for repair or where some components are stripped from the blade for inspection, the minute careful balancing and matching procedure has to be repeated so that the final overhauled product is worthy of flight as well as a brand new blade.

Absorption or entrapment of moisture within the blades of a helicopter in an uneven manner will immediately create out-of-balance conditions.

In some cases, resting the helicopter blades partially in the shade will cause uneven behavior until the relative temperature differences are again equalized.

In view of the above-mentioned facts, it is evident that some material that would be light, easily workable, impervious to severe exposure effects, highly resilient, moderate in price, and capable of long-term endurance under fatigue conditions would be ideally suited to the construction of helicopter rotor blades.

At the beginning of the company activities in this field, the only material that would permit the use of the Kaman servo flap and elastic hinge principles, with a good compromise on weight and endurance, was some rather elaborately picked and processed wood because of the low modulus and inherent resilience so obtainable.

As the size of the aircraft grew and its operating life was increased and new more powerful powerplants could be adopted, a limit was reached at which the wooden structures would not quite have sufficient strength to permit development of an adequate product within tolerable weight limits.

Since 1953, Kaman Aircraft has studied the reinforcement of some of the immediate weak points of the wooden blades by the use of fiberglass-reinforced plastic laminates.

In some cases attempts were made to use metal reinforcements, but by and large, success in transferring loads and delaying endurance damage was accomplished by the rational application of layers or various systems of fiberglass and plastic.

It must also be noted that in case of test failures the well used process of "beefing up" does not work for high-speed helicopter rotor parts because in many cases the additional weight required for strengthening, multiplied by the "G" field under centrifugal force, makes the resultant stresses more onerous than the initial ones. Therefore any correction of the situation must be achieved by cleverly redesigning a component to avoid the overloading that caused the failure in the first place.

One typical example of this procedure occurred in the development of the servo flaps where a particular problem of aeroelastic stability required a structure that would combine the proper proportion of torsional strength, bending stiffness, and extremely light weight.

After a number of test-rig failures and design improvements, the problem was solved by introducing tapered spar caps of very high strength unidirectional fiberglass-reinforced plastics, which performed properly in bending without changing the torsional tuning and did not increase the weight of the assembly to an intolerable extent.

Various series of flaps with or without less elaborate plastic reinforcing had seen service before the final solution was achieved, but in all cases they required "red line" limitations to either the speed or the flight attitude of the aircraft to avoid inducing aeroelastic trouble.

Figure II-1 is a basic sketch of the Kaman HH-43B blade.

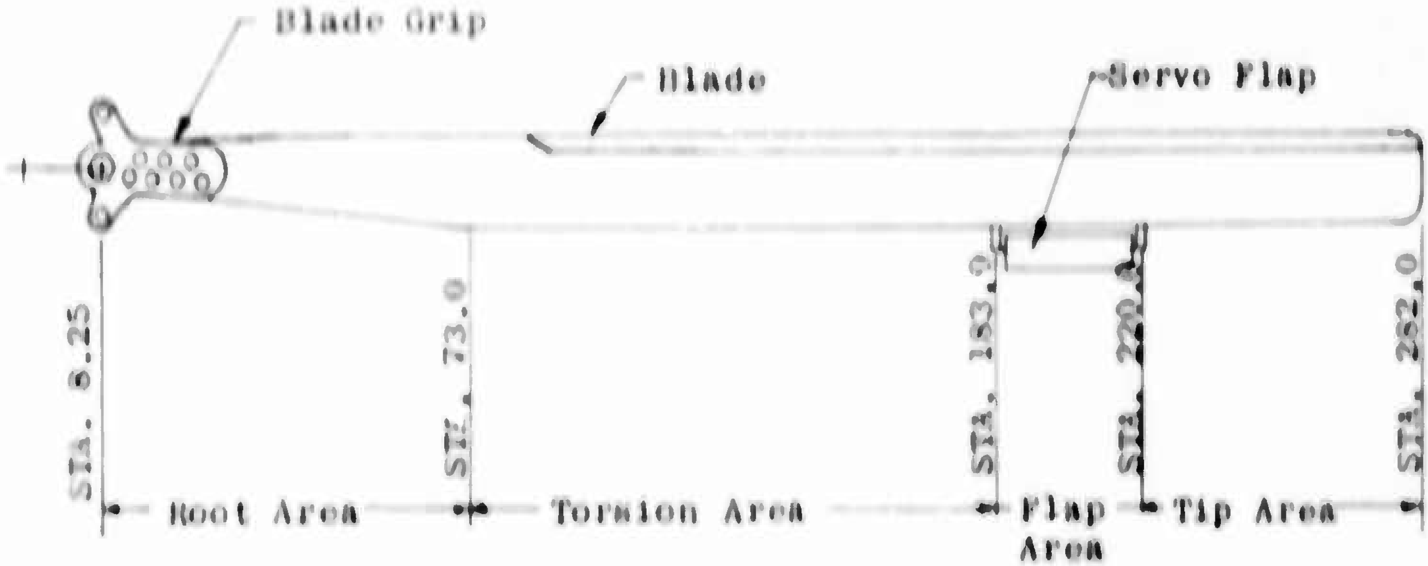

Figure II-1. Sketch of Basic Helicopter Blade

For economic and convenience reasons, the blade nomenclature is broken into areas and specimens of these areas are tested prior to complete blade final testing. Analytical data and whirl and flight test data are "cranked" into specimen test loads and revised as information is gathered to ensure integrity and safety margins.

STATIC TESTING

From a static strengthwise view, the blade root end is the weakest component of the rotor head system. It is subjected to a combination of high centrifugal force, in-plane or edgewise bending due to engine rotor torque, and flapping or flatwise bending. These loads were applied to the root end specimens in the following manner:

1. Centrifugal loads were applied to the specimen by means of hydraulic cylinders pushing on a load beam. The C.F. loads were monitored by a hydraulic pressure gage.

2. Engine torque was applied to the specimen through a stub HH-43B rotor shaft, actuated by a hydraulic cylinder in a self-contained cable system. Monitoring of the torque loads was accomplished by a strain gage line calibrated against known company standards.

3. Application and control of flapwise bending moments were accomplished by means of a vertical hydraulic cylinder attached to the center of the hub. Monitoring of the bending moment was controlled by two previously calibrated rotor blade root ends. A calibrated hydraulic pressure gage was used to obtain the shear load applied to the center of the hub.

Figures II-2, II-3 and II-4 show the specimen and fixture as described above.

The blade root end was instrumented with SR-4 type strain gages as shown in Figure II-5.

The critical static test conditions to which the specimen was tested were simulated aircraft maneuvers creating a positive (+) 3 "g" at 210 R.P.M. and a negative (-) 0.5 "g" at 260 R.P.M. Transposing this to actual forces and moments results in the following:

<u>+ 3 "g" condition</u>

213,000 in.-lb. at blade Sta. 14.0
138,000 in.-lb. at blade Sta. 31.0
110,000 in.-lb. at blade Sta. 40.0
70,000 in.-lb. at blade Sta. 57.0
21,085 lb. centrifugal force
288,000 in.-lb. engine torque

<u>- 0.5 "g" condition</u>

- 173,400 in.-lb. at blade Sta. 14.0
- 115,500 in.-lb. at blade Sta. 31.0
- 82,600 in.-lb. at blade Sta. 40.0
- 44,500 in.-lb. at blade Sta. 57.0

30,300 lb. centrifugal force
288,000 in.-lb. engine torque

These above loads are termed "limit" loads which are equivalent to what the actual part would experience for the given condition. By specification, the part must be able to withstand "ultimate" loads, which are defined as 150 percent of the limit load. It is desirable, of course, to realize higher percentages so as to create greater margins of safety.

The test procedure for the root end specimen was to apply loads in 20 percent increments up to 100 percent D.L.L. (design limit load), and in 10 percent increments to 150 percent D.L.L. Subsequently, the specimens were loaded to failure. Strain gage data were recorded and plotted to detect yielding.

Figure II-2
Typical Hub, Grip and Blade Root-End Test Setup

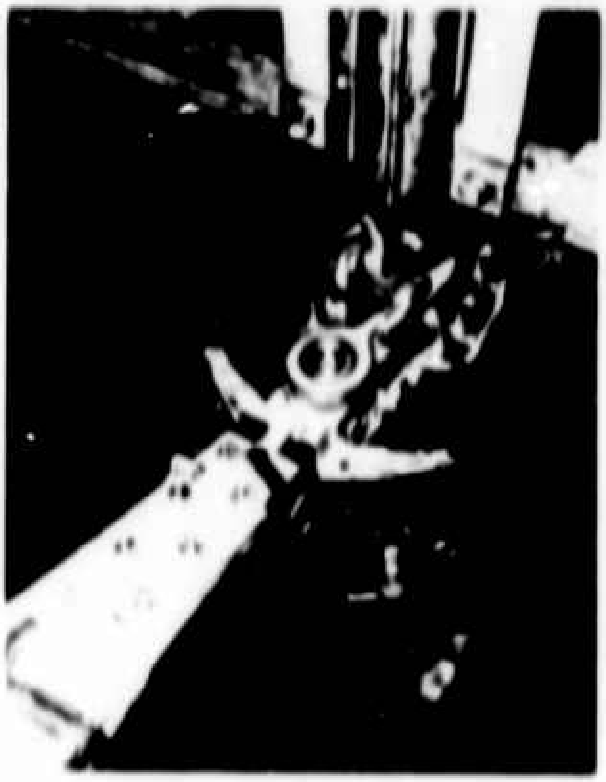

Figure II-3
Close-up of Rotor Hub Blade Grip and
Blade Root-End Installation

Figure II-4
View Showing Centrifugal Force Application Beam

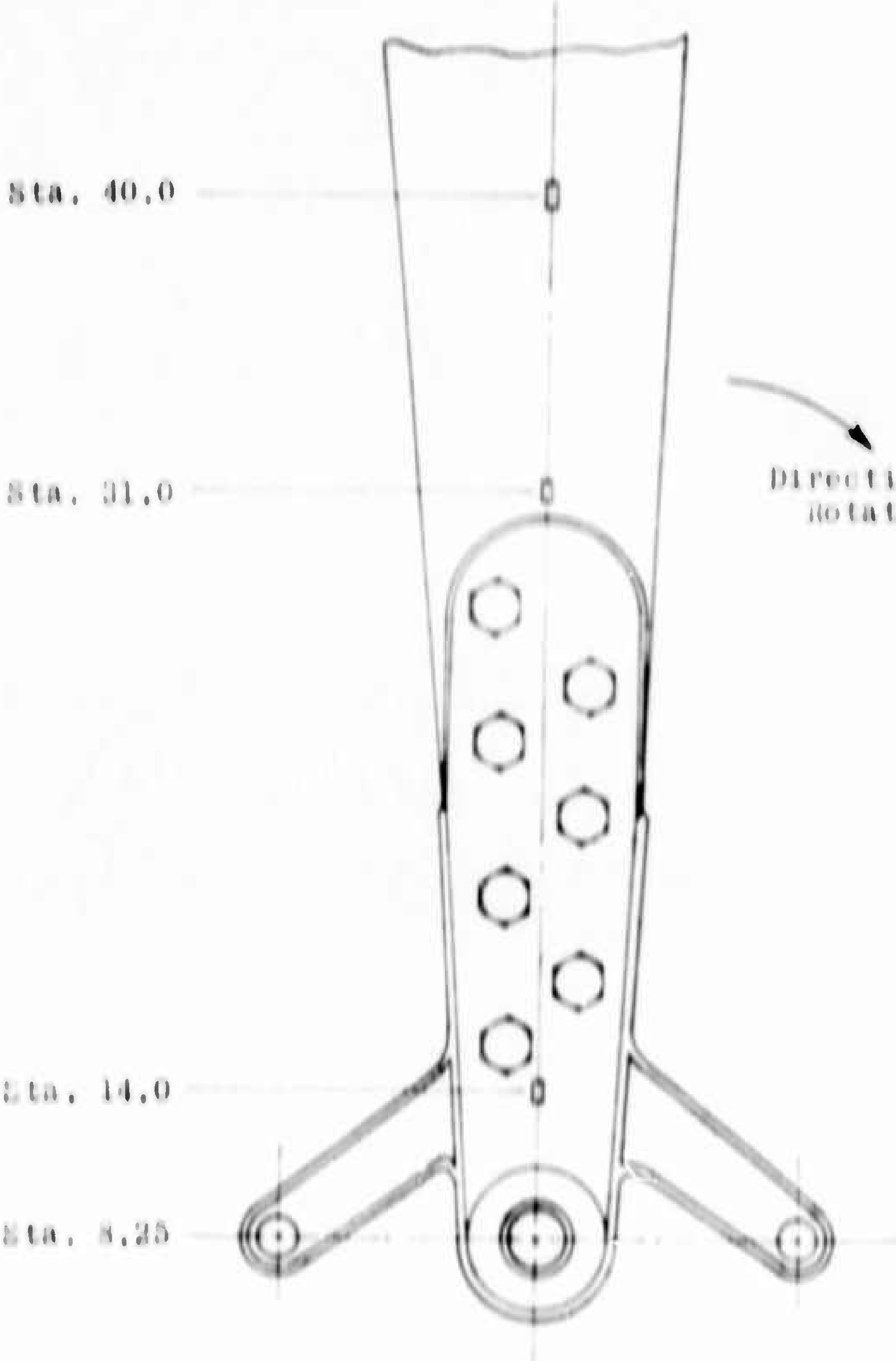

Figure II-5
Instrumentation and Bolt Hole Locations,
Blade and Grip Root-End Specimen

Figure II-6 shows the cross-sectional development of the blade root end by the application of fiberglass-reinforced plastic.

The original improvement design for the laminated spruce and maple wood spar (Figure II-6) was to shave off approximately 3/8 inch from the top and bottom surfaces and to bond in its place a reinforcing "cheek" plate comprised of a ¼-inch laminate of phenolic resin fiberglass and a 1/8-inch laminate of $\pm 5^{\circ}$ oriented layers of Scotchply (3 M Co.), with the Scotchply forming the outside of the composite sandwich. This specimen completed the 100 percent D.L.L. runs at + 3.0 g and - 0.5 g; but in an attempt to accomplish the ultimate limit load at + 3.0 g, a root-end failure occurred at 125 percent of the design limit load. Figures II-7 and II-8 reveal the failed specimen.

This premature failure necessitated a design modification in order to satisfy the strength requirements. Therefore, separate tests were conducted on single blade root-end specimens under combined centrifugal load and flatwise bending to assess these modifications.

After the prematurely failed blade root end was dissected, an investigation indicated that the primary cause was a wood shear failure between the upper and lower surfaces of the blade.

The Dynamic Stress Group suggested a fiberglass shear tie plate on both leading and trailing edges of the blade root end to eliminate this problem. A specimen was made which incorporated, in addition to the cheek plates, ½-inch shear plates of epoxy resin and No. 181 glass cloth layed up with the warp at 45° to the span (lengthwise) direction (2nd configuration, Figure II-6).

This blade root end failed at 145.5 percent of the + 3.0 g limit load condition (201,000 in.-lb. blade Sta. 31.0), just under the minimum requirement of 150 percent (207,000 in.-lbs. blade Sta. 31.0).

The vertical shear tie plate failed along its glue line where it was attached to the upper surface; thus, another design was made to increase the glue area of the shear tie by making it a channel section, hence completely boxing the blade grip retention area in fiberglass. The third configuration of Figure II-6 represents this structure. Orientation of the warp in the No. 181 glass cloth channels was at 45 degrees to the spanwise direction.

The third modification specimen surpassed the 150 percent limit load and failed under the combined centrifugal and bending

BLANK PAGE

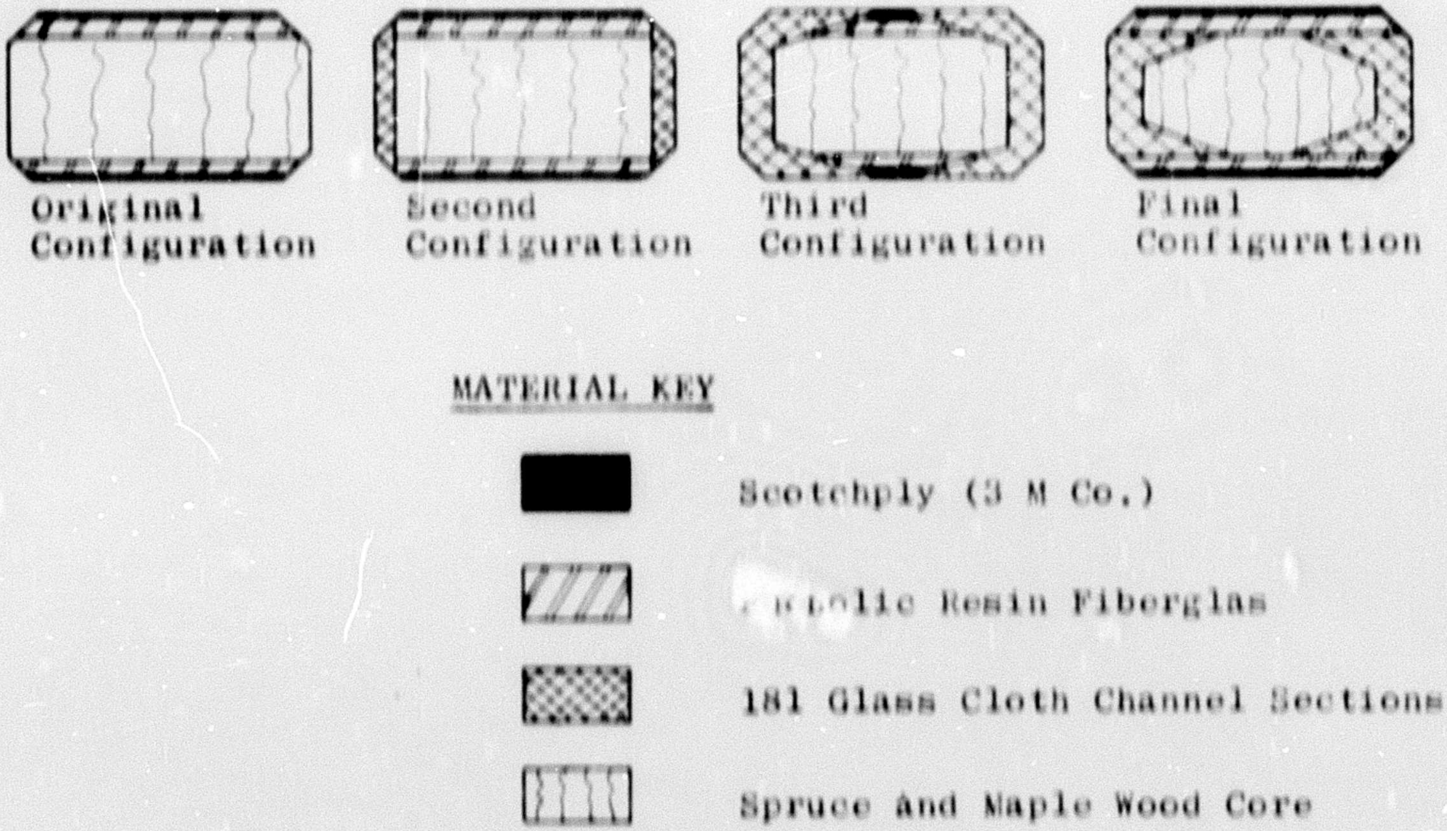

Figure II-6. Configurations of Blade Root-End Development with Fiberglass-Reinforced Plastic

Figure II-7. Original Stub Configuration Showing General Failure

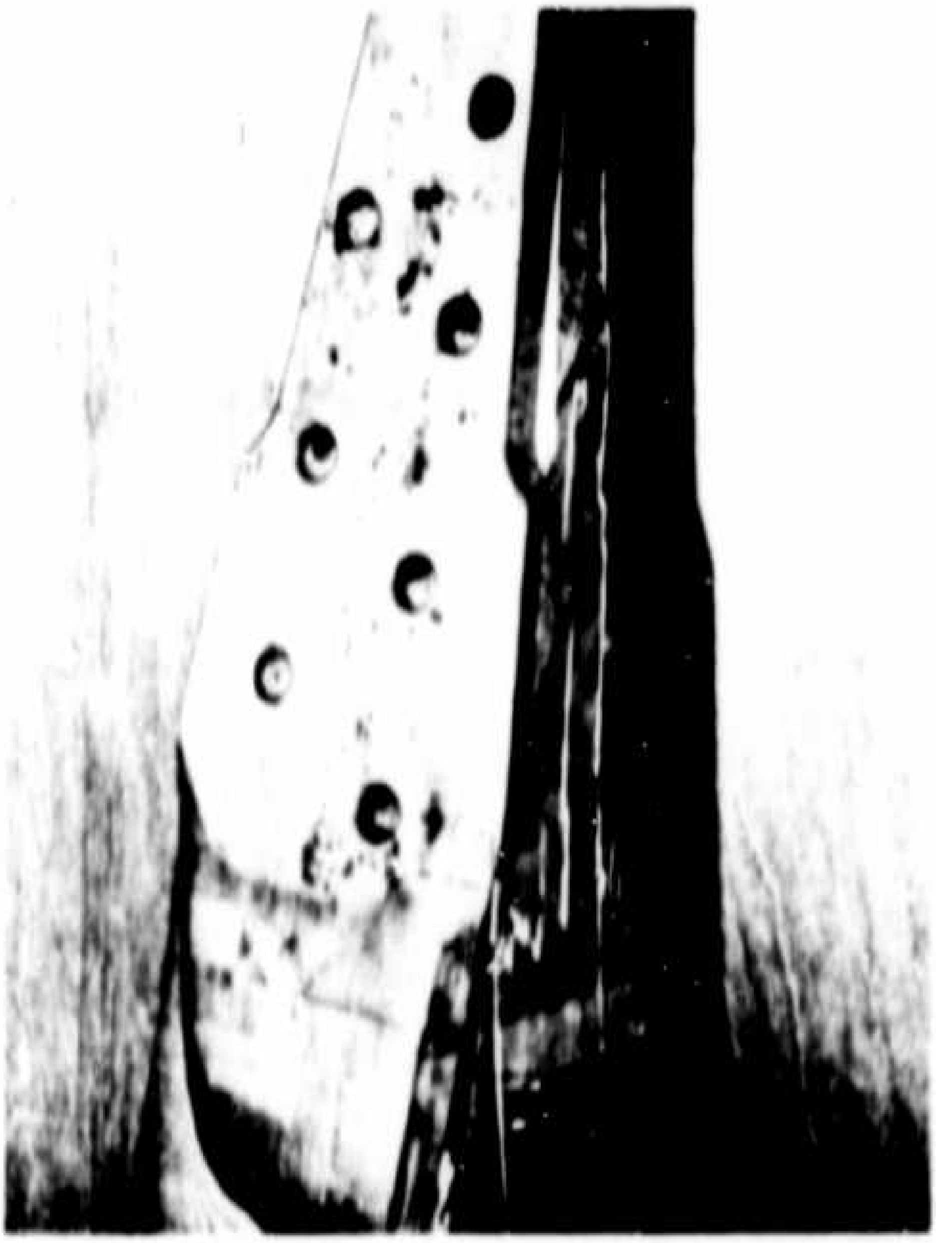

Figure II-8. Close-up View of Stub Failure effect at 163.8 percent (226,000 in.-lb. at block Sta. 31.0). This failure occurred through the outboard bolt holes in the area of the splice between side channels and cheek plates (Figure II-9).

The final modification (Figure II-6) consisted of placing the flanges of the epoxy fiberglass channels underneath the cheek plates, thus creating an uninterrupted structure for the bolt retention. Subsequent testing at the + 3.0 g limit load condition resulted in yielding of a metallic retention component at 161 percent. This is so close to the previous 163.8 percent that they may be considered the same; however, the significant deduction is lack of failure in the blade structure of the final configuration which later in this report will prove to be of value during the fatigue tests with these related parts. In addition, the opposite extreme condition of negative bending moment at - 0.5 g limit load resulted in failure at 180 percent or 208,000 in.-lbs. at blade Sta. 31.0. This failure occurred in the wooden spar structure outboard of the glass-reinforced area as shown in Figure II-10.

Also shown by these results is the more critical element of the higher bending moment at the positive 3.0 g condition.

Figures II-11 through II-33 offer the plotted results of the above testing.

Unlike the blade retention, or root-end, area where fiberglass reinforcement was paramount in deriving an adequate structure statically from the critically high bending moments and centrifugal effects, the torsion and flap areas were structurally adequate statically in the original wood configuration. For this reason, static test results for these areas are omitted. However, it will be brought out subsequently that the fatigue characteristics were greatly enhanced by the use of fiberglass-reinforced plastics in the root, torsion and flap areas.

FATIGUE TESTING

During the design and development of the HOK/HUK rotor blade (the predecessor of the H-43B rotor blade), it was recognized that the two most critically stressed areas of the blade were the blade retention area and the torsion area between the blade root and the flap. Over the years, these two critical regions of the blade became intensively developed structurally, with successive reinforcements of fiberglass as the imposed operational loads increased in severity and as time between overhaul intervals increased for economic reasons. The reinforcements incorporated in these blades were developed and resulted in structural improvements as defined below:

Figure II-9. View Showing Failure of Fiberglass Channel Reinforced Stub

Figure II-10. View Showing Failure of Static Test Stubs

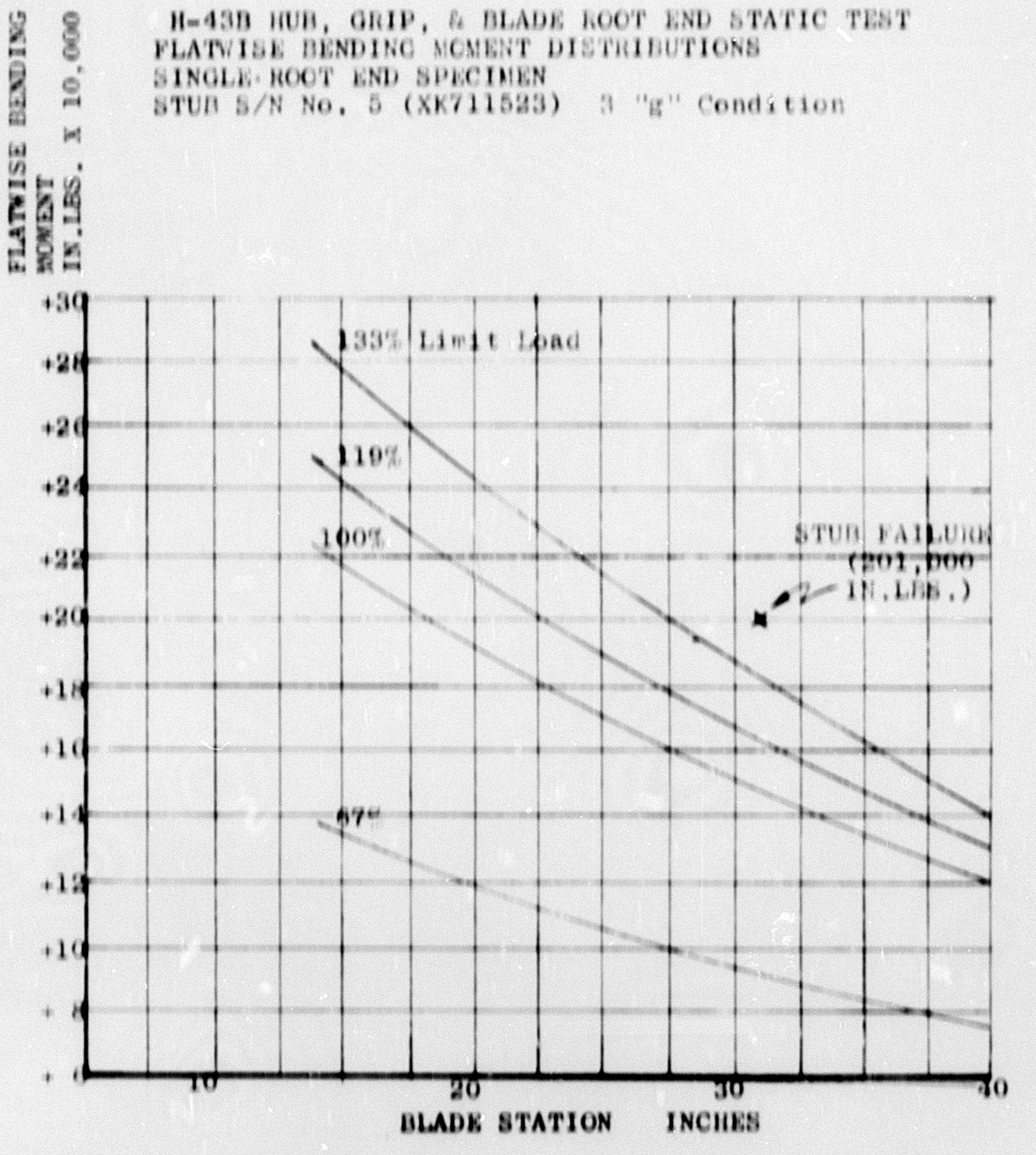

Figure II-11. Flatwise Bending Moment Distributions

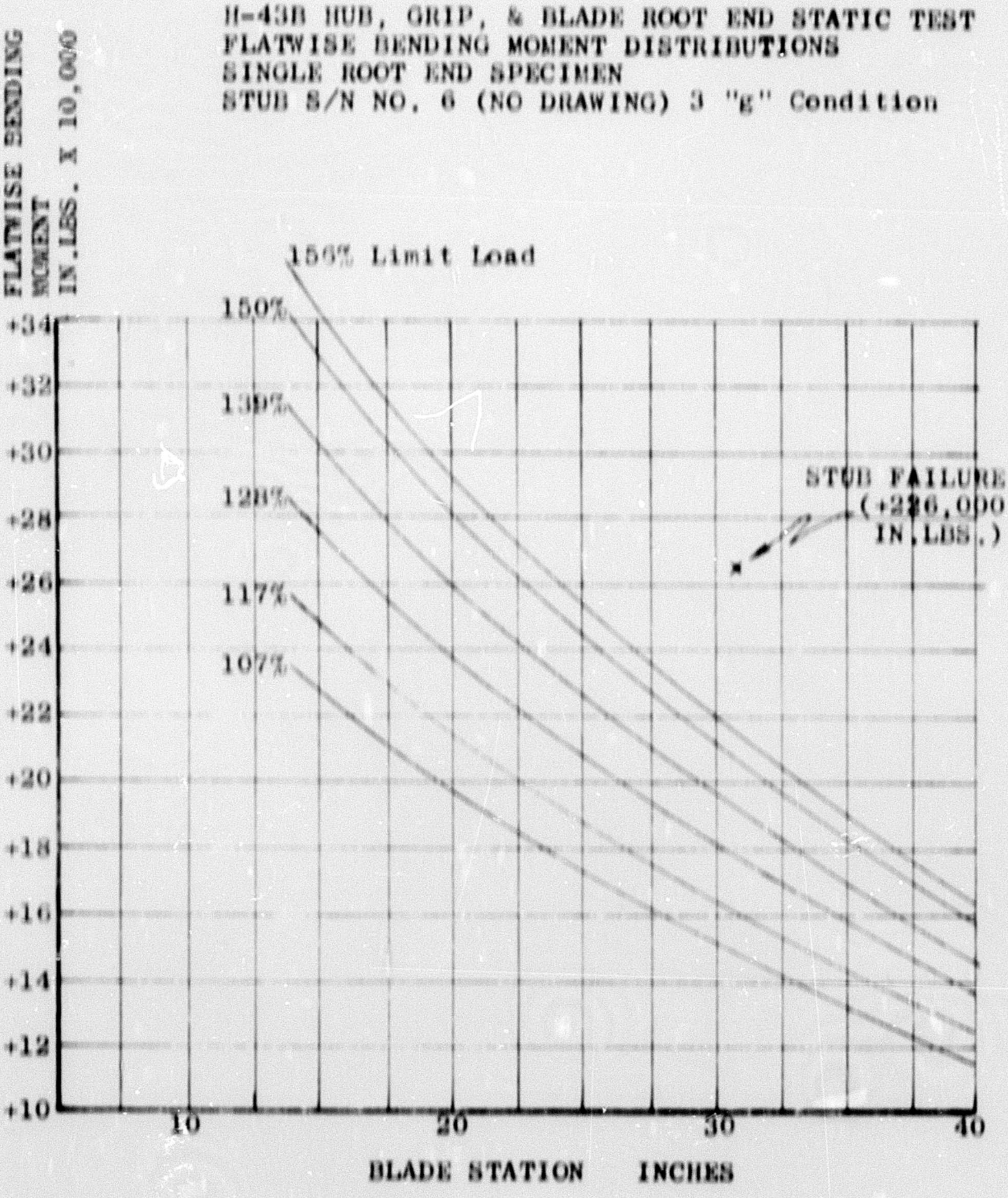

Figure II-12. Flatwise Bending Moment Distributions

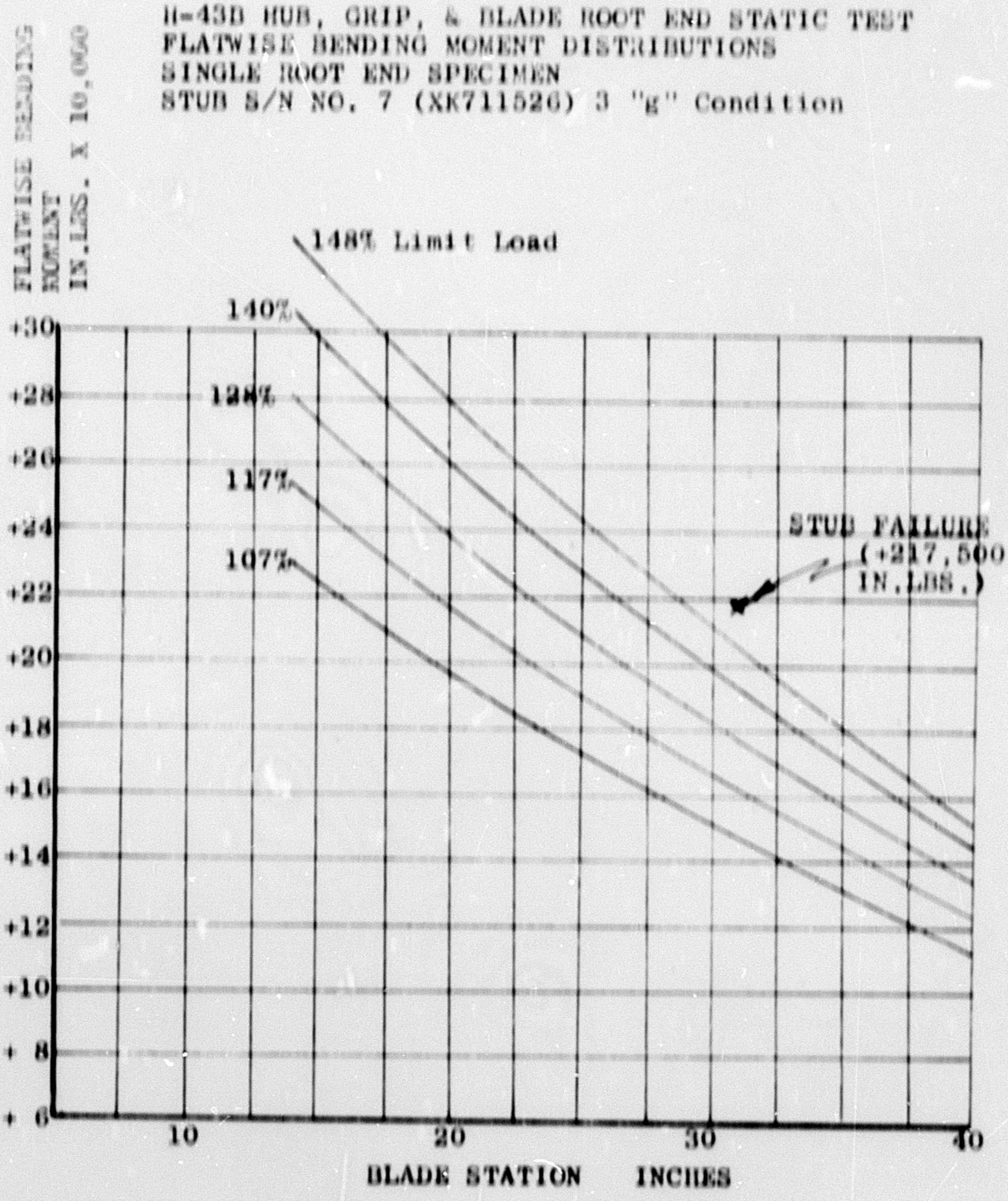

Figure II-13. Flatwise Bending Moment Distributions

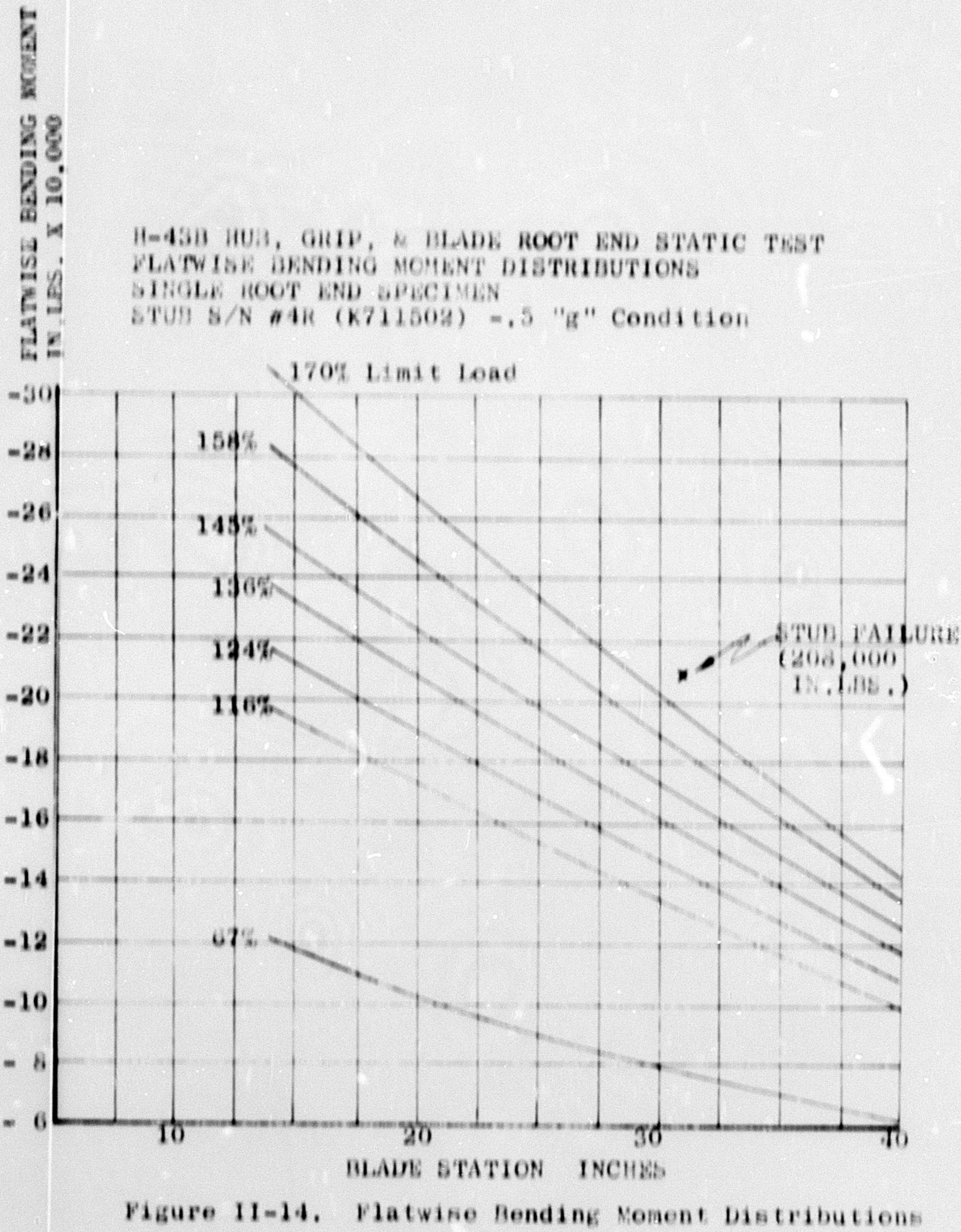

Figure II-14. Flatwise Bending Moment Distributions

BLANK PAGE

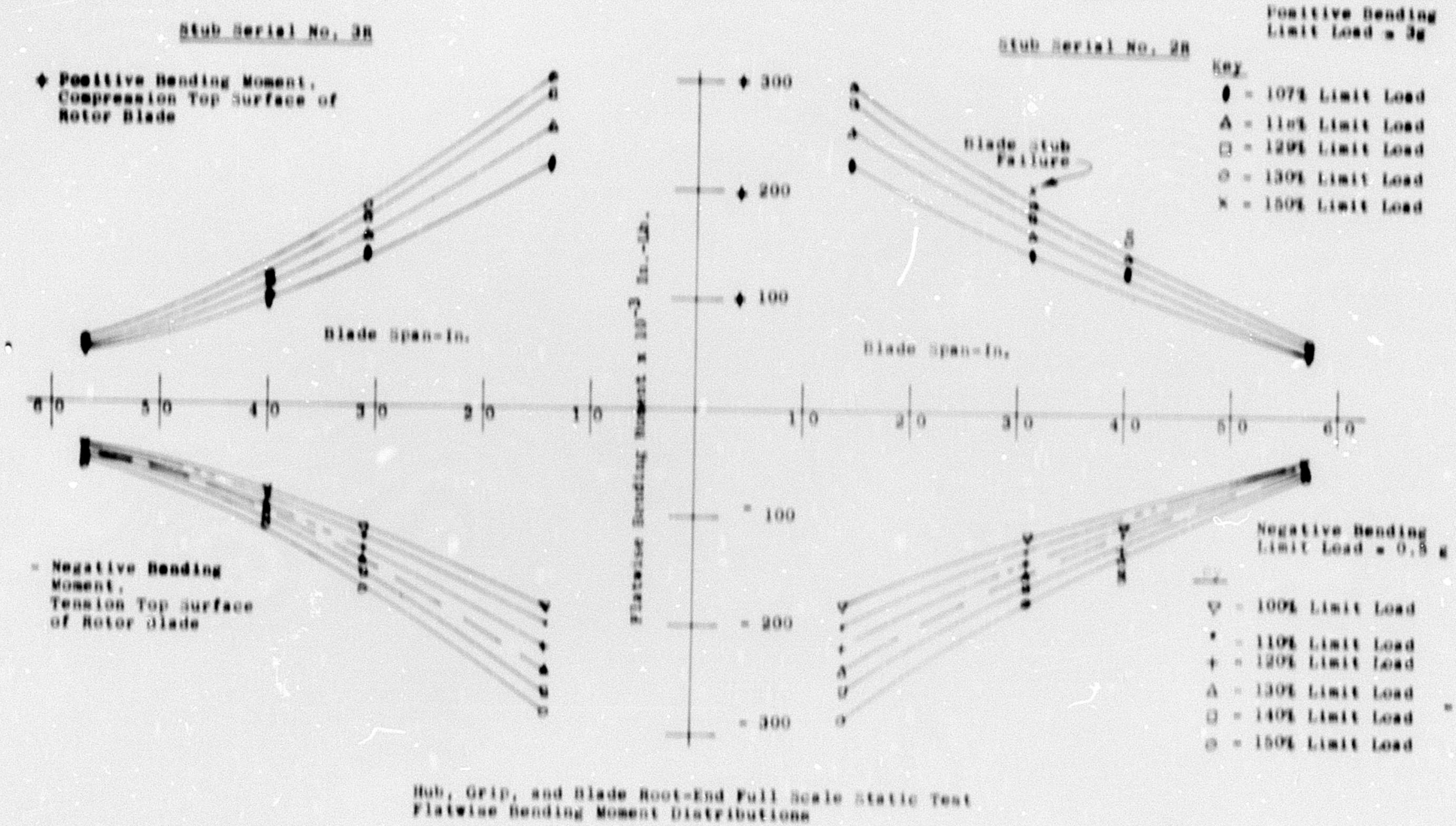

Figure II-15. Flatwise Bending Moment Distributions

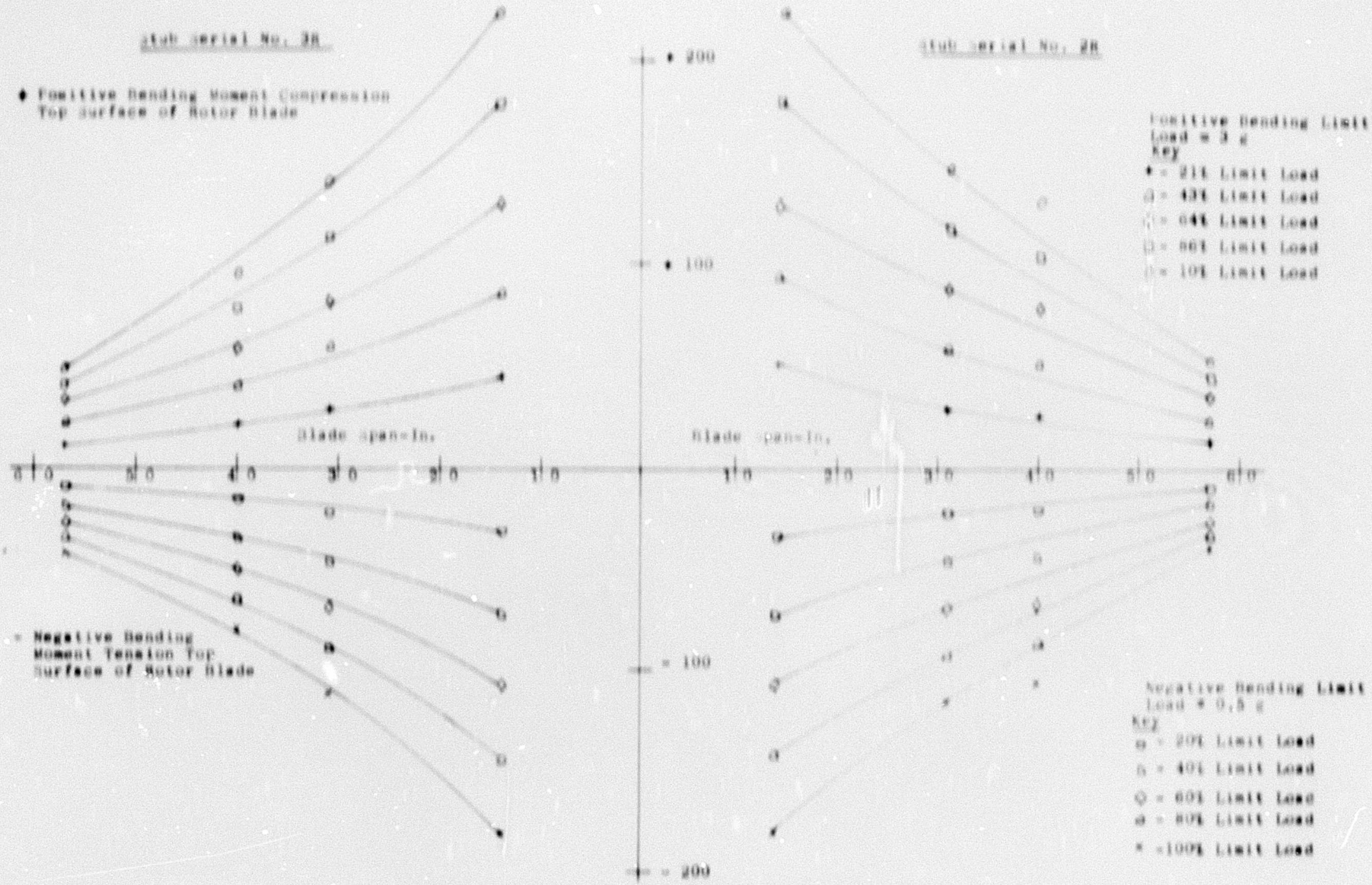

Hub, Grip, and Blade Root-End Full Scale Static Test Flatwise Bending Moment Distributions

Figure II-16. Flatwise Bending Moment Distributions

BLANK PAGE

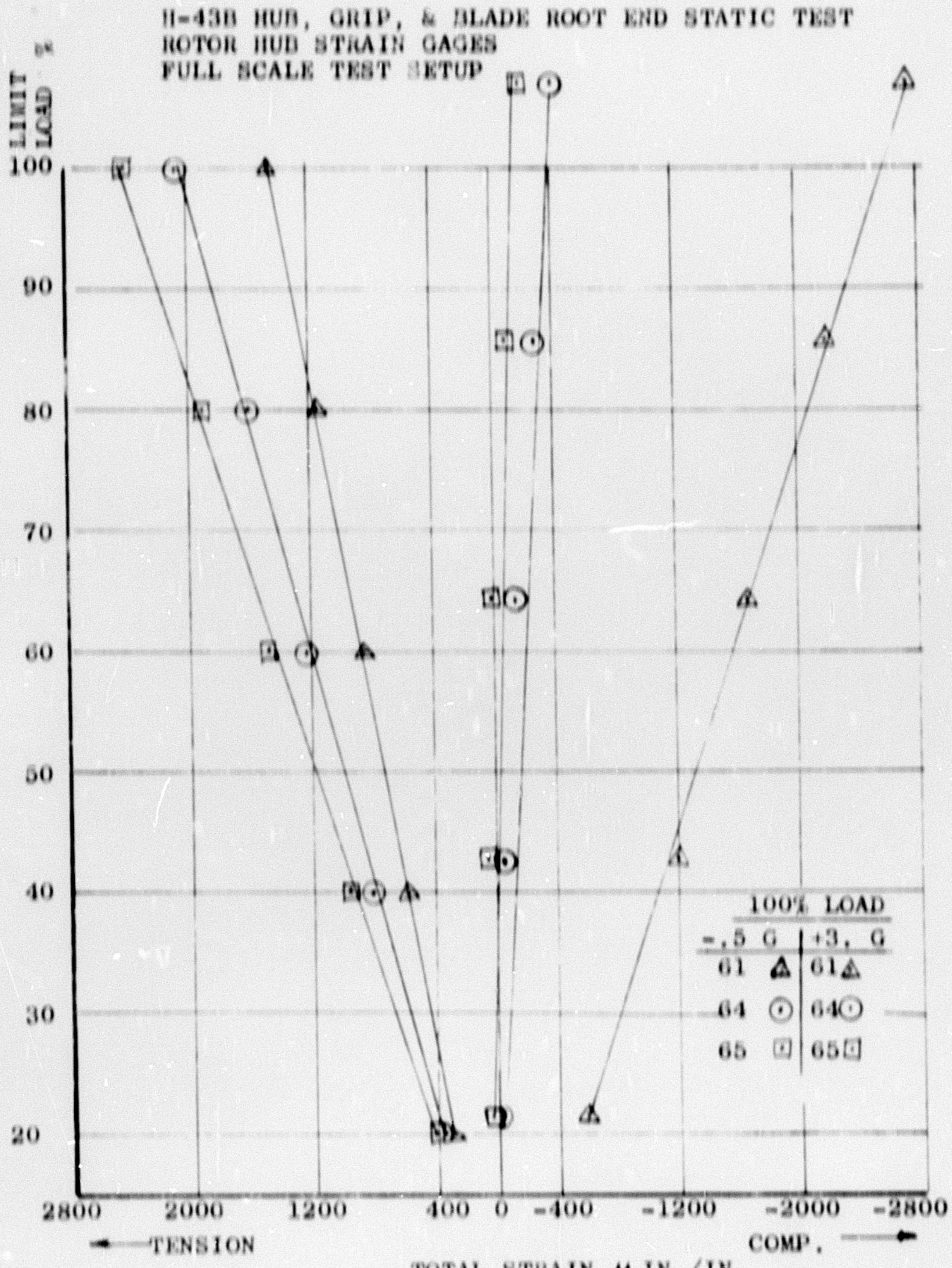

Figure II-17. Root-End Strain Distribution

H-43B HUB, GRIP, & BLADE ROOT END STATIC TEST
ROTOR HUB STRAIN GAGES
FULL SCALE TEST SETUP

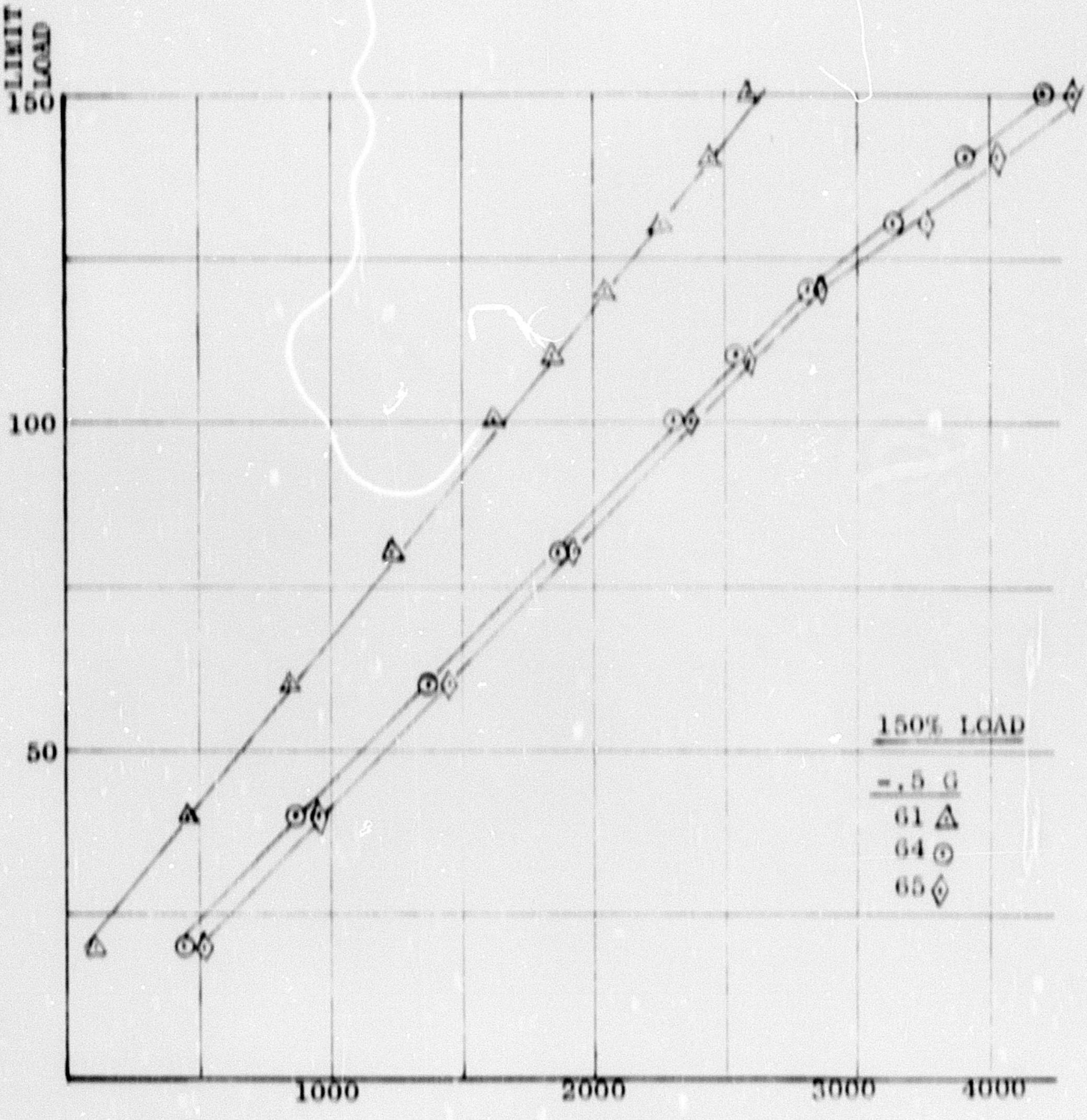

Figure II-18. Root-End Strain Distribution

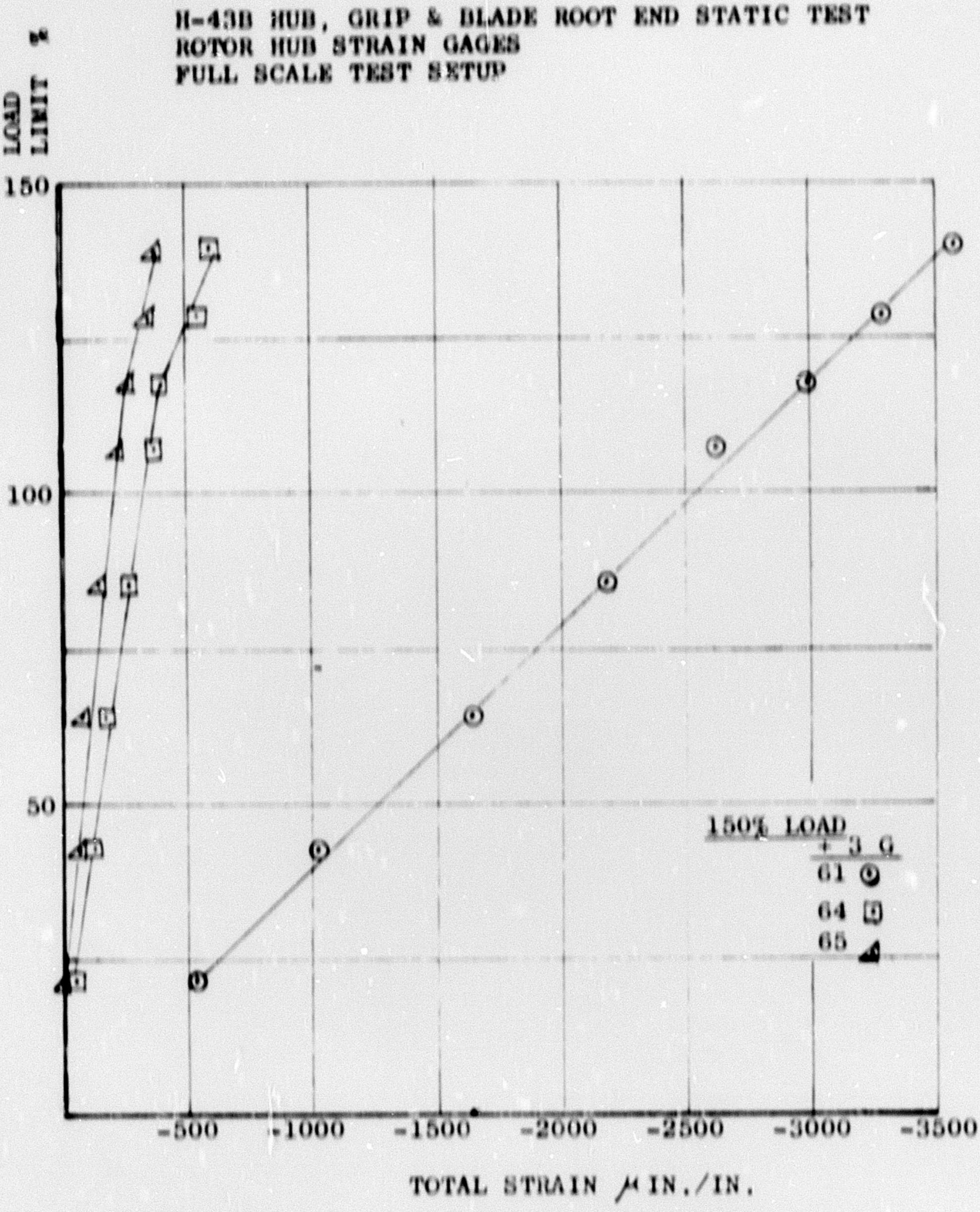

Figure II-19. Root-End Strain Distribution

H-43B HUB, GRIP AND BLADE ROOT END STATIC TEST
ROTOR HUB STRAIN GAGES
FULL SCALE TEST SETUP

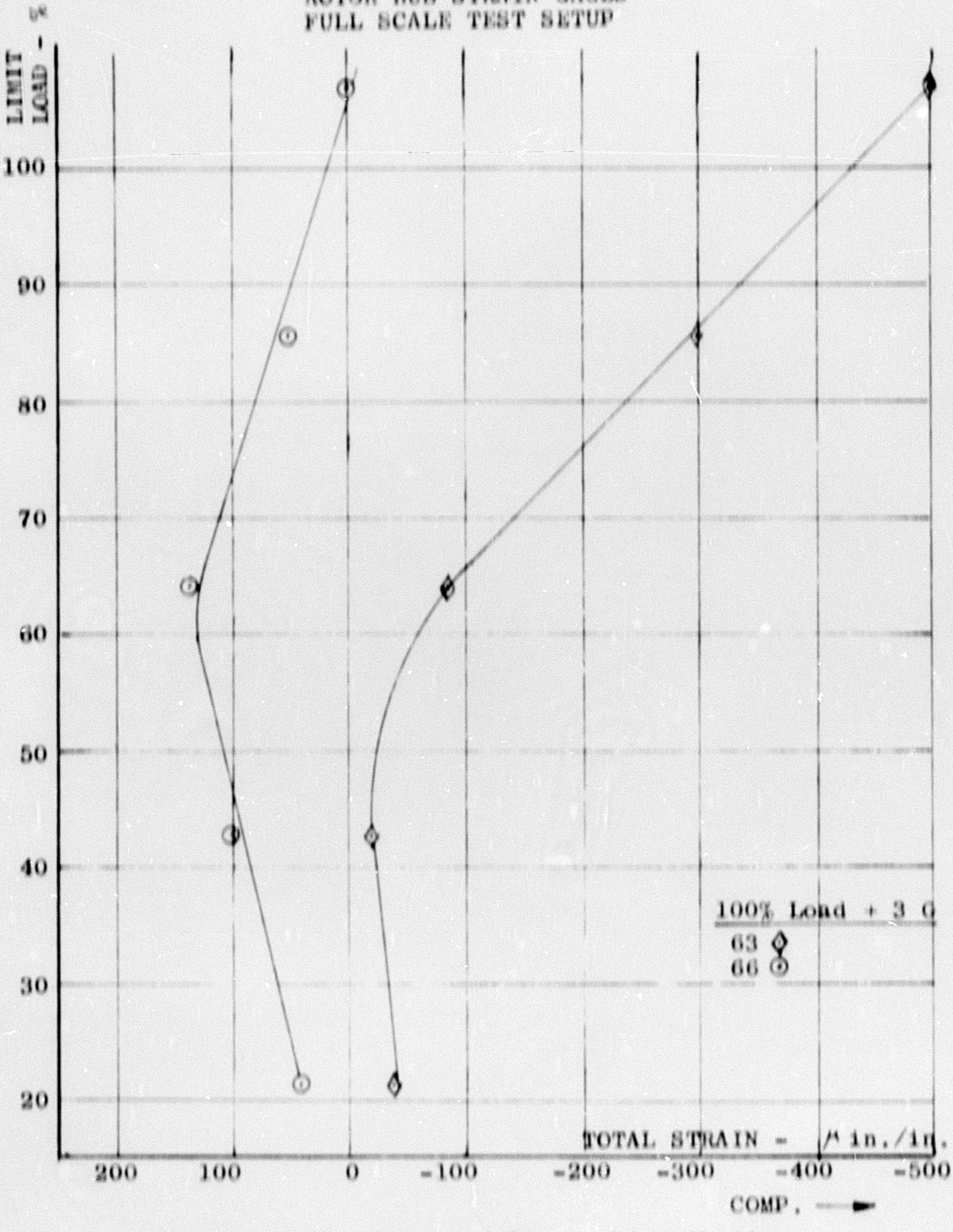

Figure II-20. Root-End Strain Distribution

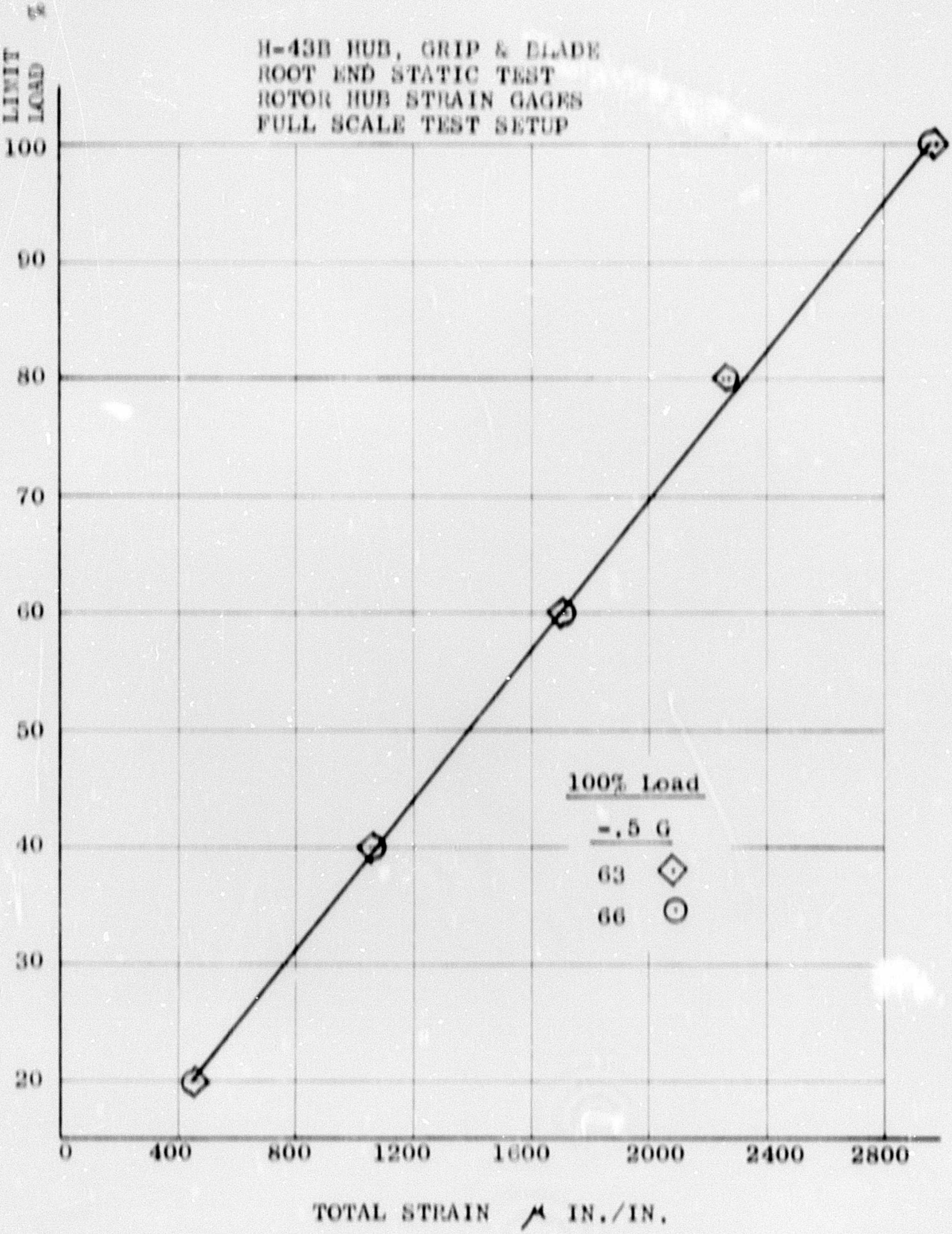

Figure II-21. Root-End Strain Distribution

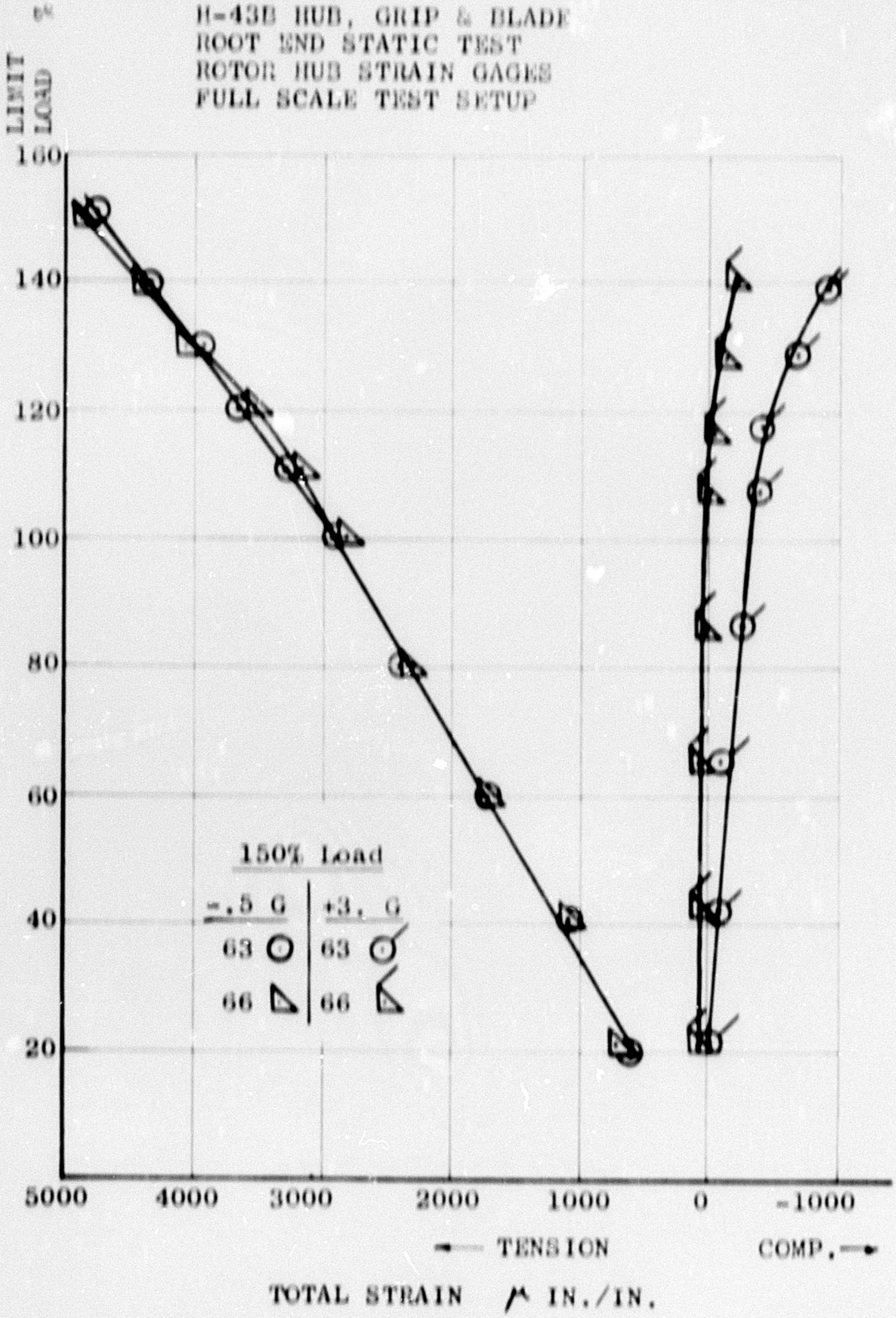

Figure II-22. Root-End Strain Distribution

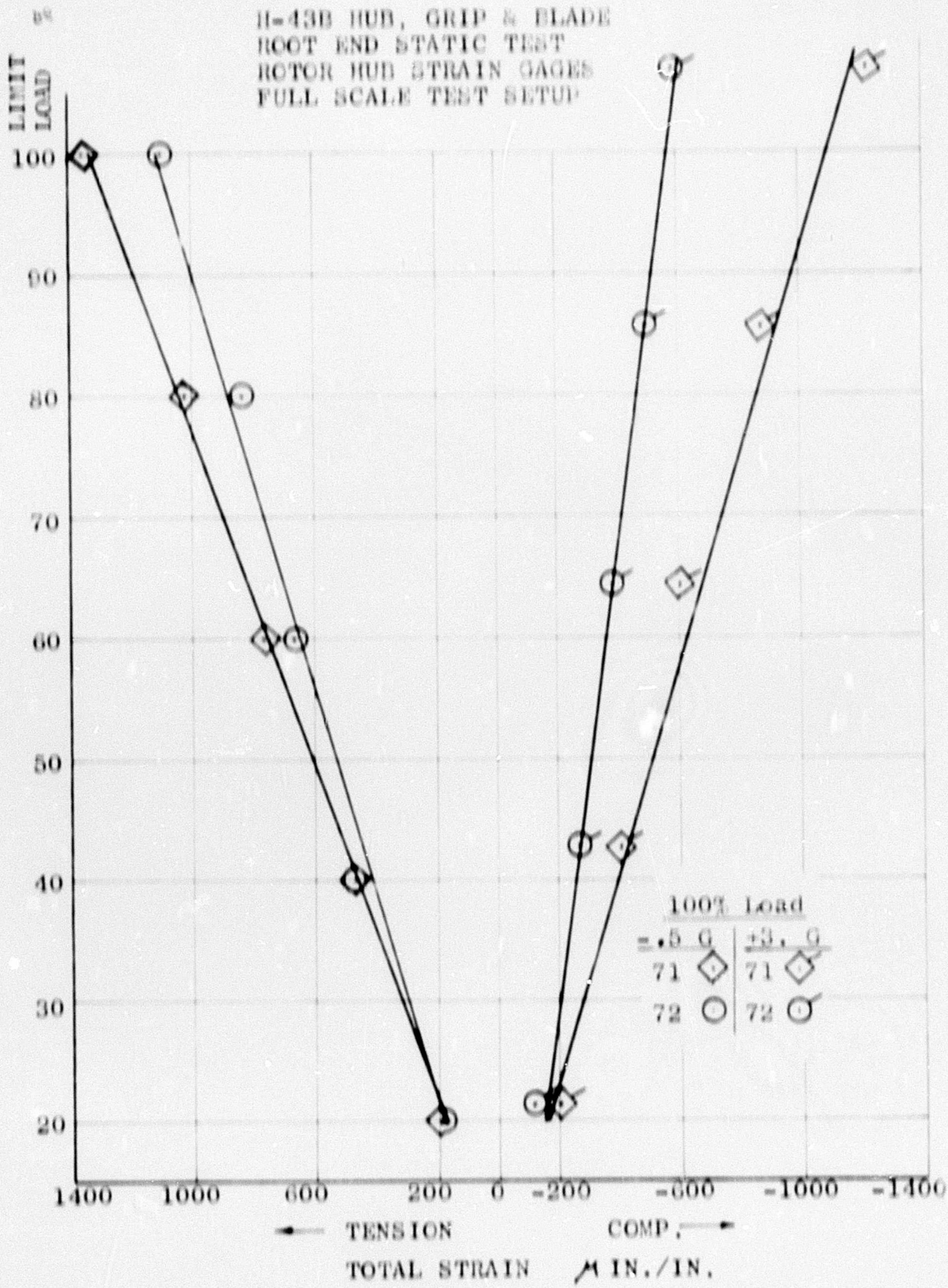

Figure II-23. Root-End Strain Distribution

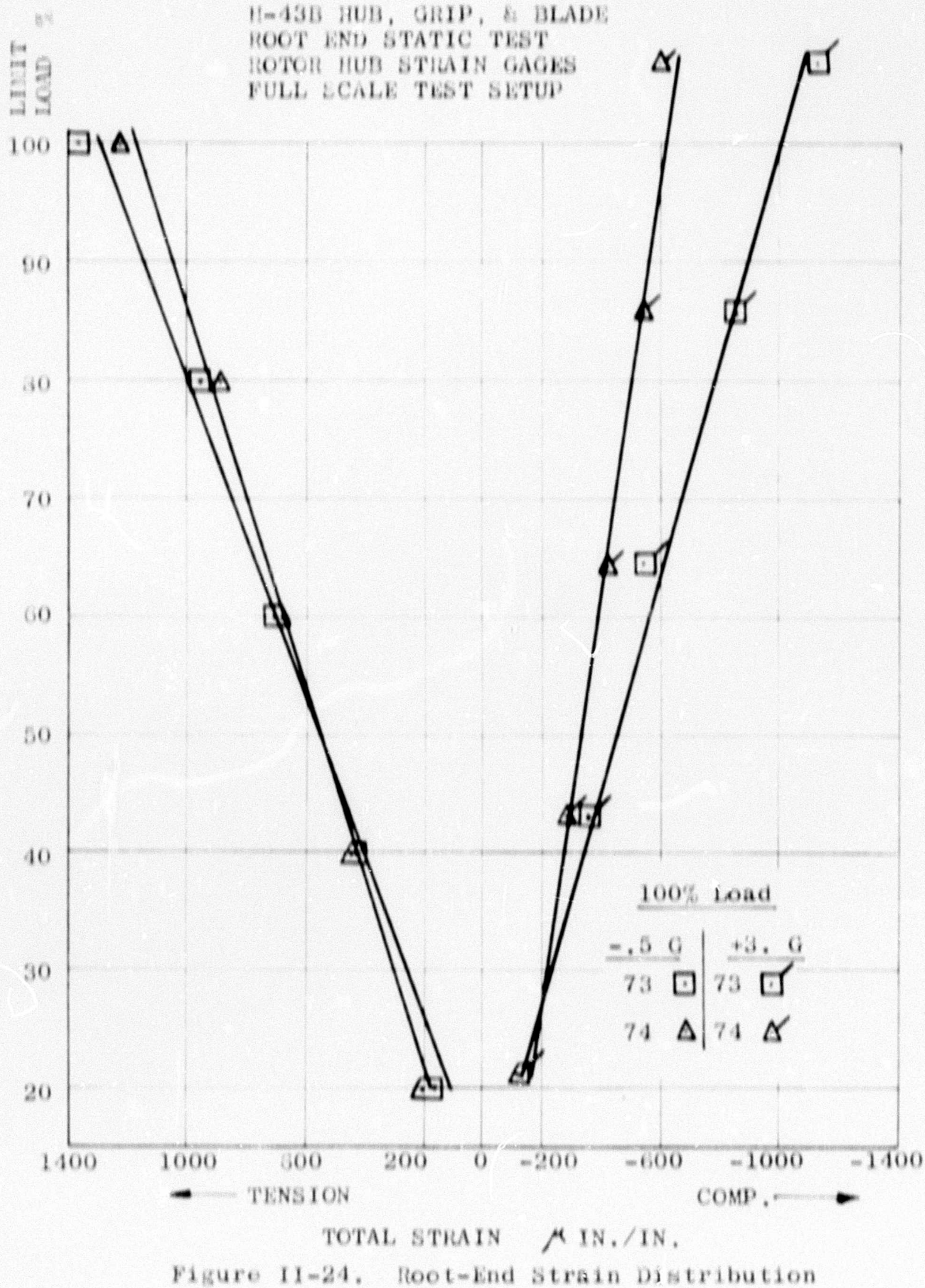

Figure II-24. Root-End Strain Distribution

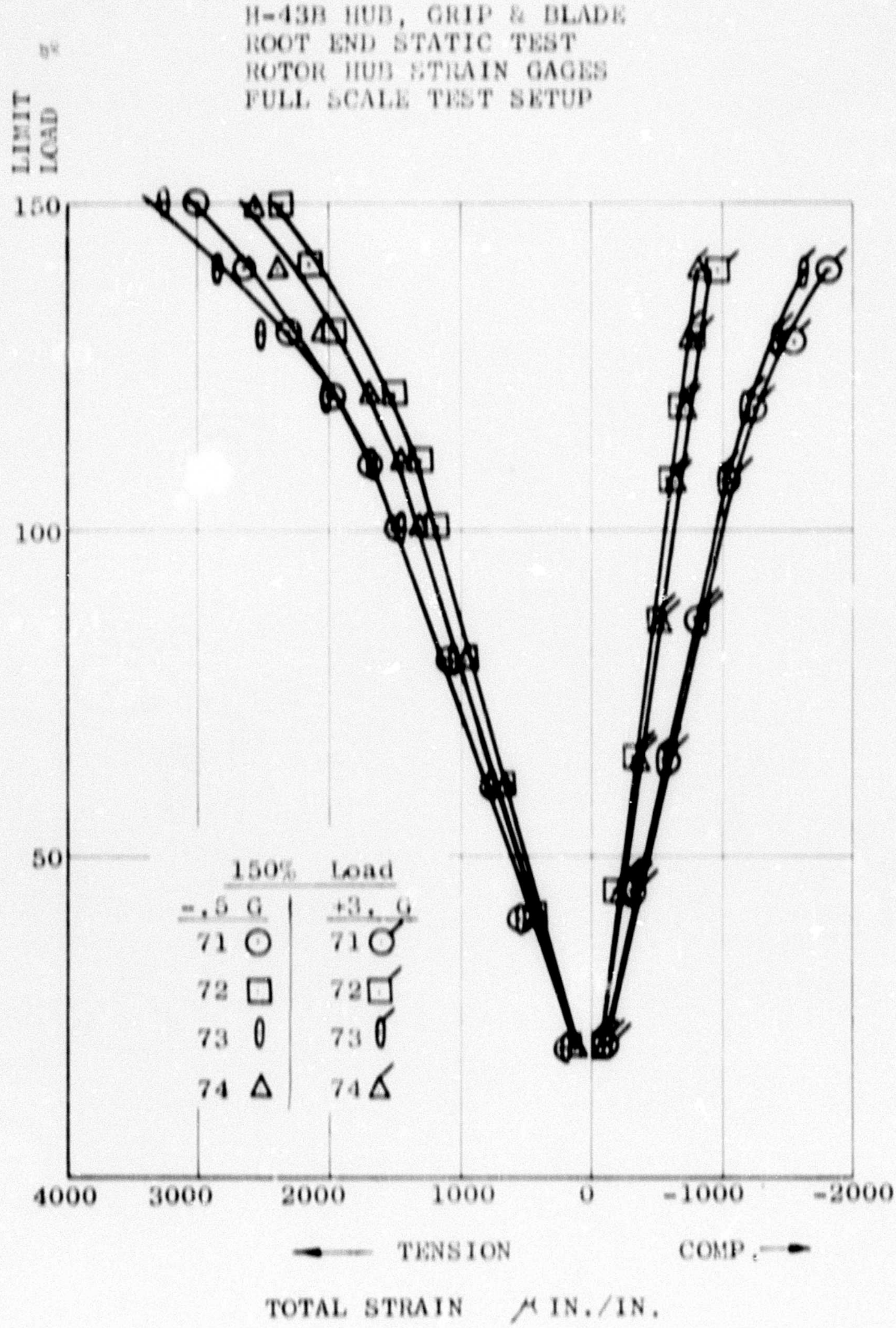

Figure II-25. Root-End Strain Distribution

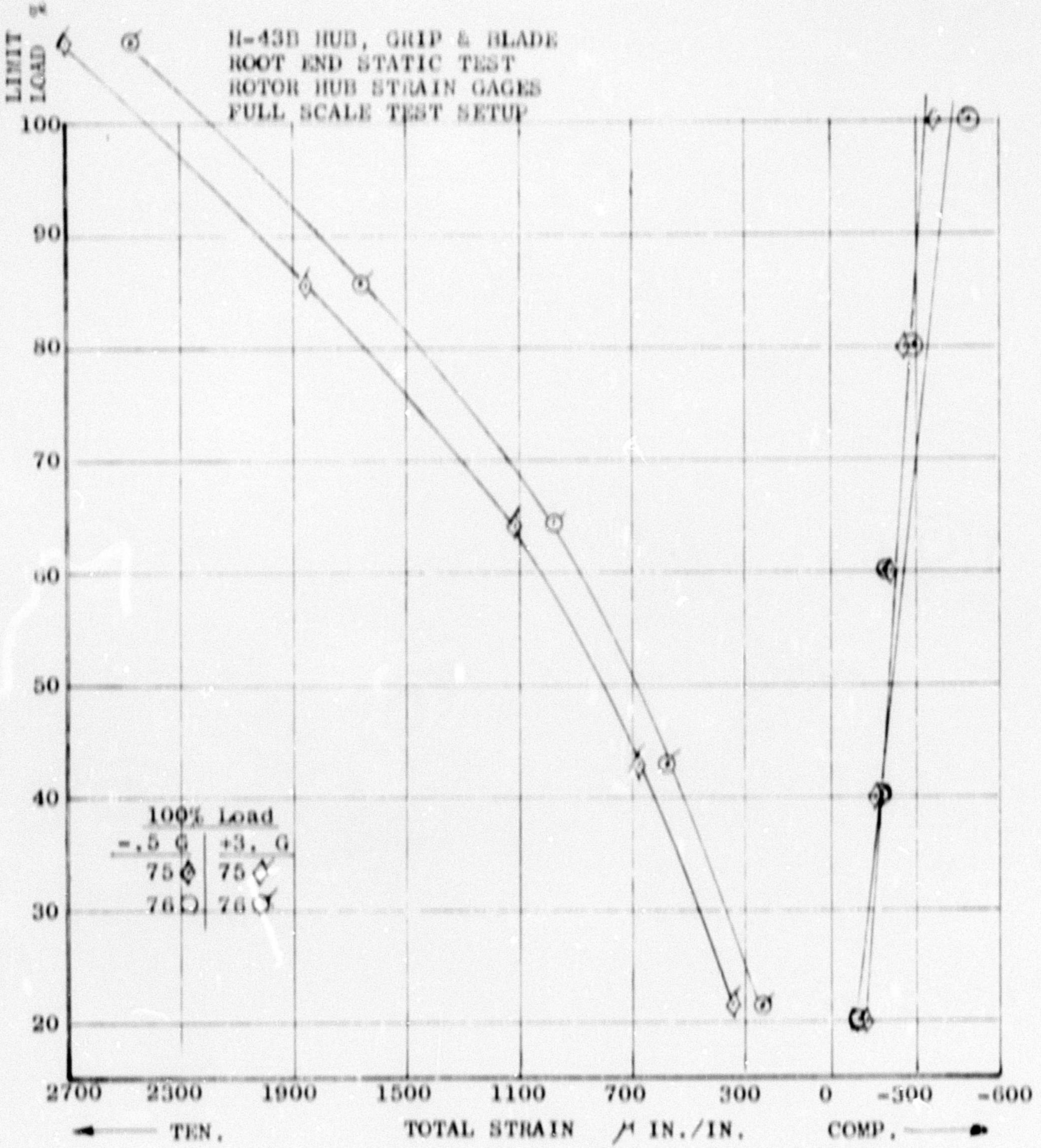

Figure II-26. Root-End Strain Distribution

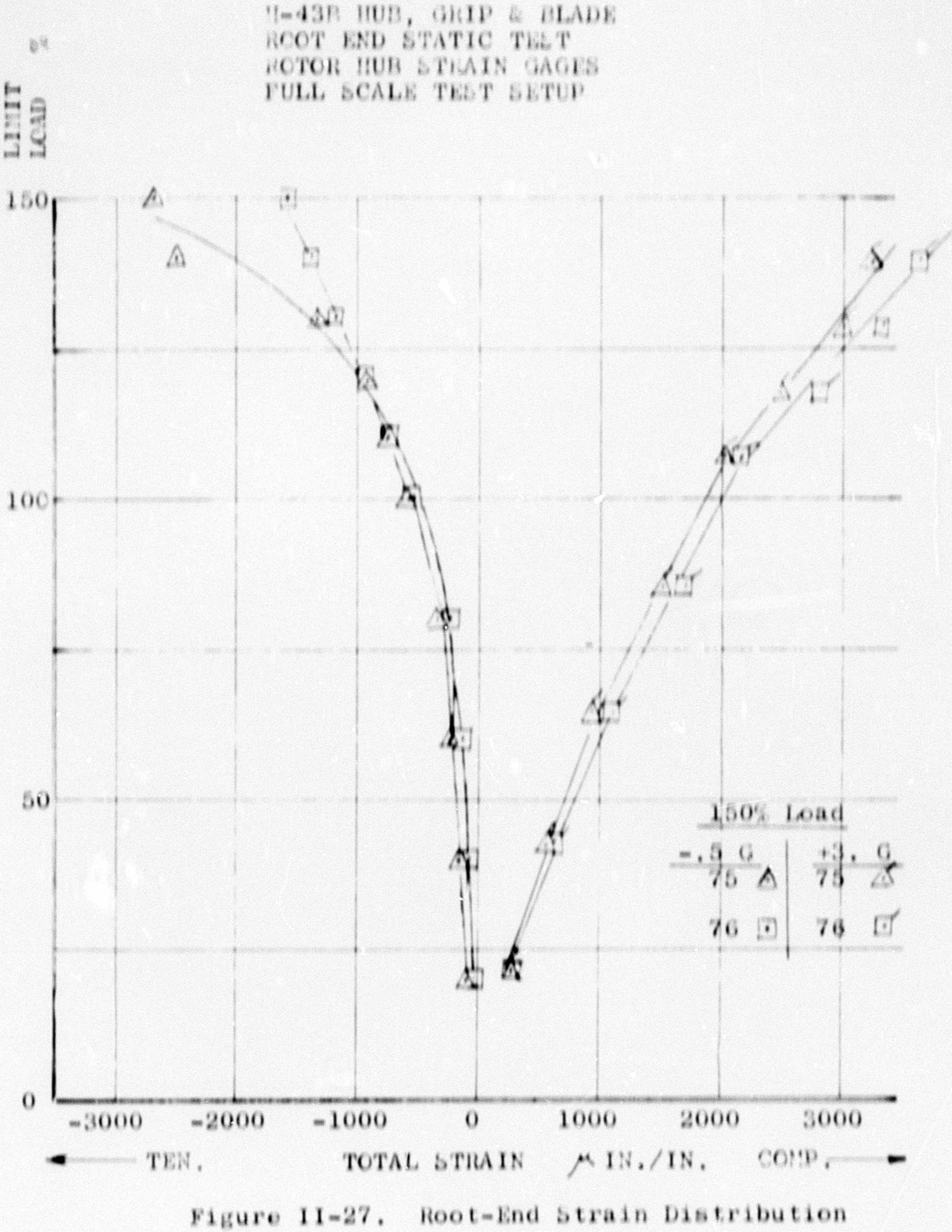

Figure II-27. Root-End Strain Distribution

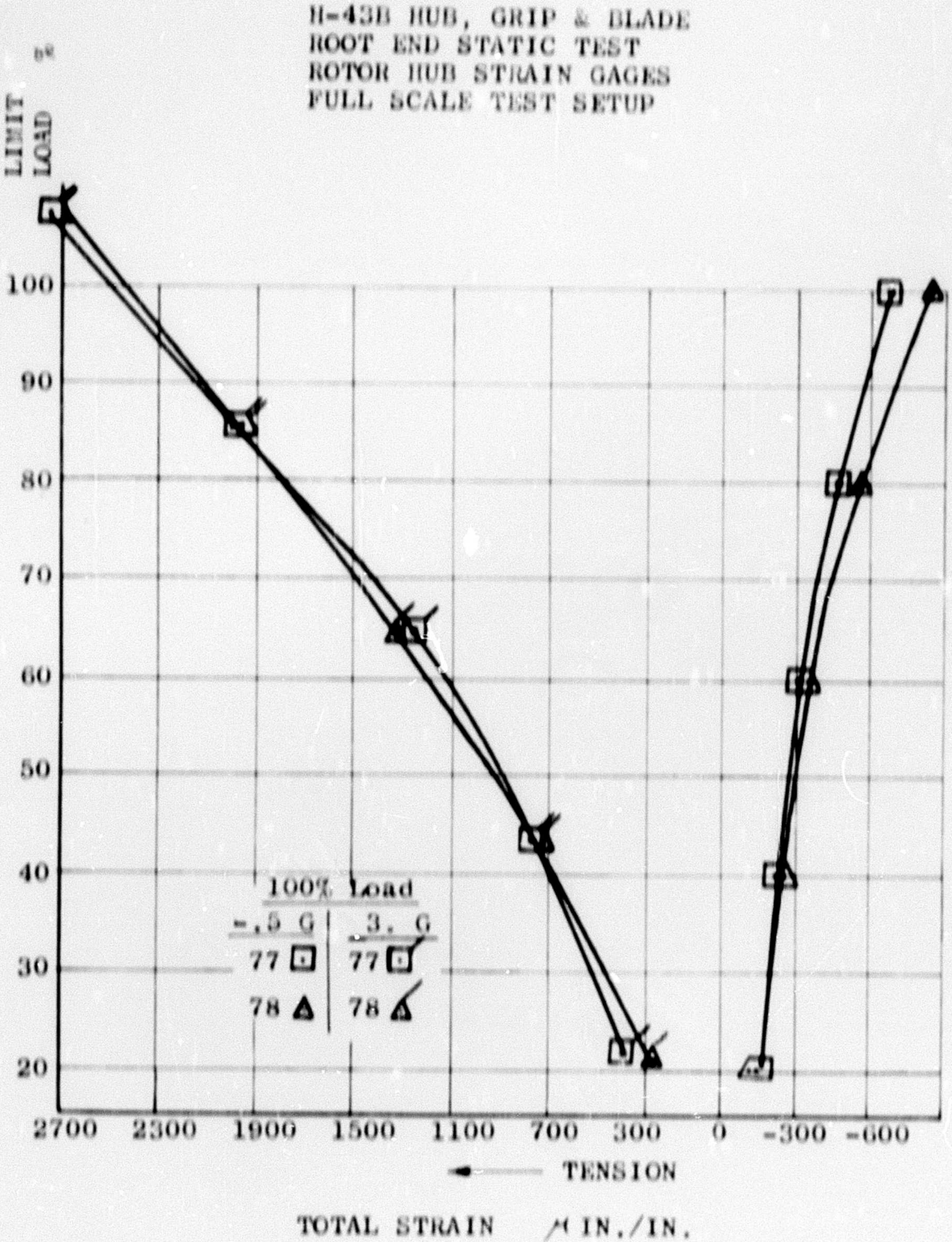

Figure II-28. Root-End Strain Distribution

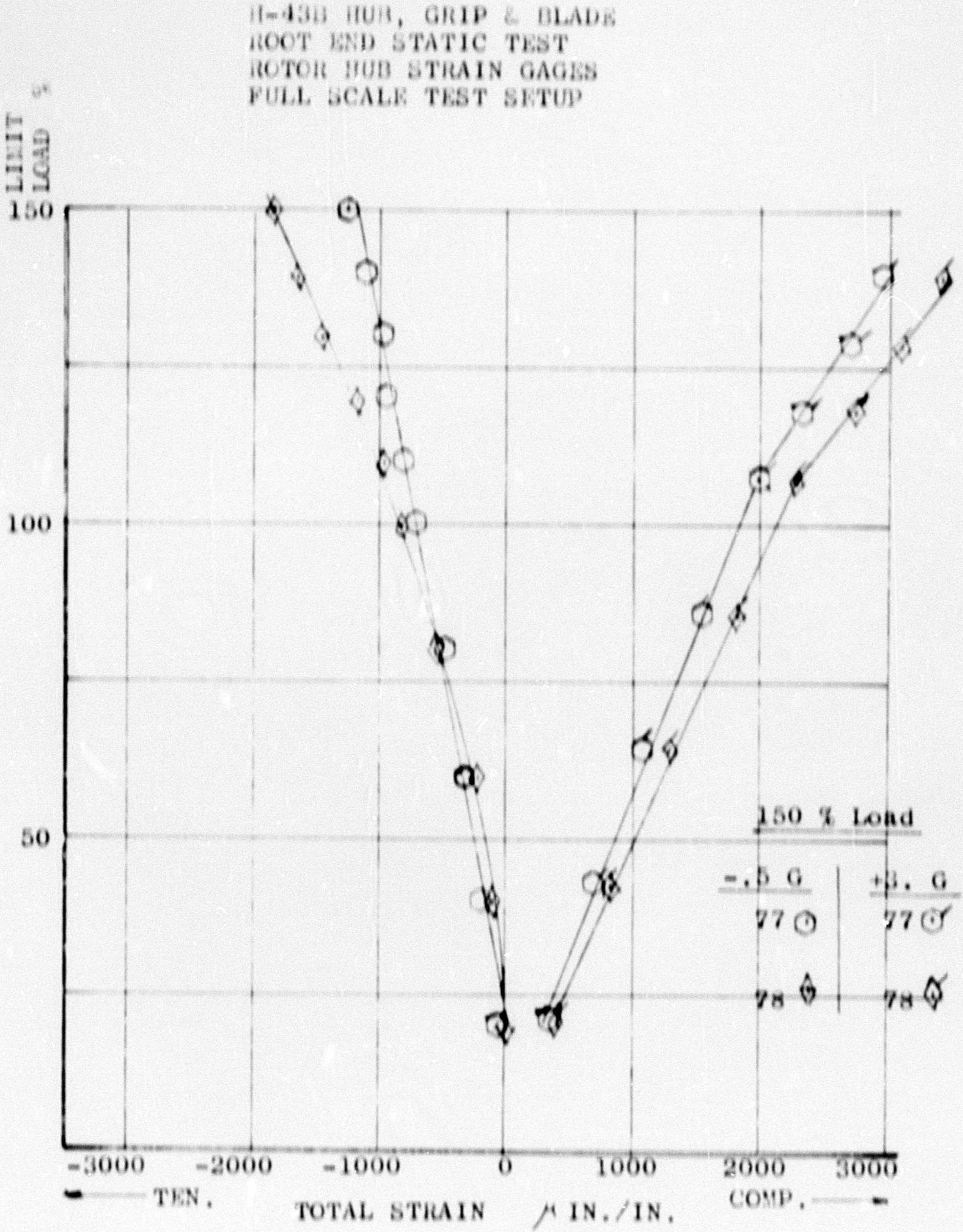

Figure II-29. Root-End Strain Distribution

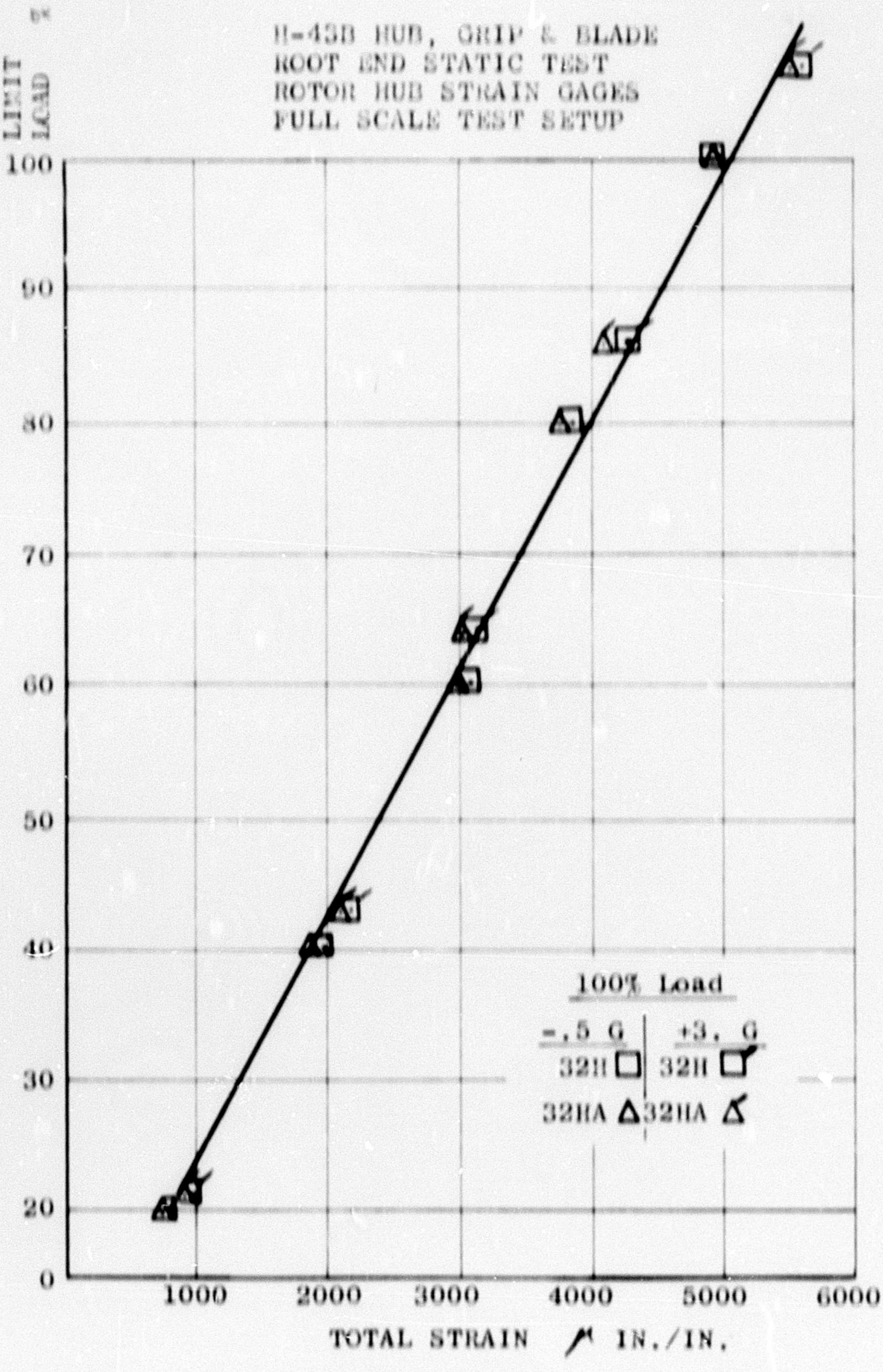

Figure II-30. Root-End Strain Distribution

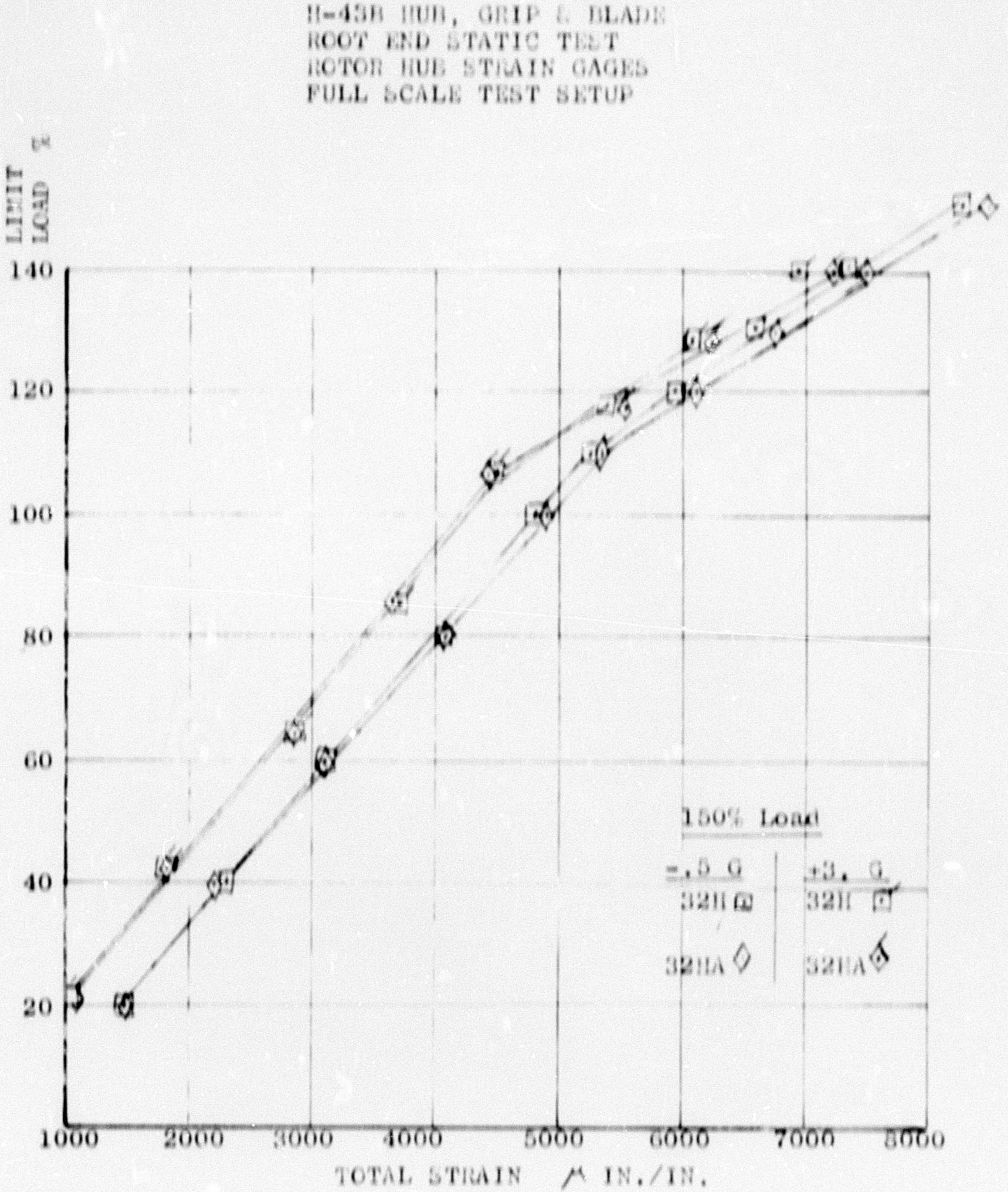

Figure II-31. Root-End Strain Distribution

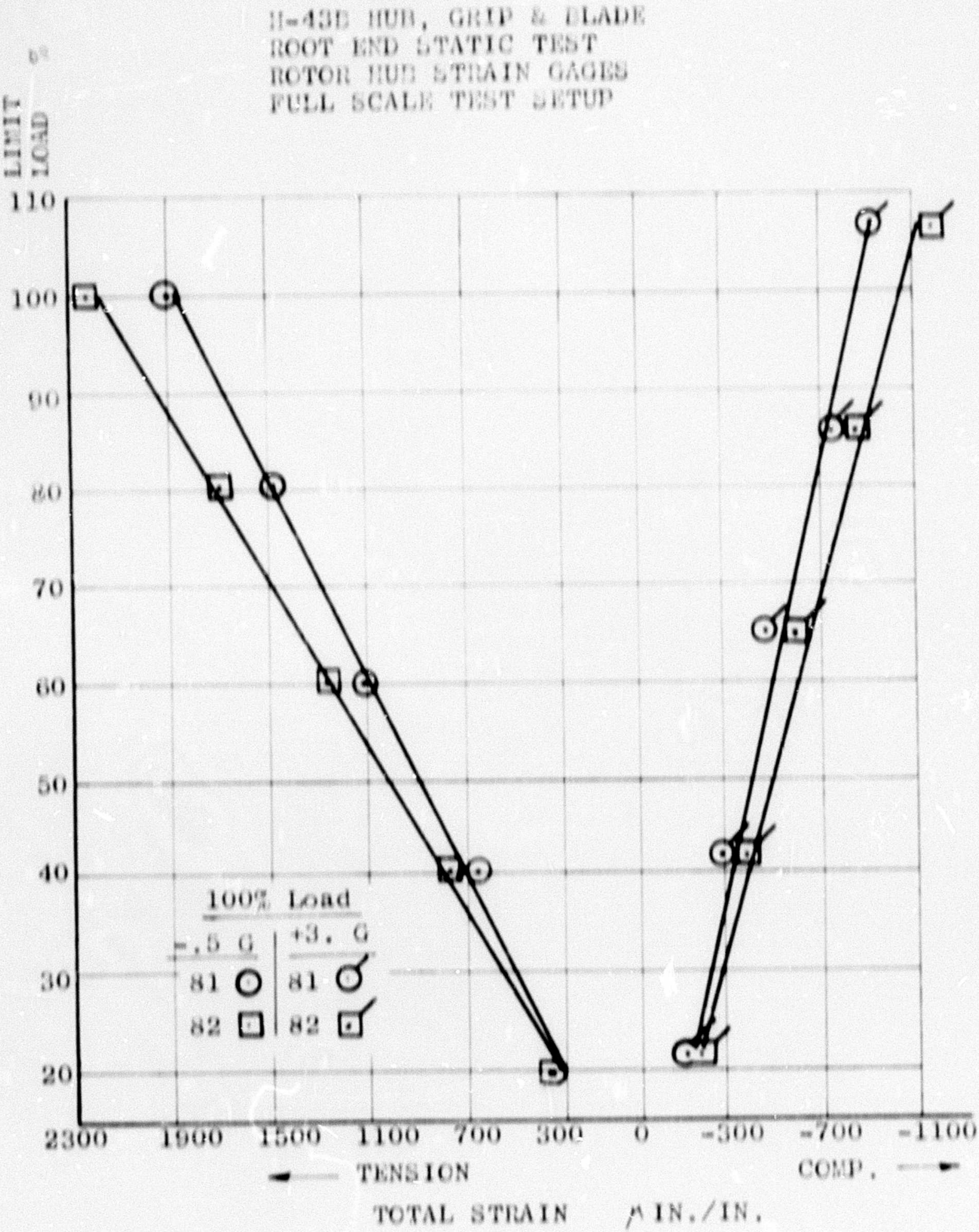

Figure II-32. Root-End Strain Distribution

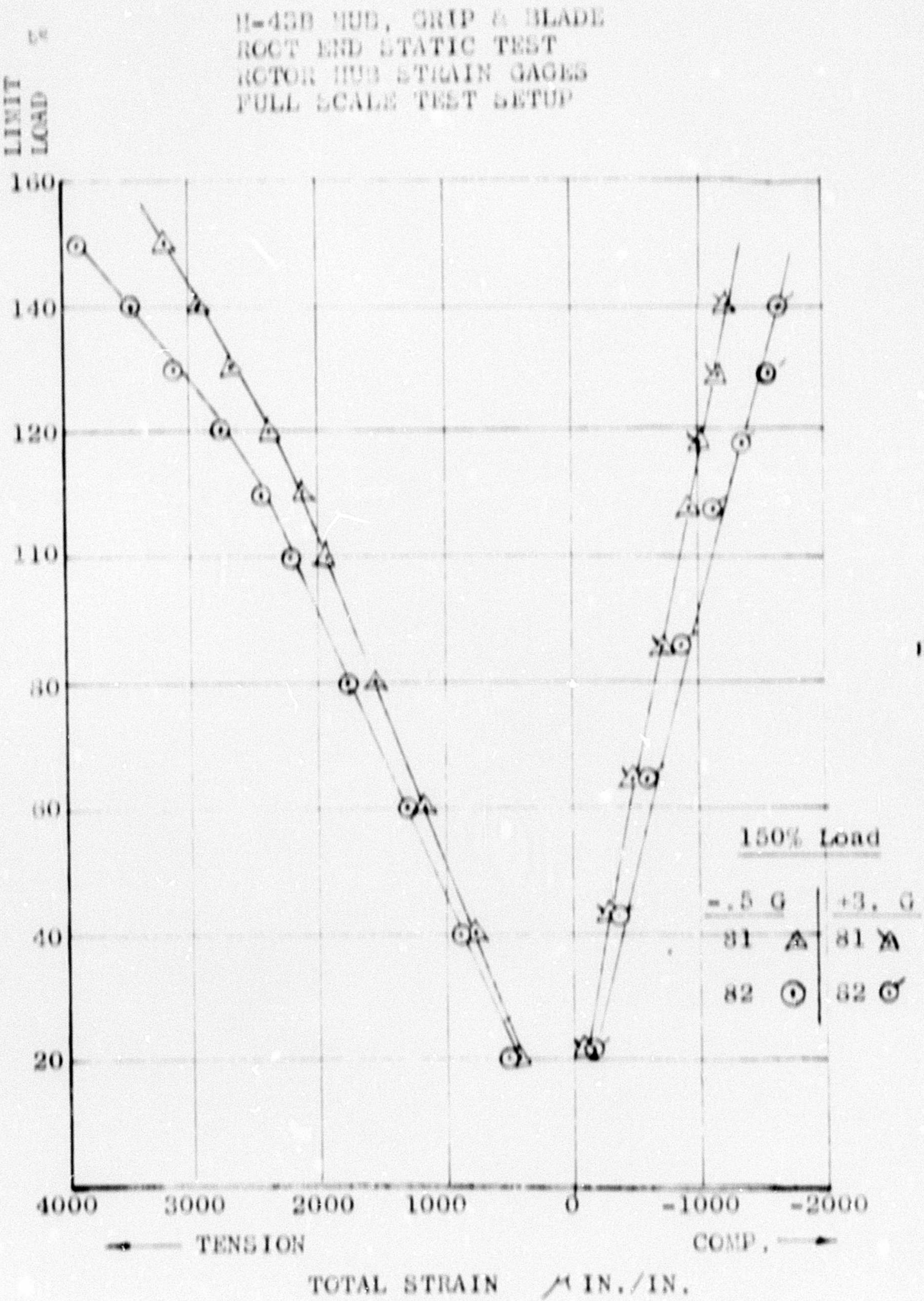

Figure II-33. Root-End Strain Distribution

Blade Retention Area: The most critical and most highly stressed region of the blade exists at the root end bolt holes where the blade is attached to the grip. The predominant load is flatwise vibratory bending in this area, and the blade section must be capable of withstanding the highest measured vibratory flatwise bending moments encountered in high-speed flight.

A. In 1953, a 3/8-inch thick fiberglass "cheek plate" was incorporated in this area of the blade to reinforce the outermost fibers of the bending section against the vibratory bending moments existing at that time in the HOK application. Fatigue tests indicated that this structure had an endurance level of ± 13,000 inch-pounds (Figure II-34).

B. As time progressed, and the flight envelope for the aircraft was expanded, the need for higher flatwise bending endurance limit in this region became apparent and we endeavored to try additional reinforcements by means of a 1/8-inch thick steel plate. Although this resulted in an increased bending moment endurance limit (± 19,000 inch-pounds), it was not deemed sufficient and development effort continued.

C. The next development step was the substitution of a 1/8-inch thick Scotchply plate in lieu of the steel plate previously mentioned. This construction of Scotchply, with its fibers predominantly spanwise oriented and the previously incorporated glass cloth "cheek plate" immediately beneath it, resulted in an endurance limit of ± 26,000 inch-pounds and was incorporated in blades early in 1957. It is interesting to note that the Scotchply, with an "E" of approximately five million, proved to be much more suitable in this particular application than a steel plate of similar thickness because of the much larger difference between the "E" of the composite structure as compared with the "E" of the steel cap. The steel plate picked up much more load than was intended because of its much higher modulus and hence was incapable of substantial increases in endurance limit; whereas the Scotchply, with a more compatible "E" and with relatively high strength characteristics (110,000 psi UTS), proved equal to the task. This structure corresponds to the "original configuration" of Figure II-6.

D. With the advent of the H-43B with its accompanying higher powers and wider performance envelope, the retention area of the blade proved to be critical in shear due to vibratory flatwise bending. Apparently

BLANK PAGE

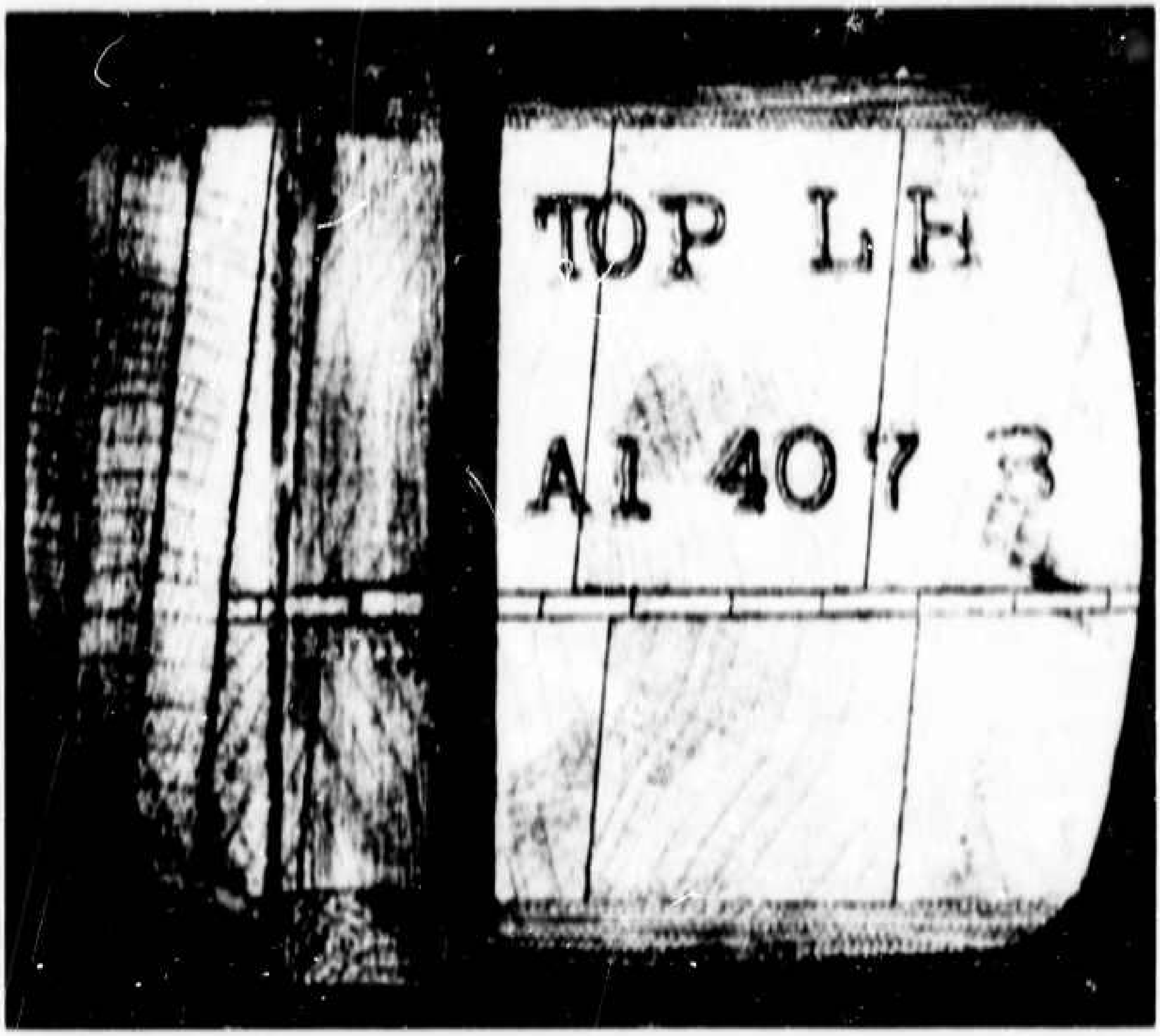

Figure II-34. Section View of Original Fiberglass Cheek Plate the tension and compression capacities of the outermost fibers by that time exceeded the shear capacities of the interposing spruce and maple. Additional shear capacity was provided by the incorporation of fiberglass cloth (wet lay-up) channels on the leading and trailing edge sides of the retention area, bonded to the previously developed cap plates of fiberglass cloth and Scotchply. This change resulted in an endurance limit of ± 45,000 inch-pounds and corresponds to the "final configuration" of Figure II-6. It is interesting to note that the envelope dimensions of this section are identical to the envelope dimensions of the original section as of 1953, when the endurance limit had been ± 13,000 inch-pounds.

The general setup of the fatigue fixture and specimen installation is shown in Figures II-35 through II-41.

The centrifugal force was applied to the specimen by two parallel hydraulic cylinders pushing on a movable load beam. When the centrifugal force is applied, a steady bending moment is introduced in the blade due to the "built-in" coning angle of the blade grips. The load beam is free to move under the hydraulic load application, but the system is backed up by an accumulator which eliminates the vibratory centrifugal loads caused by the lengthening and foreshortening of the specimen during the bending vibratory loading.

The amount of bending moment introduced by the centrifugal load is controlled by a vertical shear load applied at the centerline of the rotor hub. The vertical loading system is isolated from the jig by a spring bank, which was designed on a lever arm principle to accommodate large hub motions with small spring deflections and still maintain the necessary vertical shear to ensure the steady bending moment condition.

The engine torque is applied to the specimen through a stub rotor shaft, which simulates an actual rotor shaft and hub installation. The torque system is a self-contained cable and hydraulic unit and is reacted by the centrifugal force loading which causes the specimen to assume a "lag" blade position.

The vibratory moment is applied as a vibratory vertical shear at the hub centerline and amplified by approaching the natural frequency of the specimen. The vibratory shear loading is accomplished by a mechanical shaker with a variable-speed drive unit. The shaker is a counterrotating weight system which assures a pure linear motion output of the shaker, the output force varying with rpm.

The specimen, with the proper centrifugal force, engine torque, and steady bending moment (monitored at blade Sta. 31.0) loads applied, is excited in flatwise bending by the mechanical shaker. As the specimen approaches its natural resonant frequency, the magnitude of flatwise bending is increased with small increments of exciter force. When the proper vibratory bending moment is acquired, the variable-drive system is locked in that position. A general schematic drawing showing loads as applied to the specimen is presented in Figure II-35. The root-end stub strain gage locations are the same as for the static test specimen as shown in Figure II-5.

Test Procedure: After the blade root ends are instrumented and statically calibrated against known flatwise bending moment, the specimen is installed in the fatigue test rig. A specimen consists of a rotor hub, two blade grips, two blade root ends, and the necessary lag pins, teeter pin and blade bolts to complete the setup. This setup duplicated one-half of the H-43B rotor system.

When the specimen setup is completed, all the SR-4 strain gages are "nulled" to an arbitrary strain indicated value. From this neutral position, the centrifugal loading is applied; but due to the $4\frac{1}{2}^{\circ}$ coning angle of the blade grips, an automatic negative bending moment is introduced. This moment can be controlled, as to its magnitude, by a vertical shear load applied at the centerline of the hub. The magnitude of the vertical shear load is dependent on the desired steady bending moment required at monitor blade Sta. 31.0.

The engine torque is then applied to the specimen through a stub rotor shaft and is reacted by the centrifugal force and the lead lag angle induced to the specimen.

A set of strain readings for all blade stations were recorded. These strain readings constituted the steady loads as applied to the specimen.

The vibratory condition was setup by a variable-drive system and electric motor, driving a mechanical shaker. The specimen is excited by the shaker to a greater magnitude of load as the shaker speed approaches natural frequency. As the resonant frequency of the specimen is being approached, oscillographic records are taken to determine the vibratory bending moment levels and shaker R.P.M. When the desired bending moment level is achieved, all strain gage stations were recorded on oscillographic paper and logged.

Monitoring of the load levels during the test was accomplished at periodic intervals utilizing an oscillographic recorder.

CENTRIFUGAL	= C.F.	= As required by test conditions.
BENDING MOMENT	= M_{fb}	= As required, approximately = 48,000 inch-pounds at blade Sta. 31.0 with no F_V (Vertical) added.
ENGINE TORQUE	= M_{ETQ}	= 100,000 inch-pounds (steady).
VERTICAL	= F_V	= As required by test conditions. To reduce negative B.M. dueto C.F.
SHAKER FORCE	= $\pm F_{VS}$	= As required by test conditions to produce necessary $\pm$ bending moments at blade Sta. 31.0 (monitor).

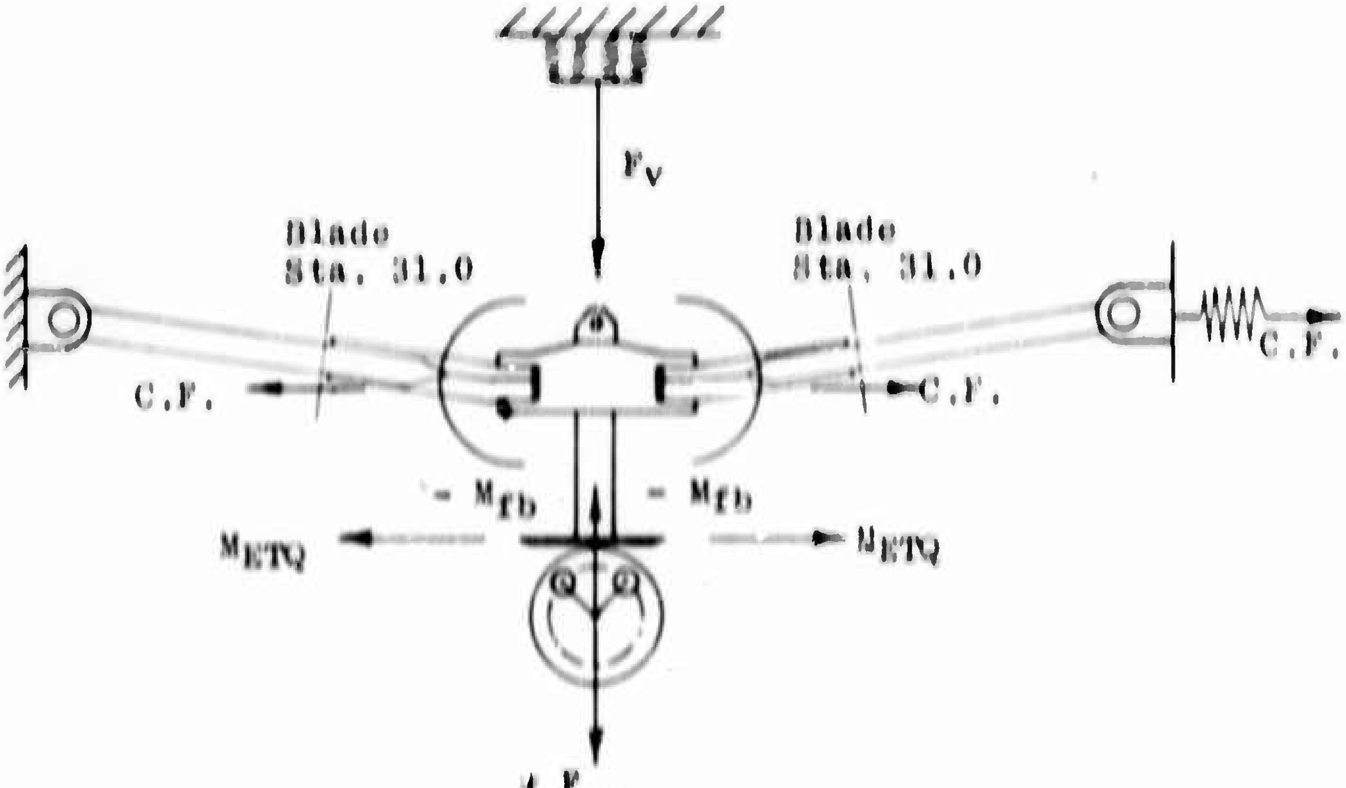

Figure 11-35. Fatigue Specimen Load Setup

Figure II-36. General Arrangement of Hub and Grip Fatigue Jig Viewed from Movable Retention End

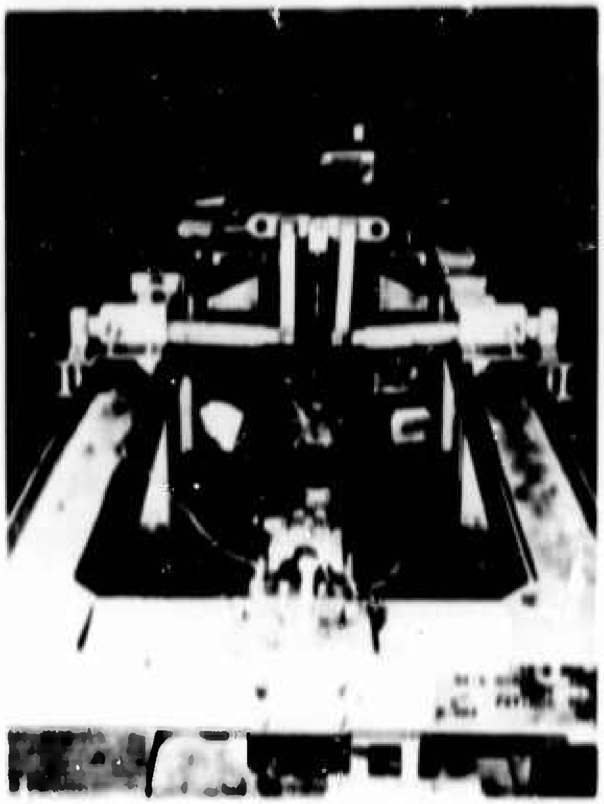

Figure II-37. General Arrangement of Hub and Grip Fatigue Jig Viewed from Fixed Retention End

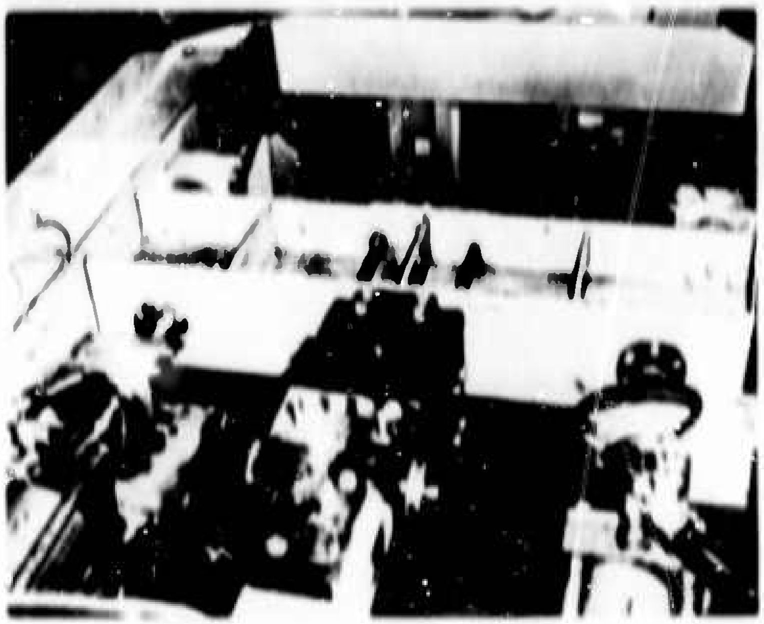

Figure II-38. General View Showing Centrifugal Force Application Load Beam

Figure II-39. Close-up of Typical Blade Root-End and Blade Grip Installed into Rotor Hub

Figure 11-40. General View Showing Mechanical Shaker and Torque Application System

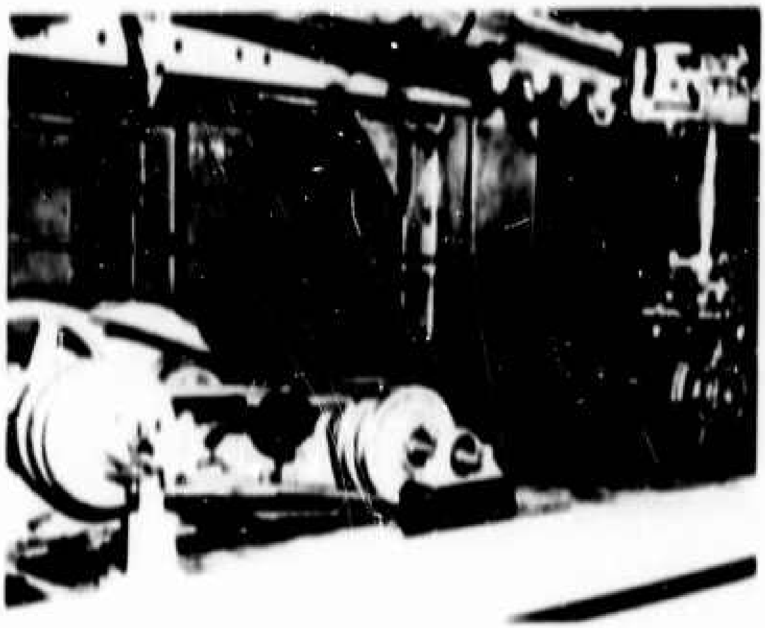

Figure 11-41. View Showing Vari-Drive System and its Attachment to Mechanical Shaker

Any load variation in the specimen was trimmed by adjusting the variable-drive mechanical shaker system to the desired level.

During the period in which the following information was obtained, 32 blade root-end specimens were fatigue tested. Six failures occurred which were classified as invalid due to propagation from the outboard centrifugal load appication pad area. Five valid failures occurred in the blade grip area; four were sustained at high level testing and one at a lower level, which was classified as a failure because of internal damage but was still capable of further fatigue testing. All other specimens either "ran out" at the desired load level or "outlived" retention metal components.

The prime fatigue location in the rotor blade retention area is the blade grip attachment bolt holes, the most critical being the outboard holes Nos. 6 and 7. Slight spanwise cracks manifest themselves in the Scotchply cheek facings. The unidirectional Scotchply has exceptional spanwise strength properties and fair chordwise strength properties. Previous experience has shown that without the Scotchply cheek plates, chordwise cracks would result with ultimate failures occurring across the net blade section. The spanwise cracks in the Scotchply have an extremely slow rate of propagation and are not considered critical.

Figure II-42 is the developed S-N curve resulting from approximately 31 separate tests of the root-end specimen. The vibratory stress level is in terms of bending moment and is a more readily usable parameter in blade analysis, rather than in actual stress values. The arrow attachments to the symbols, representing various specimens, merely indicate that the blade specimen "ran out" at the given level and/or some other retention component test run with the lower level moment being charged with the accumulated endurance time; thus, the developed curve is seen to be, in actuality, quite conservative.

Figures II-43 through II-50 give representative types of failures encountered during the fatigue test program.

Figures II-43 and II-44 show typical spanwise cracks in the Scotchply facing on upper and lower surfaces. Although this specimen did not yield and was capable of sustaining further fatigue testing, it was cut into segments to investigate internal crack propagation within the laminated wood core.

Figure II-45 shows a damaged specimen which had completed 24 x 10^6 cycles of fatigue testing, which included .624 x 10^6 cycles at the $\pm$ 60,000 inch-pounds bending moment level followed by 18.115 x 10^6 cycles at the $\pm$ 40,000 inch-pounds level. It was noted that there was extensive spanwise cracking at the chordwise edges of the bolt holes, spanwise elongation of all holes on the bottom cheek plate, considerable fretting on the top cheek plate directly under the outboard edge of the steel blade grip, chordwise cracks propagating from the bottom two outboard holes, and delamination of the fiberglass channel. The remarkable accomplishment achieved here is the fact that despite the severity of damage, this specimen still maintained the capacity for holding reduced loads. This statement, in fact, holds for all the specimens which were classified as valid failures - in no instance did a specimen succumb to complete failure.

Figures II-46 and II-47 show slight spanwise cracks on the upper Scotchply cheek plate and chordwise compression cracks at the outboard two holes on the lower Scotchply plate. This damage was sustained after 146,000 cycles at:

Blade centrifugal force	=	38,000 lbs.
Engine torque	=	100,000 inch-pounds
Blade Sta. 31.0 bending moment	=	58,000 ± 60,000 inch-pounds

Figures II-48, II-49, and II-50 are photographs of specimens which have "run out" at load levels greater than high-speed flight conditions.

Figure II-48, Photo No. 1, shows minute spanwise cracks on specimen No. 31 which accumulated 41.409 x 10^6 cycles. Photo No. 2 shows similar indications on specimen No. 37 after 30.638 x 10^6 cycles.

Figure II-49, photo No. 1, is specimen No. 38 after 30.638 x 10^6 cycles, again revealing negligible damage. Figure II-49, photo No. 2, and Figure II-50, photos Nos. 1 and 2, are respective sections of specimens Nos. 31, 37 and 38 showing internal spanwise cracks in the laminated wood core. It is interesting to note that these internal cracks were found during inspection of the bolt holes after 13 to 15 million cycles of fatigue testing. At this time, epoxy resin was forced under pressure through the bolt holes and into the cracks. After curing, the specimens were returned to the fatigue fixture and the test resumed.

Upon completion of the test, the specimens were inspected and photographed as seen in Figures II-49 and II-50 and then dissected to investigate the internal crack propagation. It was found that no further propagation occurred beyond the resin filled cracks.

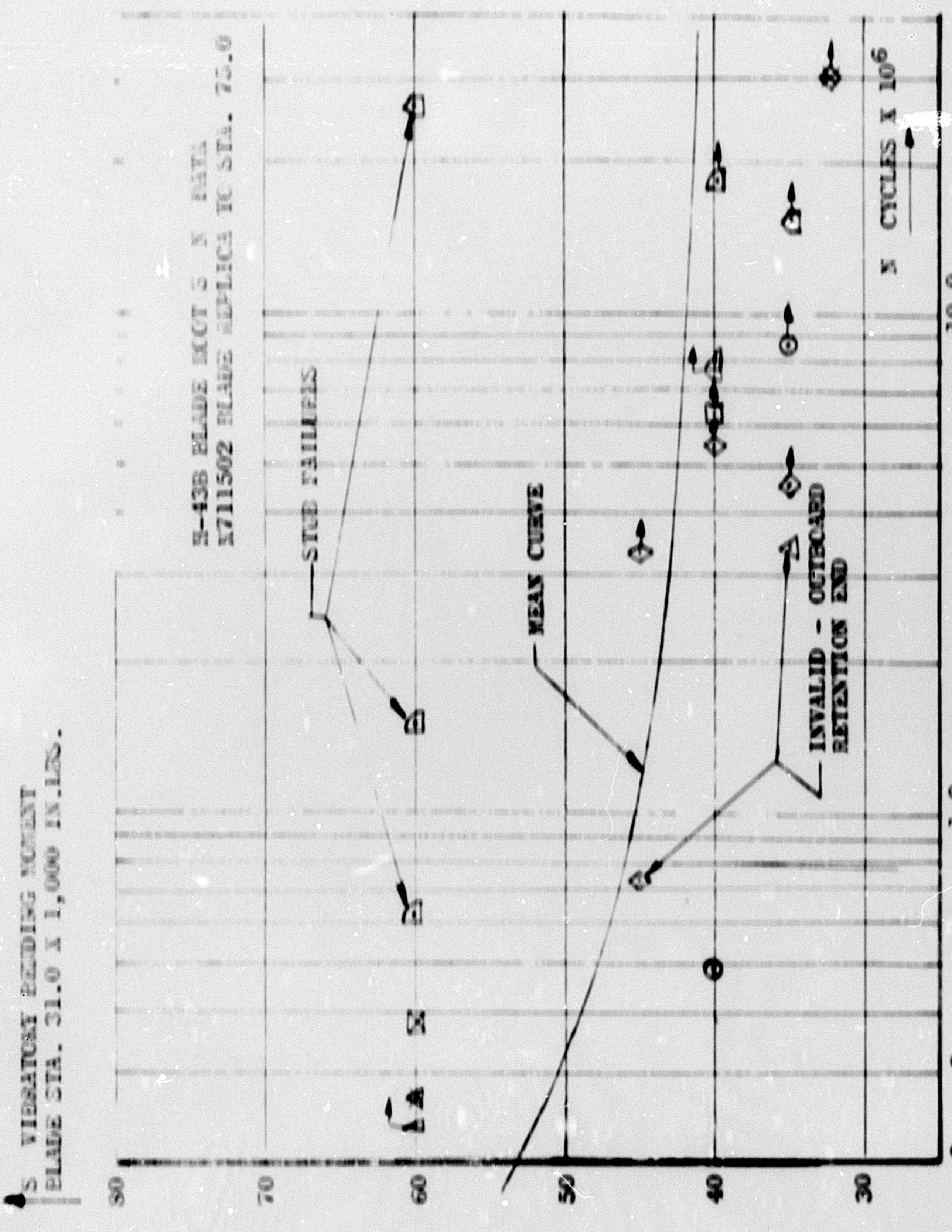

Figure II-42. Blade Root-End S-N Curve

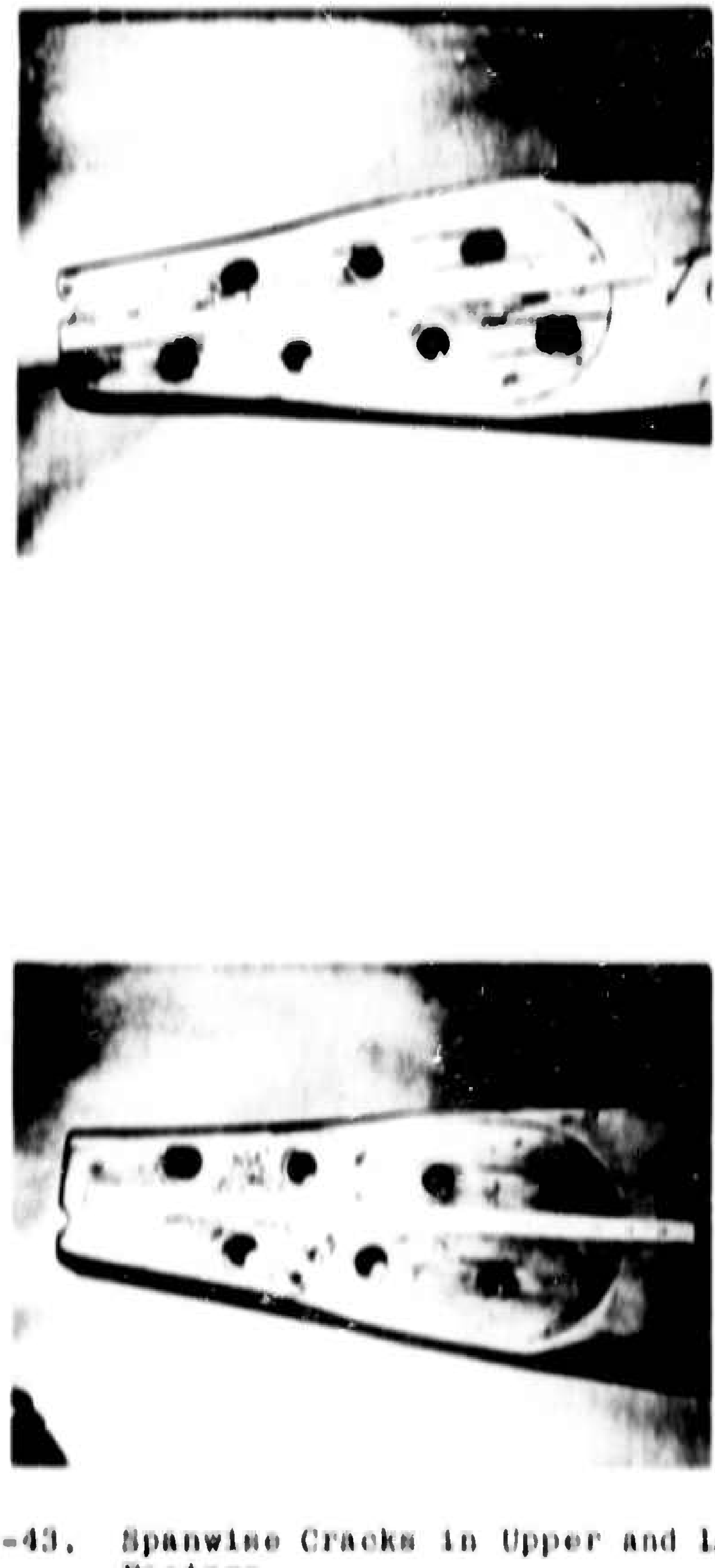

Figure 11-43. Spanwise Cracks in Upper and Lower Grip Facings

Figure II-44. Blade Root-End Crack Propagation

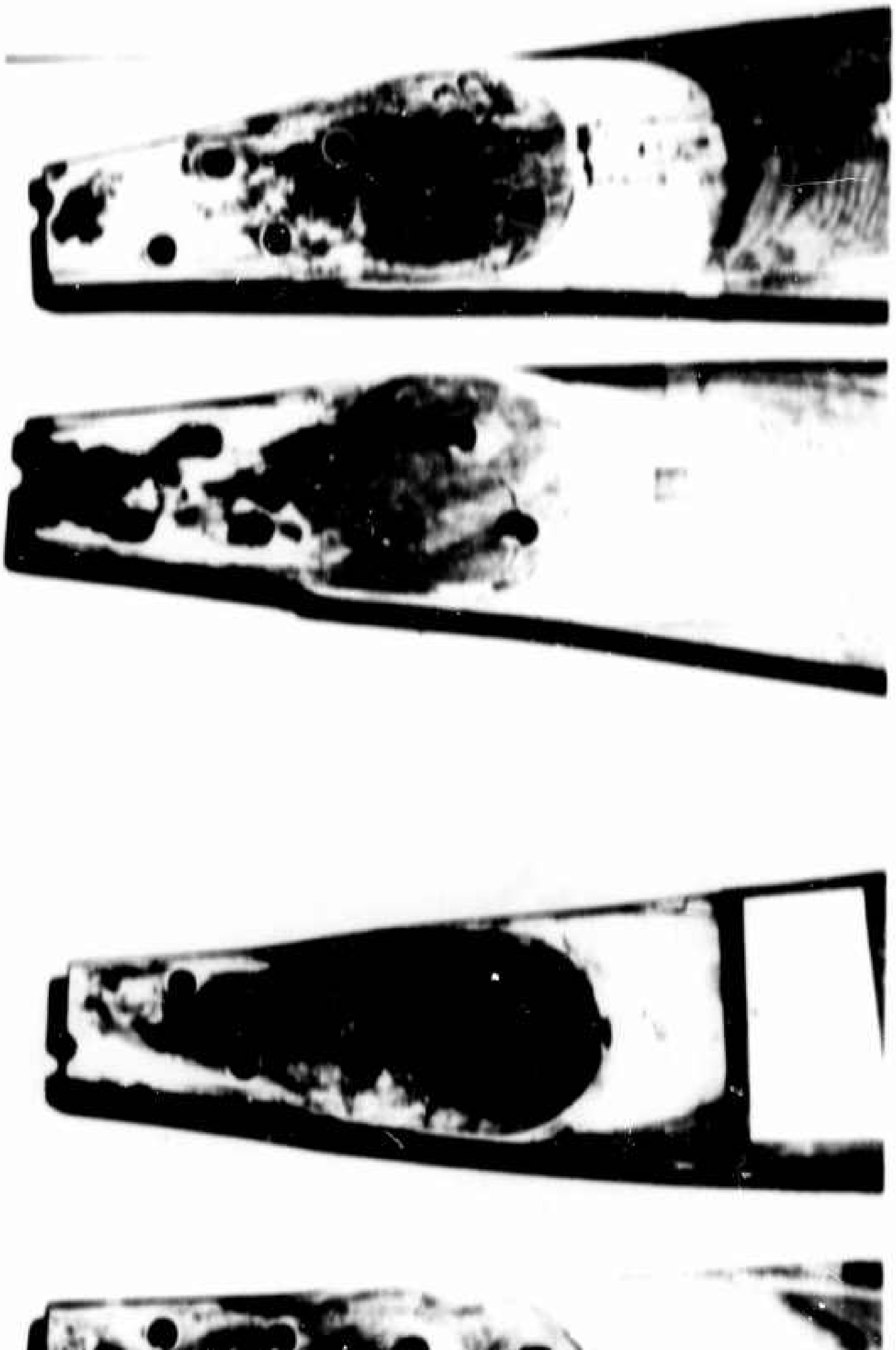

Figure 11-45. Blade Root-End Specimen Damage

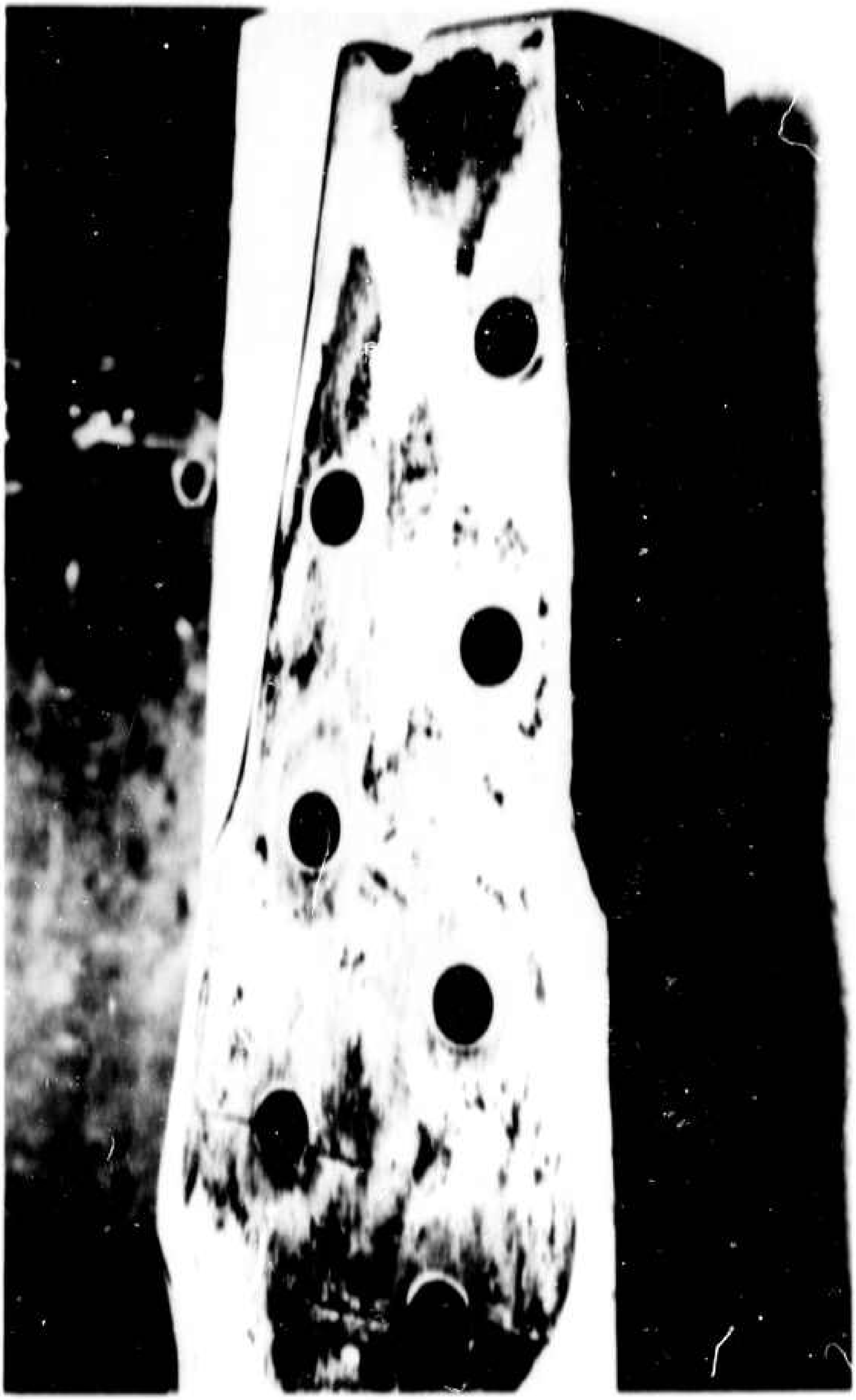

Figure 11-46. Blade Root-End Lower Surface

Figure 11-47. Blade Root-End Upper Surface

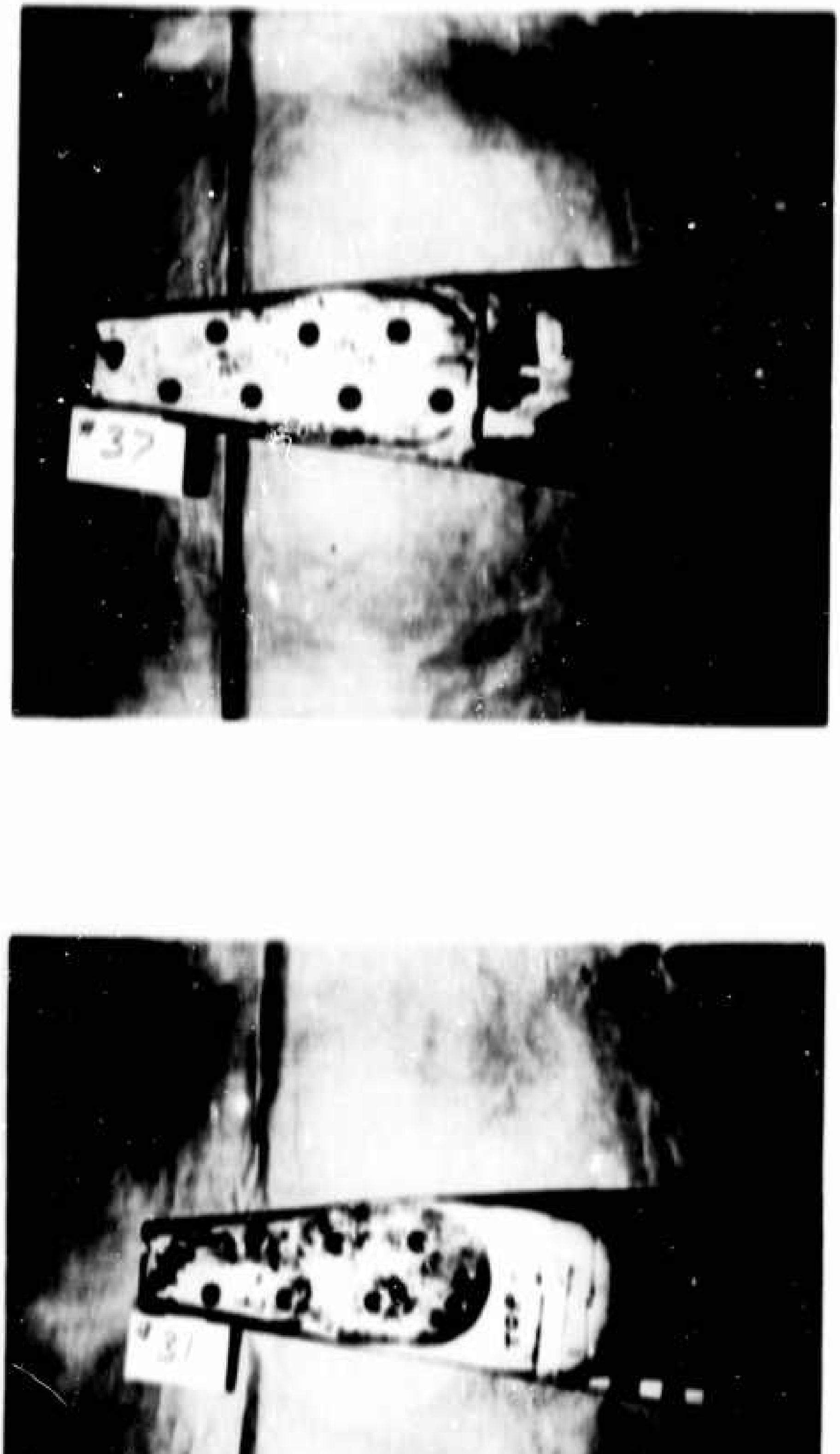

Figure II-48. Blade Root-End Spanwise Cracks

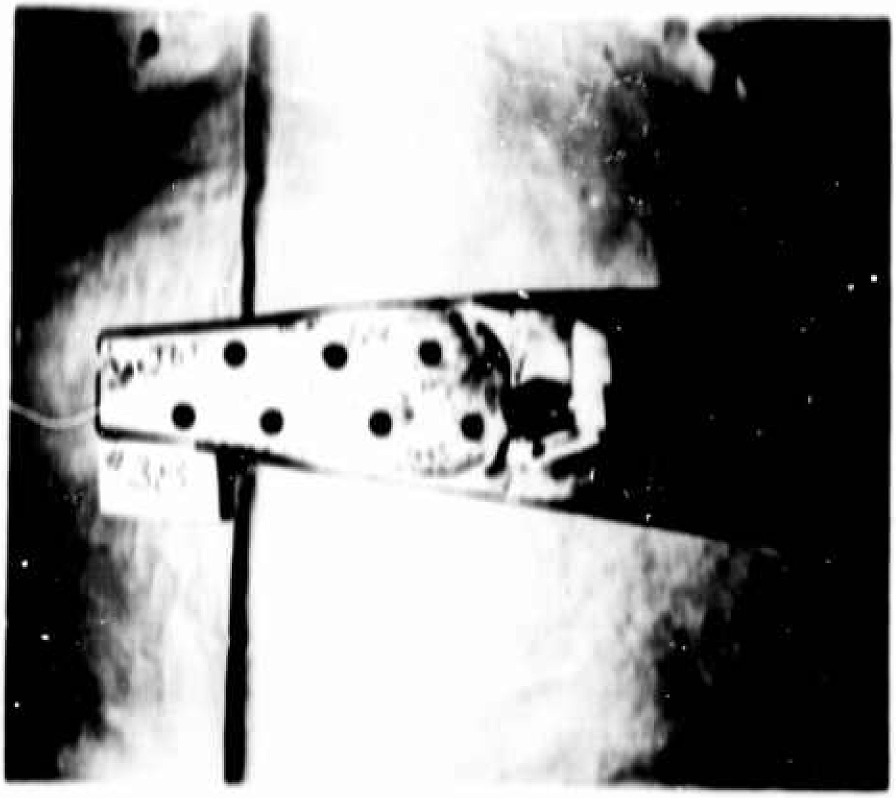

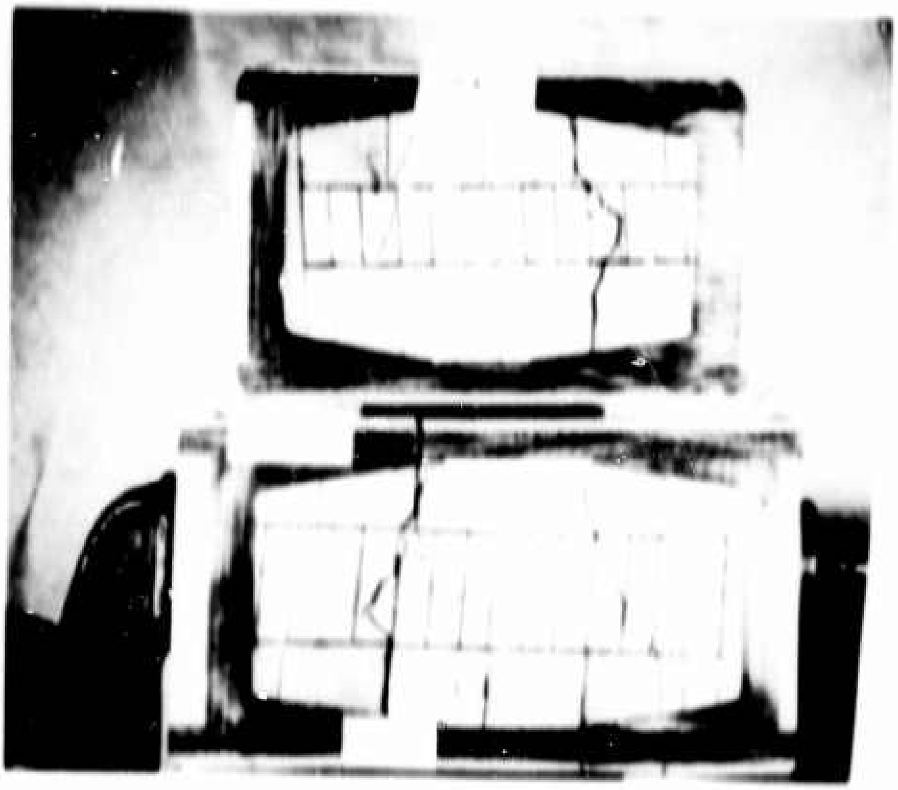

Figure II-49. Blade Root-End Spanwise Cr

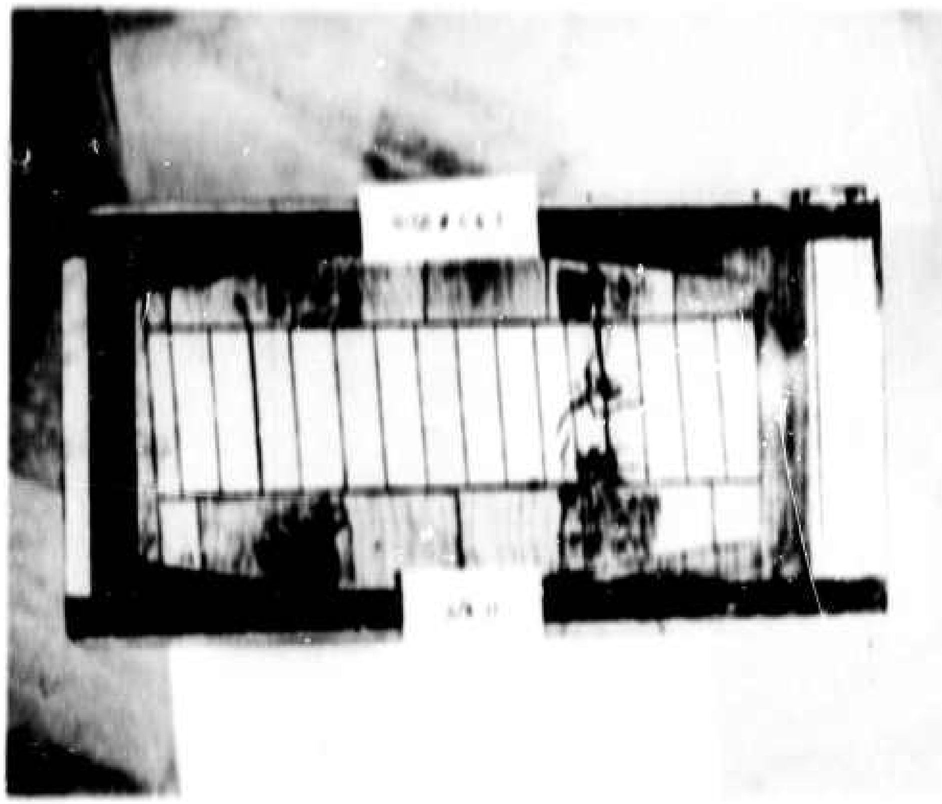

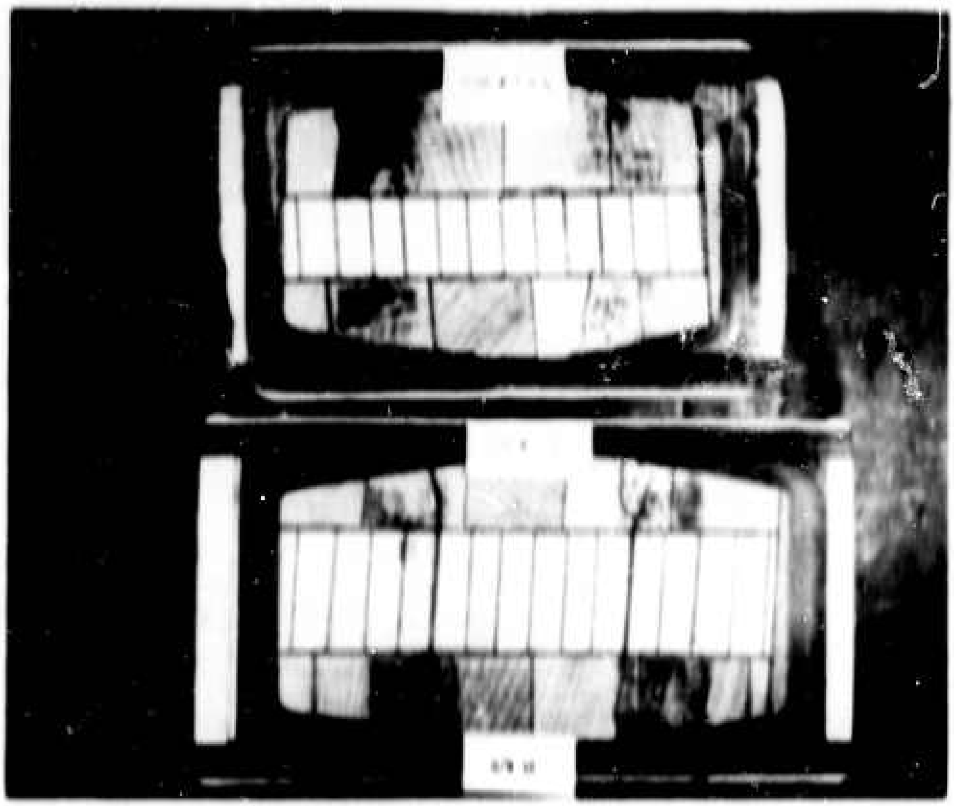

Figure II-50. Epoxy Filled Spanwise Cracks

ROTOR BLADE TORSION AREA

The torsion area of the rotor blade is a unique problem deserving of special evaluation. Due to cyclic blade pitch change, vibratory shear stresses are set up within the spar. The orientation of these stresses is both parallel and perpendicular to the blade spanwise axis, and they therefore have the same orientation with respect to spar grain direction. Under this loading, the natural failure plane is parallel to the spar axis. This is due to the orthotropic properties of wood, shear strength being a minimum parallel to the grain. Such cracks generally involve only one or two spar lamina for a portion of the thickness and are therefore readily repairable by standard methods. The propagation of such cracks tends to be limited because of the stress gradients throughout the blade. As a crack grows in depth, it enters the center of the spar where the strain level is lower; the propagation rate, therefore, decreases. As the length of a crack extends, it is limited outboard by the reduction in torsional moment occurring at the flap and inboard by the reduction in torsional strain level due to the heavier blade sections. Torsional cracks are therefore limited in length and tend to progress slowly in depth. This has been demonstrated by whirl testing which Kaman has performed on blades with simulated cracks in the torsion area. Each blade contained a knife cut 3/4 inch in depth running from Sta. 100. to 185. With 75 percent of full cyclic control applied, 150 hours of whirl testing produced crack propagation through the thickness of the spar at two locations, but no span propagation was evident. The conditions of test were conservative in that the vibratory torsional moment continuously exceeded by approximately 50 percent those measured in maximum level flight speed and subsequent overspeed test.

As the flight envelope for the HOK, predecessor of the HH-43B, expanded and the operational experience widened, it became evident that the torsional area of the main spar between Sta. inches 80 and 180 would be the next most troublesome region of the blade from a structural point of view. Spanwise checks or cracks occurred in some instances in the spruce and maple, primarily at the trailing edge of the steel nose cap. These were proven to be caused by maneuver blade torsion moments exceeding the vibratory torsional endurance limit of this area. Original construction of the HOK blade, consisting of spruce and maple laminations capped with an erosion protection of .018-inch stainless steel around the leading edge, had an endurance limit in torsion of ± 1,300 inch-pounds. (See Figure 11-51.)

A. The first structural improvement in this area, produced in 1956, consisted of one layer of glass cloth, .010-inch thick, wrapped around the spar in the shape

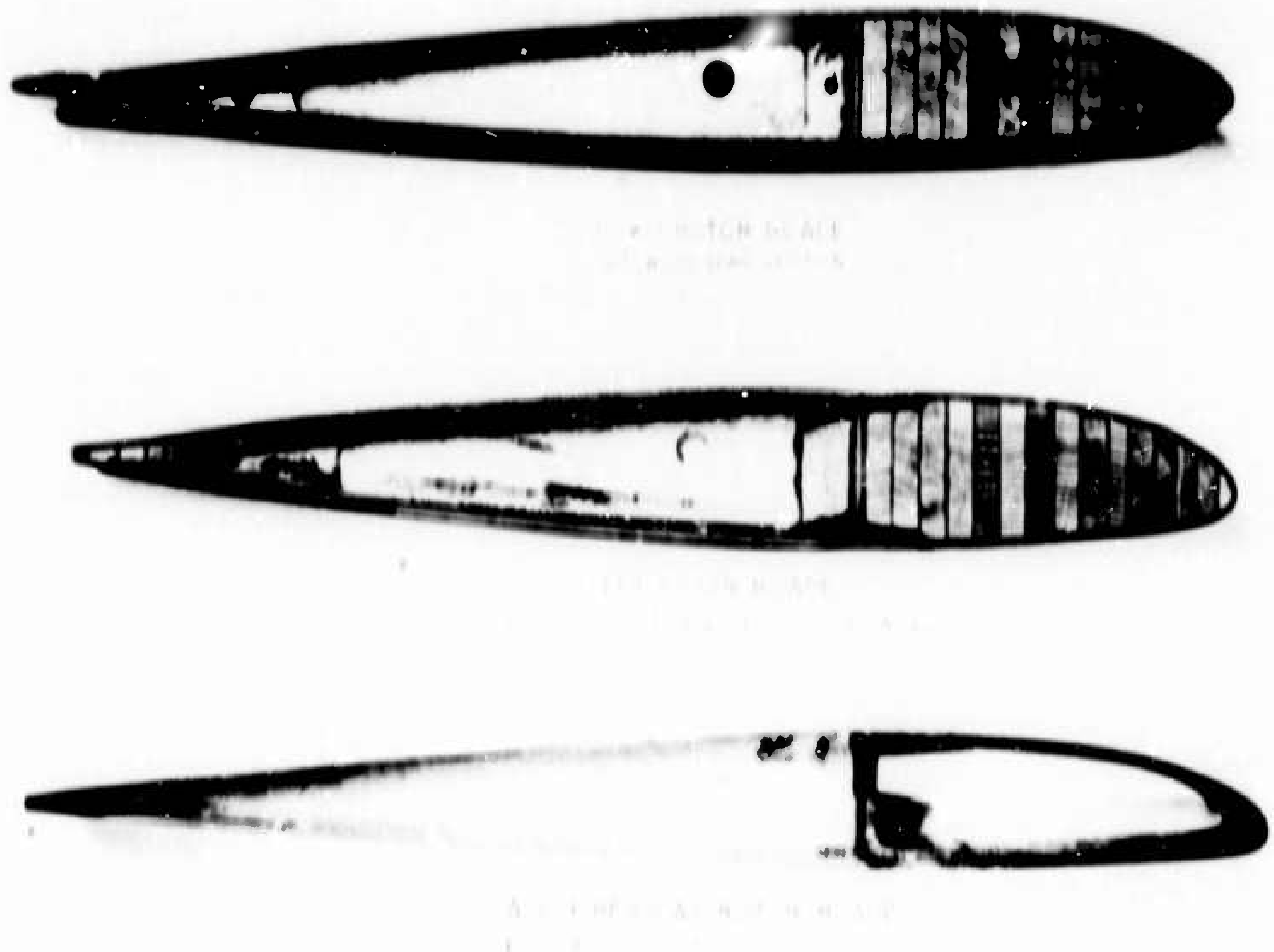

Figure II-51. Evolution of the Use of Fiberglass in Kaman Rotor Blade

BLANK PAGE

of the letter "C". After this adhered to the wooden spar, the stainless steel nose cap was then applied. This structure proved to have a torsional endurance limit of ± 1,700 inch-pounds and was a significant improvement over the previous construction.

B. The wider flight envelope of the H-43B involves greater control motions of the rotor and, specifically, a wider amplitude torsion of the blade than required in HOK installations. Hence, an additional structural improvement program was undertaken in 1958, and resulted in the introduction of the glasscloth reinforcement of the wooden spar which consisted of 6 layers of cloth wrapped completely around the wooden spar in the shape of the letter "D" as seen in Figure II-51. This reinforcement was .060-inch thick and obviated the necessity of having stainless steel over the glass cloth. Sufficient erosion protection is supplied by sprayed radome rubber. The structural torsional endurance limit for this version proved to be ± 2,100 inch-pounds and is currently incorporated on all production H-43B rotor blades. Referring once more to Figure II-51, it is again clear that with a modest increase in the total thickness of the glass cloth reinforcement around the periphery of the wooden spar, it would be quite possible to then consider the wood completely secondary and removable, leaving a complete glass cloth "D" section for the main rotor blade spar. This evolvement will subsequently be brought out in the discussion of the all-glass rotor blade.

Fatigue testing of the torsional area specimens is accomplished on the apparatus seen in Figures II-52 and II-53.

Test specimens duplicated basic production blade configuration between spanwise Sta.s 104.5 and 177.29, except as modified by fiberglass reinforcement.

Each test specimen was instrumented with strain gages, located in such a manner so as to measure torsional strain spanwise distribution. Each specimen was then calibrated to obtain the relationship between torsional moment and strain.

After calibration, the specimen was installed in the exciter clamp and supported laterally by a bungee chord. A slight torsional moment was introduced to locate the torsional node at the opposite end of the specimen. With this point located, the specimen was supported at that point. The desired moment level was introduced to start the fatigue run, and the dynamic torsional moments were checked hourly through monitored strain

Figure II-52. Overall View of Test Setup

Figure II-53. View of Exciter Attachment

Table II-A

CHRONOLOGICAL SUMMARY OF FATIGUE TESTING

Specimens	Loading Conditions	No. of Cycles (10^6)
TE8102000-1 Spring rate = 1520 inch/deg./ft. *Similar to K711502-1. Same blade structure as H-43B Blade from Sta. 104.50 to 167.25. Spar Block was made at KAC.	± 3500 inch/pound torsion & Bending	.064 cycles when skin failed spar was repaired & tested further at lower level.
	± 3000 in./lb. Torsion & Bending	.64 to failures
TE8102000-2 No spring rate determined. Similar to K711502-1. Same blade structure as H-43B blade from Sta. 104.50 to 167.25. Spar block was made at KAC.	± 3500 in./lb. Torsion & Bending	3.4 cycles to failure.
TE8102000-3 No spring rate determined. Similar to K711502-1. Same blade structure as H-43B blade from Sta. 104.50 to 167.25. Spar block was made at KAC.	± 3500 in./lb. Torsion & Bending	Failed Invalid
TE8102000-4 No spring rate determined. Similar to K711502-1. Same blade structure as H-43B blade from Sta. 104.50 to 167.25. Spar block was made at KAC	± 2300 in./lb. Torsion & Bending	3.02 cycles load increased to ± 2700 in./lb. torsion & bending.
	± 2700 in./lb. Torsion & Bending	14.4 cycles load increased to ± 3500 in./lb. torsion & bending.
	± 3500 in./lb. Torsion & Bending	.475 to failure.

*NOTE: K711502-1 refers to predessor production rotor blade as seen in Figure II-51.

Table II-A (Cont'd.)

Specimens	Loading Conditions	No. of Cycles (10^6)
TE8102000-5 No spring rate determined. Similar to K711502-1. Same blade structure as H-43B blade from Sta. 104.50 to 167.25. Spar block was made at KAC.	$\pm$ 3500 in./lb. Torsion & Bending	.225 - No cracks were evident, although test was stopped because of suspected blade failure.
TE8102000-6 No spring rate determined. Similar to K711502-1. Same blade structure as H-43B blade from Sta. 104.50 to 167.25. Spar block was made at KAC.	$\pm$ 3500 in./lb. Torsion & Bending	.25 cycles.
TE8102000-7 No spring rate determined. Similar to K711502-1. Same blade structure as H-43B blade from Sta. 104.50 to 167.25. Spar block was made at KAC.	$\pm$ 3500 in./lb. Torsion $\pm$ 2000 in./lb. Bending	.308 cycles to failure.
TE8102000-8 No spring rate determined. Similar to K711502-1. Same blade structure as H-43B blade from Sta. 104.50 to 167.25. Spar block was made at KAC.	$\pm$ 3500 in./lb. Torsion & Bending	1.35 cycles to failure.
TE8102000-9 Spring rate = 1220 lb. in./deg./ft. Similar to K711502-1, except that the spar is wrapped with fiberglass. The leading edge of the spar has a 6-ply fiberglass wrap with no fiberglass on the trailing edge of the spar. Spar block was made at KAC.	Could not be determined.	Failed Invalid

Table II-A (Cont'd.)

Specimens	Loading Conditions	No. of Cycles (10^6)
TE8102000-11. Spring rate = 1740 lb. in./deg./ft. Similar to K711502-1, except that the spar is wrapped with fiberglass. The leading edge of the spar has a 6-ply fiberglass wrap with no fiberglass on the trailing edge of the spar. Spar block was made at KAC.	Could not be determined	Failed Invalid
TE8102000-10. Spring rate = 1520 lb. in./deg./ft. Similar to K711502-1, except the spar was a 6-ply fiberglass wrap over both the trailing edge and the leading edge. Spar block was made at KAC.	Could not be determined	Failed Invalid
TE8102000-12. No spring rate determined. Similar to K711502-1, except the spar has a 6-ply fiberglass wrap over both the trailing edge and the leading edge. Spar block was made at KAC	± 2000 in./lb. Torsion - No Bending	.310 cycles
	± 2500 in./lb. Torsion - No Bending	.185 cycles
	± 3500 in./lb. Torsion - No Bending	.16 cycles
	± 3000 in./lb. Torsion - No Bending	6.0 cycles to failure
TE-8102000-13. Spring rate = 1460 lb. in./deg./ft. Similar to K711502-1, except that the spar has a 10-ply fiberglass wrap over the leading edge of the spar with none on the trailing edge. Spar block was made at KAC.	± 3000 in./lb. Torsion - No Bending	1.23 to failure

Table II-A (Cont'd.)

Specimens	Loading Conditions	No. of Cycles (10^6)
TE8102000-14. Spring rate = 1430 lb. in./deg./ft. Similar to K711502-1, except that the spar has a 10-ply fiberglass wrap over the leading edge of the spar with none on the trailing edge. Spar block was made at KAC.	± 3000 in./lb. Torsion - No Bending	.86 to failure
TE8102802-1. Spring rate = 1600 lb. in./deg./ft. Similar to TE8102000-10 and -12. Spar block was made at KAC.	± 2960 in./lb. Torsion - No Bending	1.8 to failure
TE8102802-5. Spring rate = 1162 lb. in./deg./ft. Similar to TE8102000-1 through -8 except the spar is bare and does not have the stainless steel and style No. 181 fiberglass laminated cloth over the leading edge. Spar block was made at KAC.	± 2360 lb./in. Torsion - No Bending	.15 to failure
TE8102802-7 S/N-1. Spring rate = 1400 lb. in./deg./ft. Similar to TE8102000-1 through -8 except the spar has a 3-ply fiberglass wrap over the leading edge, and a 6-ply fiberglass wrap over the trailing edge. Spar block was made at KAC.	± 2640 lb./in. Torsion - No Bending	5.1 to failure

Table II-A (Cont'd.)

Specimens	Loading Conditions	No. of Cycles (10^6)
TE8102802-7 S/N-2. Spring rate = 1590 lb. in./deg./ft. Similar to TE8102000-1 through -8 except the spar has a 3-ply fiberglass wrap over the leading edge, and a 6-ply fiberglass wrap over the trailing edge. Spar block was made at KAC.	± 2840 lb./in. Torsion - No Bending	14.4 to failure
TE8102802-7 S/N-3. Spring rate = 1500 lb. in./deg./ft. Similar to TE8102000-1 through -8 except the spar has a 3-ply fiberglass wrap over the leading edge, and a 6-ply fiberglass wrap over the trailing edge. Spar block was made at KAC.	± 2840 lb./in Torsion - No Bending	13.3 to failure
TE8102802-5. Spring rate = 1162 lb. in./deg./ft. Similar to TE8102000-1 through -8 except the spar is bare and does not have the stainless steel and style No. 181 fiberglass laminated cloth over the leading edge. Spar block was made at KAC.	± 2360 lb./in. Torsion	.15 to failure
TE8102802-7 S/N-1. Spring rate = 1400 lb. in./deg./ft. Similar to TE8102000-1 through -8 except the spar has a 3-ply fiberglass wrap over the leading edge, and a 6-ply fiberglass wrap over the trailing edge. Spar block was made at KAC.	± 2640 lb./in. Torsion - No Bending	5.1 to failure

Table II-A (Cont'd.)

Specimens	Loading Conditions	No. of Cycles (10^6)
TE8102802-7 S/N-2. Spring rate = 1590 lb. in./deg./ft. Similar to TE8102000-1 through -8 except the spar has a 3-ply fiberglass wrap over the leading edge, and a 6-ply fiberglass wrap over the trailing edge. Spar block was made at KAC.	$\pm$ 2840 lb./in. Torsion - No Bending	14.4 to failure
TE8102802-7 S/N-3. Spring rate = 1500 lb. in./deg./ft. Similar to TE8102000-1 through -8 except the spar has a 3-ply fiberglass wrap over the leading edge, and a 6-ply fiberglass wrap over the trailing edge. Spar block was made at KAC.	$\pm$ 2840 lb./in. Torsion - No Bending	13.3 to failure
TE8102802-7 S/N-4. Spring rate = 1490 lb. in./deg./ft. Similar to TE8102000-1 through -8 except the spar has a 3-ply fiberglass wrap over the leading edge, and a 6-ply fiberglass wrap over the trailing edge. Spar block was made at KAC.	$\pm$ 2840 in./lb. Torsion - No Bending	5.875 to failure
TE-8102802-9. Spring rate = 1990 lb. in./deg./ft. Similar to TE8102000-1 through -8 except the spar has a 6-ply fiberglass wrap over the leading edge, and a 10-ply fiberglass wrap over the trailing edge with a .25-inch Scotchply pad in the underside of the spar section from Sta. 104.5 to Sta. 136. Spar block was made at KAC.	$\pm$ 3500 in./lb. Torsion - No Bending	2.3 to failure

Table II-A (Cont'd.)

Specimens	Loading Conditions	No. of Cycles (10^6)
TE8102802-11 S/N-1. Spring rate = 1850 lb. in./deg./ft. Similar to TE8102802-9 with the following exception. There are no Scotch-ply inserts under the fiberglass wrap. Spar block was made at KAC.	± 3500 in./lb. Torsion - No Bending	1.08 to failure
TE8102802-11 S/N-2. Spring rate = 1850 lb. in./deg./ft. Similar to TE8102802-9 with the following exception. There are no Scotch-ply inserts under the fiberglass wrap. Spar block was made at KAC.	± 3500 in./lb. Torsion - No Bending	8.72 to failure
TE8102802-13 S/N-1. Spring rate = 1860 lb. in./deg./ft. Similar to TE8102802-11. On these specimens the 6-ply fiberglass "D" wrap over the leading edge was applied to the wooden spar in two steps of 3-ply each. Spar was made at KAC.	± 3500 in./lb. Torsion - No Bending	1.15 to failure
TE8102802-13 S/N-2. Spring rate = 1620 lb. in./deg./ft. Similar to TE8102802-11. On these specimens the 6-ply fiberglass "D" wrap over the leading edge was applied to the wooden spar in two steps of 3-ply each. Spar was made at KAC.	± 3500 in./lb. Torsion - No Bending	.083 to failure

Table II-A (Cont'd.)

Specimens	Loading Conditions	No. of Cycles (10^6)
TE8102802-15. Spring rate = 2040 lb. in./deg./ft. Standard spar block grain laminations with .030 thickness Scotchply strips added to top and bottom surfaces of the basic wooden spar, subsequently wrapped with a 6-ply leading edge, and a 10-ply trailing edge fiberglass wrap. Spar block was made by Pratt-Reed.	± 3500 in./lb. Torsion - No Bending	8.5 to failure
TE8102802-17. Spring rate = 2000 lb. in./deg./ft. Torsion specimen incorporating selected spruce grain laminae - 6-ply leading edge, and 10-ply trailing edge fiberglass wrap. Spar block was made at KAC.	± 3500 in./lb. Torsion - No Bending	3.3 to failure
TE8102802-19. Spring rate = 2000 lb. in./deg./ft. Three horizontal cuts made through the spar incorporating one layer of No. 181 fiberglass cloth sandwiched between each cut - same fiberglass wrap as for -17. Spar block was made at KAC using selected grain principal.	± 3500 in./lb. Torsion - No Bending	24.05 to failure
TE8102802-21. Spring rate = 2200 lb. in./deg./ft. Similar to TE8102802-11, but has .015-inch thick Scotchply strips running full length of the specimen on top and bottom.	± 3500 in./lb. Torsion - No Bending	19.5 to failure

Table II-A (Cont'd.)

Specimens	Loading Conditions	No. of Cycles (10^6)
TE8102802-23. Spring rate = 1900 lb. in./deg./ft. Similar to TE8102802-19, but has only two horizontal cuts. Spar block was made at Pratt-Reed.	$\pm$ 3500 in./lb. Torsion - No Bending	8.22 to failure
TE8102802-25. Spring rate = 1910 lb. in./deg./ft. Similar to TE8102802-19, but spar block was made at Pratt-Reed.	$\pm$ 3500 in./lb. Torsion - No Bending	8.00 to failure
TE8102802-27. Spring rate = 2030 lb. in./deg./ft. Combination of TE8102802-21 and -25. Spar block was made at Pratt- Reed.	$\pm$ 3500 in./lb. Torsion	5.65 to failure
TE8102802-29 S/N-1. Spring rate = 1746 lb. in./deg./ft. Three horizontal cuts, No. 181 cloth sandwiched between each cut, staggered glue lines with five wrap fiberglass on L.E. and ten wrap on T.E.	$\pm$ 3140 in./lb. Torsion	3.87 to failure
TE8102802-29 S/N-2. Spring rate = 1800 lb. in./deg./ft. Same configuration as -29 S/N-1.	$\pm$ 3140 in./lb. Torsion	6.40 to failure
TE8102802-29 S/N-3. Spring rate = 1826 lb. in./deg./ft. Same configuration as -29 S/N-1.	$\pm$ 3140 in./lb. Torsion	1.66 to failure
TE8102802-11 S/N-3. Spring rate = 1780 lb. in./deg./ft. Same configuration as -11 S/N-1.	$\pm$ 2320 in./lb. Torsion	Failed Invalidly

Table II-A (Cont'd.)

Specimens	Loading Conditions	No. of Cycles (10^6)
TE8102802-11 S/N-4. Spring rate = 1820 lb. in./deg./ft. Same configuration as -11 S/N-1.	$\pm$ 2100 in./lb. Torsion	30.0 No Failure
TE8102802-11 S/N-5. Spring rate = 1965 lb. in./deg./ft. Same configuration as -11 S/N-1.	$\pm$ 2570 in./lb. Torsion	30.0 - No Failure
TE8102802-7 S/N-5. Spring rate = 1555 lb. in./deg./ft. Same configuration as -7 S/N-4.	$\pm$ 2030 in./lb. Torsion	30.0 - No Failure

gages. Frequency adjustments were made as required for optimum tuning.

Failures occurred in the spar near the center of the span and were not visible until propagation had reached the fiberglass. At no time had the primary origin been determined to be in the fiberlgass. The resonant frequency and external force were therefore used to detect a failure; the resonant frequency would decrease and the external force required to maintain the load level would increase in the event of failure.

As previously stated, spanwise cracks occurred in the laminated wood spar, and it was felt that by reinforcing the periphery with glass structure, support would be given the outermost wood fibers to resist the torsional shear forces.

Table II-A is a chronological summary of this fatigue testing, starting with the basic blade structure with no fiberglass modifications (similar to Figure II-51) and continuing through the various combinations of fiberglass build-up over the leading and trailing edges of the blade spar. Ultimately it is shown that an optimum configuration is obtained with a 6-inch to 10-inch lay-up, which signifies that 6 plies of No. 181 cloth are wrapped over the leading edge or "C"-shaped portion of the "D"-shaped spar, and 10 plies of No. 181 cloth close the "C" to complete the "D" structure. The wood spar is, of course, routed down proportionately so that with the glass build-up, the outside airfoil coordinates are maintained. Physically, the trailing edge fiberglass is in the form of a channel, enclosed by the leading edge "C" wrap. It is significant to mention that the spring rates of the fiberglass wrapped and the previous unwrapped blade are comparable, thus ensuring the same order of loading magnitude for a given flight condition, while at the same time more than doubling the blade life between overhaul periods.

Original testing of the blade torsional area was to improve the spar from its susceptibility to spanwise cracking. As noted in Table II-B, the testing first employed combined loading of torsional and flatwise bending moments but later excited the specimen in torsion only. This was done because experience had shown that flatwise bending had little effect upon the spanwise shear failures in the spar, yet hampered spar testing by causing aft structure (skin) failures in the form of chordwise cracks. It must be stated that quality plywood used for blade skins was not plentiful; therefore, in torsional area testing for spar improvement, inferior-grade plywood was used for aft structure, thus explaining the skin failures in the previous sentence.

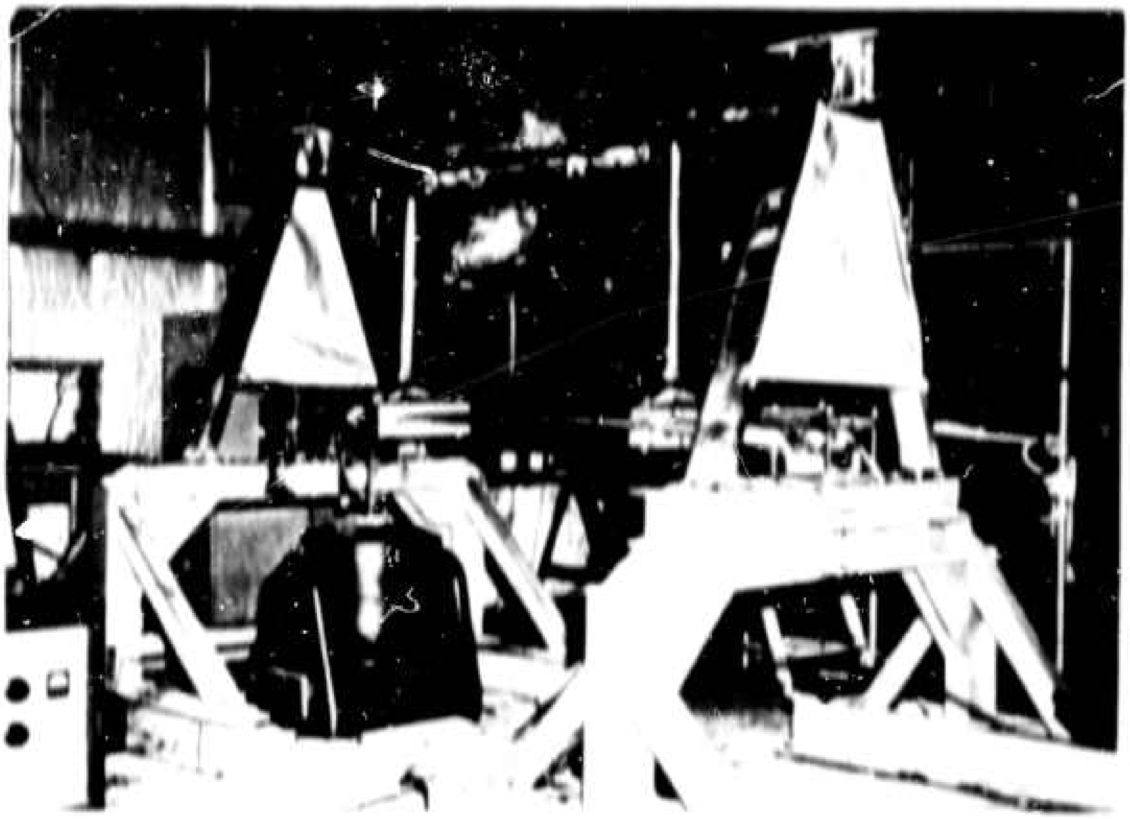

Figure 11-54. Test Setup for Steady Plus Vibratory Flatwise Bending

The above explanation of availability of quality plywood must be carried further. In general, little trouble was encountered with skins in service use; however, despite rigid quality control inspection, occasional skin failures did occur "in the field". Indications were that the cracks started near the forward edge of the skin and propagated rapidly to the trailing edge of the blade in the bottom skin only. At this point the crack stopped and was discovered; or paused and propagated slowly through the trailing edge and then rapidly through the complete chordwise extent of the top skin, at which time the pilot was able to feel control changes and/or visually observe the disturbance in the blur of the whirling blades.

Failures were judged to be fatigue, although the development was known to be rapid. In every case the failure origin was located in a region of "short-grain" plywood.

Assessment of all the evidence concluded that initial failure was incurred on the ground either during tie-down of the helicopter or during inadequate tie-down in high winds, and subsequently propagated in flight. In order to reduce dependence upon the properties of wood and to increase the probability against failure, a test program was entered to evaluate plywood skin reinforcement with fiberglass. The test apparatus used is shown in Figure II-54.

To duplicate this low cycle type failure as it occurred in the field, a high steady flatwise bending (to simulate static droop) with a high superimposed vibratory bending moment (to simulate heavy wind gusts) was proposed. After several trials, it was found that a loading of - 7500 $\pm$ 9000 in.-lb. flatwise bending moment resulted in simulating the actual failures. Various skin reinforcement configurations were then subjected to this loading for evaluation. Table II-B and Figure II-55 offers a condensed tabulation and plot of the results.

In conjunction with the above test, slight modifications were incorporated in the blade to reduce the droop loading. This included, as noted in the test tabulation, a thin "Scotchply" plank formed into the lower spar surface, and maple stringers which were inset into notches cut into the rib flanges. Both plank and stringers were tapered so as to distribute stiffness rationally.

It was found in the course of the development program that the application of fiberglass had substantial effects upon results. As finally developed, this process involves a high-pressure cure of a single ply of Type 120 glass cloth applied to both sides of the .070-inch-thick plywood bottom skin and the top side only of the .070-inch-thick plywood top skin with an epoxy resin used as an impregnant. Reinforcement

BLANK PAGE

Table II-B

SUMMARY OF ROTOR BLADE SKIN FATIGUE TESTING
(High Bending Moment - Low Cycle Condition)

Specimen Number	Spar Wrap	Top Skin Plies/Cloth	Bottom Skin Plies/Cloth	Scotchply Plank	Flatwise Bending (in.-lb.)	No. Cycles	Failure - Remarks
7-8-11-1	3-16	1/116	2/116		7500 ± 9000	396,000	Bottom Skin
29-5- 5-4	5-10	1/181	--			57,300	
29-6- 5-3	5-10	1/181	--			15,100	
11-7-11-2	6-10	1/116	2/116			10,000	
11-6-11-4	6-10	1/116	2/116			235,000	
11-7-11-3	6-10	1/116	2/116			70,500	Bottom Skin
7-9- 9-2	3- 6	1/116	2/116			6,500	
7-9- 9-2	3- 6	1/116	2/116			1,600	Bottom Skin
7-8-15-1	3-6	--	--			8,000	
11-3-17-1	6-10	--	--			55,400	
29-6- 5-6	5-10	1/181	--			213,000	
33-1- 5-7	6-10	1/181	--	X		27,800	
29-5- 5-7	5-10	1/181	--			12,100	Bottom Skin
33-2-23-1	6-10	1/181	--	X		151,000	Bottom & Top Skin
7-8-19-2	3- 6	1/120	2/120			149,000	Top Skin
7-8-25-1	3- 6	1/120-181	2/120			301,000	
11-3-27-1	6-10	1/120	2/120			477,000	
7-8-21-2	3- 6	1/120	2/120			311,000	Top Skin
33-2-23-2	6-10	1/181	--	X		28,000	Bottom Skin
31-1-21-1	6/10	1/120	2/120			1 x 10^6	No Failure
31-2-21-3	6/10	1/120	2/120		7500 ± 9000	1 x 10^6	No Failure

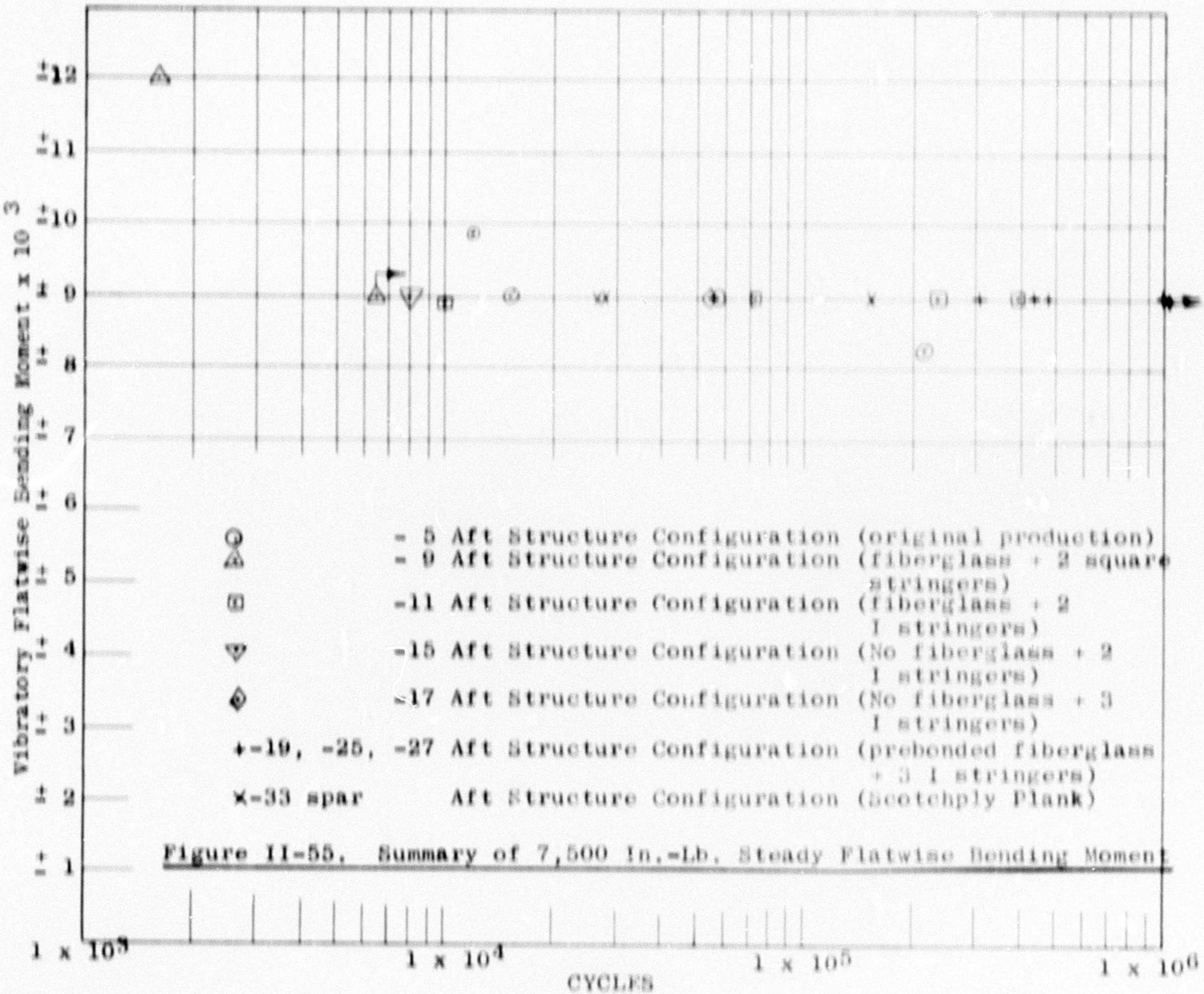

Figure II-55. Summary of 7,500 In.-Lb. Steady Flatwise Bending Moment

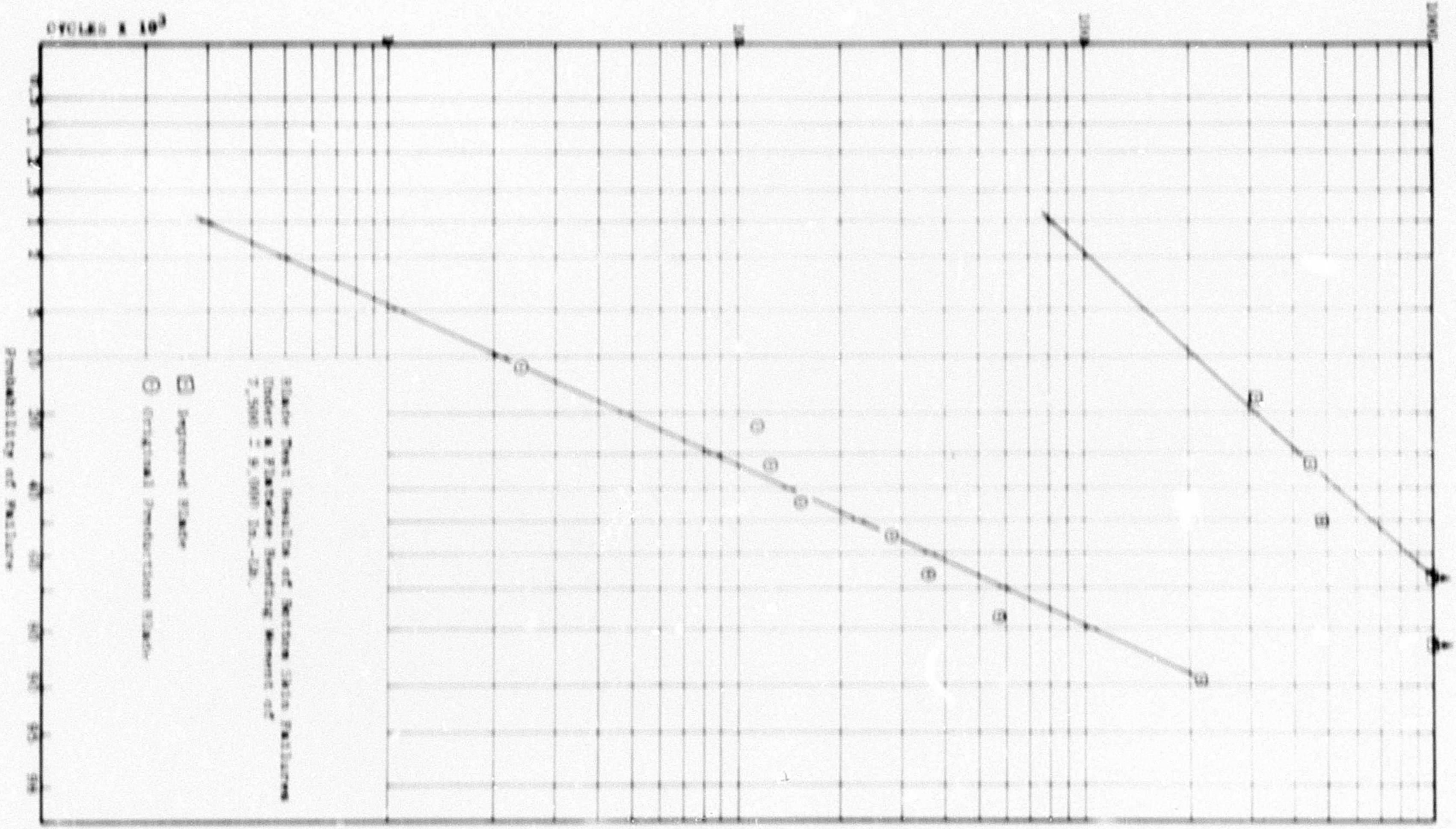

Figure II-56. Blade Test Results - Cycles vs. Probability was applied to the top skin as insurance that solving of the bottom skin problem would not, at some later date and after greater exposure to service usage, cause the top skin to become critical.

Specimens of the "old" configuration subjected to this test exhibited failure after as little as 2400 cycles at 7500 $\pm$ 9000 in.-lb. bending. The relative life of the "old" design as compared to the final developed configuration is depicted in a long-life-probability plot in Figure II-56. Here it is clearly seen that the crack resistance of the skin has been substantially improved, particularly at low probability of failure. As an example, at a failure rate of 1 part in 100, the life of the improved blade is 270 times that of the original configuration.

SECTION III

ALL FIBERGLASS-REINFORCED PLASTIC BLADE DEVELOPMENT

BACKGROUND

As previously stated, all helicopters produced by Kaman have used elastic structures as primary load-carrying members in the servo-flap controlled rotor. The basic wood structure originally used has been improved and has gradually been replaced by directed glass fibers in the more critically stressed blade areas. Referring again to Figure II-6, it is obvious that the existence of the spruce and maple in the latest section now serves as a filler between the various glass fiber elements and does not serve any primary structural purpose. Also with reference to Figure III-3, it appears clear that with a modest increase in glass cloth reinforcement around the periphery of the wooden spar, it would then be possible to consider the wood secondary and removable, leaving a complete glass cloth "D" section for the outboard portion of the main rotor blade spar. It is then logically concluded that it would be quite possible to remove all the wood, leaving only the primary load-carrying structure, namely, the glass cloth and unidirectional glass fiber structure for the entire spar.

The design parameters involved in developing these helicopter blades within the very restricted weight limits are quite onerous; for instance, the centrifugal force at the root end of our blades is of the order of 60,000 pounds and must be combined with vibratory bending moments of the order of $\pm$ 20,000-inch pounds for normal flight and up to $\pm$ 45,000 inch-pounds for short maneuvers.

Torsional loading of the order of $\pm$ 3,600 inch-pounds can be generated in the twisting part of the blade, and all these vibratories are continuously applied at a frequency between 220 to 260 cycles per minute as part of the normal flight behavior of the aircraft.

The current design requirements establish 1,000 flight hours, or in other cases full endurance to 30,000,000 cycles, for the moving parts of a helicopter.

In the early stages of the blade development, experimental fabricating operations were used. As the technology was adopted and developed, better equipment was obtained, such as a heat-controlled oven of a size big enough to handle large units, and the use of many plastic and metal tooling devices was introduced and mastered to augment the original wood tooling capability.

As soon as a geometrically and structurally acceptable blade was produced, the aerodynamic and dynamic problems inherent in any new helicopter rotor blade design had to be solved by a number of runs on test rigs, vibration response studies, and the attending changes in local stiffness and weight management that could be found only be detailed testing.

At this point some of the attractive properties of the fiberglass material came to the fore. On many occasions the existing structure had to be cut into to make subtle changes, and the repairs could be restored to the strength and endurance of the whole assembly by judicious use of scarfing and joining without losing the integrity of the final product.

While it may sound as if the goal had been reached at this point, actually the test sections had to take over at this point and run endurance tests for the blades by accumulating hundreds of hours of continuous running under high stress and broad control inputs on one or more of the test rigs to prove that changes would not occur in behavior through extensive use and that the fatigue resistance surmised from individual component tests was actually present in the completed blades.

In addition to the ground testing, a limited program of flight testing was conducted with these blades installed on the military helicopters operating from the manufacturer's plant. Outstanding success was achieved.

To prove satisfactory structural criteria, very exhaustive tests must be conducted, especially since the helicopter is designed by fatigue endurance requirements rather than static strength.

In many cases the stress analysis that can be achieved is an idealization of the actual phenomena and is used to determine the signposts for setting up "component oriented" rather than "material oriented" tests.

This is the main reason why actual material strength or endurance data have not been published, while statements can be made precisely on the differential of behavior between design solutions achieved with different materials for the same component.

As a good example of this situation is shown in Table III-C and Figure III-33, where some of the developments discussed in this section are summarized.

The bending stresses corresponding to the most advanced of the tests reported above are estimated at 2,000 psi steady plus or minus 4,750 psi vibratory with a correction for fastening notches bringing the actual vibratory stress to ± 8,700 psi at the edge of the mounting holes.

The torsional stress can be assumed to be neutral-steady, plus or minus 8,000 psi vibratory.

When such values are corrected for modulus and lightness of weight and are compared with the allowables for wood and available metals, the advantage to be found in the use of reinforced-plastics appears in full force.

Work on this concept has culminated in the development of an all-glass fiber blade that is completely interchangeable with and greatly superior to the wooden blade.

DEVELOPMENT

Calculations based upon the fiberglass manufacturer's data and Kaman's experience led to a spar section of 38 plies of cloth at the root end, varying according to spanwise requirements to 9 plies at the tip (approximate Sta. 280.0). The ease in forming with fiberglass allowed the outboard end to be "pocketed", as sketched in Figure III-1, to accommodate leading edge mass balance weight.

Figure III-1. Spar Tip Section

Basic spar material was Type 143 glass cloth with the innermost and outermost plies being Type 181 glass cloth. An epoxy resin system was used in the wet lay-up operation.

The leading edge of the spar was formed over a male mold in its entire length. The trailing edge of the spar was formed in two sections: the inboard (thick) end, and the outboard "closing channel". The cured parts were then mated with the

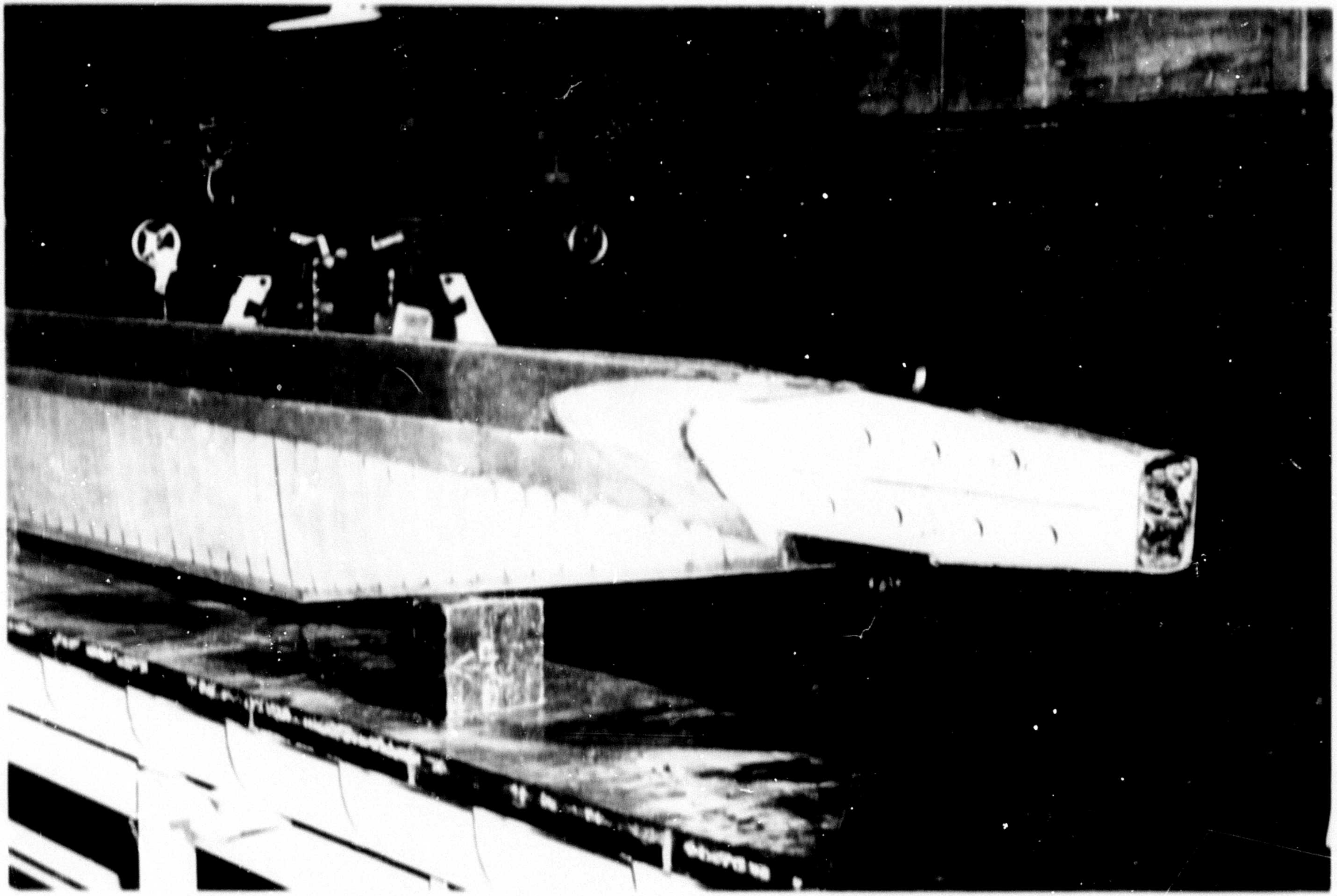

Figure III-2. Original Fiberglass Blade Root-End Construction

BLANK PAGE

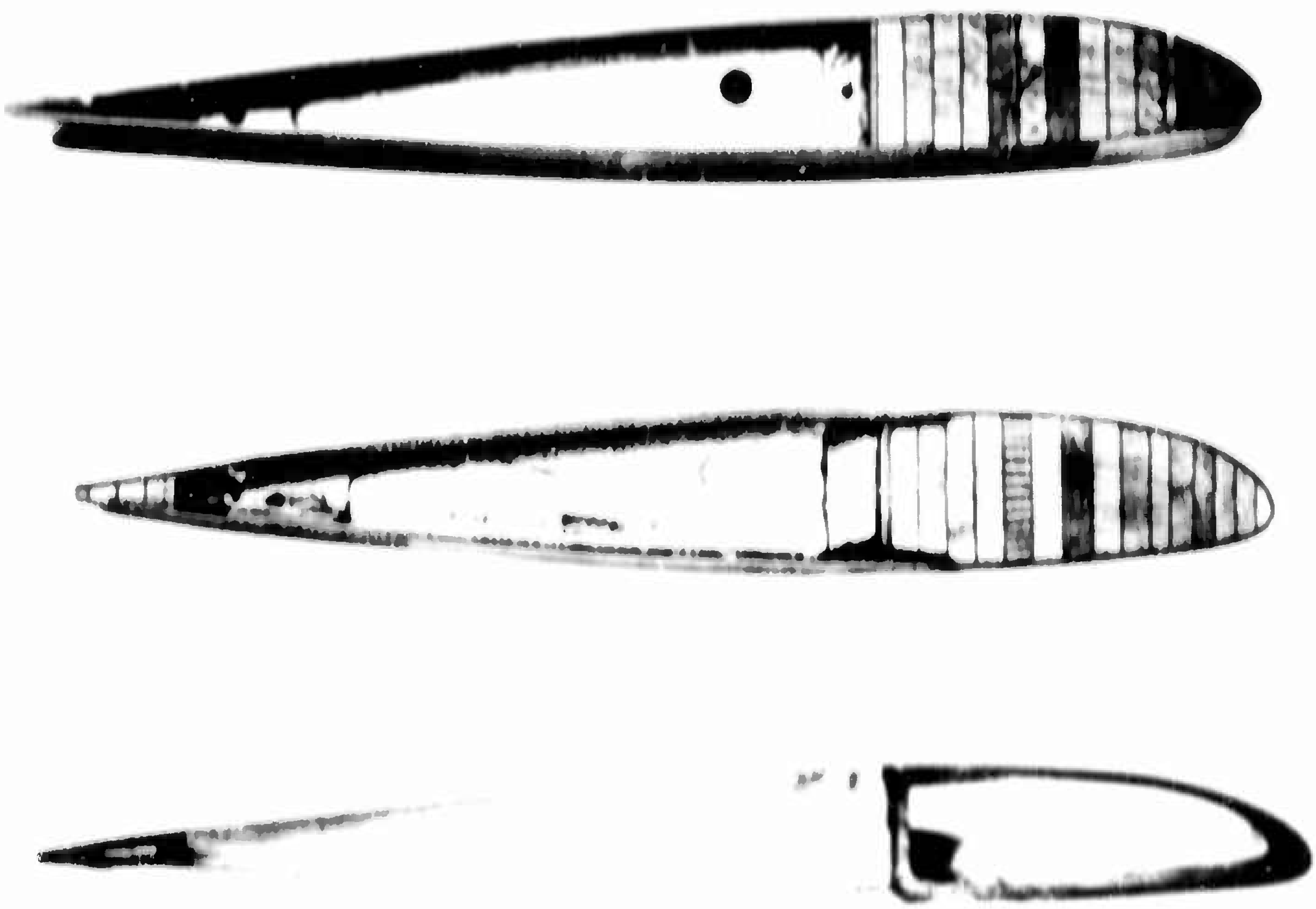

Figure III-3. Evolution of the Use of Fiberglass in Kaman Rotor Blades

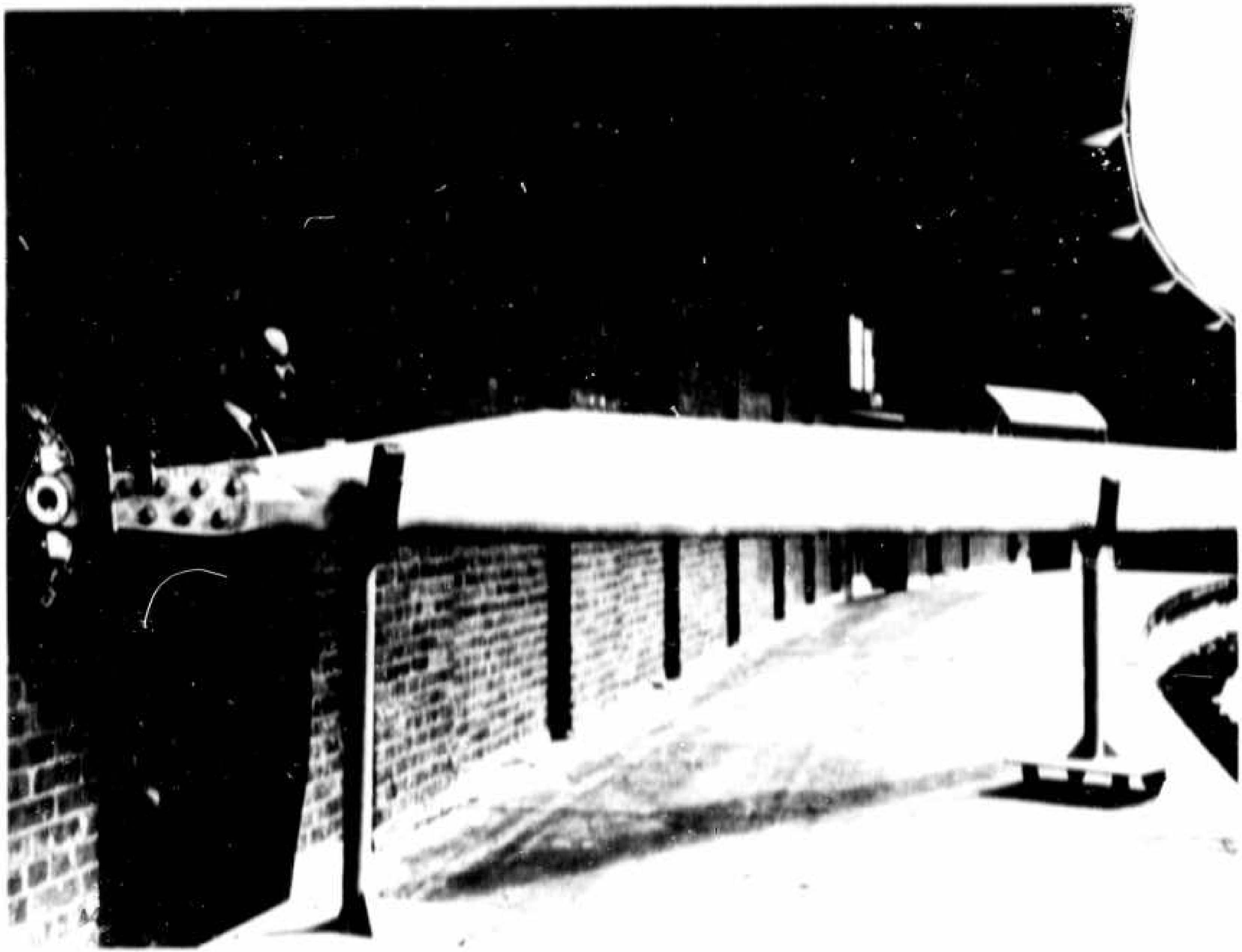

Figure III-4. Original Fiberglass Blade Completed

BLANK PAGE

the inboard sections being bonded with a rabbeted joint; the closing channel, overlapped by the inboard trailing edge outboard end, completed the closing of the spar leading edge "C" section to form the "D" section. Phenolic spools 1½ inches in diameter were bonded into the root end to form back-up spacers for the retention bolts.

The phenolic and Scotchply cheek plates were added along with I-section ribs formed as back-to-back channels of Type 181 glass cloth. A Scotchply spline spliced into a Type 181 glass cloth tapered inboard channel formed the trailing edge structure, and a 2-ply skin of Type 181-150 glass cloth completed the basic blade structure (see Figures III-2, III-3, and III-4).

This very first effort in fabricating an all-glass blade was not only aesthetically appealing but with attached flap, controls, hardware, and calculated mass balance weight additions, exhibited outstanding properties from preliminary static tests.

Encouraged by the results, Kaman commenced a series of whirl tests using the all-glass blade paired with a standard wood blade. Initial runs indicated the need for improved pitch stability, which was obtained by a slight weight addition in the leading edge to move the chordwise center-of-gravity forward. This was easily accomplished by removing the 4-ply outboard leading edge balance weight cover (Figure III-1), bonding in the required weight, and replacing the 4 plies of glass cloth in a simple wet lay-up. Changes in blade torsional stiffness were also found to be necessary. This, too, was easily rectified by simply adding 2 plies of Type 181 glass cloth around the blade between Sta. 80 and 120. Obvious here is the great adaptability of fiberglass-reinforced plastics to be reworked or modified without affecting adjacent areas. To plagiarize from a manufacturer's publication, it is so easy to "put the strength and stiffness where you need it". It must be emphasized in this regard, however, that prerequisites for this type of rework and/or modification are proper surface preparation and contamination-free environment. Much lack of confidence in the use of glass structures stems from failures which can be attributed to the aforementioned prerequisites as well as design inexperience.

Following the previously mentioned modifications, the glass-fiber glade was installed on a 1,000 HP electrically powered whirl rig, where the blade strength and stability permitted exploration of the complete thrust range from -½ g to +3 g at 240 to 330 RPM. Oscillograph data showed the feathering stability, bending moments, and torsion moments to be equivalent to those of the standard blade.

The corporate investment of this development proved so fruitful that Kaman sponsored further work in glass-blade research. Fabrication of a matched pair of blades capable of actual flight trials was the next endeavor. The mass balance information from the first blade was "cranked in", the elastic hinge adjustment was made in the form of a mold modification to give a more gradual transition in the spar torsion area, and the Type 143 glass cloth in the spar was replaced with ± 15° oriented Scotchply. The manufacturer supplied the Scotchply in 2-ply rolls, which aided considerably in the handling of the material by the mutual cross support of one ply to the other.

When the fabrication, weight and balance, torsional properties, etc., were completed, the two blades were whirl tested to substantiate their structural and dynamic stability prior to initial flight trials. Test runs were conducted at rotor speeds of 240, 260, and 280 RPM. At each of these speeds, the blades were subjected to 1 g, 2 g, and minimum power loadings. Cyclic control inputs up to ± 5.5° were applied at 1 g thrust, inducing a maximum torsional moment of ± 2,800 in.-lbs. at Sta. 138.0. Throughout the entire range of RPM and power, blade stability and track were found to be satisfactory. Five hours of operation were accumulated with no deterioration of track or stability observed. Figure III-5 shows the glass blades installed for whirl testing. Figure III-6 is an interesting study of the translucent structure of the blade; this characteristic has become an aid in the inspection of subsequent area test specimens, where, by normal viewing or by viewing with a light from the opposite side of the blade, certain flaws in bonding, resin dry areas, cast resin pockets, etc., can be ascertained.

After completion of the above whirl testing, the blades were installed on an aircraft for initial flight trials. The glass-fiber blades were mounted on the left-hand rotor head, while a pair of standard wood blades was mounted on the right-hand side of the intermeshing helicopter. The program consisted of a ground run-up and flight evaluation from hover into translational lift to a forward velocity of approximately 10 knots. No quantitative data were obtained during this evaluation. In general, the blades performed well according to pilot reports; the only different characteristic from the standard rotor was the increased sensitivity of the glass blades to control movements.

Following the flight trials, the blades were again installed on the whirl test stand, where they were successfully operated for 151 hours in an endurance test program. During this operation, the blades were run at a torsional moment of ± 3,400 in.-lb. (twice the HH-43B high-speed level flight condition of ± 1,750 in.-lbs.).

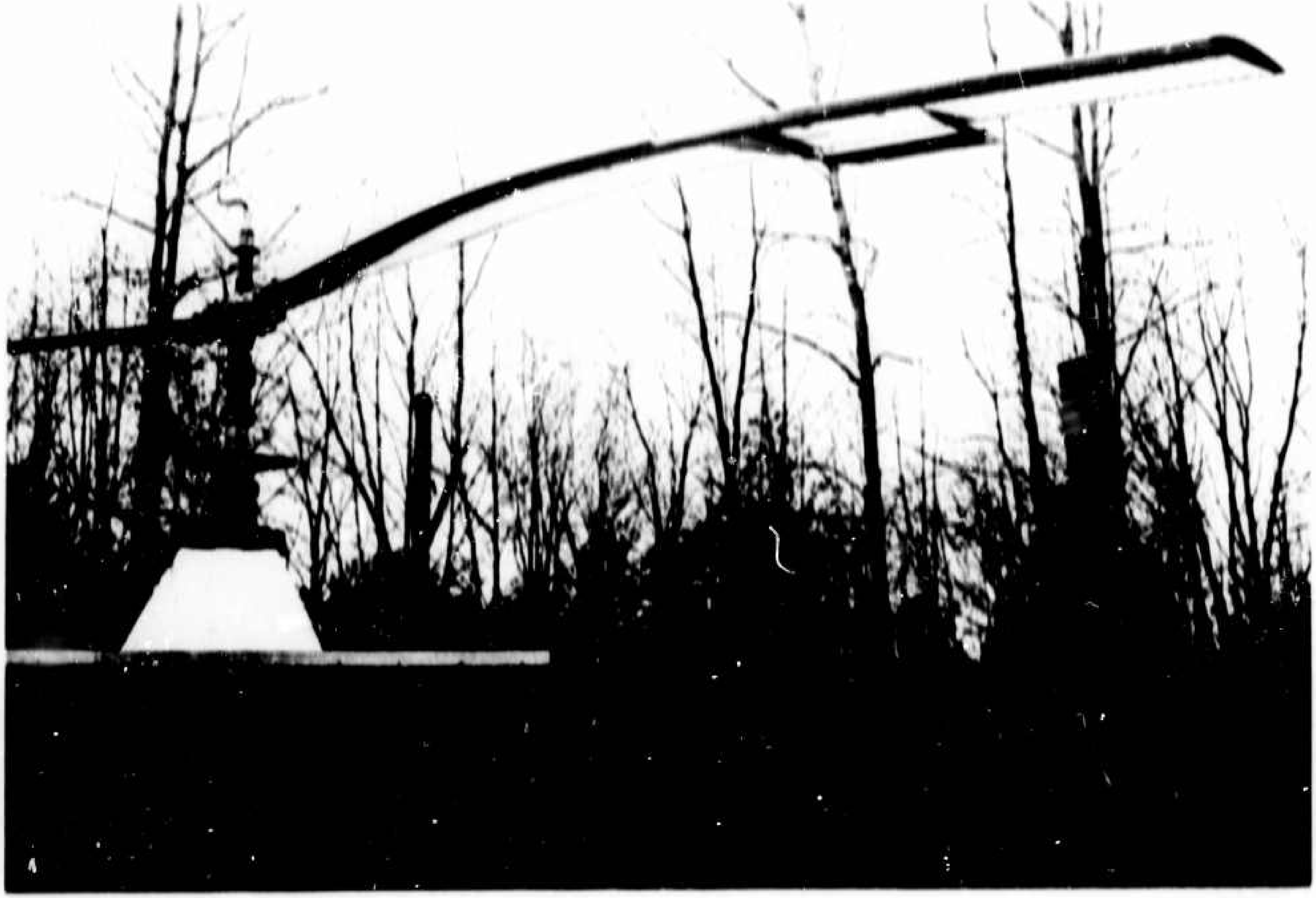

Figure III-5. Fiberglass Blade Whirl Test Rig

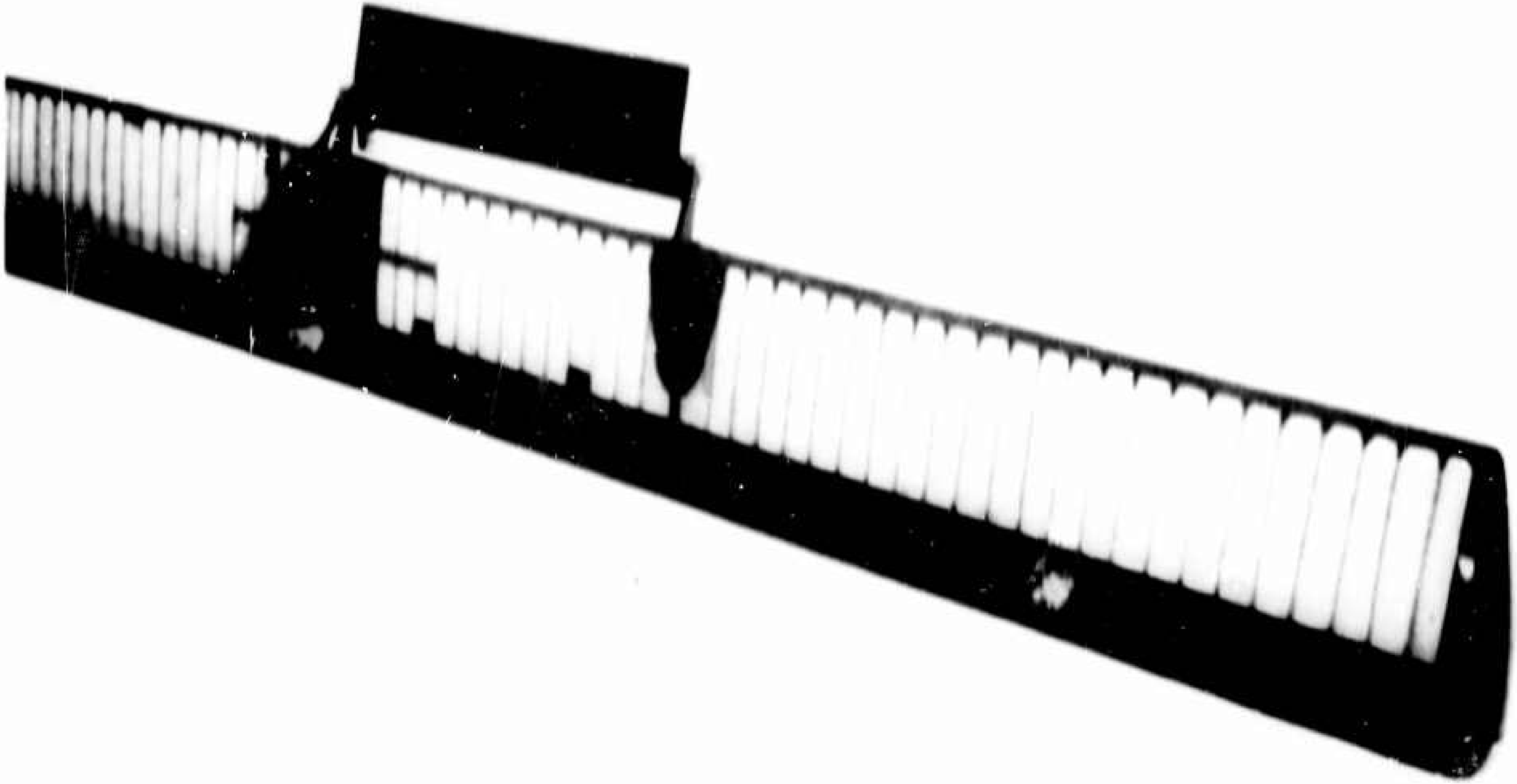

Figure III-6. Translucent Structure of Fiberglass Blade

BLANK PAGE

Kaman management, feeling the great potential of these blades, again authorized corporate funds to build a complete ship set of blades (two left-hand and two right-hand blades). The blades fabricated were the same as the previous pair with one exception: the modification of the top and bottom skins to include "built-in" stringers as sketched in Figure III-7. Because of the low modulus of the fiberglass-reinforced plastic, the stringers offer stiffness to overcome the static droop tendency.

Figure III-7. Fiberglass Blade Skin Construction

The completed ship set of blades is shown in Figures III-8, III-9, and III-10, where the stringers are clearly visible.

Prior to flight test trials, a preflight whirl test was conducted to check structural integrity and to establish the flutter clearance limit. A total of four hours was run with no instability or structural deficiencies occurring. The blades were then installed on a HH-43B helicopter for flight evaluations (Figures III-9 and III-10).

Due to the increased stiffness caused by the stringer modification, a reduction in cyclic controllability was noted during the early stages of the flight program. After completion of the flight program, the blades were reworked by removing two plies of material from the torsional section of the spar; these were reflown at the 6,100-pound weight condition. The cyclic sensitivity was then shown to be equivalent to production wood blades.

INSTRUMENTATION:

Stress and motion parameters were recorded as follows:

a) Blade Station 14 flatwise bending moment
b) Blade Station 31 flatwise bending moment
c) Blade Station 40 flatwise bending moment
d) Blade Station 90 flatwise bending moment
e) Blade Station 138 torsion moment
f) Flap centerline bending moment
g) Collective control stick positio.
h) Fore and aft cyclic control stick position
i) La.eral cyclic control stick position
j) Rudder pedal position
k) Pilot seat vertical acceleration
l) Ship's C.G. vertical acceleration (load factor)

TEST RESULTS

Nineteen flights were made with the glass-fiber blades; the forward speed envelope of the helicopter was explored from hover to 107 knots, maneuvering flight was performed from 0.3 g to 2.0 g load factors, power-off autorotations were made up to 100 knots, full lateral control sideward flight maneuvers were made up to about 25 knots, high-power climbs and climbing turns were done at 80 knots. Three gross-weight conditions were flown: a low weight, forward C.G. condition; a normal weight, aft C.G. condition; and an overload weight, aft C.G. condition.

No structural deterioration problems were encountered during the entire flight program of the glass-fiber blades, nor were there any unfavorable dynamic stability characteristics noted.

The measured maximum vibratory torsion moments at blade Station 138 were well below the level at which fatigue runout occurred on test specimens and the level at which sustained whirl testing was previously demonstrated on a ground test rig. The measured root vibratory bending moments at Station 31 are also well below demonstrated fatigue strength capabilities.

The blades appeared to behave in generally the same way as standard wooden blades with the exceptions of the greater blade stretch due to centrifugal force and the higher torsional stiffness that required more servo-flap control input. Compensation for blade stretch was made by the addition of an axially flexible control rod installed in the nonrotating collective control system of each rotor, which provided additional spanwise motion of the blade control rod. The effectiveness of this modification can be seen in Figure III-11.

BLANK PAGE

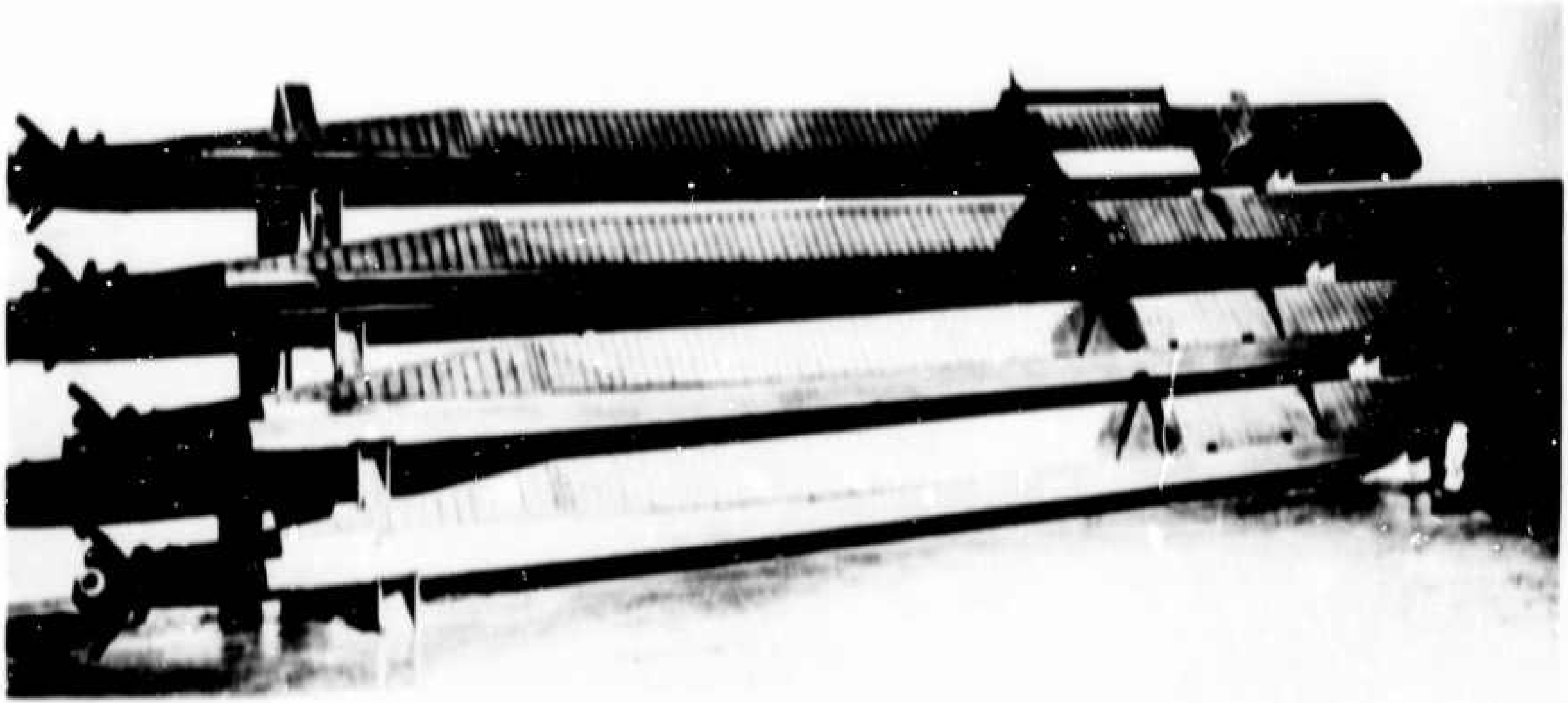

Figure III-8. Fiberglass Blades with Stringers Visible

Figure III-9. Fiberglass Blades (with Stringers) Mounted on Jet Powered HH-43B Helicopter

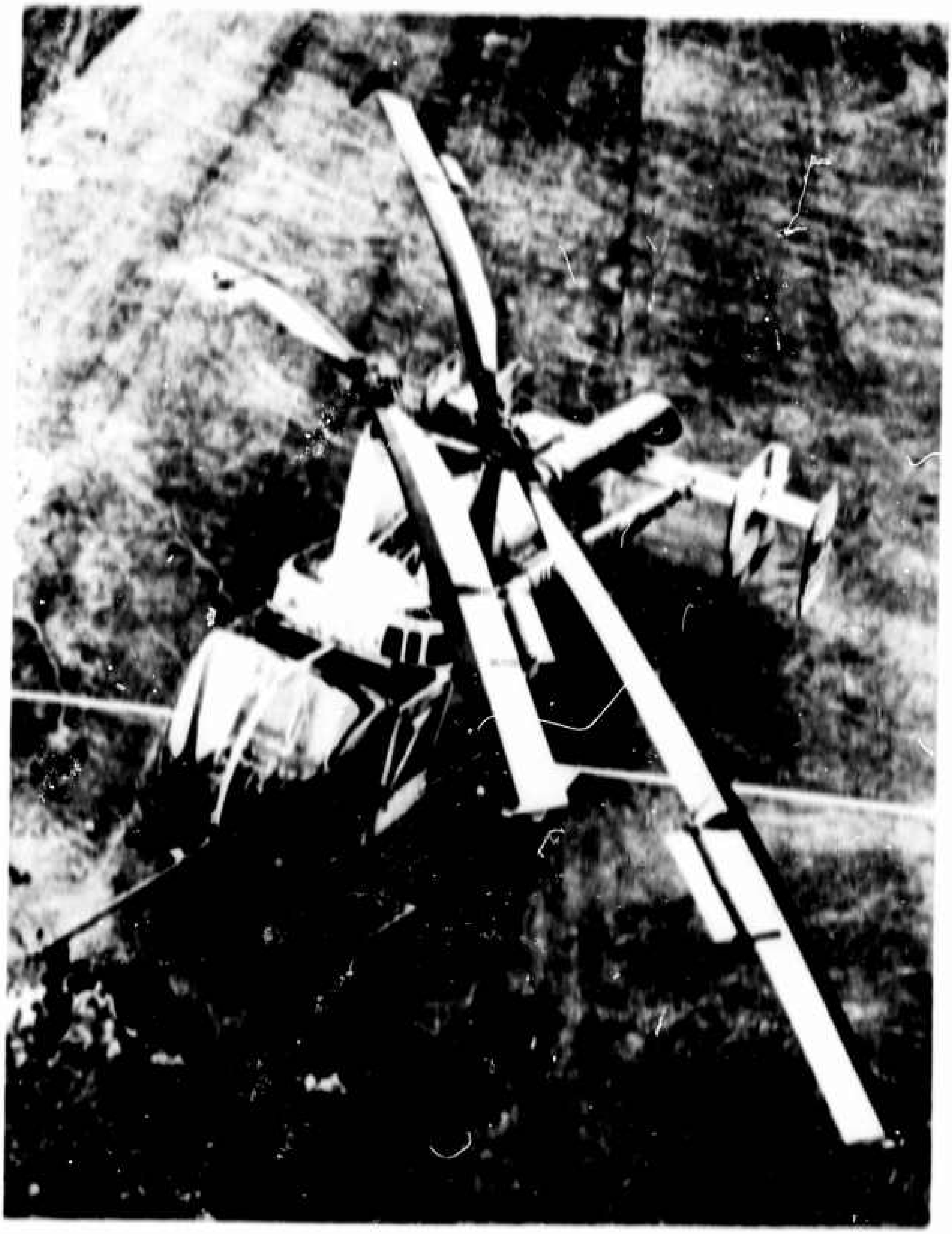

Figure III-10. Fiberglass Blades (with Stringers) Installed o
Helicopter for Flight Test Evaluation

Standard production wooden blades have a torsional spring rate of 285 - 305 inch-pounds/degree, while the prototype glass-fiber blades had a spring rate of 365 - 380 inch-pounds/degree during the first part of this flight program. The added torsional stiffness made it necessary to apply more collective flap to produce the same thrust at a given rotor speed and more cyclic flap to produce the same control moment at a given rotor speed. This slight reduction in controllability was corrected by the reworking done on the prototype glass-fiber blades, which reduced their torsional stiffness to 304 - 314 inch-pounds/degree. Helicopter response to control input after the working was judged by the pilot to be as rapid as with standard wooden blades. A standard HH-43B will normally attain 26 - 28 knots sideward flight at full lateral control; the glass blades were limited to 18 - 20 knots before working and reached 23 - 25 knots after reworking. Full-pedal and partial-pedal hovering turns showed that the glass blades have sufficient control power to meet the directional requirements set forth in MIL-H-8501 (General Requirements for Helicopter Flying and Ground Handling Qualities).

A reduction in vibratory flap bending moments and vibratory blade Station 128 torsion moments was also realized by the reworking to lower torsional stiffness, because less cyclic flap deflection was required to provide the same rotor response. The vibratory root bending moments at Station 31 were not significantly changed by the stiffness change and are within the range of current wooden blade data.

The comparison of vibratory loads illustrated in Figure III-23 and III-25 is somewhat deceptive, because the test helicopter used for the standard blade comparison was not equipped with the more recent 60° engine tailpipe that reduced the amount of longitudinal trim required in forward flight. A basis for comparison can be obtained by noting in Figure III-21 that the vibratory blade root bending moments at Station 31 are reduced 35% at 100 knots by the addition of the 60° tailpipe and that the vibratory flap loads and blade torsional moments would follow this reduction. Application of this correction to data in Figures III-23 and III-25 shows that the vibratory loads for the glass-fiber blades are about the same as for the production wooden blades.

It is important to note that the fatigue life of the prototype glass-fiber blades is about three times that of production wooden blades at the same torsional moment levels, based on fatigue tests conducted by the contractor on torsion area specimens. The glass blade configuration "after rework" corresponds to the torsion area specimens tested.

Blade root flatwise bending moments at Station 31, both steady and vibratory, agree very well with those of the standard production configuration, as illustrated in Figures III-15 and III-21. Bending moment distributions along the blade are also shown in Figures III-12, III-13, and III-14 at the three gross weights flown. Another check on the flatwise bending moment comparison can be observed in Figure III-27, where the engine differential torque pressures for the two types of blades are seen to agree quite well. Since both rotor configurations are absorbing the same engine power and they are similar in mass distribution, flatwise stiffness and aerodynamics, the lift and centrifugal force distributions are the same; hence, the steady root bending moments are the same. By the same reasoning, the trim moments applied by the rotor must produce the same vibratory root bending moments.

In order to assess the vibratory characteristics of the blades and their effect on the helicopter more completely, a 24-point Fourier analysis was done on each blade parameter recorded to extract the first four rotor harmonics from the vibratory loadings. The total vibratories were also read separately for selected parameters of interest.

The vibratory flatwise bending moments at four stations along the blade are presented by harmonics in Figures III-16 through III-19, where it can be seen that the 2/rev. component is the most significant and is typical of a two-bladed rotor. Total vibratory flatwise bending moments are plotted in Figures III-20, III-21, and III-22.

Vertical accelerations at the pilot's seat were also reduced to four rotor harmonics to evaluate the contribution of each harmonic component to the total vibratory acceleration. The results can be seen in Figure III-28, where the major components are 2/rev. and 4/rev. The total vibratory levels at the pilot's seat are slightly lower than those of the production configuration at the high-speed end of the flight envelope for the prototype glass-fiber blades after they were reworked to reduce torsional stiffness. The levels with the glass blades installed before reworking are slightly higher than production levels, which demonstrates the importance of proper tuning of the blade torsional natural frequency.

A typical time history of the mild maneuvers which were performed is presented in Figure III-29; the 60-knot cyclic and collective pullout case is listed in Table III-A. The maneuvers listed in Table III-B are those performed after the blade reworking was accomplished.

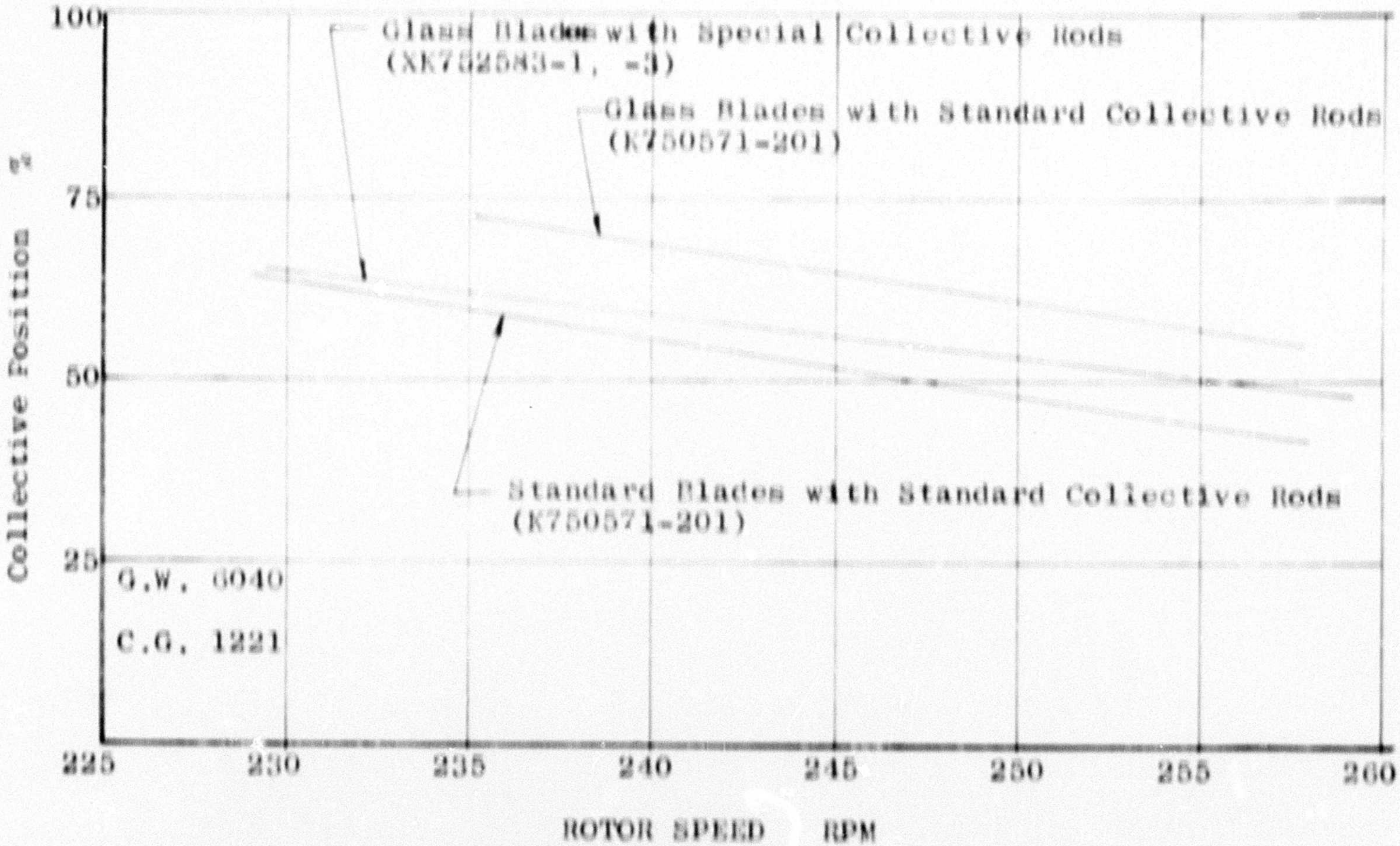

Figure III-11. Collective Stick Position vs. Rotor Speed (Hover)

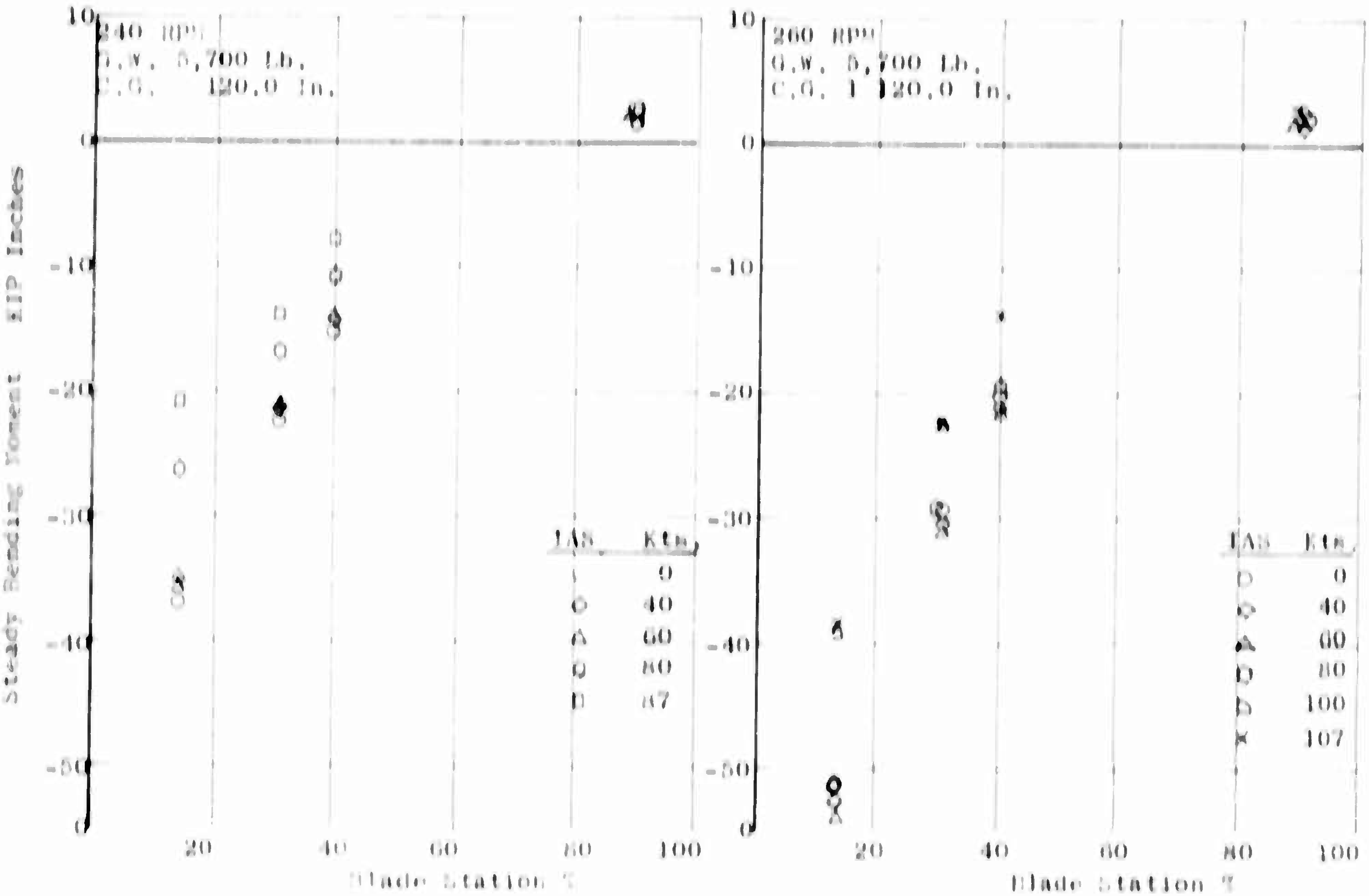

Figure III-12. Steady Flatwise Bending Moment Distribution

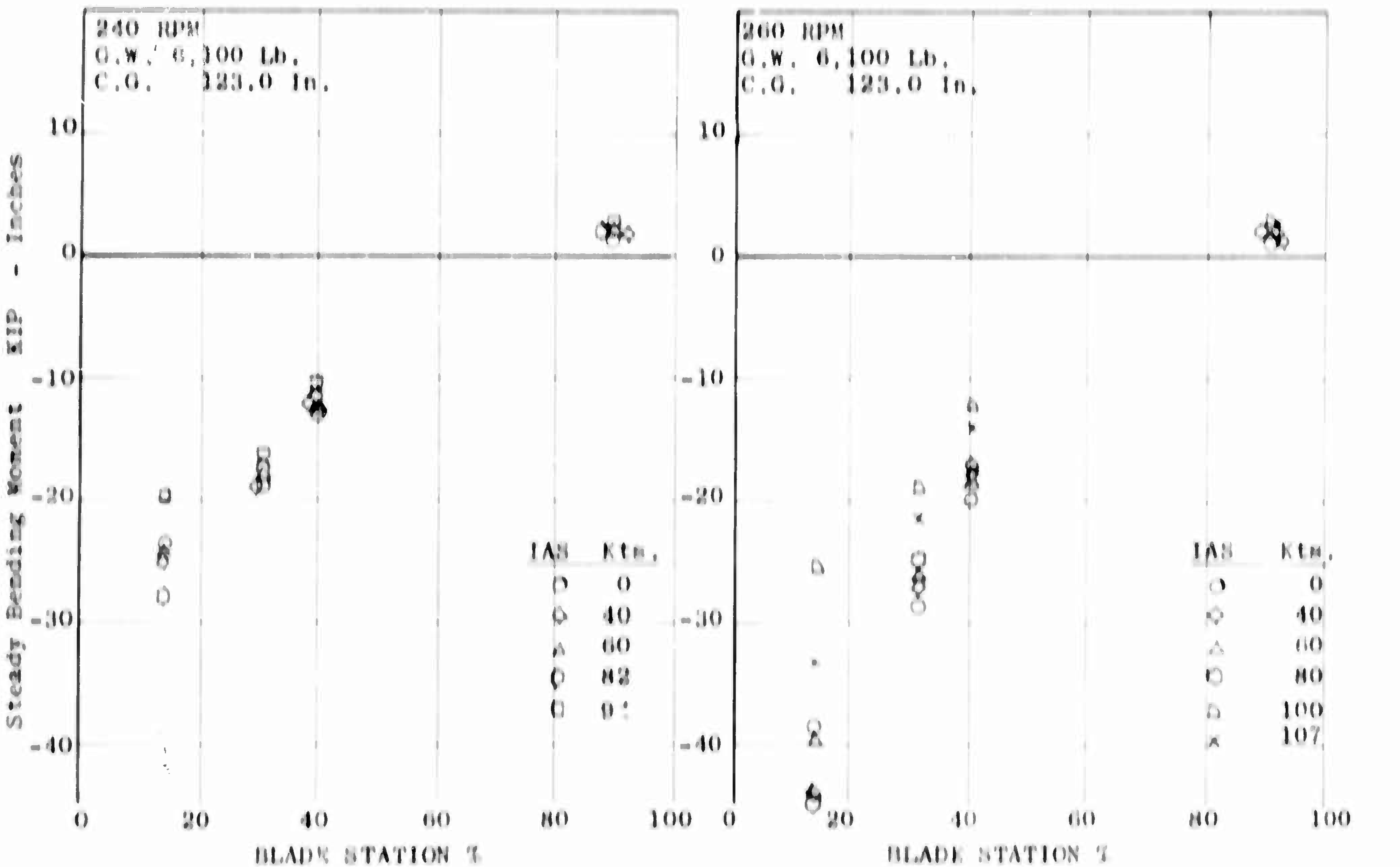

Figure III-13. Steady Flatwise Bending Moment Distribution

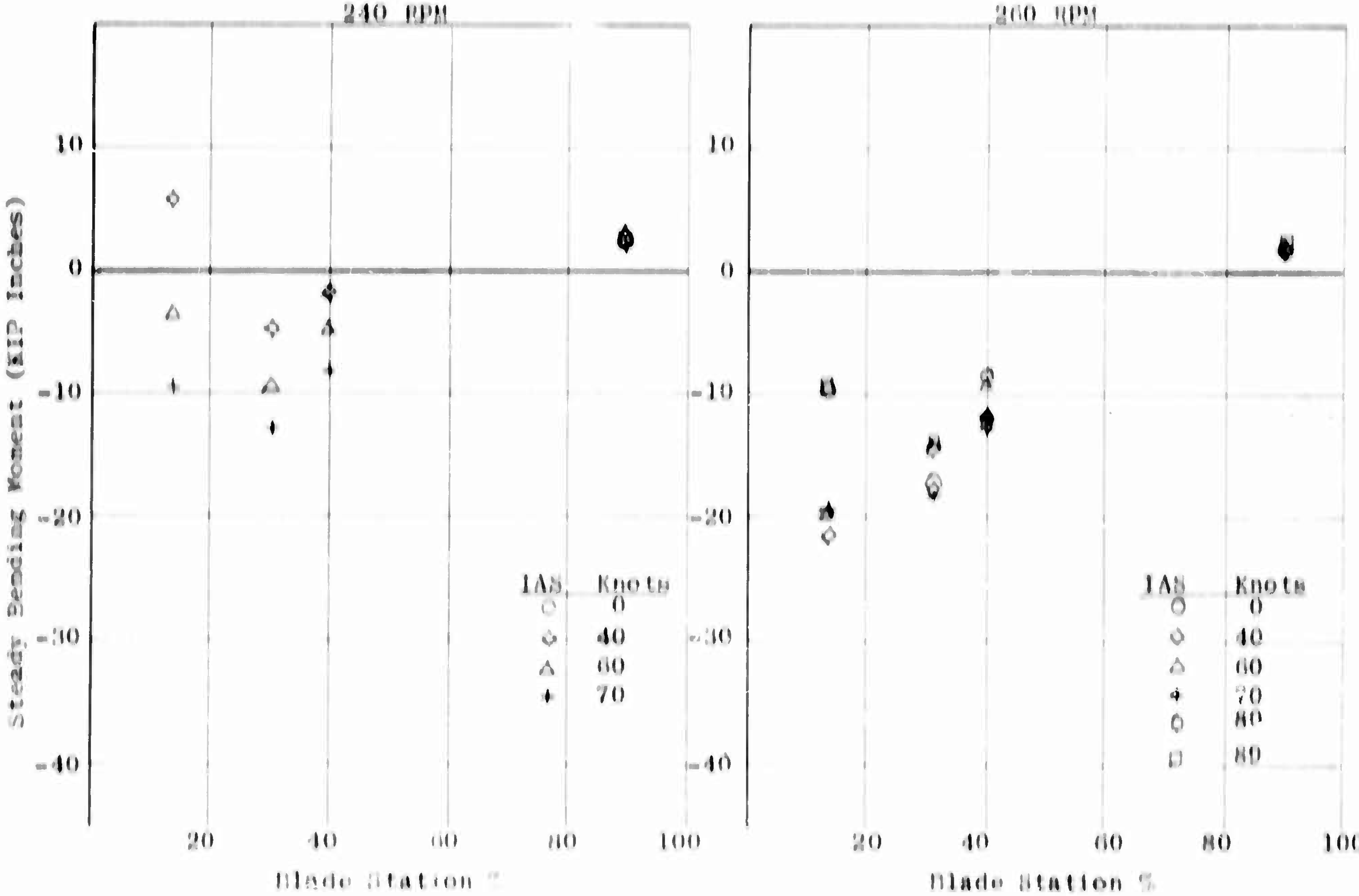

Figure III-14. Steady Flatwise Bending Moment Distribution

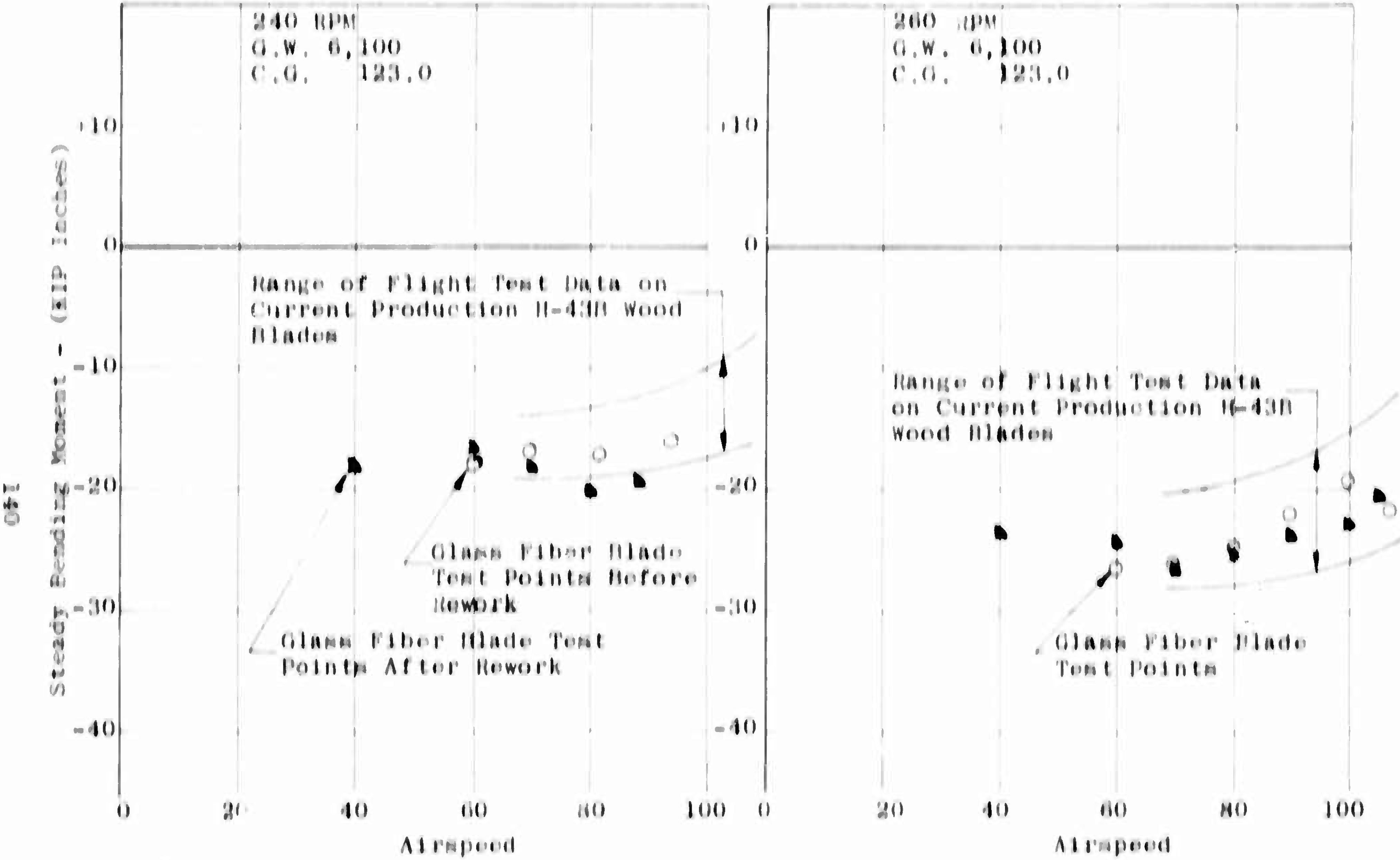

Figure III-15. Steady Flatwise Bending Moment vs. Airspeed

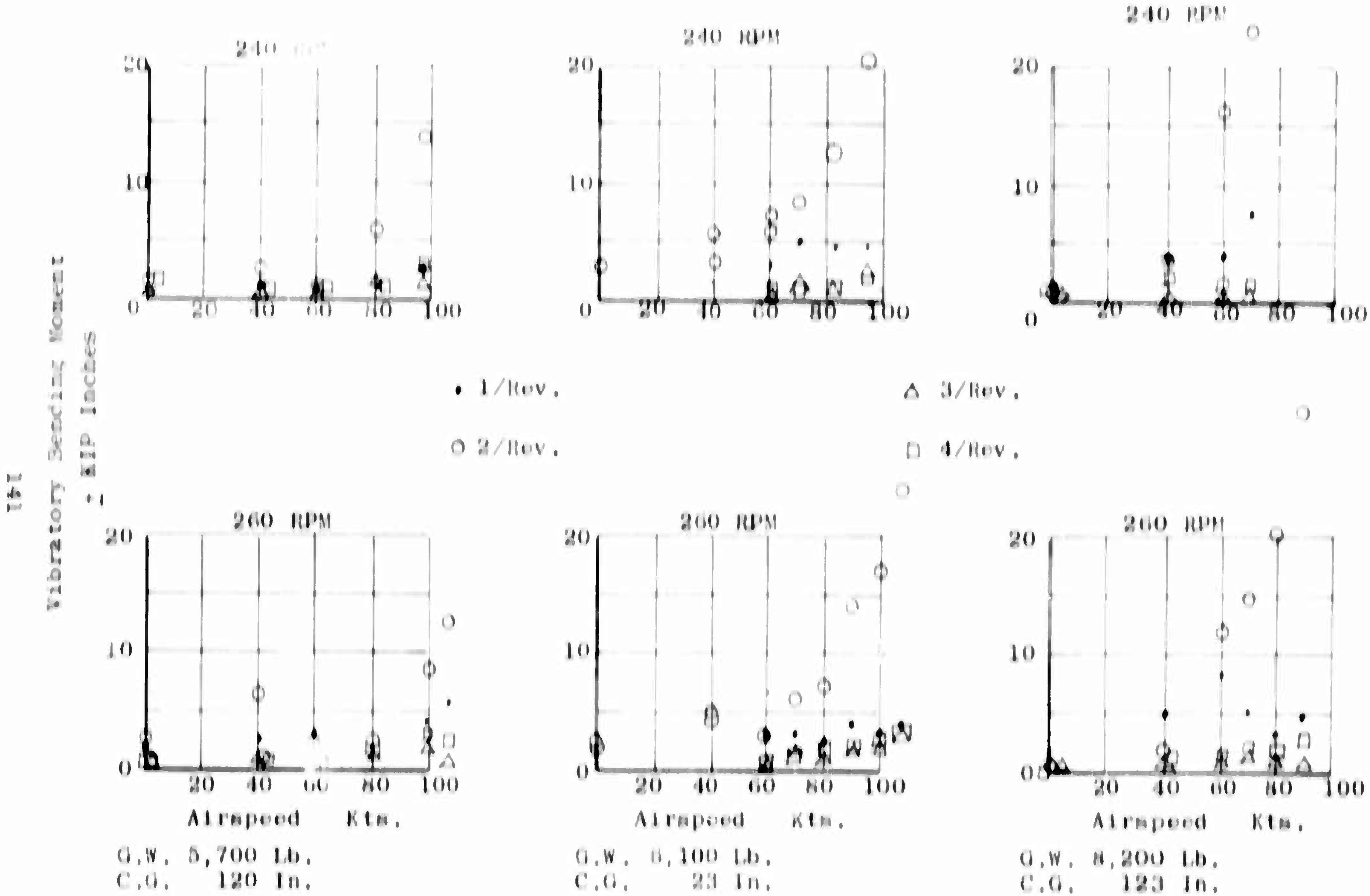

Figure III-16. Vibratory Flatwise Bending Moment vs. Airspeed

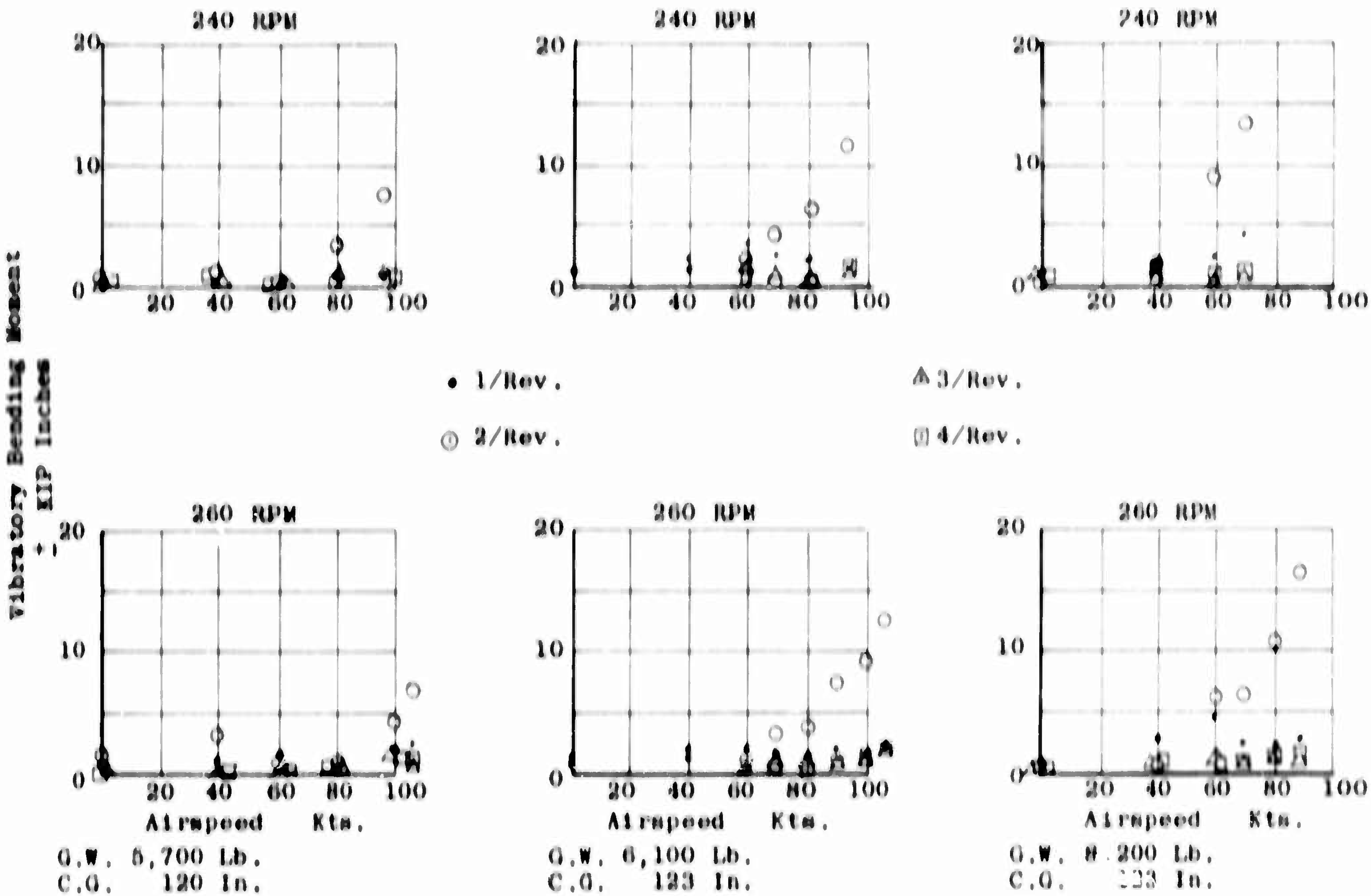

Figure III-17. Vibratory Flatwise Bending Moment vs. Airspeed

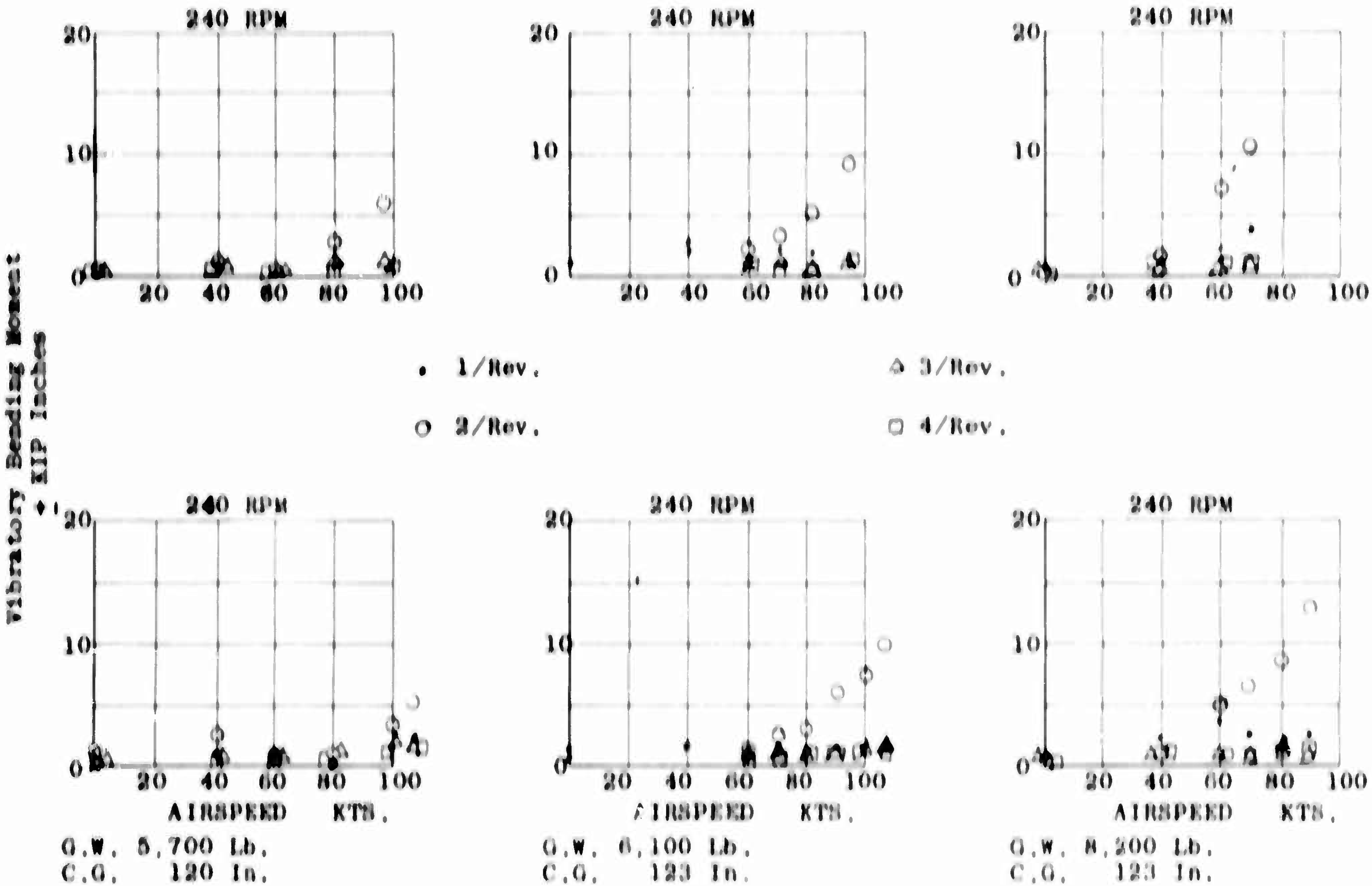

Figure III-18. Vibratory Flatwise Bending Moment vs. Airspeed

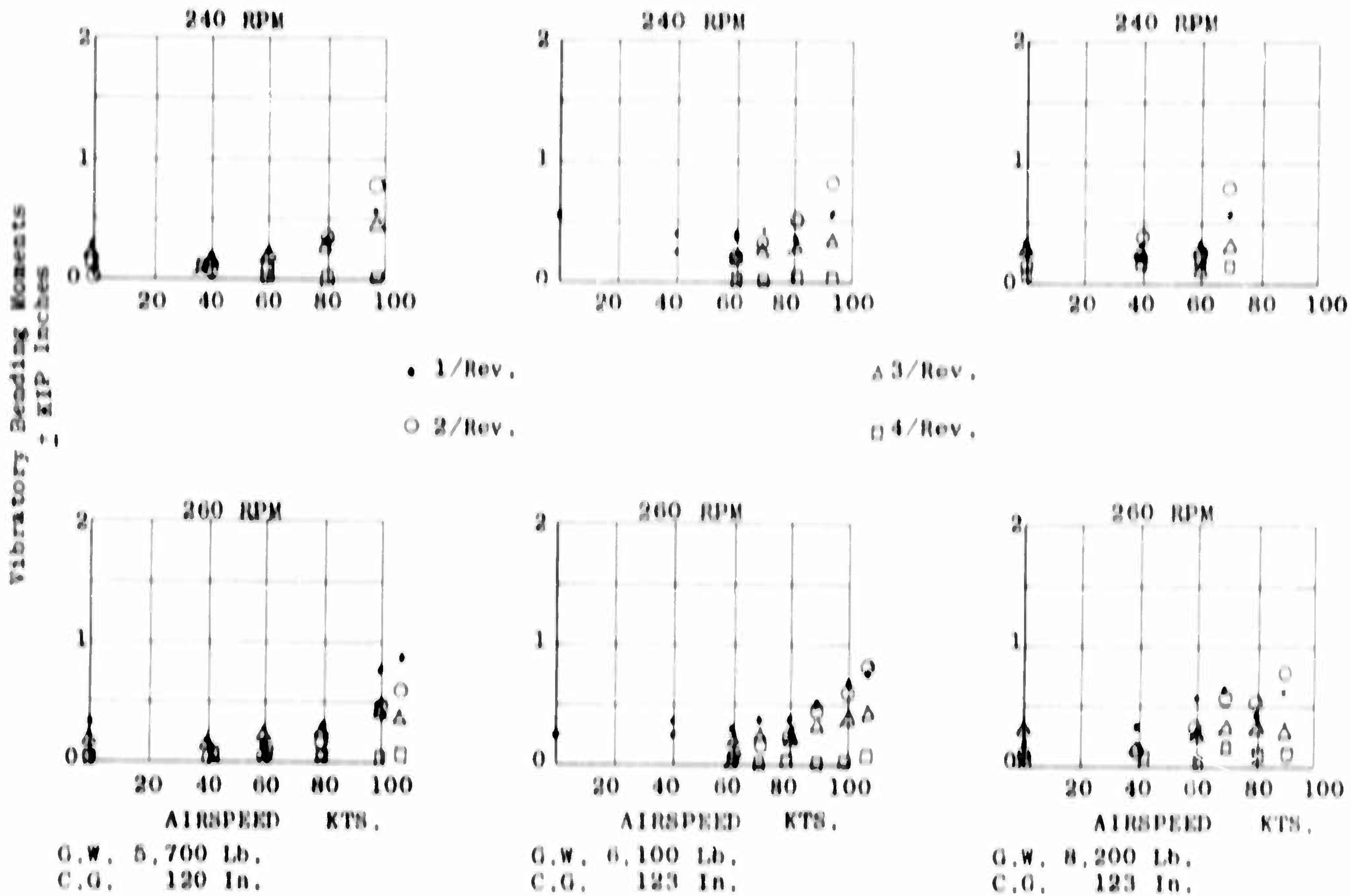

Figure III-10. Vibratory Flatwise Bending Moment vs. Airspeed

BLANK PAGE

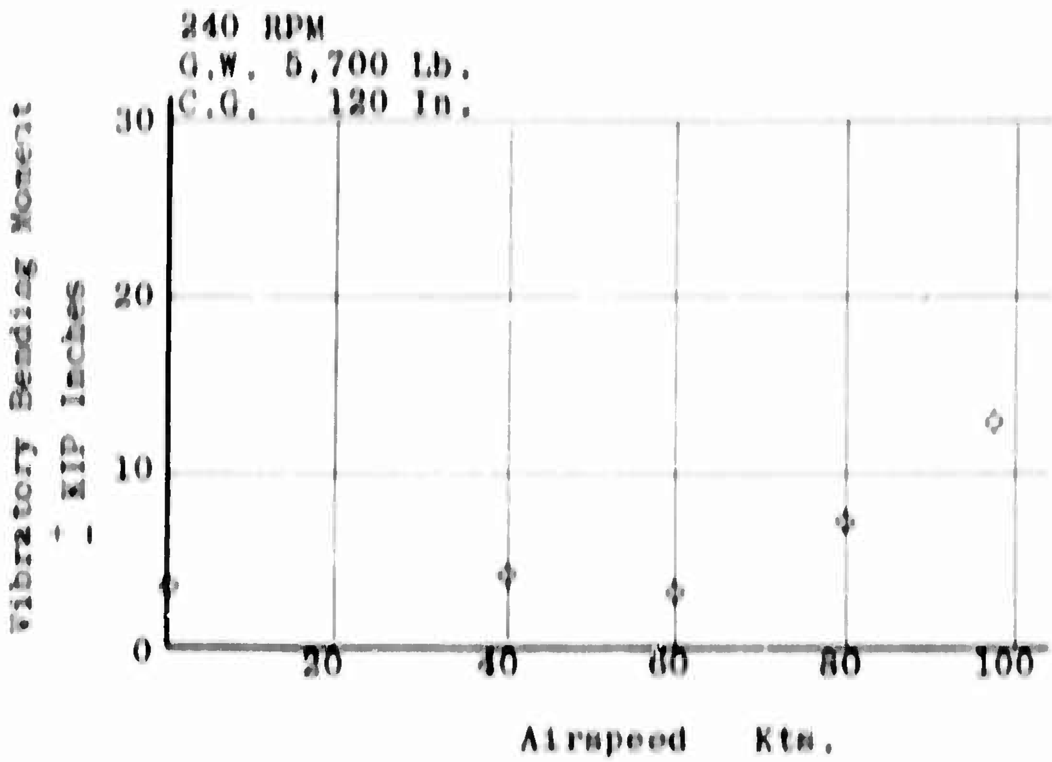

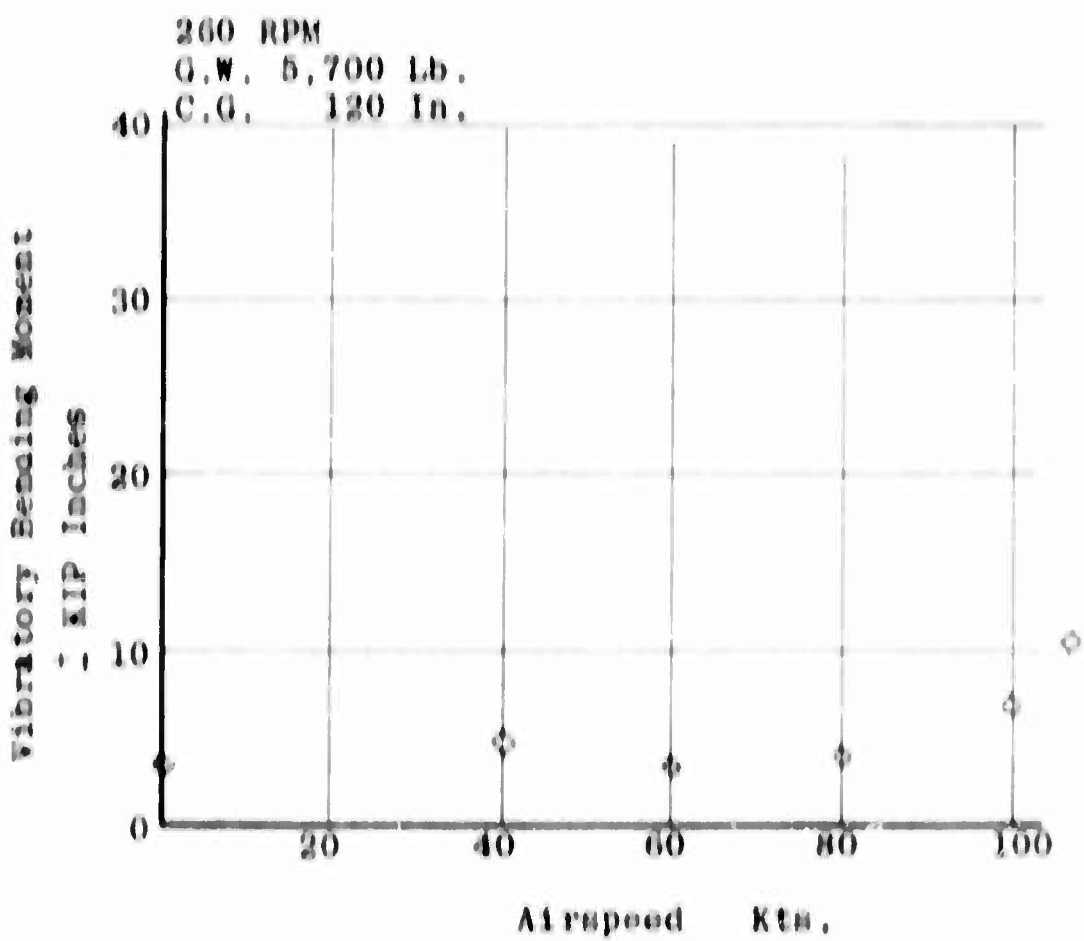

Figure III-20. Total Vibratory Flatwise Bending Moment vs. Airspeed

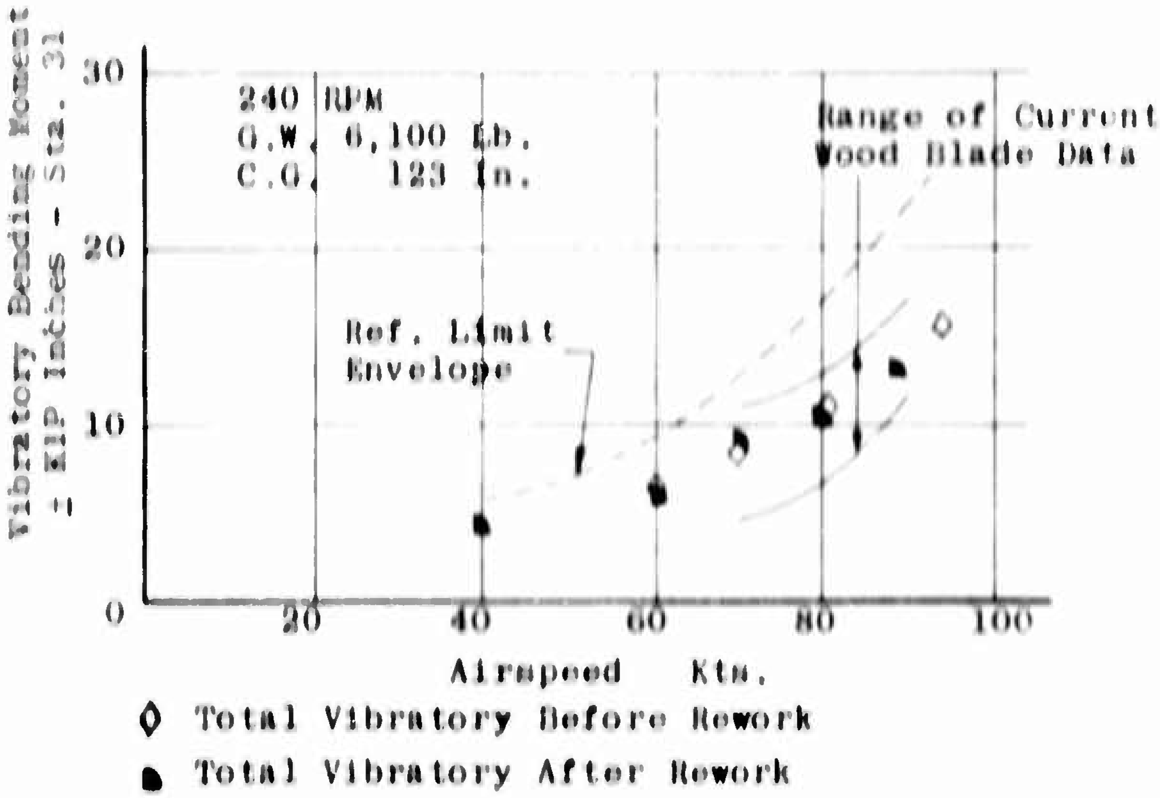

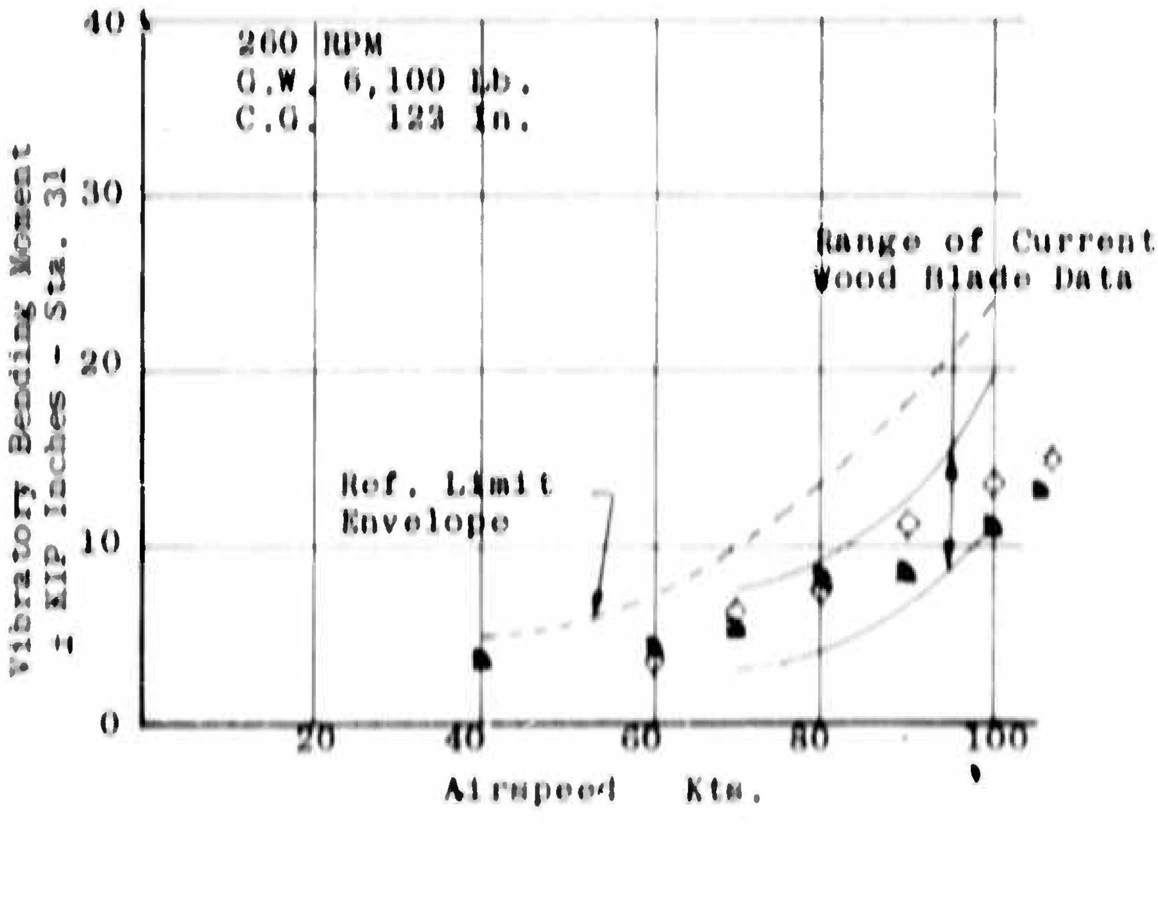

Figure III-21. Total Vibratory Flatwise Bending Moment vs. Airspeed

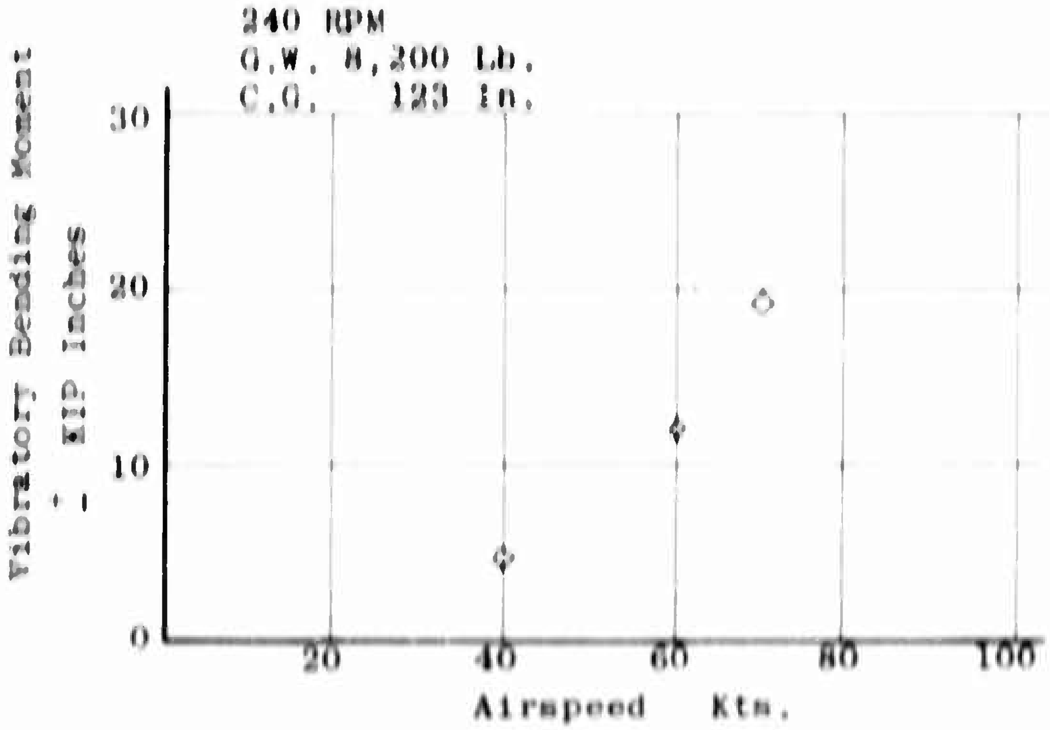

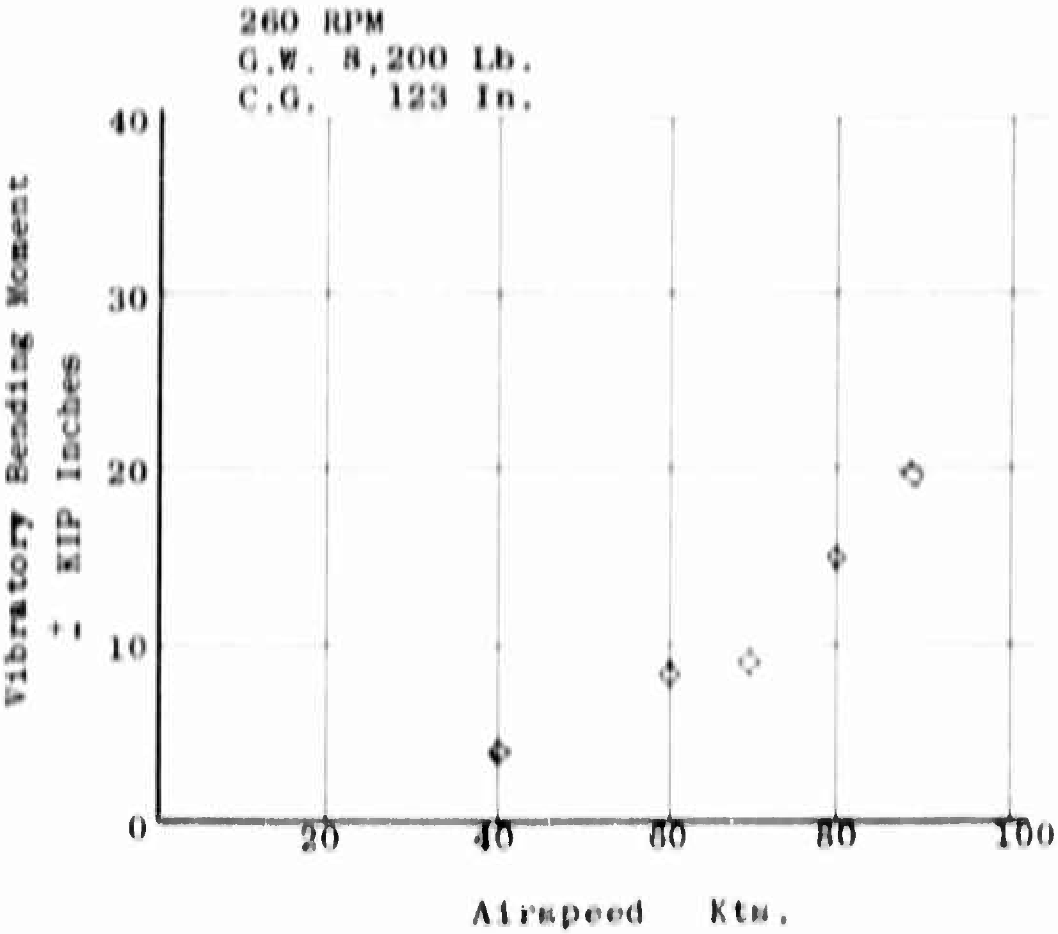

Figure III-22. Total Vibratory Flatwise Bending Moment vs. Airspeed

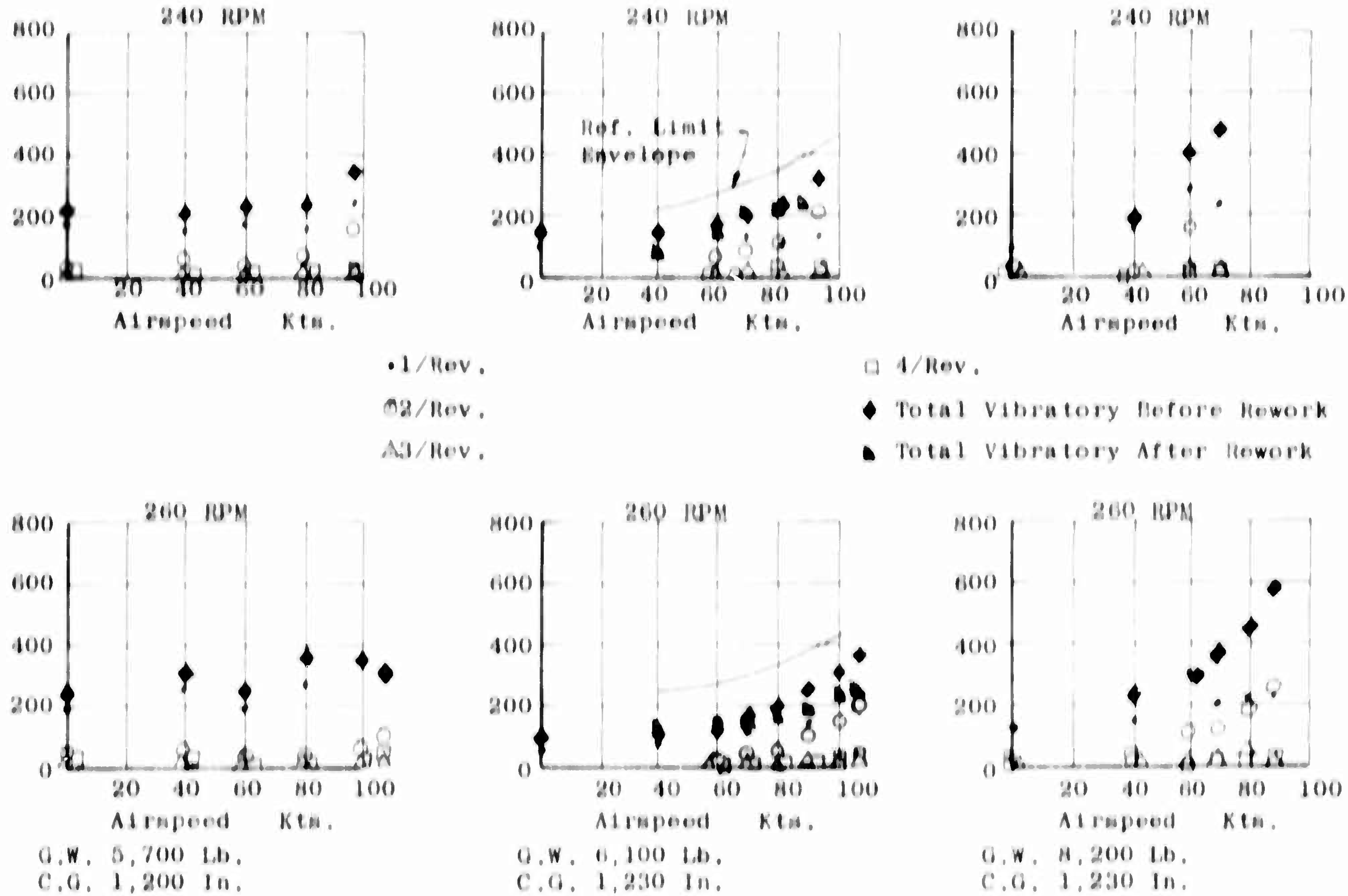

Figure III-23. Vibratory Flap ℄ Bending Moment vs. Airspeed

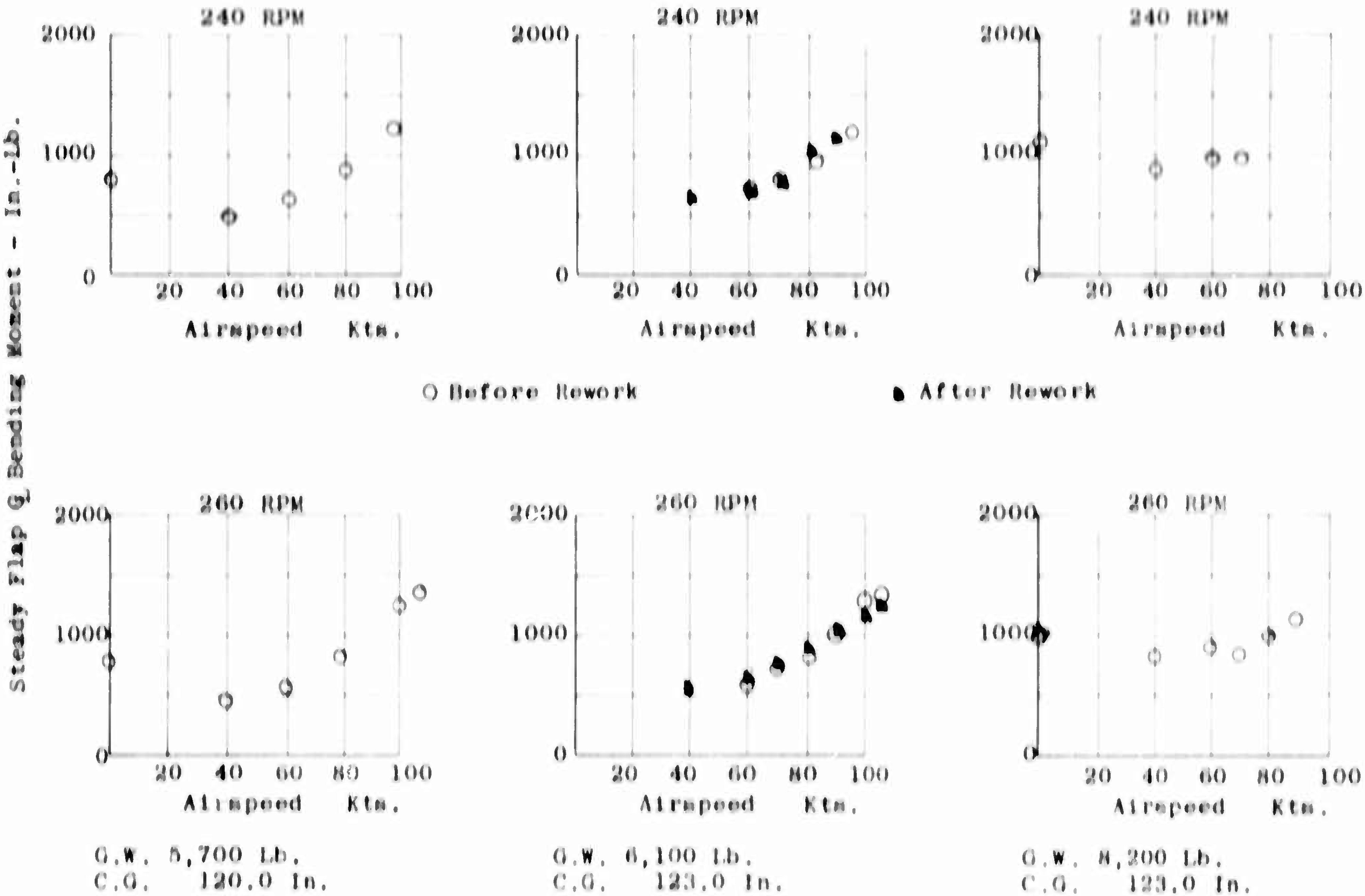

Figure III-34. Steady Flap ℄ Bending Moment vs. Airspeed

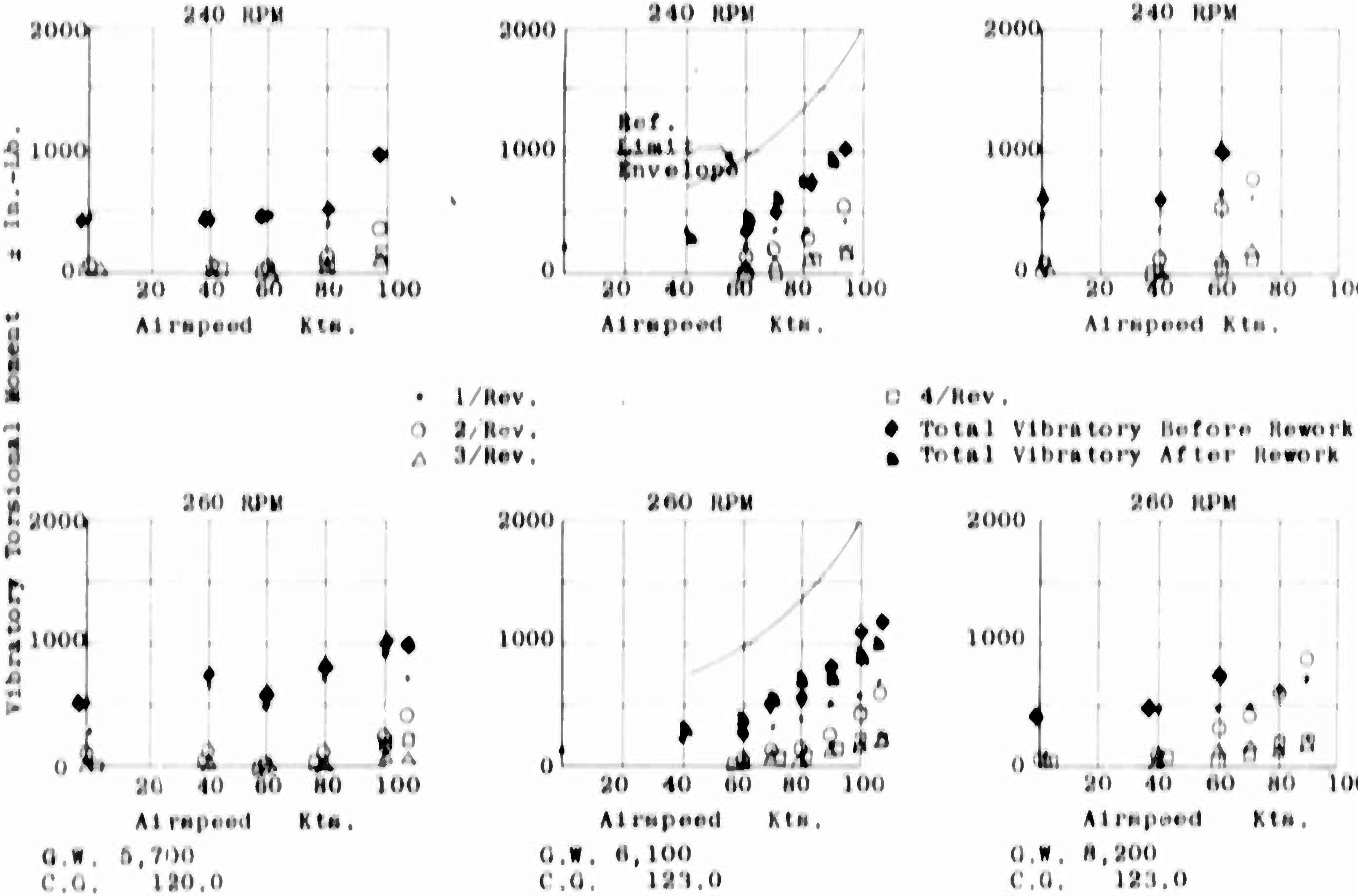

Figure III-25. Vibratory Torsional Moment vs. Airspeed

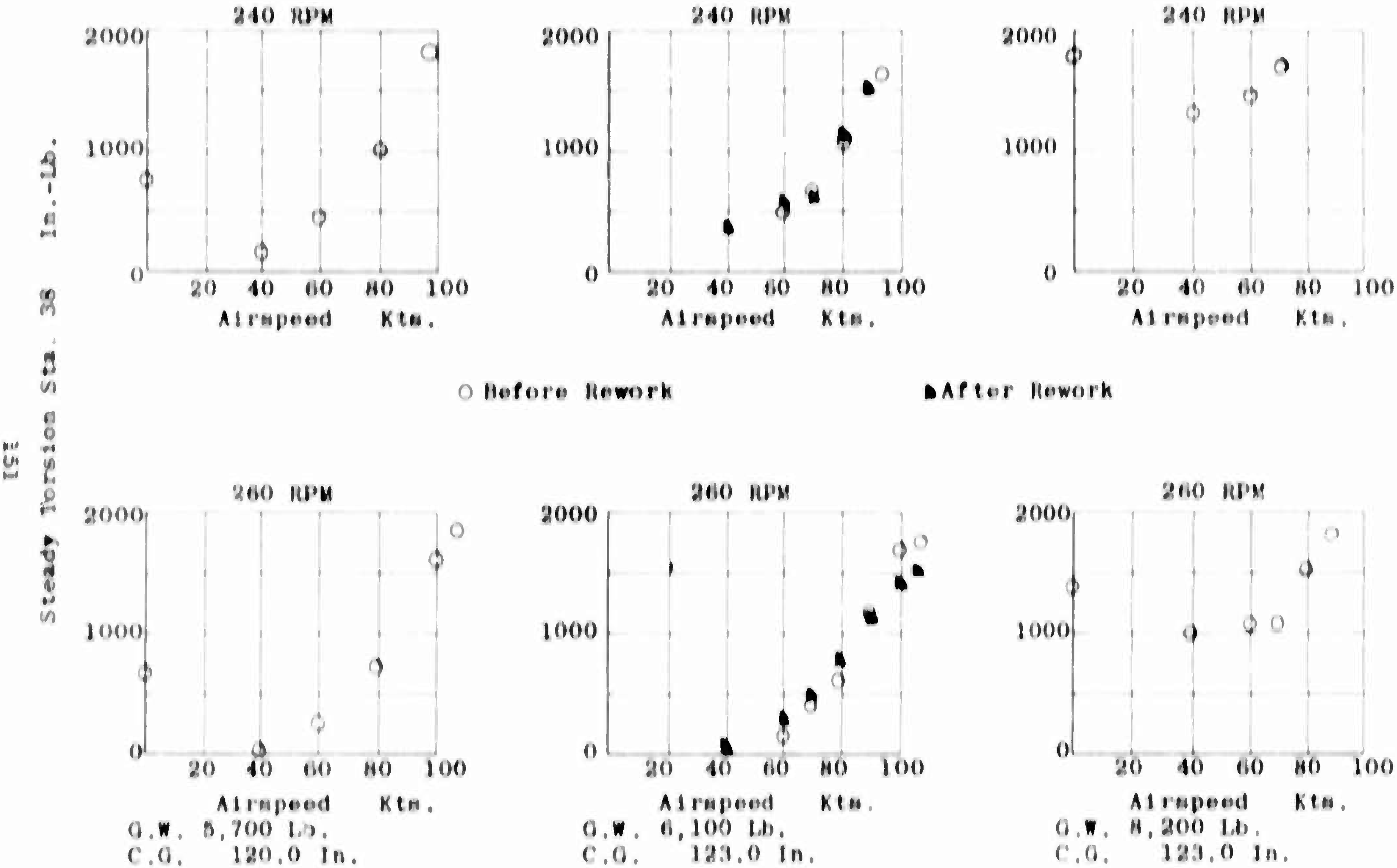

Figure III-26. Steady Torsional Moment vs. Airspeed

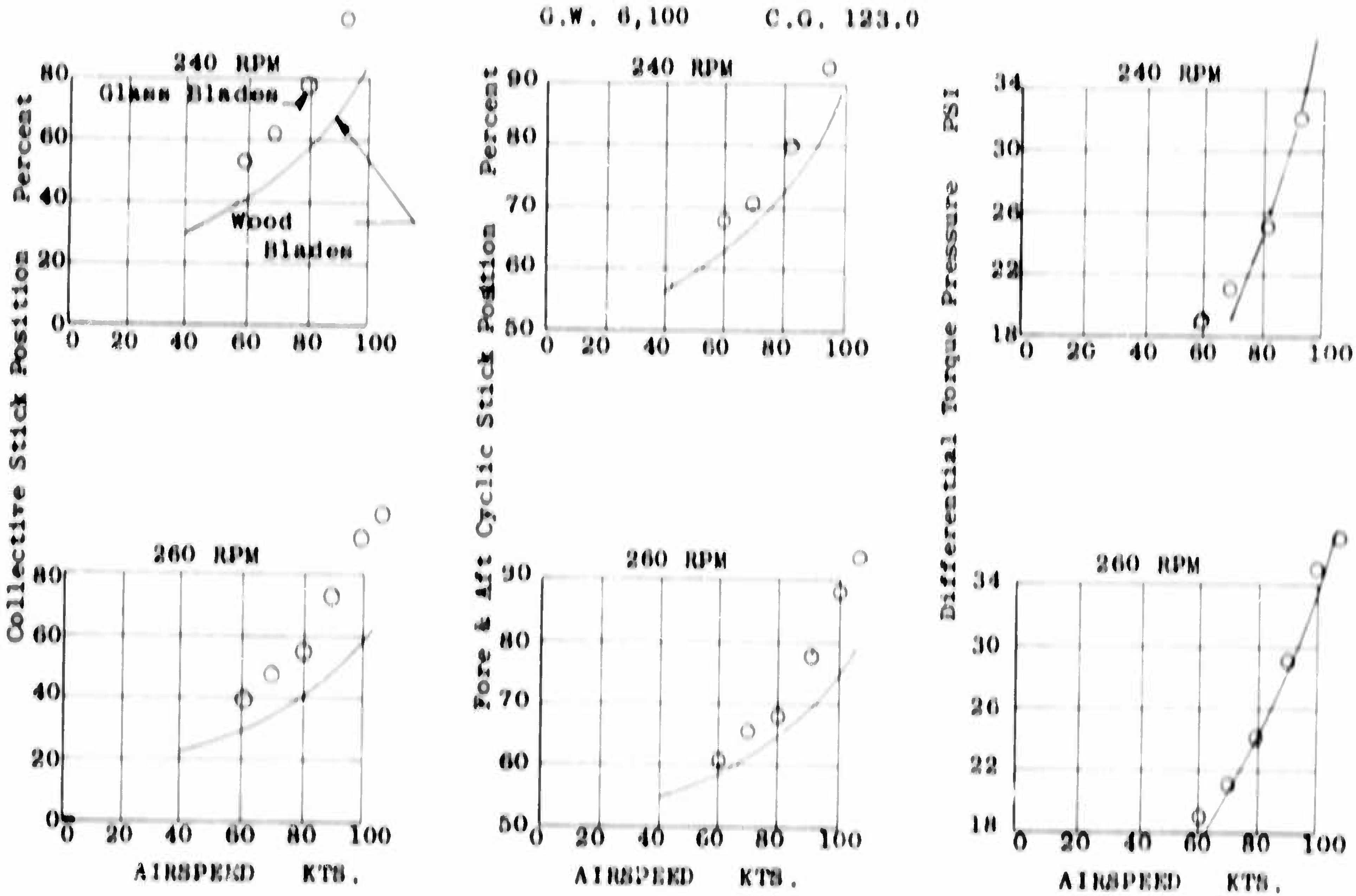

Figure III-27. Controllability and Power

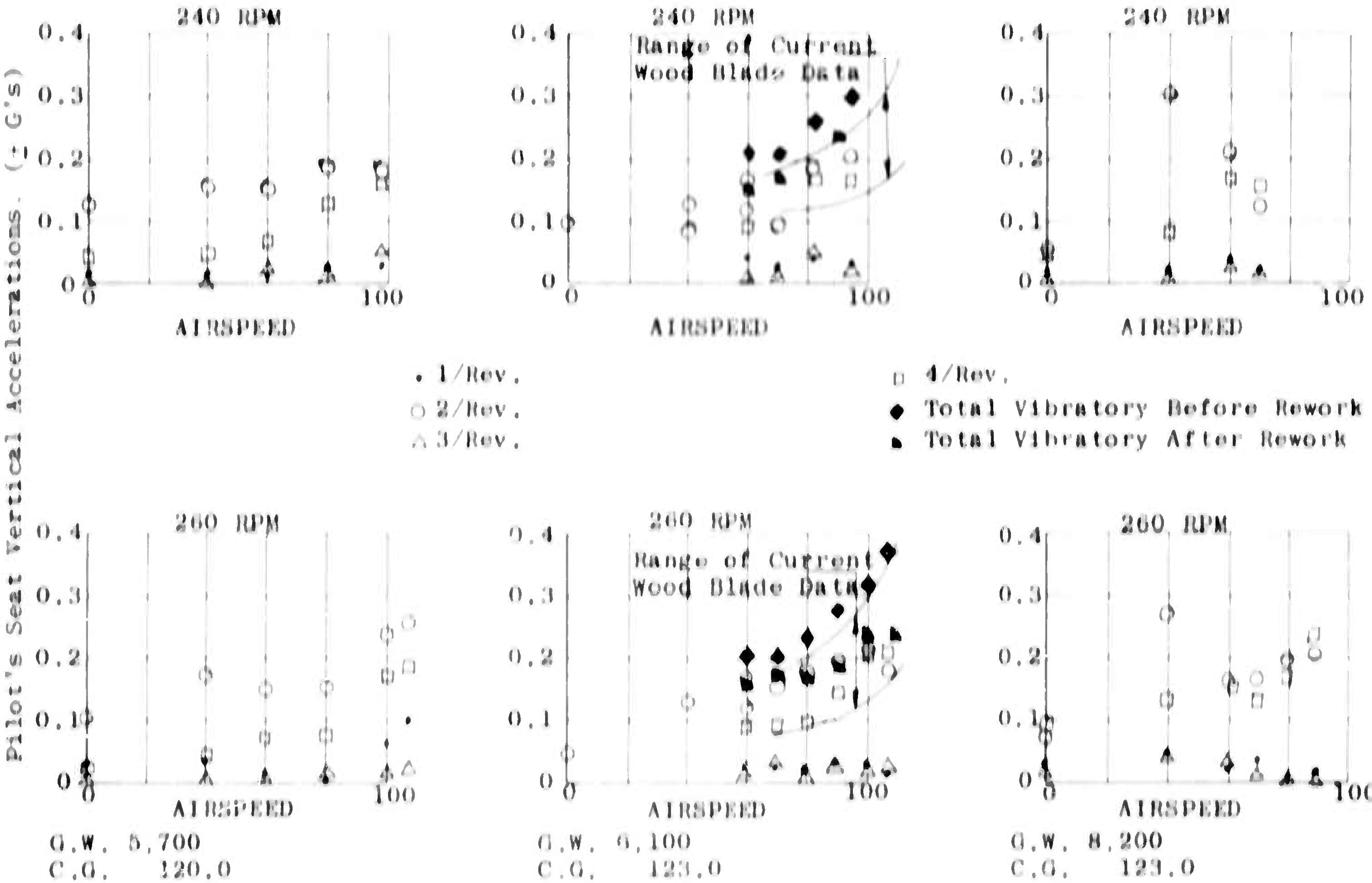

Figure III-28. Pilot Seat Vertical Accelerations vs. Airspeed

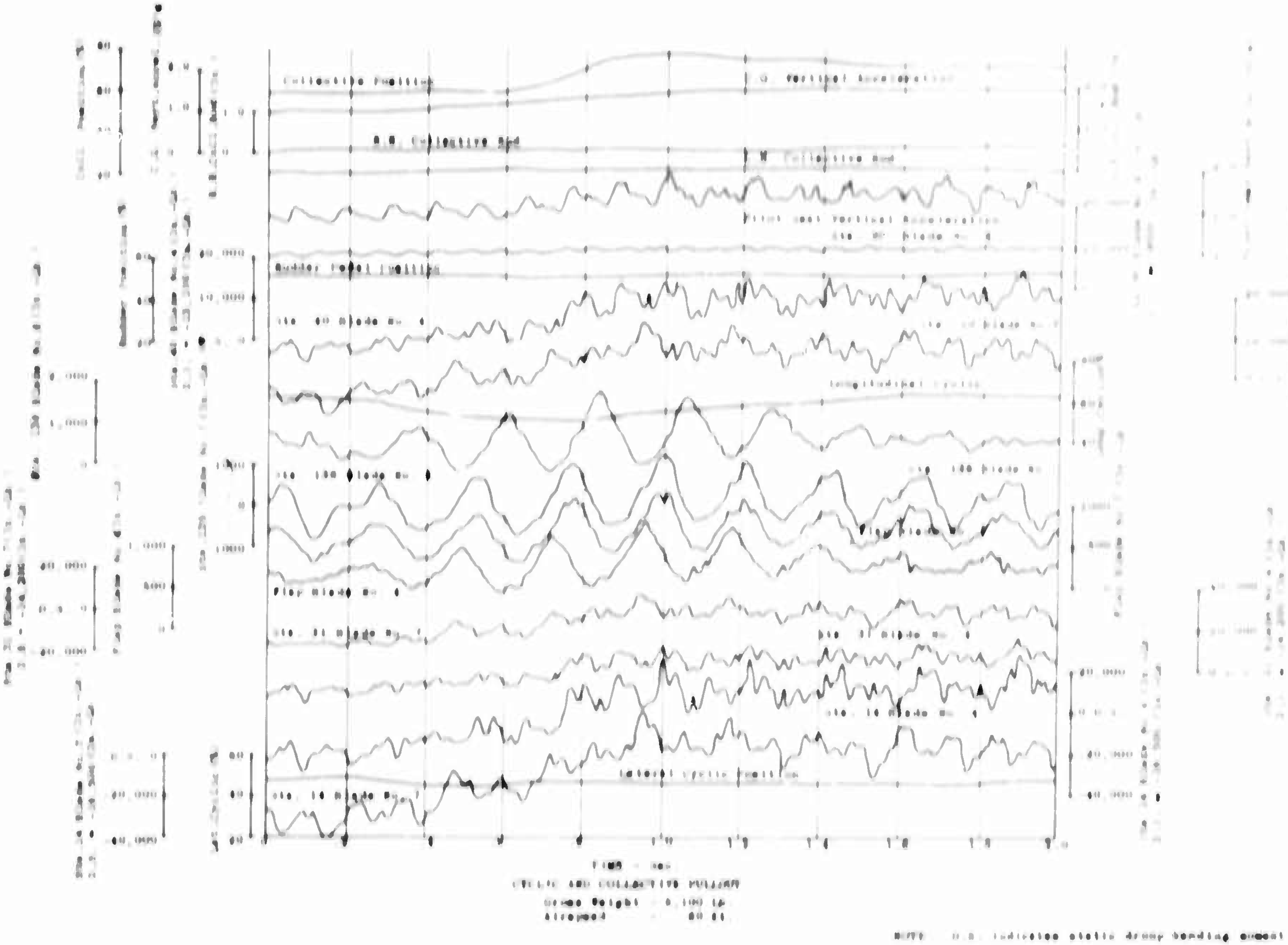

Figure III-20. Cyclic and Collective Pullout

Table III-A

Summary of Maximum Moments recorded in Mild Maneuvers and Cyclic Flares with the C.G. located at Station 123, Gross Weight as noted. All maneuvers were done at 260 RPM Rotor Speed.
BEFORE TORSIONAL STIFFNESS REDUCTION

Maneuver	Gross Weight	Station 31 Steady ± Vibratory		Station 138 Steady ± Vibratory		Flap ℄ Steady ± Vibratory		Max. G's
Cyclic & Collective Pullout 60 Kts.	6100	-8,200 ±	5,000	800 ±	900	- 800 ±	375	1.50
	8200	800 ±	7,000	1,200 ±	695	- 750 ±	250	1.55
Cyclic & Collective Pullout 80 Kts.	6100	-5,100 ±	10,700	1,100 ±	800	-1,050 ±	350	1.55
	8200	6,800 ±	12,500	1,560 ±	830	- 950 ±	350	1.50
Cyclic & Collective Pushover	6100	-31,200 ±	3,000	-1,000 ±	1,150	0 ±	475	0.45
	8200	-42,200 ±	4,000	- 570 ±	1,310	0 ±	400	0.50
Cyclic Pushover 30 Kts.	6100	-47,200 ±	6,000	-1,150 ±	1,150	100 ±	450	0.50
	8200	-42,200 ±	8,000	- 650 ±	925	- 200 ±	450	0.50
100% Right Pedal Sideslip 80 Kts.	6100	-19,685 ±	4,550	1,000 ±	1,070	-1,000 ±	425	1.00
	8200	5,500 ±	7,350	1,760 ±	1,420	-1,160 ±	460	1.00
100% Left Pedal Sideslip 80 Kts.	6100	-20,954 ±	3,400	1,425 ±	670	-1,170 ±	310	1.00
	8200	-15,250 ±	14,700	1,540 ±	1,680	-1,060 ±	520	1.00
Cyclic Flare 40 Kts.	6100	-22,200 ±	11,000	- 500 ±	2,250	- 200 ±	900	1.20
	8200	-21,200 ±	7,000	280 ±	1,460	- 300 ±	600	1.20
Cyclic Flare 60 Kts.	6100	-17,200 ±	13,500	- 300 ±	2,550	- 300 ±	1,050	1.40
	8200	-16,200 ±	9,000	- 370 ±	1,540	- 50 ±	650	1.35

Table III-B

Summary of Maximum Moments Recorded in Mild Maneuvers and Cyclic Flares at a Gross Weight of 6,100 pounds and C.G. at Station 123.0 Inch.

AFTER TORSIONAL STIFFNESS REDUCTION

Maneuver	Max G's	Station 31 Steady ± Vibratory	Station 128 Steady ± Vibratory	Flap ℄ Steady ± Vibratory
Cyclic & Collective Pullout 60 Kts.	1.88	+ 648 ± 15,940	+1,457 ± 2,010	-1067 ± 733
Cyclic & Collective Pullout 80 Kts.	2.03	+ 3,294 ± 13,102	+1,520 ± 1,696	-1,137 ± 641
Cyclic & Collective Pushover 30 Kts.	.28	-43,242 ± 15,285	-1,243 ± 1,645	+ 124 ± 647
Cyclic Pushover 30 Kts.	.42	-46,209 ± 8,734	- 967 ± 1,570	+ 27 ± 608
100% Right Pedal Side Slip 80 Kts.	1.06	-21,406 ± 4,367	+ 741 ± 402	- 782 ± 119
100% Left Pedal Side Slip 80 Kts.	1.07	-28,176 ± 3,275	+ 485 ± 879	- 729 ± 345
Cyclic Flare 40 Kts.	1.23	-17,257 ± 6,551	+ 25 ± 1,281	- 415 ± 496
Cyclic Flare 60 Kts.	1.20	-21,624 ± 3,275	+ 38 ± 502	- 534 ± 253

BLANK PAGE

The prototype glass-fiber blades completed the flight program in excellent condition, and no problems were incurred by the use of fiberglass-reinforced plastic as a structural material.

On the basis of the strain data taken during this flight program and the parallel fatigue testing of specimens, the prototype glass-fiber blades represent a substantial improvement over the current production wooden blades because of the greater fatigue strength of the glass blades.

Further test and development work has been done on area test specimens. A tendency for the root end bolt holes to enlarge under high-load-level fatigue conditions was eliminated by pressing in steel bushings so as to increase the projected area of resisting glass structure. A flap bracket area specimen containing honeycomb filler between ribs in the inboard bracket region accrued 15 x 10^6 cycles before the test was terminated due to a failure of a metallic hardware part. Load levels at the flap centerline for this test represented moderate maneuver conditions.

Blade centrifugal force	5500 lb.
Blade bending	± 1950 in.-lb.
Flap centrifugal force	1040 lb.
Flap bending	- 600 ± 1350 in.-lb.

Torsion specimens with the Scotchply spar and various configurations for aft structure have also been investigated, including rib intercostals, fiberglass honeycomb of various cell sizes, and aluminum honeycomb. A specimen using ¼-inch cell aluminum honeycomb was static tested and then fatigue tested to 30 x 10^6 cycles without failure under a centrifugal load of 18,000 pounds, a torsional vibratory load of ± 3,300 in.-lb., and a flatwise bending moment of ± 330 in.-lb. This torsional loading far exceeds the runout value for wooden blades.

Figures III-30, III-31 and III-32 show typical test plots of the standard wooden blade as compared to the improved all-glass fiber blade.

Figure III-30 represents the lowest mean curve for retention area parts. It is seen that the wooden blade with the original fiberglass cloth reinforced cheek plate was more critical than the weakest hub hardware. The blade was, of course, improved as stated previously in this report; and finally it is seen that the all-fiberglass blade root end with the laminated Scotchply cheek plate exceeds the capabilities of other retention hardware.

Figure III-31 shows the minimum life curve for the torsion area of the production blade. Recalling that the problem with the wooden blade was the spar failures, it is here shown that the fiberglass blade spar "ran out" at projected load levels higher than those at which the wooden spar failed.

Figure III-32 gives the mean curve for the flap bracket area of the standard blade. This area has not been troublesome even with the standard wooden blade, but here again the glass-fiber blade shows at least equal capabilities as evidenced by the test "run outs".

A chronological summary of the glass blade development is shown in Table III-C and Figure III-33.

DAMAGE FROM SMALL-ARMS FIRE

Of recent interest in helicopters is their vulnerability to small-arms fire. In this regard, Kaman initiated a test to determine the damage effect of bullet "hits" upon the rotor blades.

The test was conducted on a torsional area specimen using 30-06 ball ammunition. A .30 caliber rifle was mounted in a vertical plane above the specimen, to which was applied a centrifugal load of 26,000 pounds. An excitation, by means of an electro-magnetic shaker, was also applied to produce vibratory flatwise bending and torsional moments upon the specimen. One round of ammunition was fired into the oscillating blade, which maintained its loading for a short period after the firing, to determine if rapid propagation of the break in the specimen would result. This procedure was repeated until five rounds had pierced the blade: two in the spar, two in the aft structure, and one at the junction of the spar and aft structure.

At the completion of the firing, the blade specimen was subjected to a sustained run at the following loads:

Centrifugal force	26,000 lb.
Torsional moment	± 2,000 in.-lb.
Flatwise bending moment	± 710 in.-lb.

The centrifugal load represents normal flight load, while the vibratory torsion loading exceeds the flight measured values during high-speed level flight. After 182,000 cycles (equivalent to nearly six hours of flight at the 2/rev. loading), a failure in the test fixture terminated the test.

Post-test inspection of the specimen revealed no propagation or delamination in the damaged area. Figures III-34 and III-35 show photographs of the blade specimen after the test.

BLANK PAGE

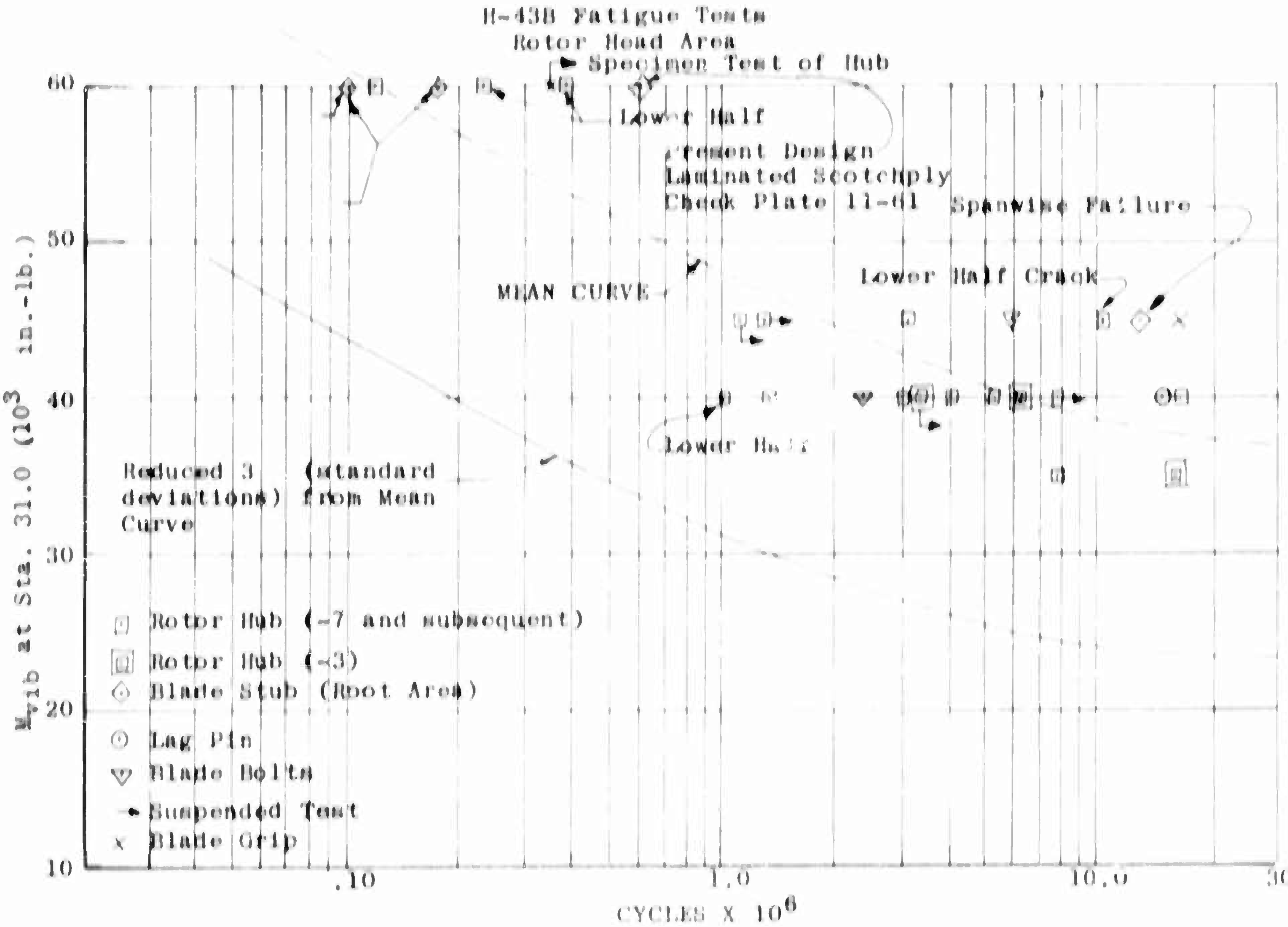

Figure III-30. Rotor Head Fatigue Tests

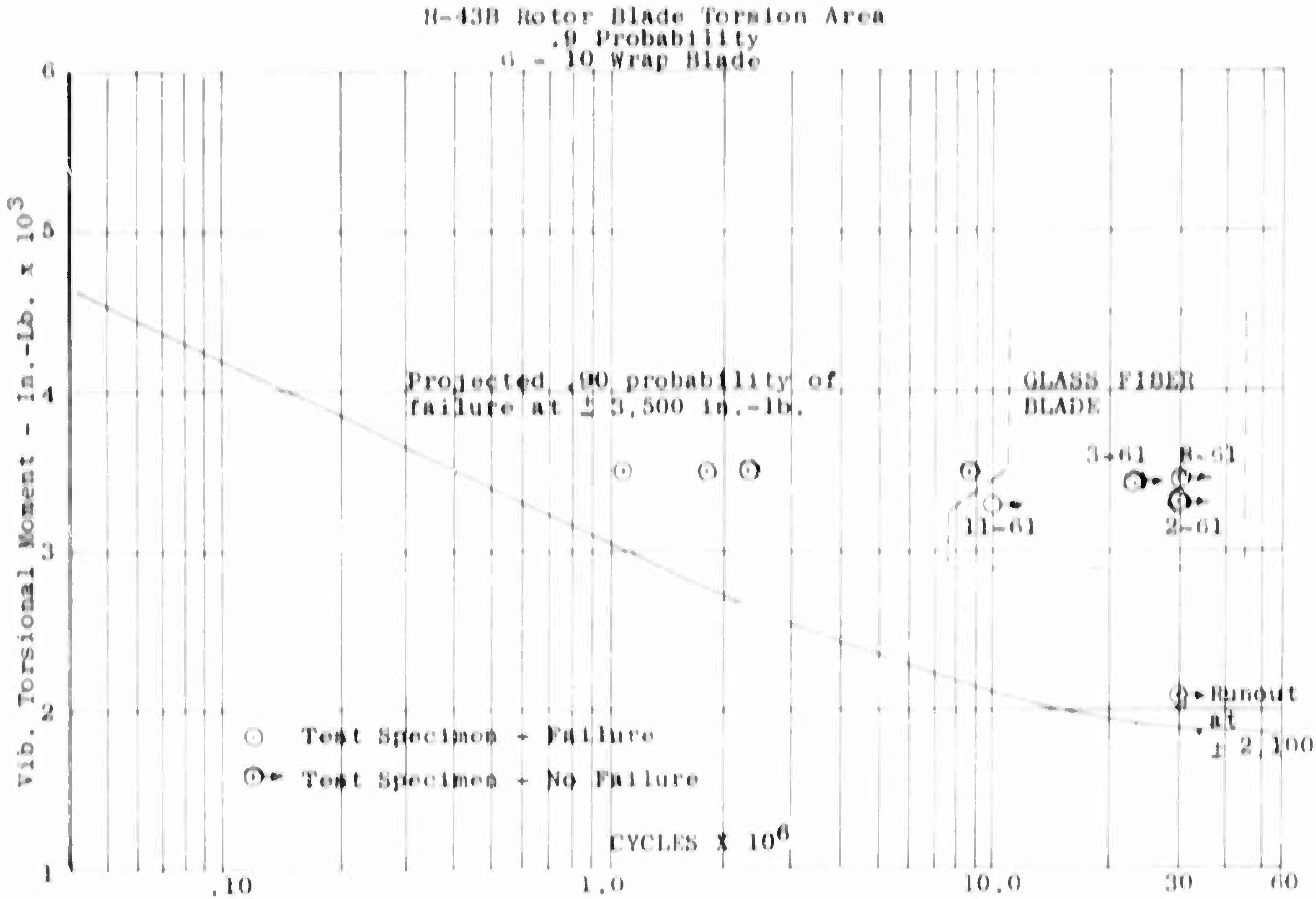

Figure III-31. Rotor Blade Torsional Fatigue Tests

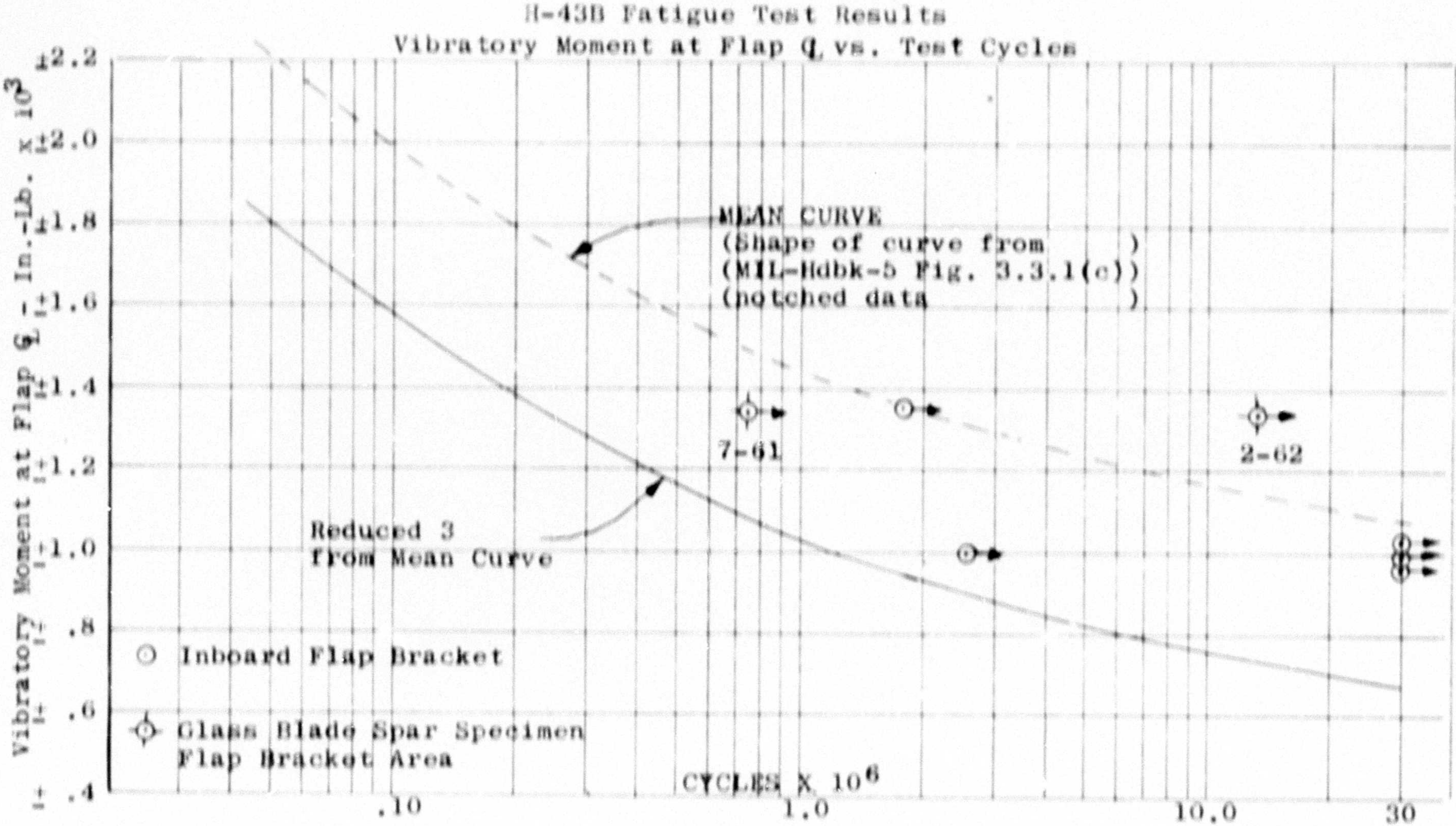

Figure III-32. Rotor Blade Flap Area Fatigue Tests

Table III-C

Load Oriented Glass Fiber Construction in Kaman Rotor Blades (Chronological Summary of)

Note	Development Completed	Structural Description	Proven Endurance Limit
1	1953	3/8" thick No. 162-114 glass cloth plates	± 13,000 in.-lb. (flat-wise bending)
	1956	1/8" thick (SAE 4130) steel plate	± 19,000 in.-lb.
	1957	3/8" thick No. 162-114 glass cloth plates plus 1/8" thick Scotchply plate (unidirectional glass fibers oriented ± 20° to span axis).	± 26,000 in.-lb.
	1959	3/8" thick No. 162-114 glass cloth plates plus 1/8" thick Scotchply plate (unidirectional glass fibers oriented ± 20° to span axis). No. 181 glass cloth shear channels.	± 45,000 in.-lb.
2	1953	Spruce-Maple-.018" steel cap spar	± 1,300 in.-lb. (torsion)
	1956	Spruce-Maple +.010 (1 layer No. 181) glass cloth "C" wrap +.018 steel cap	± 1,700 in.-lb.
	1958	Spruce-Maple +.060" (6 layers No. 181 glass cloth) "D" wrap.	± 2,100 in.-lb.
	1960 (June)	.150 (15 layers No. 181) glass cloth "D"	(Approx. ± 2,100 in.-lb.)

Table III-C (Cont'd.)

Note	Development Completed	Structural Description	Proven Endurance Limit
2 (Cont'd.)	1960 August	.120 in. (12 layers, unidirectional $\pm$ 20^{o} to span axis) plus .150 in. (No. 181 glass cloth) aft channel	$\pm$ 3,600 in.-lb.

Note: 1. Affected Blade Region - Retention (Sta. 12-55)

2. Affected Blade Region - Torsion (Sta. 82-180)

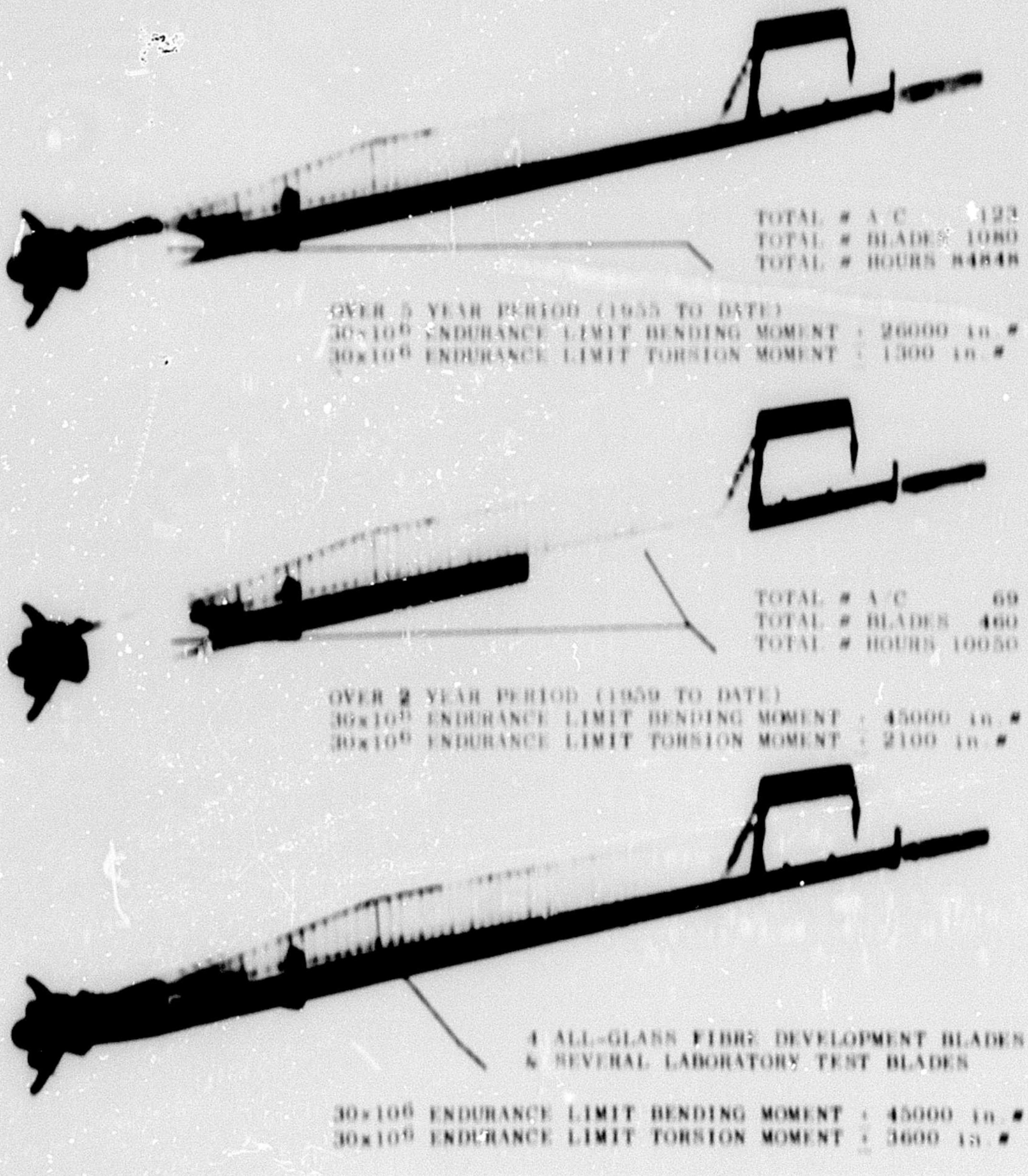

Figure III-33. Applications of Glass Fiber Reinforced Plastic Construction

BLANK PAGE

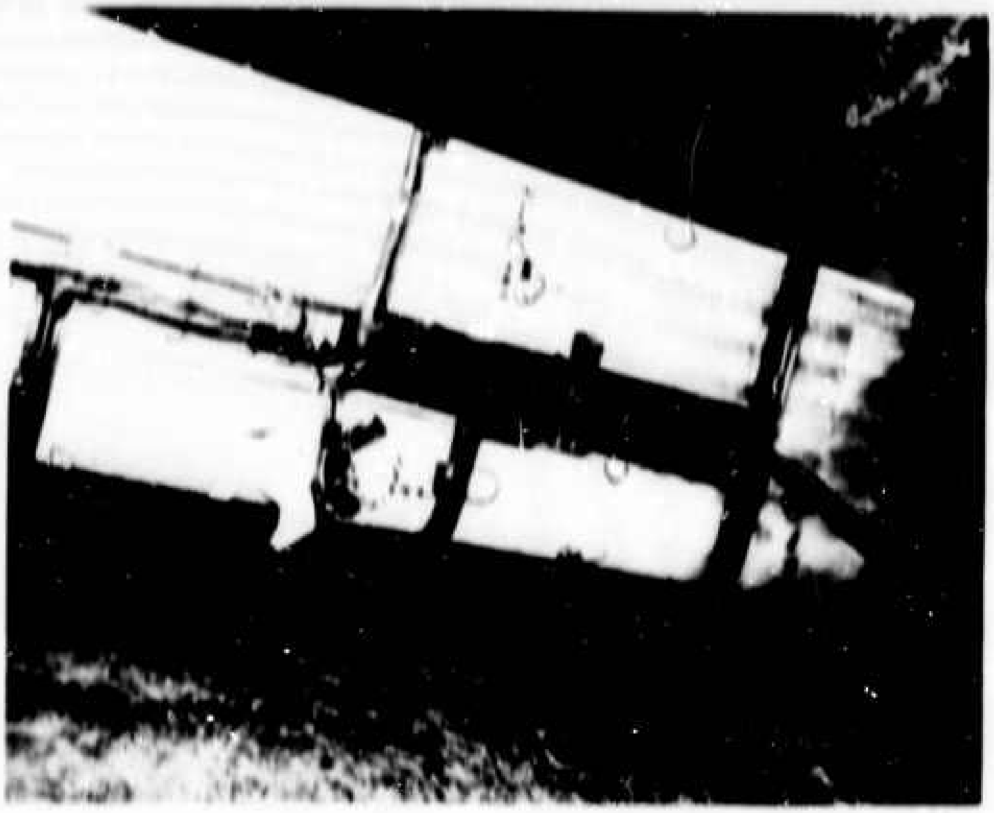

Figure III-34. Fatigue Test of Blade Section Damaged by Rifle Fire

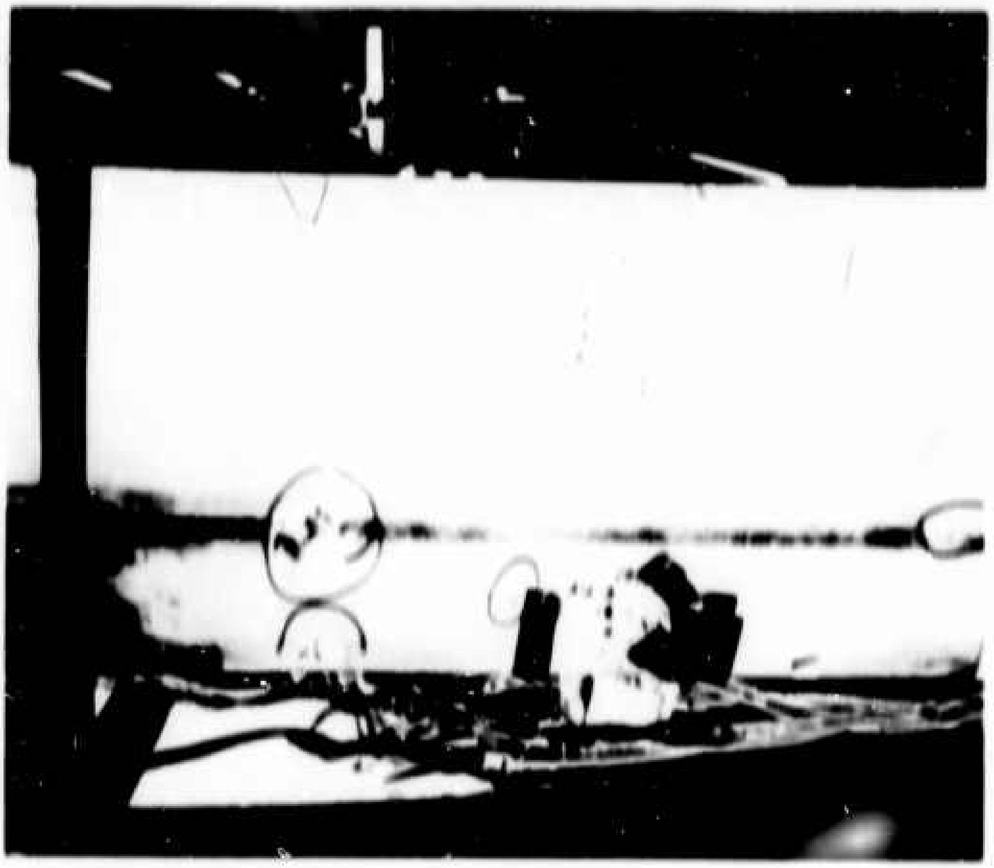

Figure III-35. Fatigue Test of Blade Section Damaged by Rifle Fire

CONCLUSIONS

From the experience gained with fiberglass reinforcements of the highly stressed helicopter wooden rotor blades, the confidence in glass structures is apparent by the Kaman corporate investment of nearly $400,000 to fabricate, test, and develop the afore-discussed all-glass fiber rotor blade. The testing done thus far has authenticated the belief and confidence in the use of fiberglass for primary load-carrying members.

Much more testing can be proposed; however, necessity for financial austerity has precluded the gathering of further desired data at present.

Additional flight strain measurements along with quantities of fatigue tests should be completed to substantiate statistically the strength improvements as mentioned in this report. Maintenance abuses and ground handling problems can be thoroughly investigated to further prove the capability of the all-glass blade as a practical operational component. A test program is also needed to subject this blade to the complete gamut of weather conditions, including the influence of extreme atmospheric environments and the effects of all forms of precipitation and abrasive solid particles, etc. Damage from weapons fire is to be investigated more completely for military applications. The knowledge gained from the use of fiberglass in a complex system such as a helicopter rotor blade indicates unlimited potential for use in other design areas where weight, strength, and endurance are prime parameters.

SECTION IV

EVALUATION OF THE EFFECT OF WEATHERING AND PROTECTIVE COATING SYSTEMS ON A FIBERGLASS-REINFORCED PLASTIC HELICOPTER ROTOR BLADE SPECIMEN

SUMMARY

As a result of the investigation into the effects of 18 months of outdoor exposure at Bloomfield, Connecticut, it appears that fiberglass specimens or blades of similar design and fabrication technique will maintain their elastic properties for long periods of exposure under load.

An early change in deflection of the specimen observed during the first three months was attributed to the need for post cure and faster settling.

After the 18-month exposure period, DeSoto Super Koropon Fluid Resistant Coating and the aluminized acrylic lacquer finishes withstood the elements and remained in good condition on the top surface. The epoxy antistatic coating and the clear urethane epoxy varnish were eroded to a condition where minute fiberglass "fuzz" was evident.

The unprotected surfaces had the resin completely eroded away, exposing the fiberglass strands.

The bottom surface, being exposed primarily to moisture but not to erosive effects, showed no evidence of deterioration on the protected or unprotected surfaces.

TEST INFORMATION

Under corporate sponsorship, a research program was undertaken to build a fixture, out-of-doors in an exposed location, upon which a fiberglass blade specimen could be cantilever mounted and observed under the influence of weather under a droop weight.

During the fiberglass blade development program, several torsion area specimens were made. One of these specimens, which had failed at 23×10^6 cycles under a torsional excitation of $\pm$ 3,420 inch-pounds (developed torsion area specimens ran out to 30×10^6 cycles), was repaired and assigned for this weathering test.

Four different coatings were sprayed in 10-inch-wide areas on both sides of the blade specimen, with approximately 6 inches between the coated areas. Surface preparation consisted of solvent wiping, abrading lightly with No. 180 emery paper, and solvent wiping again to obtain a clean surface. The coatings used in this test were:

1. Clear Marine Urethane Epoxy Varnish,
   Miller Stephenson Chemical Co.
   Danbury, Conn.
   Application - 3 cross coats

2. R.S.E. 100 Epoxy Aircraft Antistatic Coating
   Micro-Circuits Co.
   New Buffalo, Michigan
   Application - 3 cross coats

3. DeSoto Super Koropon Fluid Resistant Coating
   DeSoto Chemical Coating, Inc.
   Philadelphia, Pa.
   Application - 1 cross coat (.5 - .7 mils) No. 1910091 primer
   - 2 cross coats (1.2 - 1.8 mils) No. 3308086 white epoxy enamel

4. Aluminized Acrylic Lacquer Finish, per Kaman Aircraft Specification G-102 Code WL-1, which is:
   1 coat of wash primer per MIL-C-8514
   1 coat of lacquer primer per MIL-P-7962
   2 coats of acrylic-nitrocellulose lacquer per MIL-L-19537

5. Pressure sensitive Polyethylene erosion resistant tape (.010-inch thick)
   Minnesota Mining & Manufacturing Co.
   St. Paul, Minn.
   Application - two pieces 1 foot long by 4 inches wide were placed on the leading edge. No sealant was applied to the exposed joint edges.

Periodic inspections were made and static deflections were recorded during the exposure period from 1 June 1961 to 2 December 1962; these are shown in Figure IV-2. The calculated stiffness for the composite specimen, (EI) composite, was 3.1 psi.

A permanent set of 2-7/8 inches resulted with the specimen loaded as shown in Figure IV-1.

Figure IV-1 illustrates the test setup.

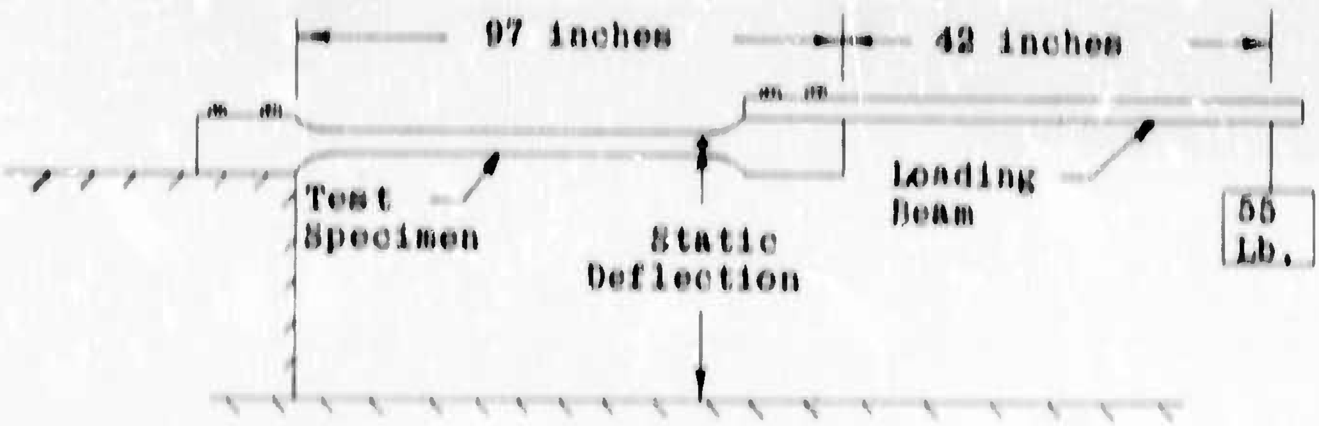

Figure IV-1. Glass Blade Exposure Test Setup

In the unprotected areas, the upper surface was severely eroded, as seen in the photographic reproduction (Figure IV-3). The surface resin had completely vanished, leaving exposed fiberglass strands from the outer ply of the laminate. There was no deterioration of the unprotected areas on the bottom surface.

Coating 1. The Urethane Epoxy Varnish was almost completely eroded from the upper surface, with moderate disintegration of the epoxy resin in the laminate exposing fibers from the outer ply. There was no evidence of deterioration on the bottom surface.

Coating 2. The R.S.E. 100 Epoxy Aircraft Antistatic Coating exhibited moderate erosion by a heavy chalky residue on the surface, which upon removal brought out the outline of the substrate glass fabric. The bottom surface appeared to be free from deterioration.

Coating 3. The DeSoto Super Koropon Fluid Resistant Epoxy Coating showed but slight chalkiness on the upper surface, which when polished slightly was restored to its original sheen. Here, again, the bottom surface was found to be free from defect.

Coating 4. The Aluminized Acrylic Lacquer Finish also showed a slight chalkiness comparable with the DeSoto coating. Upon wiping, a hard, nondeteriorated surface was revealed. There was no deterioration of the lower surface.

The above coatings were then subjected to a dry tape adhesion test similar to that of specification MIL-F-18264 except that the paint surface was dry. All of the finishes exhibited a good adhesion quality.

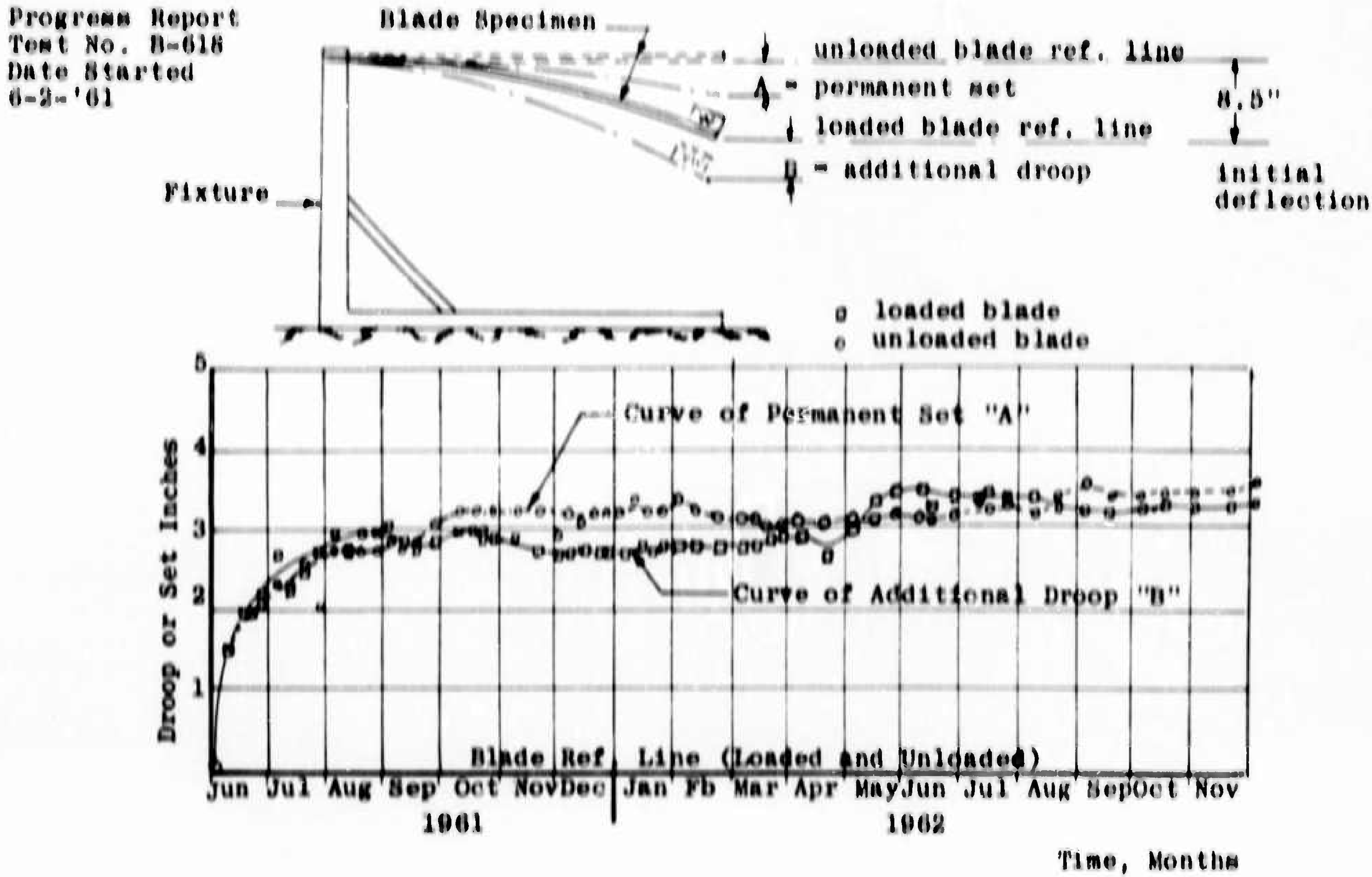

Figure IV-2. Evaluation of Effects of Weathering on Glass Blade Specimen

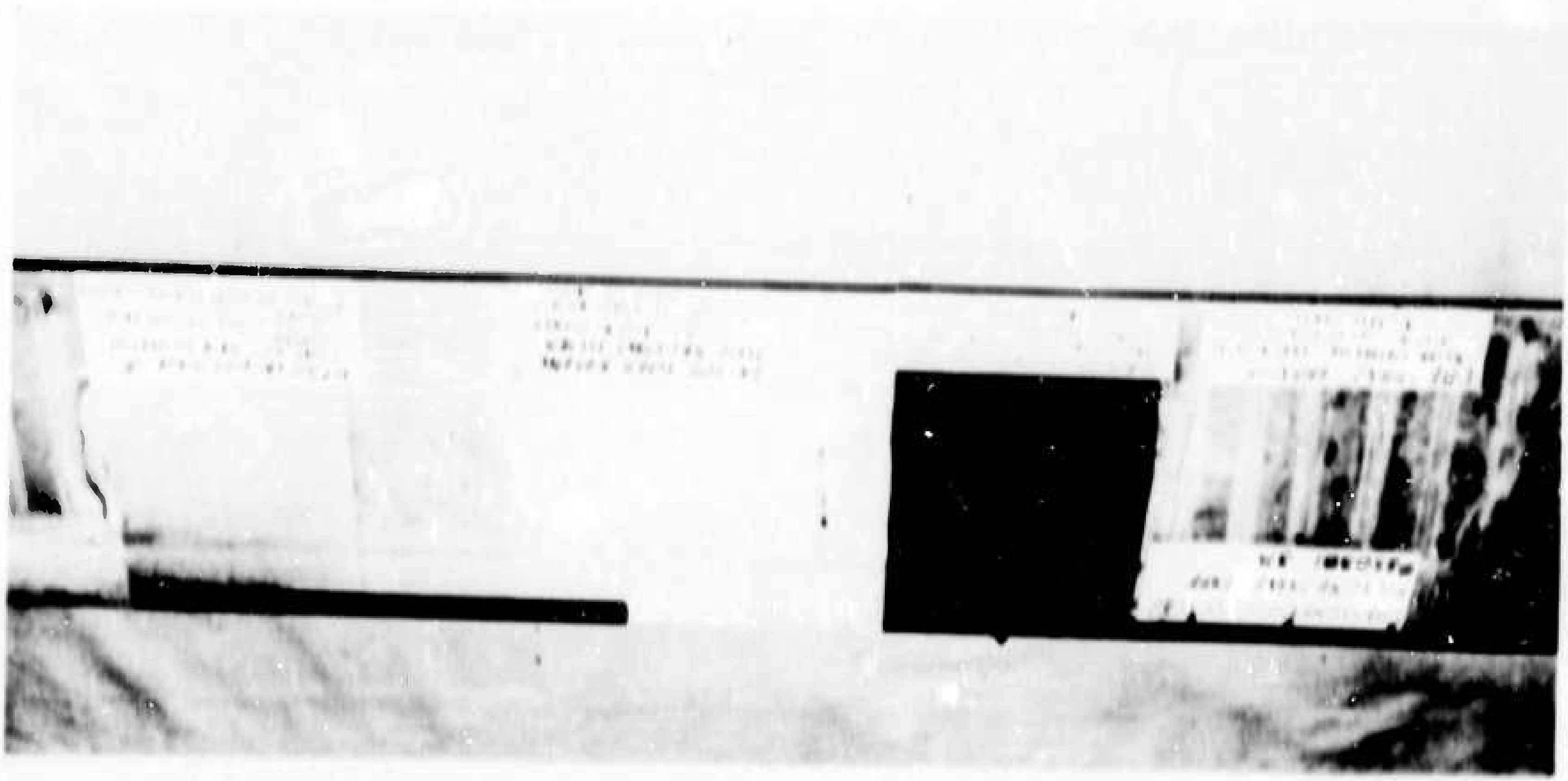

Figure IV-3. Effects of Weathering on Coated and Uncoated Surfaces

The polyethylene erosion-resistant tape experienced no deterioration in itself; however, with no sealant applied to the edges, the tape eventually did separate at the edges from the glass-blade structure.

DISCUSSION

It can be concluded that coating systems exist which fully protect fiberglass-blade (and other glass-laminated) structures from exposure to the environmental weather conditions as associated within the extremes of the test area. This does not, however, mean that the coatings tested would or would not exhibit similar results under flight erosion environment.

It is further concluded from this single investigation that a fiberglass blade or structure of similar design and fabrication, when exposed to similar environmental conditions, will stabilize its elastic properties after a period of time and assume no further permanent set, thereby reaching a repeatable static deflection. It is felt that additional environmental testing should be accomplished before conclusions can be drawn as to whether the initial droop and/or set is a function of design, fabrication technique (post cure), faster settling, or other phenomena as an inherent characteristic of the fiberglass epoxy laminate aging process.

The environmental test specimen is stored for the purpose of gaining valuable data on the effects of weathering versus fatigue integrity through possible future testing.

SECTION V

EVALUATION OF A ONE-PIECE, TWO-BLADED TAIL ROTOR SPAR OF DIRECTED FIBERGLASS-REINFORCED PLASTIC

SUMMARY

A tail rotor design approach proposed by Kaman Aircraft offers the potential of a completely maintenance-free unit. Teeter bearings and control rod ends allow relative motion on surfaces of Teflon and therefore have no lubrication requirement. The oriented glass-fiber spar material, which is continuous from tip-to-tip, is molded into an elliptical cross section on either side of the central hub and provides an effective elastic pitch spring. The induced tail-rotor pitch, which is purely collective, is accomplished by torsionally deflecting this section, and no pitch bearings are required (pitch bearings have been a potential trouble spot in all helicopters).

Other loadings carried by this section are the flatwise bending, edgewise bending, and centrifugal force. The principal bending and centrifugal force stresses are normal stresses on the net cross section, while the pitch change causes steady shear stresses which are maximum where the minor axis of the ellipse intersects the surface. It is the characteristic of the material that normal stresses are carried primarily as tension in the filaments of glass, while shear stresses are reacted in the plastic matrix. Shear and normal stresses are therefore not combined in the usual fashion, as in isotropic material. The analysis shows margins based on both shear and normal stress considerations.

In a material whose properties have vast variation for the orthogonal principal axes, the mode of failure for any general loading will be greatly influenced by the orientation of the axes. It has been Kaman's experience that material of the type used for tail-rotor structure will normally fail in shear only in planes adjacent to discontinuous fibers. For this reason, the tail-rotor design provides a continuous path for fibers from one blade to the other, and permits terminations only in the outboard blade sections where loads are reduced. Normal loadings of inboard sections should, therefore, develop the full potential of the unidirectional glass filament material.

Structural members were constructed and tested for comparison with analytical data. Although the specimens were not completely homogeneous (the section was formed from three precured laminates of Scotchply secondary bonded together), the test information which follows shows that the twist angles applied with

static loads are more than double that required; the fatigue specimen was run out to 30×10^6 cycles at six times the design load without failure.

Description of Tail Rotor

The tail-rotor assembly has two fiberglass blades with an overall dimeter of 5 feet and a chord of 5 inches with a 12 percent thickness ratio. The main spar has a "C" section with a molded channel which completes the member to make it a typical "D" spar. The aft portion of the structure is constructed of carved glass-fiber honeycomb bonded between glass-fiber skins. The outer layer of skin laminations is wrapped entirely around the spar and rib box to form a smooth, continuous surface. Toward the root end of the table, the layers of skin are gradually increased to form the required reinforcement for a shear load path from trailing edge to spar. Pitch arms extend forward to attach with the control links. The interconnecting hub region is pierced for a centering guide which affords control rod passage. The rotor driving mechanism is a steel yoke which clamps against the flat phenolic pads shown in Figure V-2.

Both tips of the blades are closed by a molded tip cap to fair the end ribs. The leading edge of these tip caps is covered by small stainless-steel shields. Under the tip caps, two spanwise holes with threaded inserts are provided to permit addition of small weights for final blade balance before final tip cap installation.

Figures V-1 and V-2 show sketches of the proposed tail rotor.

Test Information

To substantiate the calculated data for the proposed tail rotor, a series of tests were conducted. The test specimens were constructed of monofilament glass fibers with an elliptical cross section simulating the tail rotor pitch spring section and set up in static and fatigue test fixtures (Figures V-3 and V-4 respectively).

In the static test, the specimen was subjected to a simultaneous axial load of 3,400 pounds and a torsional moment applied as a couple. Figure V-5 is the plot of torque versus twist, where it is seen that up to 31 degrees (twice the maximum expected value), a linear rate of 24.5 in.-lb. per degree occurs. At this point, the slope then changes to a softer linear rate of up to 42.5 degrees where the applied torque has reached approximately 1,780 in.-lb. The plot is twice the actual spring rate, since two torsional section specimens were tested back-to-back. The knee, or break, in the slope is explained by the partial failure of the secondary bond between

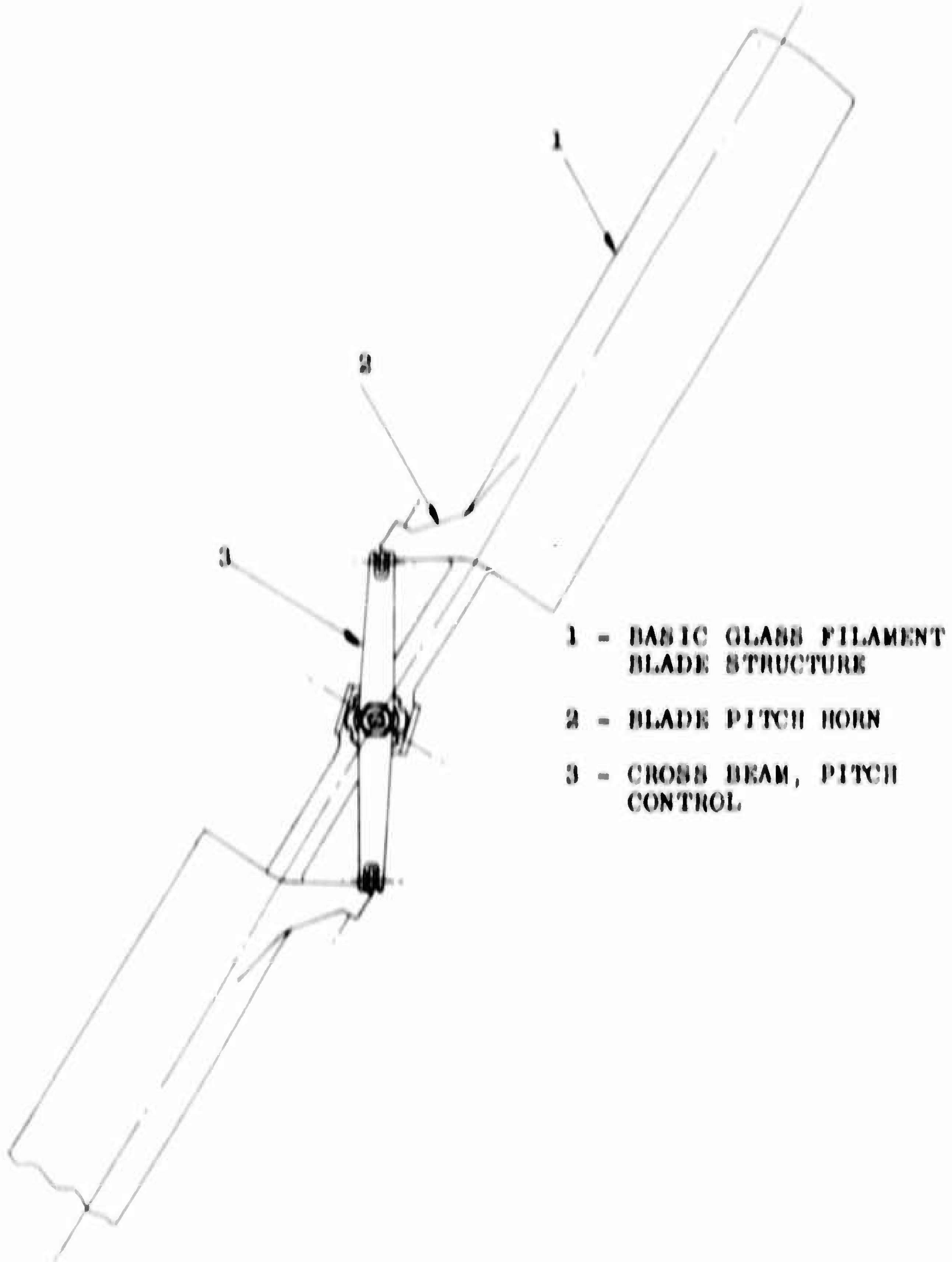

Figure V-1. Elastic Hinged Tail-Rotor

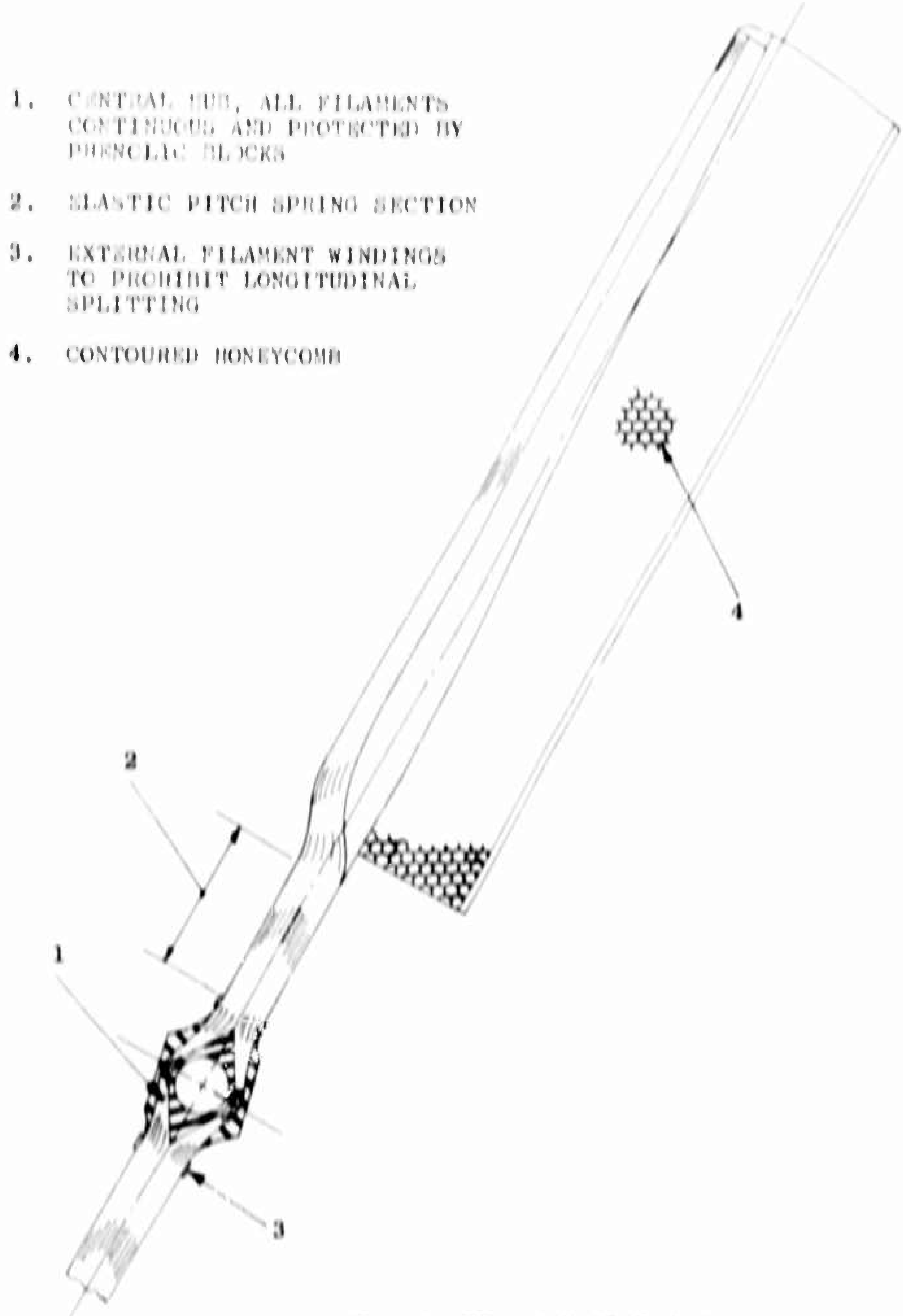

Figure V-2. Elastic Hinged Tail-Rotor

the laminates of precured unidirectional Scotchply. It must be emphasized that there was no interlaminar failure of the Scotchply, and deflecting to larger angles was not achieved only because of test equipment limitations.

The calculated spring rate of 62 in.-lb. per degree was based upon a shear modulus of .827 x 10^6 psi, deducted from thin-shell testing. The difference in section and attendant strain rates and the lack of homogeneity of the specimen are probable sources of error; however, the lower stiffness is advantageous in this case, since it leads to lower control forces.

The truly significant contribution of this test is the value of the assumed ultimate shear stress. Known published information on shear stresses for unidirectional fiberglass-reinforced plastic appears to be limited to the block shear or interlaminar shear test data, which of course yields very low values (less than 6,000 psi). However, in this torsional shear application, it is shown that the assumed value of 35,000 psi for the ultimate shear strength used in this analysis is quite conservative.

The dynamic program produced similar positive results. The predicted maximum tail-rotor vibratory edgewise moment was ± 133 in.-lb. with a steady centrifugal load of 3,400 lb. The fatigue test was carried out first at ± 150 in.-lb. and then at ± 300 in.-lb. with the steady 3,400 lb. axial load; both levels resulted in runouts, that is, 30 x 10^6 cycles. In an attempt to promote a valid failure, a moment level of ± 800 in.-lb. was induced on the same specimen; this, too, ran out to 30 x 10^6 cycles, as plotted in Figure V-6. The strains at the point of maximum bending moment associated with the above runs were:

Steady strain due to centrifugal loading	=	1,440 micro inch/inch
Vibratory strain for ± 150 in.-lb. run	=	± 250 micro inch/inch
Vibratory strain for ± 300 in.-lb. run	=	± 500 micro inch/inch
Vibratory strain for ± 800 in.-lb. run	=	± 1,333 micro inch/inch

The vibratory strains when superimposed over the steady value of course give the maximum and minimum strain excursions experienced by the specimen.

Visual examination and electrical monitoring devices were unable to determine any evidence of failure in the specimens.

Calculations

Torsion Area - Edgewise Fatigue Stress Analysis

Station 2.18

$A = .3976 \text{ in.}^2$

$I_{yy} = .03145 \text{ in.}^4$

$M_{Steady} = -59 \text{ in.-lb.}$

$M_{Vib} = \pm 133 \text{ in.-lb.}$

$C.F._{Steady} = 3,400 \text{ lb.}$

$a = 1.125 \text{ in.}$

$b = .45 \text{ in.}$

Steady

$$f = \frac{M\ C}{I} + \frac{CF}{A} = \frac{59(.5625)}{.03145} + \frac{3,400}{.3976}$$

$$= 1,056 + 8,550 = 9,606 \text{ psi}$$

Vibratory

$$f = \frac{M\ C}{I} = \frac{\pm 133(.5625)}{.03145} = \pm 2,380 \text{ psi}$$

$F_{Allow} = \pm 5,320 \text{ psi}$

$$M.S. = \frac{5,320}{2,380} - 1 = 1.23$$

Torsion Section - Flatwise Fatigue Analysis

Station 2.18

$A = .3976 \text{ in.}^2$

$I_{xx} = .00503 \text{ in.}^4$

$M_{Steady} = 176 \text{ in.-lb.}$

$M_{Vib} = \pm 28.5 \text{ in.-lb.}$

C.F. = 3,400 lb.

Steady

$$f = \frac{M\,C}{I} + \frac{CF}{A} = \frac{170(.23)}{.00503} + \frac{3,400}{.3976}$$

$$= 7,775 + 8,551 = 16,326 \text{ psi}$$

Vibratory

$$f = \frac{M\,C}{I} = \frac{\pm 28.5(.23)}{.00503} = \pm 1,303 \text{ psi}$$

$$F_{Allow} = \pm 4,900 \text{ psi}$$

$$M.S. = \frac{4,900}{1,303} - 1 = 2.76$$

Torsion Section

Station 2.18

$$I_{xx} = \frac{ab^3}{64} = .00503 \text{ in.}^4$$

Torsion Spring Rate

$$T/_{\theta} = \frac{KG}{L} = 62.8 \ \frac{\text{in.-lb.}}{\text{degree}}$$

Max. Pitching Travel $= \pm 15^{\circ}$

$$\therefore T = 62.8\ (15) = 942 \text{ in.-lb.}$$

$$P = \frac{942}{3.0} = 314 \text{ lb.}$$

$$M = 314\ (3.03) = 951 \text{ in.-lb.}$$

Tension Due to Bending

$$S_t = \frac{M\,C}{I} = \frac{951\ (.45)}{2(.00503)} = 42,538 \text{ psi}$$

$$F_{tu} = 90,000 \text{ psi}$$

$$M.S._u = \frac{90,000}{1.5\ (42,538)} - 1 = .41$$

Torsional Shear

$$S_s = \frac{16T}{ab^2}$$

$$= \frac{16(942)}{(1.125)\ (.45)^2}$$

S_s = 21,062 psi

$F_{s_{u_{Allow}}}$ = 35,000 psi

$$M.S. = \frac{35,000}{(1.5)(21,062)} - 1 = \frac{35,000}{31,593} - 1 = 1.108 - 1 =$$

+ .108

It is to be noted here that the allowable shear stresses used elsewhere in these calculations are based upon the Goodman Diagram presentation for the steady and superimposed vibratory stresses anticipated. The allowable stress given for the static torsional condition above, although seeming overly optimistic, is substantiated in the test information which follows. This is considered to be an extremely important contribution.

Edgewise Fatigue Stress Analysis

Station 12.0

A = .5784 in.^{2}

I_{yy} = .4078 in.^{4}

M_{Steady} = − 25 in.-lb.

M_{Vib} = ± 55 in.-lb.

$C.F._{Steady}$ = 2,585 lb.

Stress at Trailing Edge C = 5 − 1.46 = 3.54"

Steady

$$f = \frac{MC}{I} + \frac{CF}{A} = \frac{25(3.54)}{.4078} + \frac{2,585}{.5784}$$

= 217 + 4,470

= 4,687 psi

Vibratory

$$f = \frac{M\,C}{I} = \frac{\pm 55(3.54)}{.4073}$$

$$= \pm\ 477 \text{ psi}$$

$$F_{Allow} = \pm\ 5{,}680 \text{ psi}$$

$$M.S. = \frac{5{,}680}{477} - 1 = \text{LARGE}$$

Flatwise Fatigue Stress Analysis

Station 12.0

$$A = .5784 \text{ in.}^2$$

$$I_{xx} = .028 \text{ in.}^4$$

$$M_{steady} = 27 \text{ in.-lb.}$$

$$M_{vib} = \pm\ 48 \text{ in.-lb.}$$

$$C.F. = 2{,}585 \text{ lb.}$$

$$C = \frac{.60}{2} = .3 \text{ in.}$$

Steady

$$f = \frac{M\,C}{I} + \frac{C.F.}{A} = \frac{27(.3)}{.028} + \frac{2{,}585}{.5784}$$

$$= 289 + 4{,}469 = 4{,}758 \text{ psi}$$

Vibratory

$$f = \frac{M\,C}{I} = \frac{\pm 48(.3)}{.028} = \pm 514 \text{ psi}$$

$$F_{Allow} = \pm 5{,}670 \text{ psi}$$

$$M.S. = \frac{5{,}670}{514} - 1 = \text{LARGE}$$

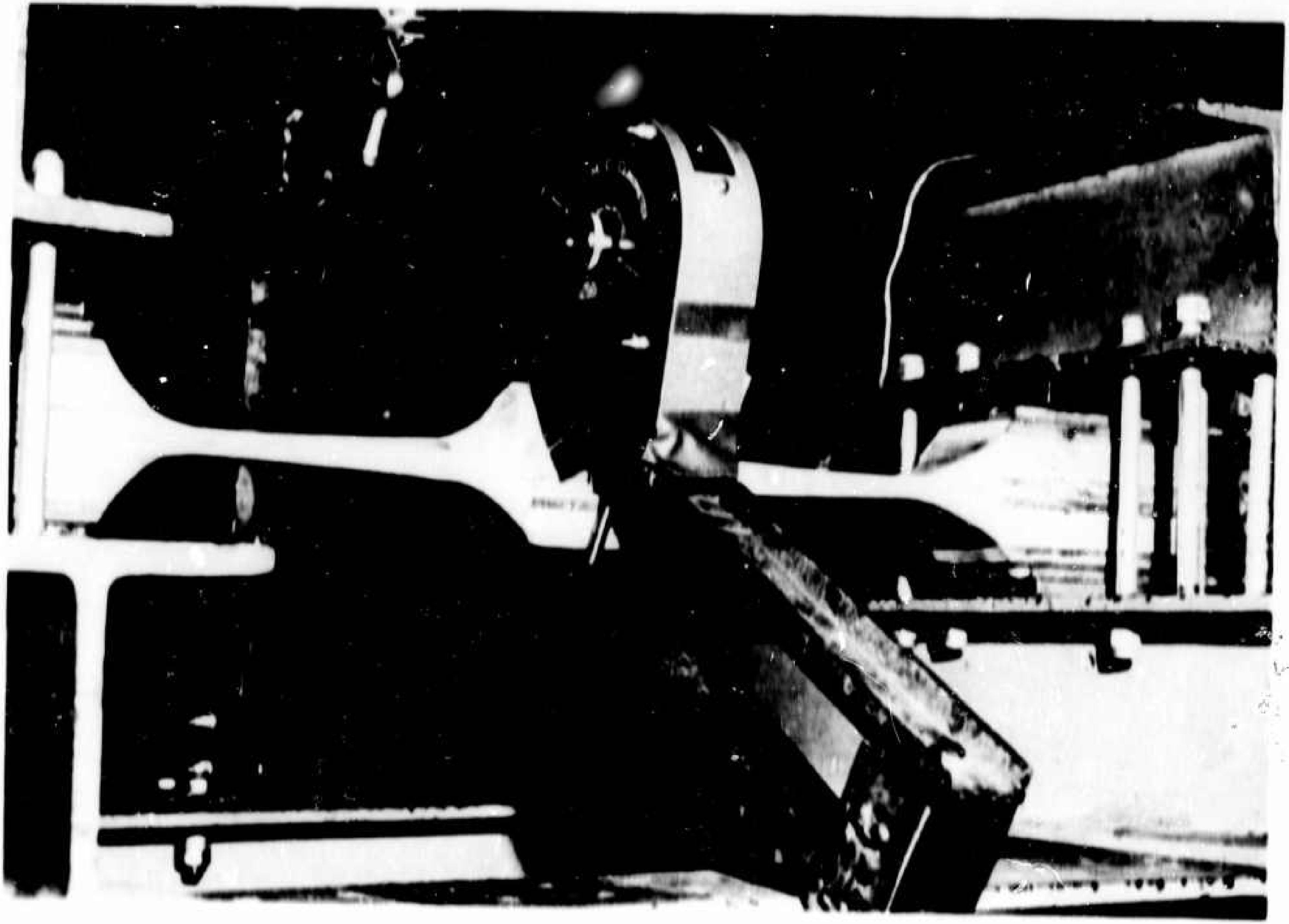

Figure V-3. Tail-Rotor Torsional Section Static Test

BLANK PAGE

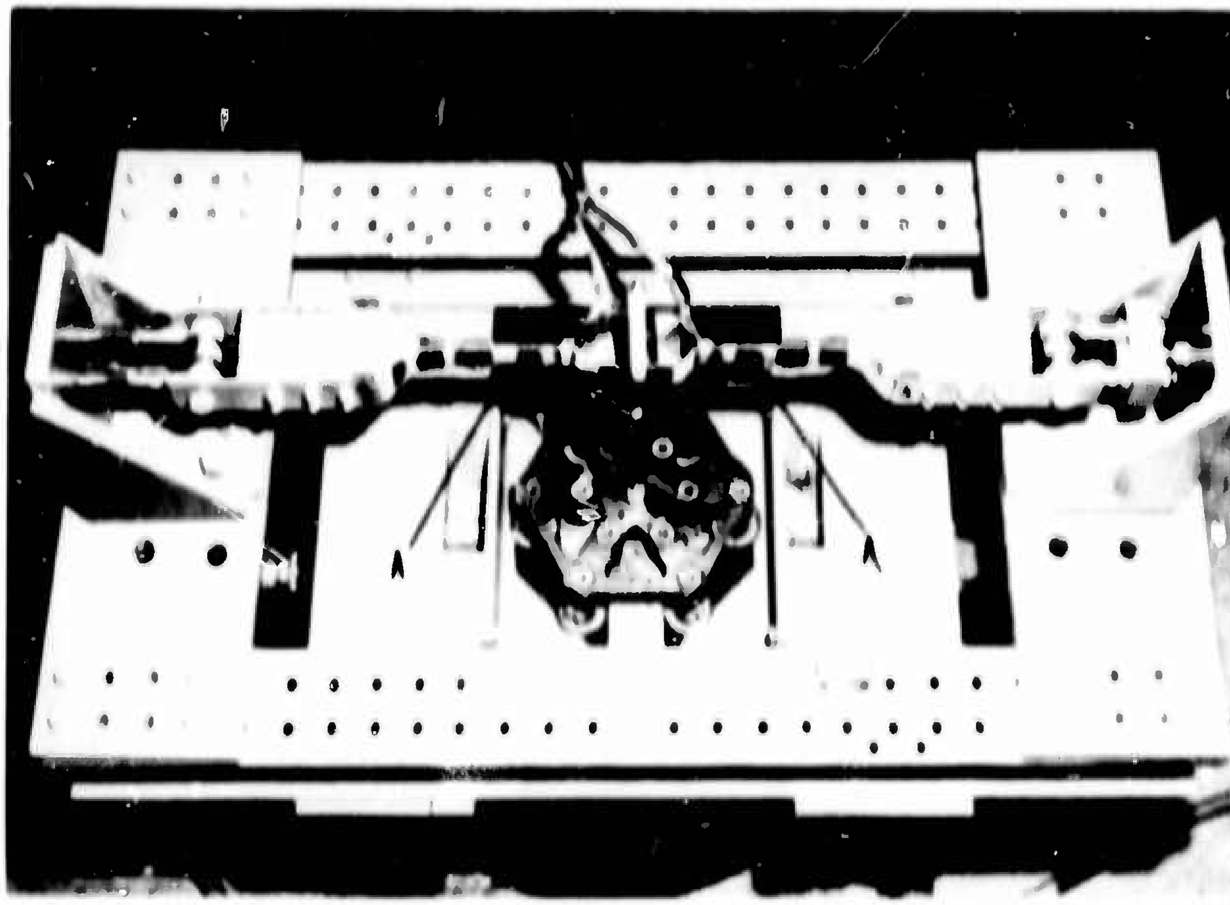

Figure V-4. Tail-Rotor Torsional Section Fatigue Test

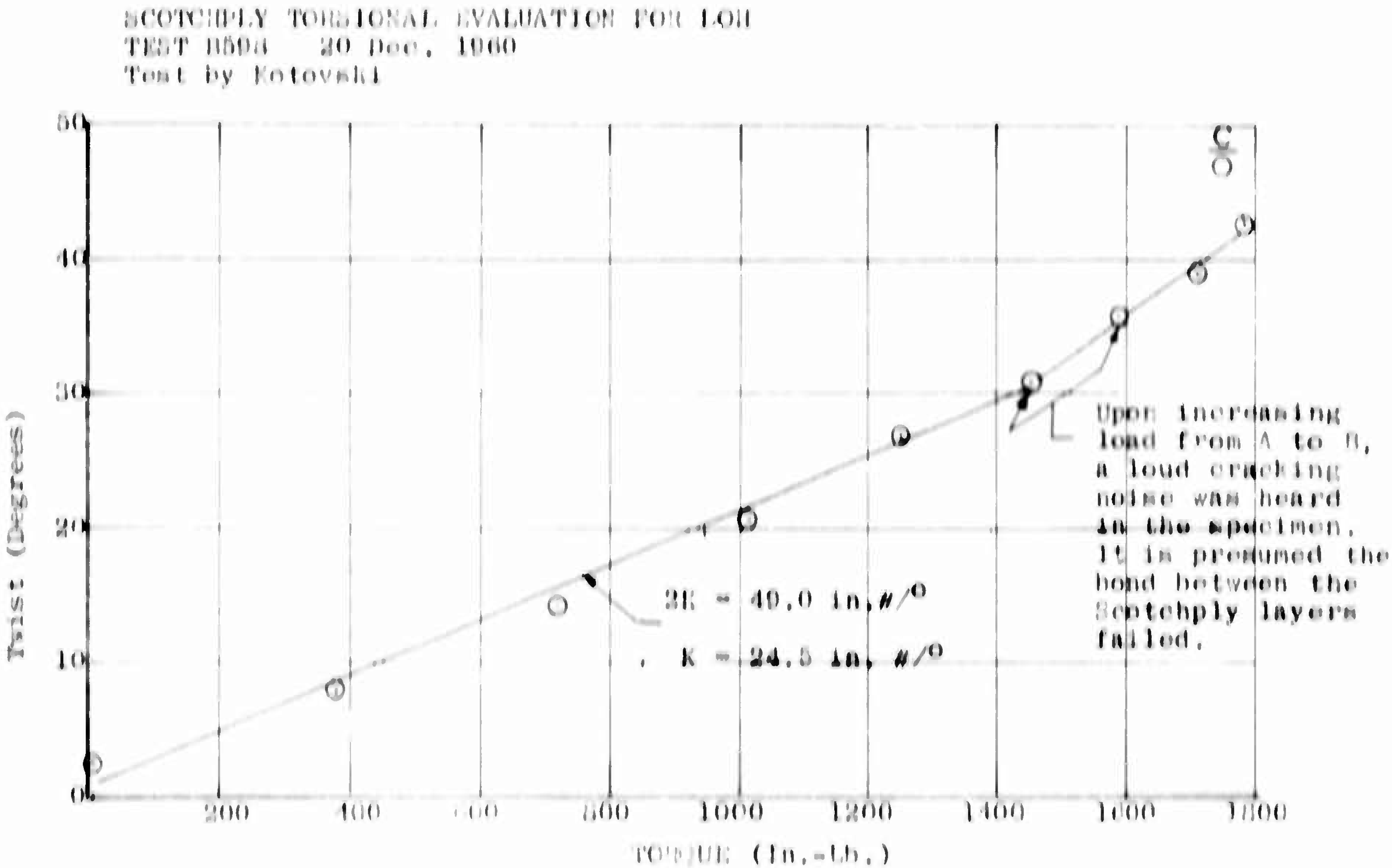

Figure V-5. SCOTCHPLY Torsional Evaluation

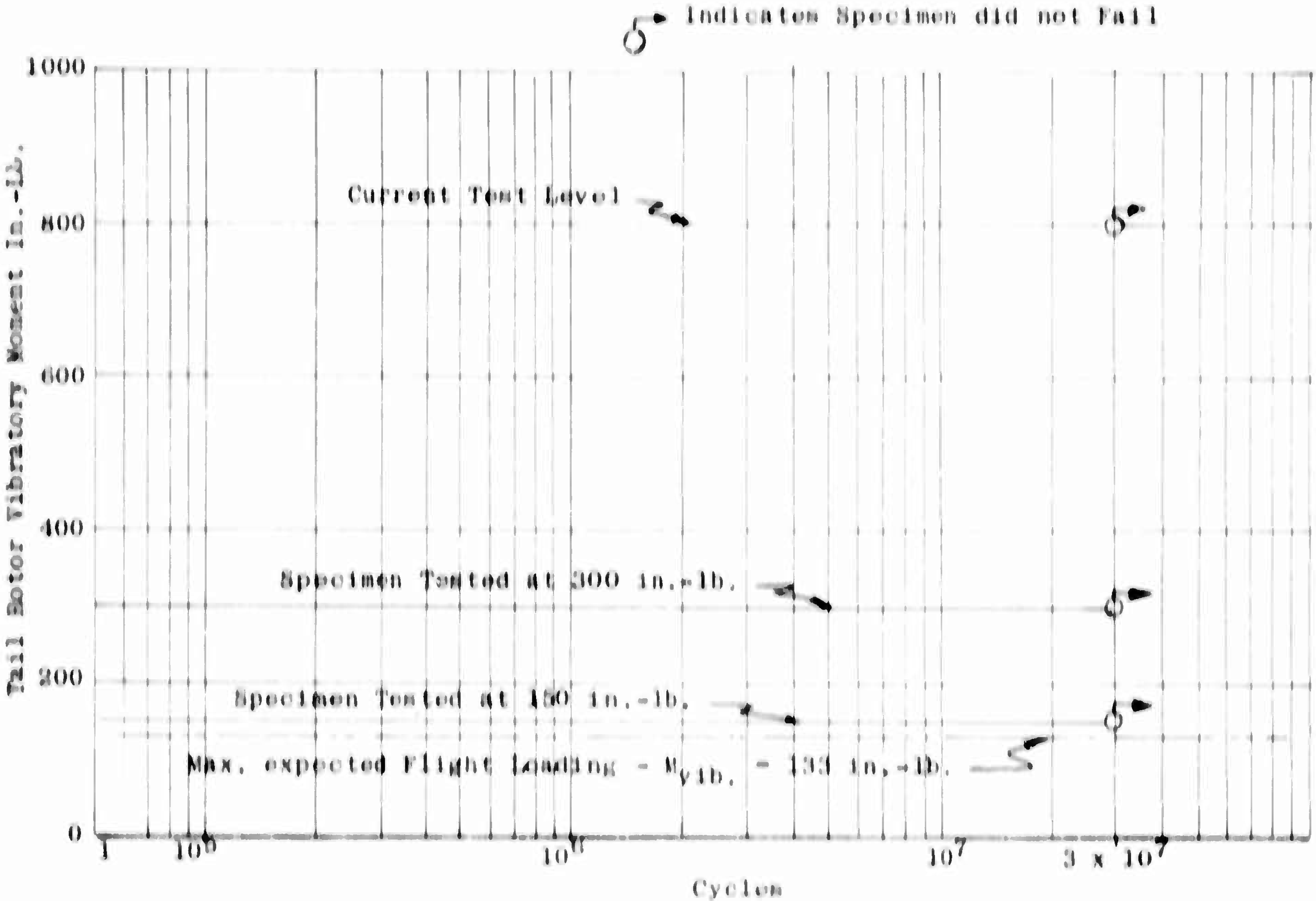

Figure V-6. Tail-Rotor Spar Endurance Test

DISCUSSION

Although the operating conditions of a tail rotor are not identical to those of a main rotor, they are basically similar with regard to hinges and fatigue requirements. The test results have indicated that this same basic principle can be applied not only to tail rotors but to main rotors as well, but would of course require additional design study and evaluation.

Some of the advantages of directed glass fibers over metallic structure are:

- High strength-to-weight ratio
- Greatly improved fatigue characteristics due to reduced notch sensitivity
- Damping of vibratory peaks
- Exposure and moisture resistances
- Lower tooling costs
- Freedom with regard to placement of fibers in a manner to provide greater strength in the load paths required for optimum structures.

The above-mentioned advantages coupled with sound engineering understanding of the problems involved and the ability to use directed glass fibers to their fullest extent indicate that great potential exists in the design of an elastically hinged rotor hub system.

SECTION VI

V/STOL ROTOPROP DEVELOPMENT

BACKGROUND

The Kaman K-16B (see Figure VI-1) is a twin-engined, tilt-wing, vertical take-off and landing (V/STOL) experimental aircraft developed to study the capabilities of directed vector rotoprop (roto-propeller) and the effectiveness of the tilt-wing/roto-prop combination.

The rotor development study started in 1954.

Test rig ground testing was done in 1957-1958, although feasibility testing of a large-scale rotor was done in 1955-1956.

The aircraft was designed, and fabrication was completed in 1960.

Ground and wind-tunnel testing took place at Kaman and at NASA (Ames) in 1961-1962.

Data reduction and studies for further application of the results are being carried on at the time of this writing.

This aircraft was equipped with many fiberglass-laminated parts, such as the spinners, air inlet fairings for the powerplant nacelles, and other secondary structural applications, all such applications were very effective and presented no trouble in operation - their study is considered routine and no report is made on their performance.

The primary structural uses of fiberglass laminates were devised to solve problems of strength, weight, and endurance in the rotor system and are the subject of this report.

SUMMARY

In the development of the Kaman K-16B rotoprop system, extensive testing was done on both the whirl rig, which imposed actual centrifugal force and air loads, and on the flap fatigue test stand, which simulated the centrifugal force and bending air loads.

A total of 94.6 hours was accumulated on the whirl rig, of which 40.3 hours was credited to endurance time for planned control inputs. During this time, the glass-reinforced retention of the rotor blade created no problems. The control flap,

Figure VI-1. K-16B Experimental V/STOL Aircraft

BLANK PAGE

however, required several modifications of glass reinforcement before becoming acceptable.

The running of the flap fatigue was concurrent with the whirl rig operation tests.

From a valid failure at 2.64 x 10^6 cycles, glass reinforcement modification brought the endurance life to 14.7 x 10^6 cycles; here the failure occurred outside the reinforcement. A final modification was made, and these flaps were used on the aircraft in full-scale wind-tunnel tests. The tests accumulated 24 hours, or slightly over 1 x 10^6 cycles, with no perceptible detrimental indications.

Statement of Problem

The configuration established was a three-bladed rotor having a 15-foot 3-inch diameter with 18-inch-chord blades. The system was to operate at 725 rpm and to develop 5,200 pounds of thrust in each of the two rotoprops.

To produce the helicopter type of control with cyclic and collective actuation, a control flap acting as an aileron on each propeller blade is used. The submerged flap is 50 percent of the blade chord and covers the outer 42 percent of the blade span.

The difficulties involved with the design configuration and operating conditions are the high rpm and vehicle maneuvers which impose very high loads and stresses on the blades and flaps. The blades must withstand a centrifugal force of 41,500 lb., an edgewise bending moment of 35,000 in.-lb., and a flatwise bending moment of 23,000 in.-lb.; these combine into a 42,400 in.-lb. limit bending moment at the root. Fatigue requirements are the steady edgewise moment of 1,000 in.-lb. with a superimposed vibratory moment of ± 12,000 in.-lb.

The lightweight control flap, occupying the outer portion of the high rpm blade, must resist a centrifugal force of 5,250 lb. and endurance loadings such as a steady bending moment of 720 in.-lb. with a superimposed vibratory moment of ± 740 in.-lb.

DESCRIPTION OF PARTS

Blades

The airfoil section used is an NACA 16509 and is constant from blade Station 32.00 to the tip (Station 91.00). The blade has a constant chord of 18 inches and incorporates a spanwise washout of 0.3387 degrees per inch of span.

The core is of laminated maple and is full chord at the butt end. The trailing edge is then tapered so that at 50 percent of the actual blade span the width of the spar is 40 percent of the chord measured from the leading edge and remains constant at this width to the tip.

Aft of the taper in the spar, the blade profile is obtained with laminated spruce and plywood ribs and plywood skin. A .020-inch corrosion-resistant steel doubler is bonded into a routed out-section of the spar from Station 34.00 to Station 64.00 for added strength. A similar .020-inch stainless-steel skin is then bonded over the entire core and doubler, completely covering the top and bottom surfaces.

At the butt end, fiberglass retention reinforcing pads were bonded inside and outside of both the upper and lower surfaces, thus forming a sandwich structure with the steel skin. A machined steel retention fitting was socketed into the blade shank and mechanically attached with three 5/8-inch-diameter bolts.

The spar tip was reinforced with fiberglass cloth to give support where material had been removed for the accommodation of the flap control mechanism. The mechanics of the flap control are unimportant to this report, and its description will therefore be omitted.

The tip cap was a 4-ply No. 181 glass-cloth fairing which enclosed the tip fitting, its mounting bolts, and control mechanism pivots. The cap was attached to the tip fitting with screws and was designed to reduce the turbulence associated with tip airflow.

Flaps

The basic flap (sketched in Figure VI-2) consists of a .25-inch laminated birch plywood spar with spruce spar caps; .25-inch spruce ribs; birch plywood spline; laminated spruce nose block (for retention cable); .032-inch birch plywood skin that covered an .032-inch birch plywood nose skin, which extended to the spar aft edge; and laminated maple pad for mounting the control horn.

The flap is centrifugally restrained by a steel tension armored cable which passes through a hollow stud in the flap nose block, through a tunnel in the blade spar, and attaches to the blade retention fitting. The stud also serves as a pivot axis for the inboard flap bearing (radial) which is housed in the spar. Control motions of the flap are permitted by elastic twist of the retention cable.

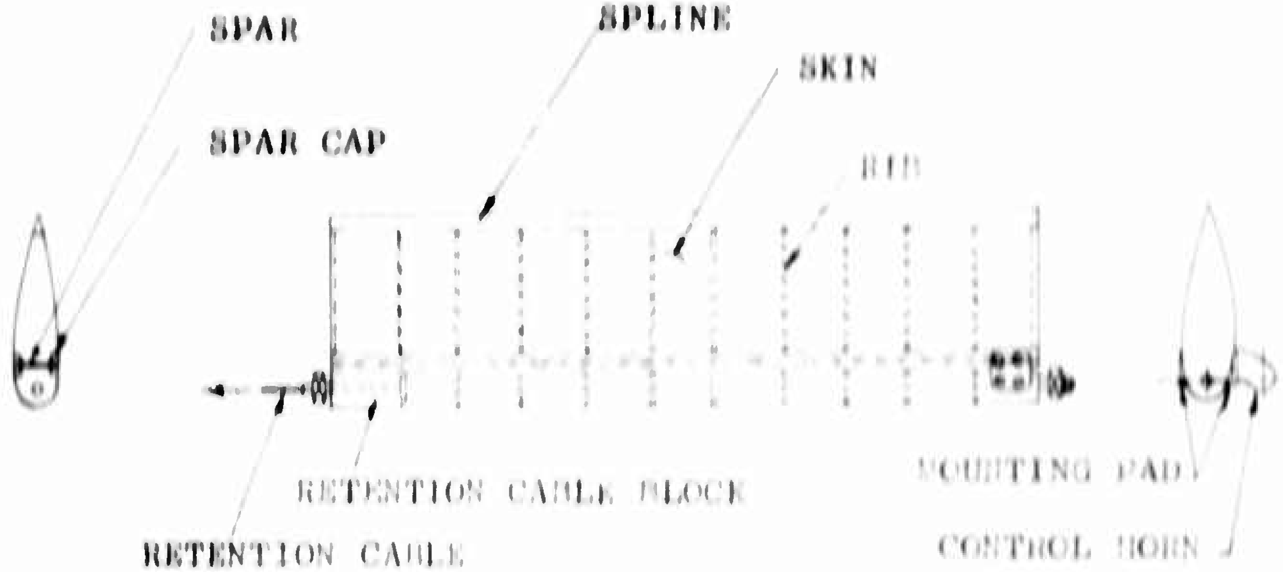

(a) Basic Flap

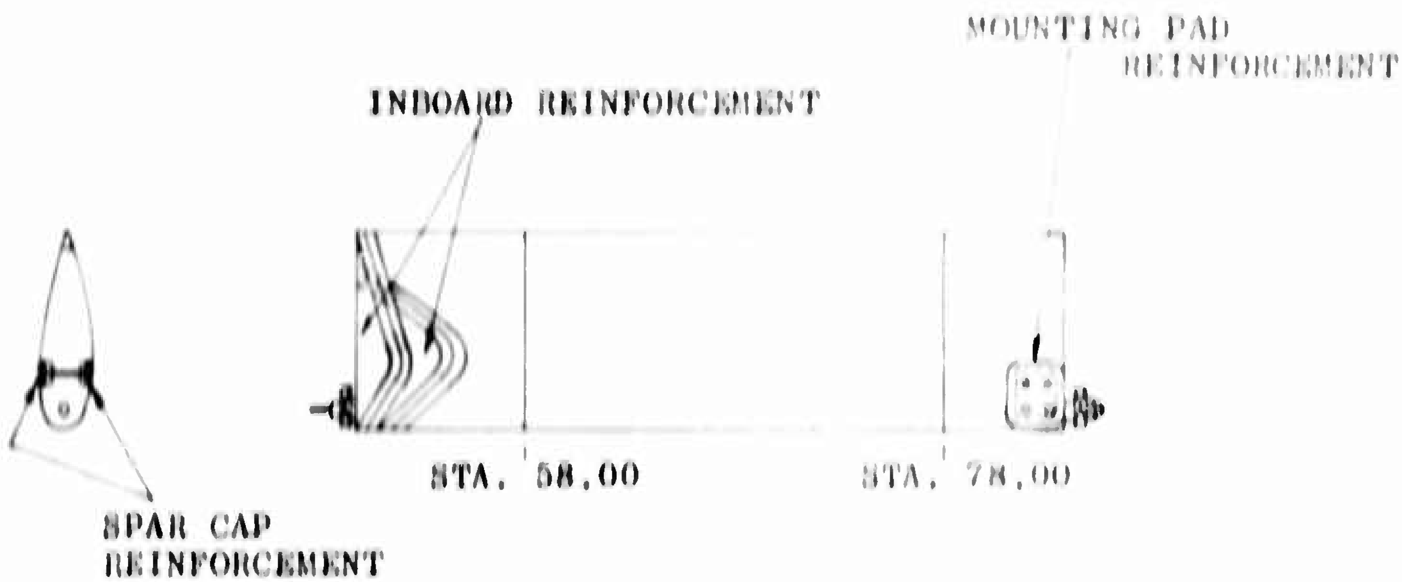

(b) Reinforced Flap

Figure VI-2. K-16B Rotoprop Control Flap

At the outboard end, a second stud is bonded into the flap and is used as the pivot axis for the outboard radial bearing. The outboard bearing is housed in an aluminum tip fitting that is bolted to the blade. The attaching bolt thread into metallic inserts which are buried in the spar.

The flap bearing housings are lined with phenolic bushings, thus allowing the flap to float axially under the centrifugal field while being restrained at the butt end by the cable. In this manner, high local loads from the flap are avoided at the blade tip.

Control moments are introduced by a crank arm bolted to the outboard end of the flap through skin pads and shear block reinforcements.

TEST INFORMATION

Prior to the installation of the K-16 vehicle into the NASA wind tunnel, the rotor system had to accumulate 40 hours of endurance time on the whirl rig (Figure VI-3). In order to provide continuous instrumentation coverage and to observe operating limitations on the engine, the entire program was run in dry weather.

The following control inputs were to constitute the required whirl testing:

Collective Flap	Collective Blade Pitch	Cyclic Flap	Hours	Total
deg.	deg.	± deg.		
2	16	0	5.00	5
13	10	0	6.50	11.50
2	16	2.0	7.00	18.50
13	10	2.0	8.25	26.75
10	14.5	4.0	1.00	27.75
10	13	6.5	3.10	30.85
13	13	7.5	2.15	33.00
13	13	8.5	2.00	35.00
13	13	9.0	2.10	37.10
13	10	10.5	2.00	39.10
13	10	11.0	1.00	40.10
13	18	11.5	0.15	40.25

The 40-hour endurance program was run at a normal rotor speed of 725 rpm. Collective flap was preset statically and a meter reading corresponding to a measured cyclic flap condition was obtained prior to each run.

Figure VI-3. Rotoprop Whirl Stand

The engine was started, and the rotor was brought up to speed. Collective blade pitch was applied until the desired setting was reached as indicated by a meter reading on the instrument console in the block house (protective operation and observation building); the cyclic flap was then applied. Endurance timing was started after the required conditions had been reached. The levels established were maintained for the duration of the run, after which the cyclic flap was reduced to zero, the collective blade pitch was reduced to zero, the rotor speed was brought to idle, and the engine was shut down.

Throughout the entire running, the blade itself remained undamaged by the tested loads. One small area did require attention, however; this was because of the large amount of instrumentation mounted on the hub which created awkward access to areas requiring ordinary maintenance. Due to inadvertent tool contact to the blade trailing edge corner, a skin separation occurred. This was quickly and easily remedied with the incorporation of a 2-ply fiberglass reinforcing patch over the corner of each blade. No recurrence of damage followed.

The tip cap required some development to sustain the loading at the tip. Under the 1,200 "g" field, the 4-ply cap exerted approximately 1,020 pounds on the six attachment screws securing it to the tip fitting. It was necessary to locally reinforce each of the attachment holes with 2 plies of No. 181 fiberglass cloth. Also, because of the wide chord and the amount of tip cap overhang from the aft top and bottom attaching screws, the aft portion of the cap experienced a failure in separating from the forward half of the cap. The integrity was restored by removing the 2-ply hole reinforcement on the top and bottom aft holes and replacing it with a 2-ply reinforcement which extended toward the trailing edge for 2 inches beyond the attachment holes, thus strengthening the highly stressed area. No further problem was encountered with the tip caps on the whirl rig or during the 24-hour NACA wind-tunnel test.

The flap created quite a unique development program. Because of its operation in a high centrifugal field, it must necessarily be of light weight construction; yet because of the air forces it reacts against, it must possess superior structural integrity.

The original flap, as described previously, contained no fiberglass reinforcement. After 0.7 hour of endurance whirling, the retention cable nose block separated from the spar to which it was bonded, failing the skin around it. Examination also disclosed compression failure in the spruce nose block under the head of the retention stud. A similar failure also occurred during testing on the fatigue bench stand (Figure VI-10). The retention area was redesigned, at a slight sacrifice in weight, by replacing the wooden nose block with a phenolic laminate block having greater bonding area and better shear distribution. In addition to the new nose block, the plywood skin over the block and the inboard flap edge was reinforced with No. 181 glass cloth, as shown in Figure VI-2 (b), which aided in transferring the retention stresses over the spar and skin. A 2-ply reinforcement of glass cloth was also placed over the outboard control horn mounting pad because of evidence of pad-to-skin separation. The flap and cable units were then pull-tested at 5,400 pounds to ensure the integrity of the bond.

To utilize the whirl stand for the other units of the aircraft's power and drive system, the flaps were allowed to be used at reduced life levels while parallel flap testing and development proceeded on the fatigue bench.

Early testing at the heavy load levels caused the flap to experience deflections so great that the skins would buckle after a low number of cycles. A major fix was required to stiffen the spar. This was done by fabricating new spars and incorporating a glass reinforcement, running the length of the spar (top and bottom) of 8 plies with the unidirectional fibers oriented alternately at $\pm$ 5 degrees from the spanwise axis. Rebuilding the flaps with the previously mentioned changes resulted in lower bending deflections, and the whirl and fatigue tests were resumed.

Two invalid failures occurred next to the fatigue load actuating clamp. The concentrated effect of the clamp was diluted by the blending of a fiberglass pad bonded to the flap under the clamp area. The succeeding test produced a valid skin failure at 530,760 cycles; however, the quality of the plywood was questionable due to its "short grain". The flap was repaired with a new skin being spliced into the top surface and retested. This time a mid-span failure occurred in the new top surface skin at 2,643,000 cycles.

The flap was again repaired, and this time the top skin was reinforced with a single ply of No. 181 glass cloth between Station 58.00 and 78.00; a complete covering of the top surface was avoided so that the end strain gages would remain on the plywood. The flap completed 230,400 cycles when the retention cable, which had accumulated 3,404,000 cycles, failed (Figure VI-11).

A new flap of the same specifications using a single ply of No. 120 glass cloth (instead of No. 181 cloth) on the top and bottom surfaces between Stations 58.00 and 78.00 was next installed in the fatigue apparatus. The deflection of this flap under the tested load was only one-third that of the original wooden flap, and ran to 14.7 x 10^6 cycles before the top and bottom skin

Table VI-A

Test History of Flaps

Test No.	Flap S/N	Flap Type and Differences	Cycles at Failure	Remarks
1	17	Original test specimen rectangular retention block at flap inboard end	2,136,000	Cable retention pulled out at inboard end of flap. Valid failure for this configuration. Retention corner fiberglass-wrapped for next test.
2	25	Improved retention block; modified load distribution path	5,520,000	Flap failed at Sta. 79, adjacent to actuating clamp. Failure due to load concentration by corner of clamp. Clamps modified for next test.
3	31 1st run	Same flap type as S/N 25	323,400	Flap failed near actuating clamp. Failure initiated by clamp. Modified clamps to obtain greater flexibility before next test. Rework flap.
4	31 2nd run	Flap S/N 31 reworked. New skin spliced in failed area and fiberglassed under clamp.	530,700	Fracture in top skin at approximately center of spar. Due to short grain plywood. Rework flap.
5	31 3rd run	Flap S/N 31 reworked. New skin spliced in failed area	2,564,000	Failed in new skin approximately 2-inch outboard of center spar. Definite evidence of short grain failure. Rework flap.

Table VI-A

Test History of Flaps

Test No.	Flap S/N	Flap Type and Differences	Cycles at Failure	Remarks
6	31 4th run	Flap S/N 31 reworked. Fiberglass covering on top skin	3,404,200	Failure on retention cable adjacent to flap inboard end. Cycles noted are those on cable.
7	63	New flap S/N 63. Modified with thin layer of No. 120 fiberglass from Sta. 58 to 78, top and bottom	14,700,000	Failure in skins approximately 7 1/8-inch from outboard end in top, and 5[illegible]-inch from outboard end in bottom. Fractures not in areas covered by fiberglass.

failed outboard of the glass reinforcement (Figures VI-12 and VI-13). Table VI-A is a summary chart of this fatigue testing.

The loads used in the fatigue test were as follows: a steady centrifugal force of 5,250 lb., applied at the outboard end; a steady bending moment of 720 in.-lb., applied at the center of the flap; and a superimposed vibratory bending moment of $\pm$ 740 in.-lb.

The speed of excitation was selected to provide the required vibration output: 200 rpm for the first 1.5×10^6 cycles of the first test, 600 rpm for the last 100,000 cycles of the second test, and 480 to 490 rpm for the remainder of the testing. As for the effect of speed of testing on the fatigue specimen, a study by the American Society of Testing Materials indicates that, at least in the range of 200 to 7,000 cycles per minute, there is no effect caused by varying the frequency except when accompanied by a noticeable temperature rise. Also, the effect of rest periods has no significant effect on fatigue life.

Figures VI-4 through VI-8 show the fatigue testing apparatus and the method of testing.

Figure VI-9 is a close-up view of the rotoprop, without the tip caps, mounted on the whirl stand.

Figures VI-10 through VI-13 are photographs of the type of failures experienced during this test and development program.

Figures VI-14 through VI-30 are the plotted results of the vibratory flap bending moments versus the number of cycles as reduced from the oscillograph recordings which were taken each hour.

Figure VI-31 shows the rotoprop in operation on the K-16B test vehicle in the tilt-wing configuration prior to the aircraft's departure for full-scale wind-tunnel testing at the Ames Laboratory in California.

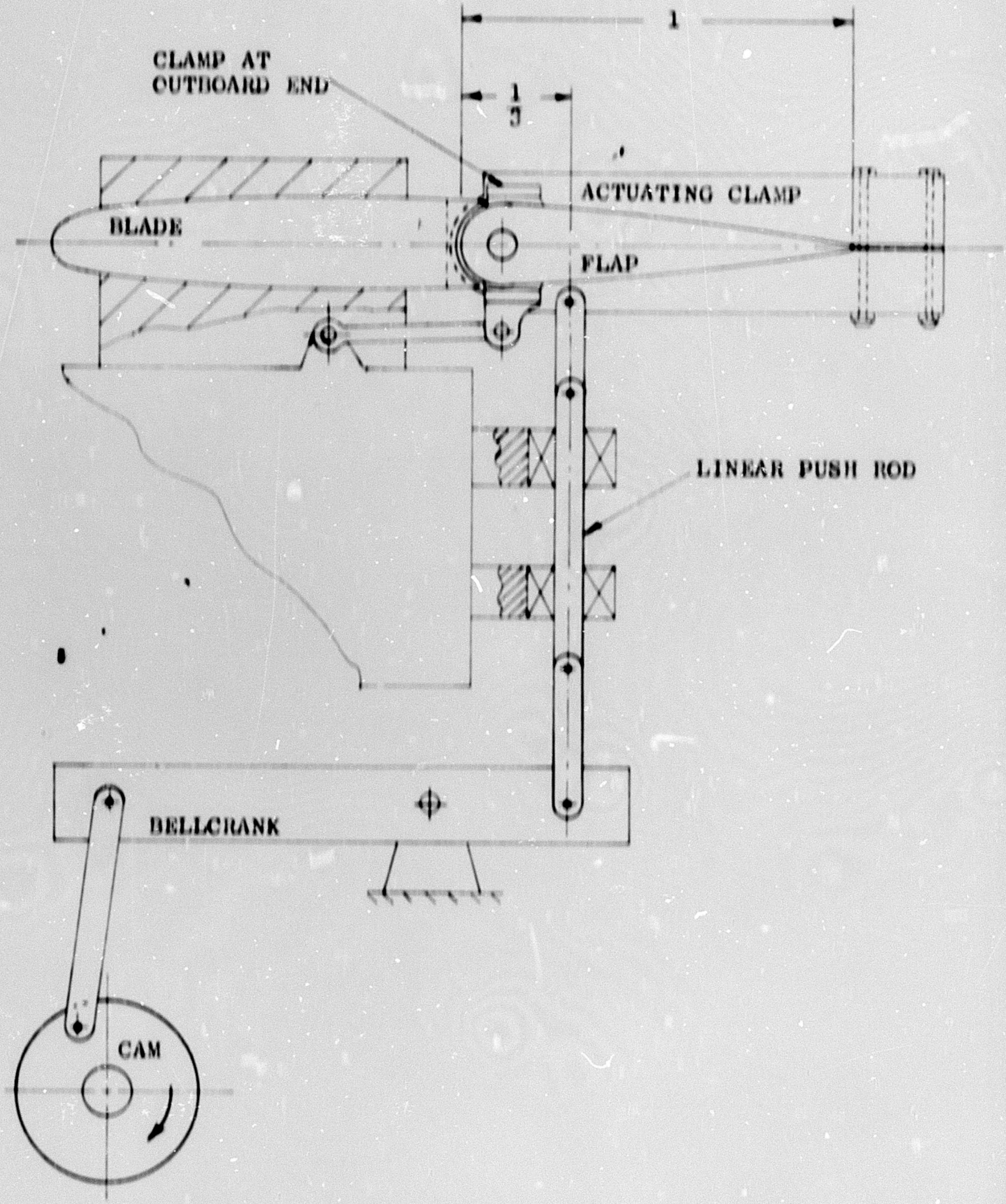

Figure VI-4. Sketch of K-16 Flap Fatigue Jig

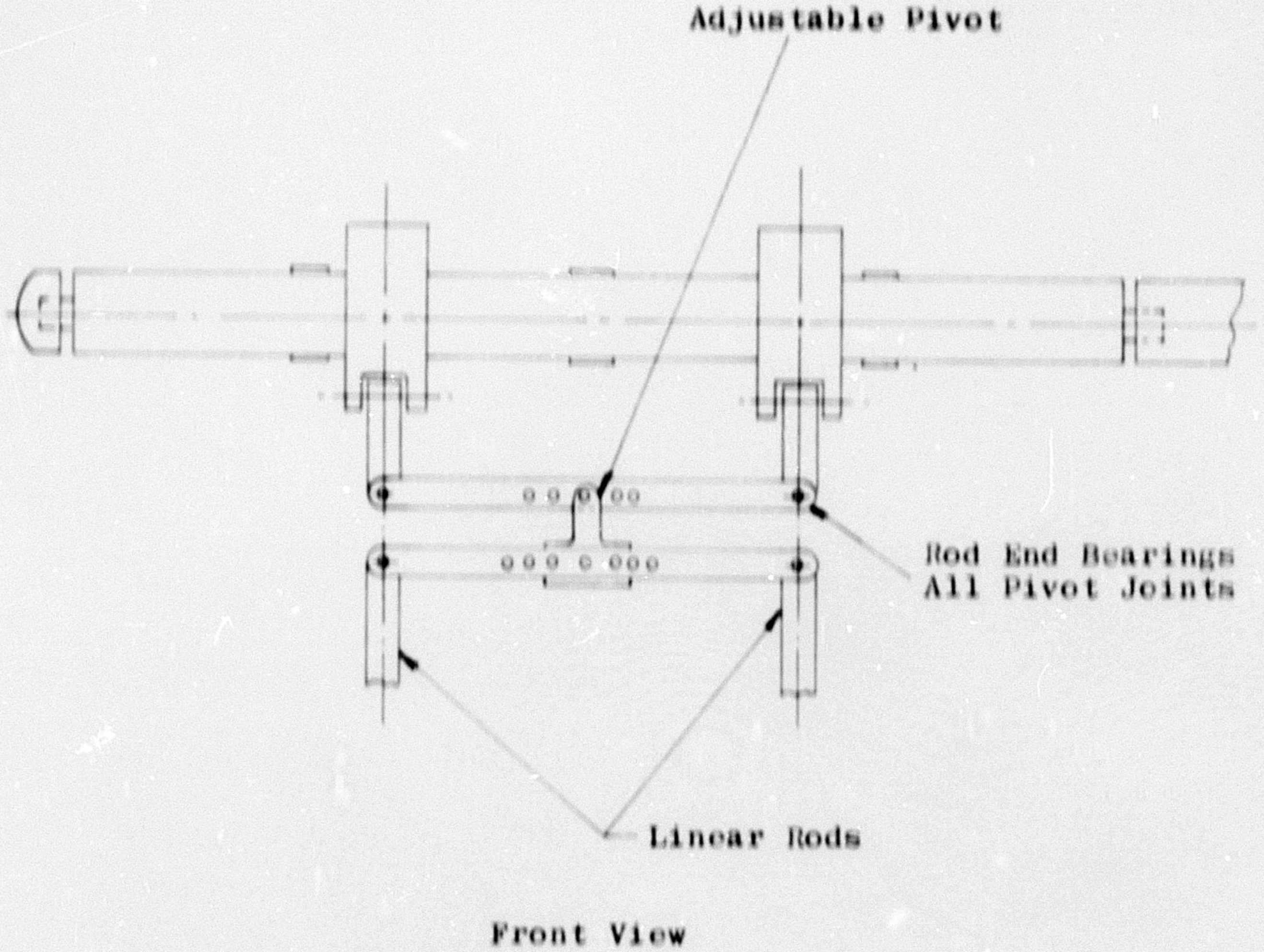

Figure VI-5. Flap Fatigue Test Drive System

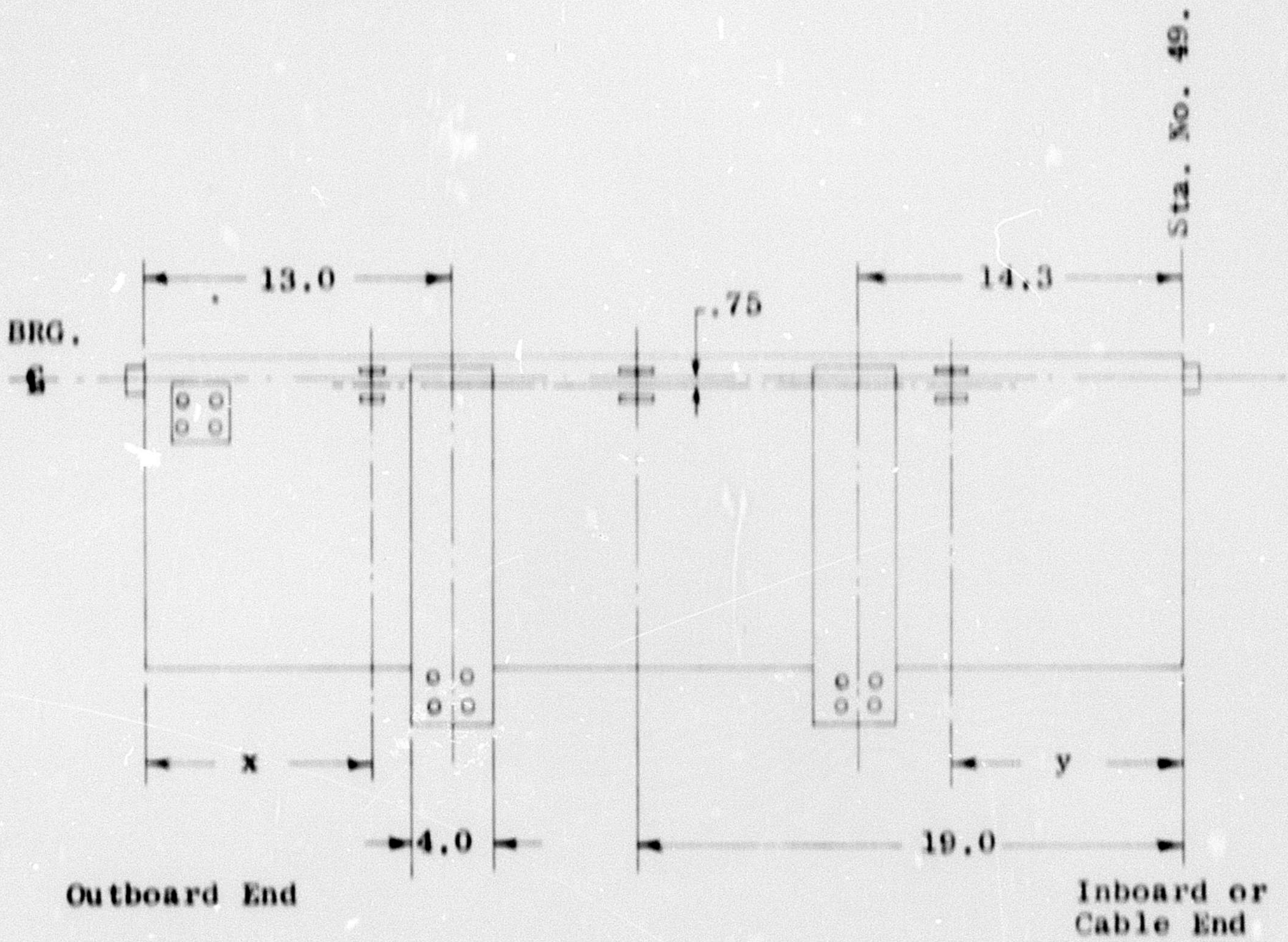

x = 8.0 y = 9.0 on Tests No. 4, 5, and 6

x = 10.25 y = 11.0 on Tests No. 1, 2, 3, and 7

Figure VI-6. Flap Fatigue Test Clamp and Gage Positions

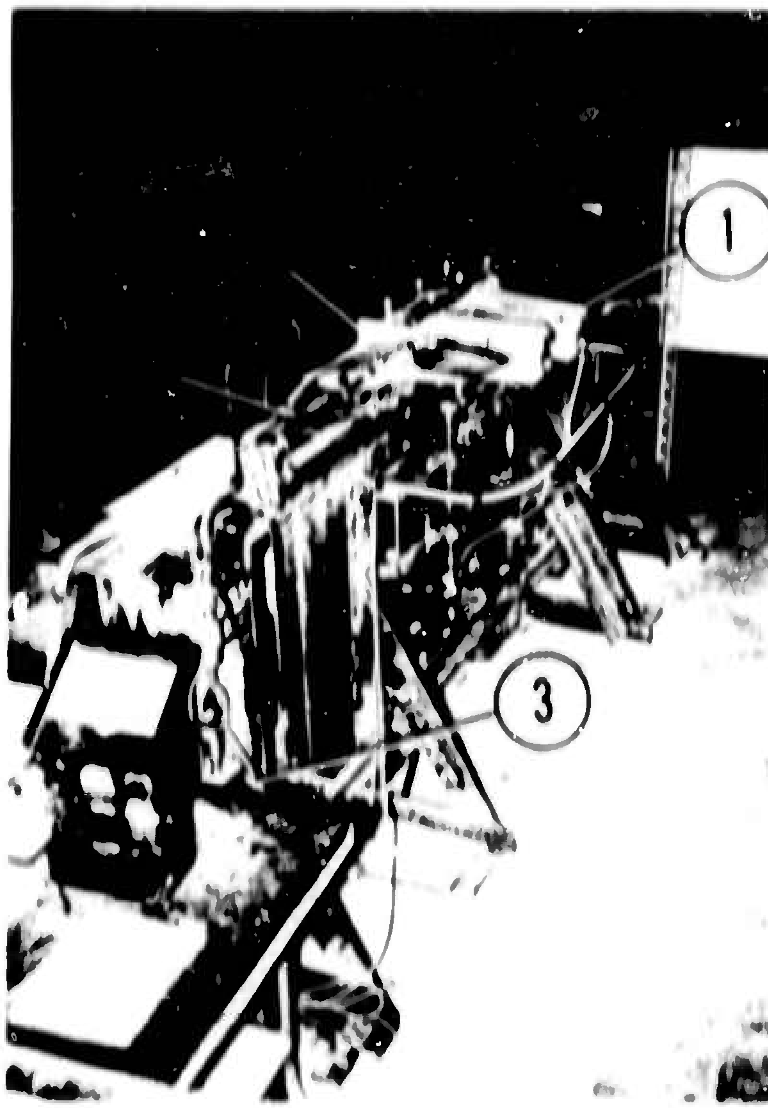

View of Front of Jig Showing

1. Actuating clamps connected to linear drive rods and bellcranks.
2. Steady load cables running to attaching clamp.
3. Steady load cylinder.
4. Strain gage cables.

Figure VI-7. Flap Fatigue Test Apparatus

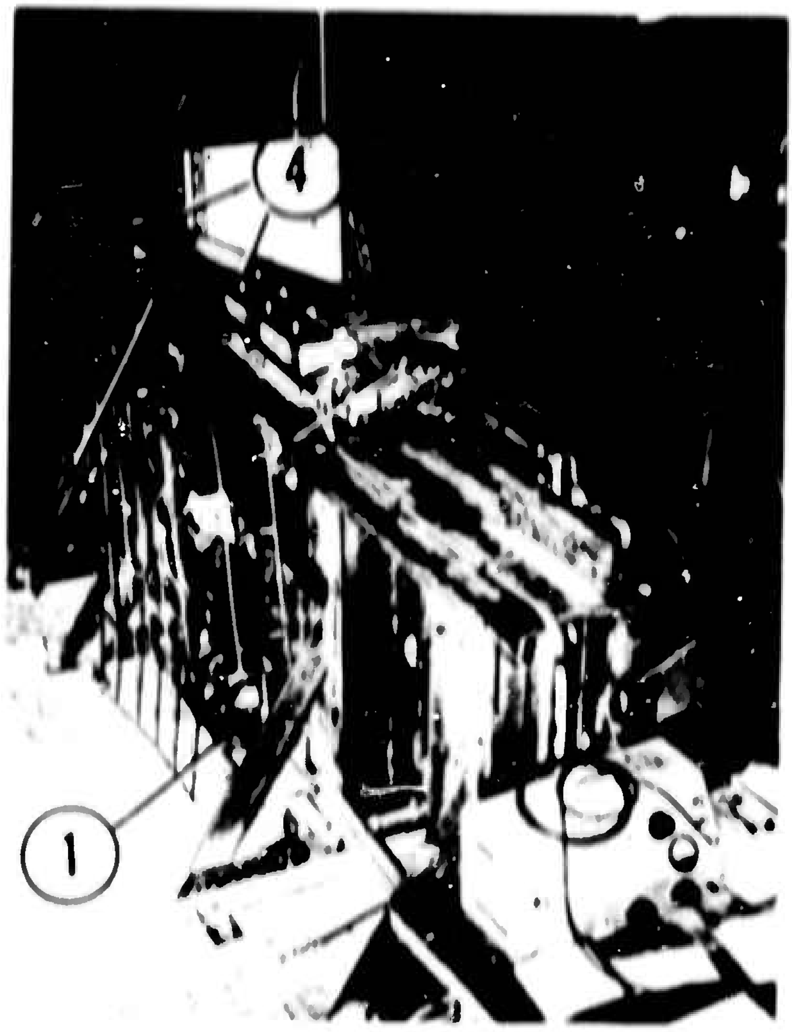

View of Rear of Jig Showing

1. Actuating cams and other drive components.
2. Steady load link.
3. Fixed blade spar.
4. Retention clamps.

Figure VI-8. Flap Fatigue Test Apparatus

Figure VI-9. Close-up of Rotoprop on Whirl Stand

BLANK PAGE

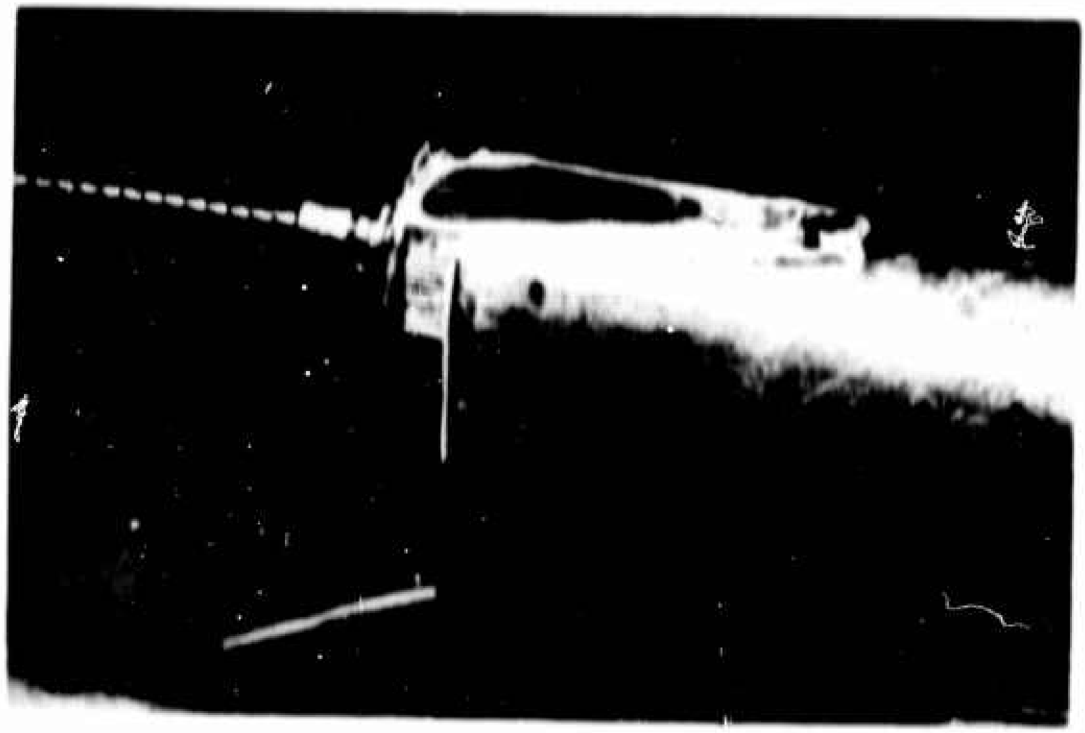

Figure VI-10. View of Flap Retention Failure

Figure VI-11. View of Flap Cable Failure

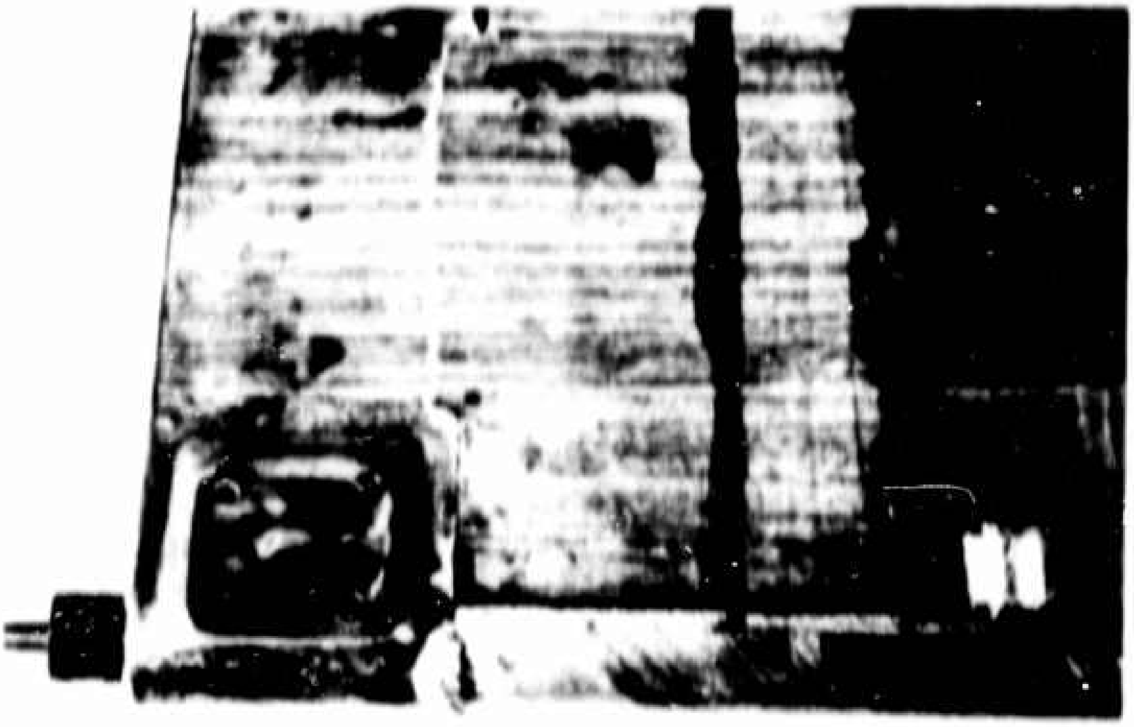

Figure VI-12. View of Flap Failure

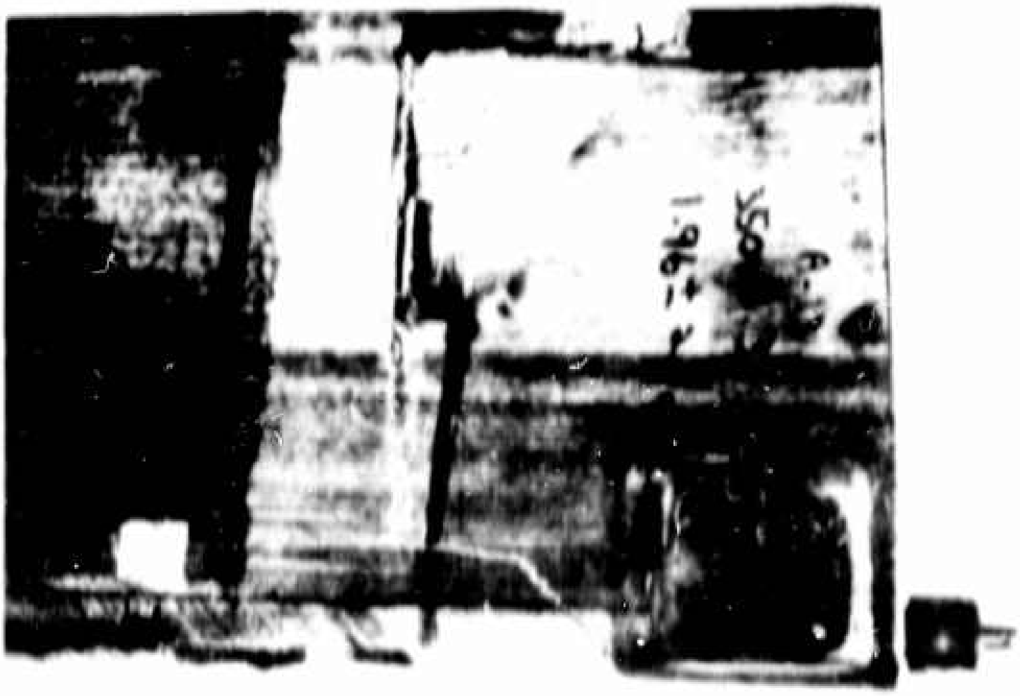

Figure VI-13. View of Flap Failure

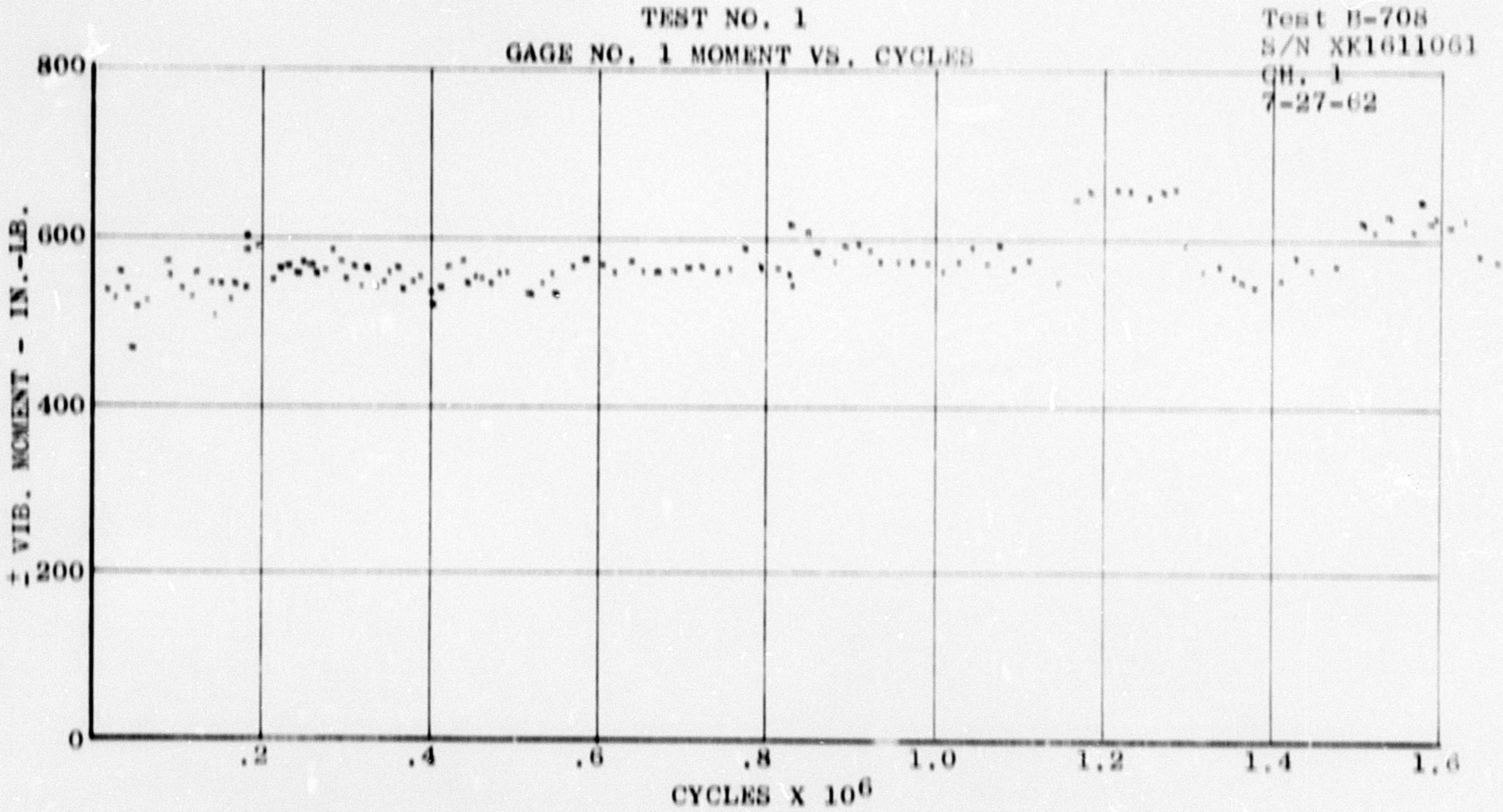

Figure VI-14. Flap Endurance

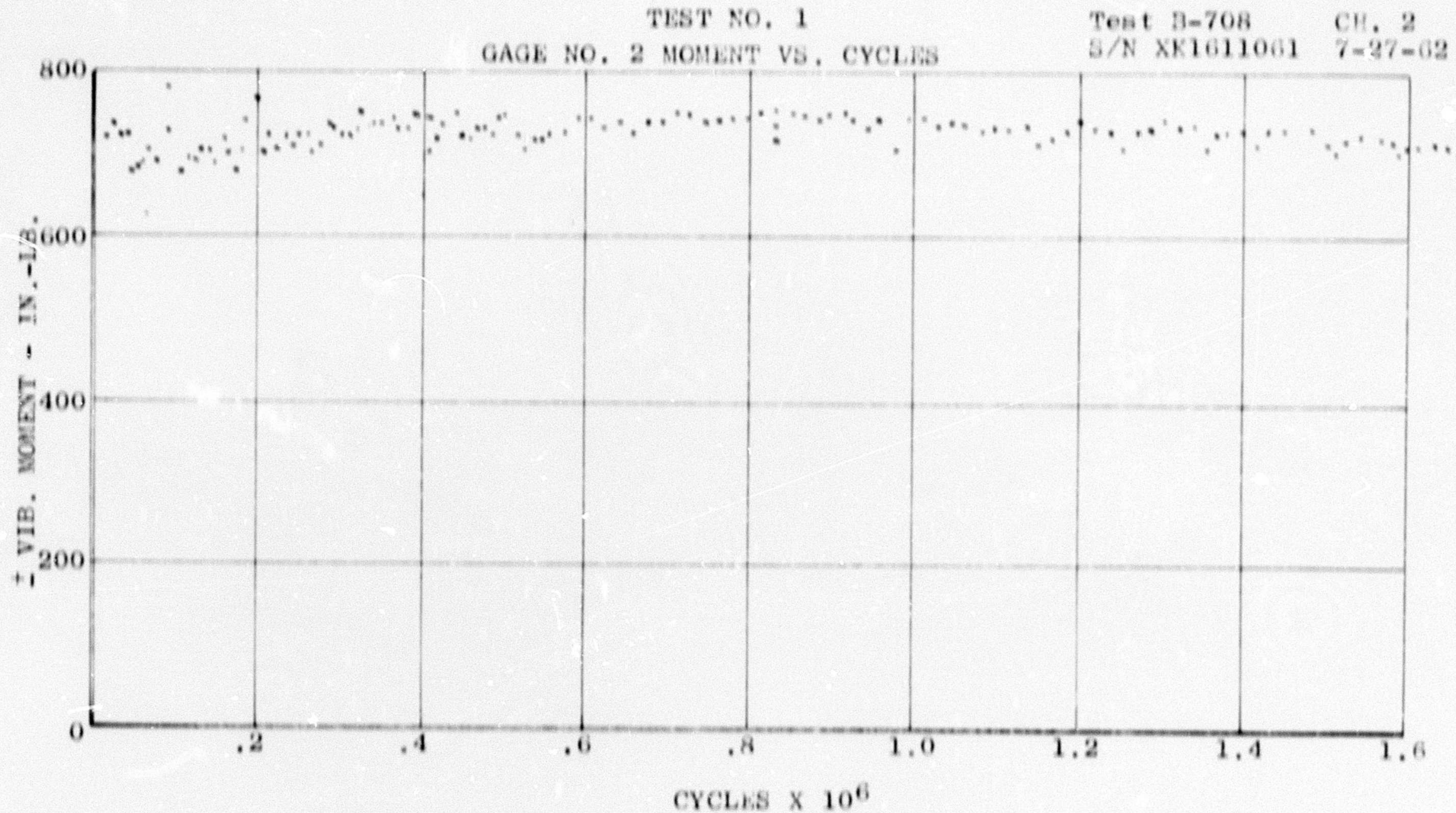

Figure VI-15. Flap Endurance

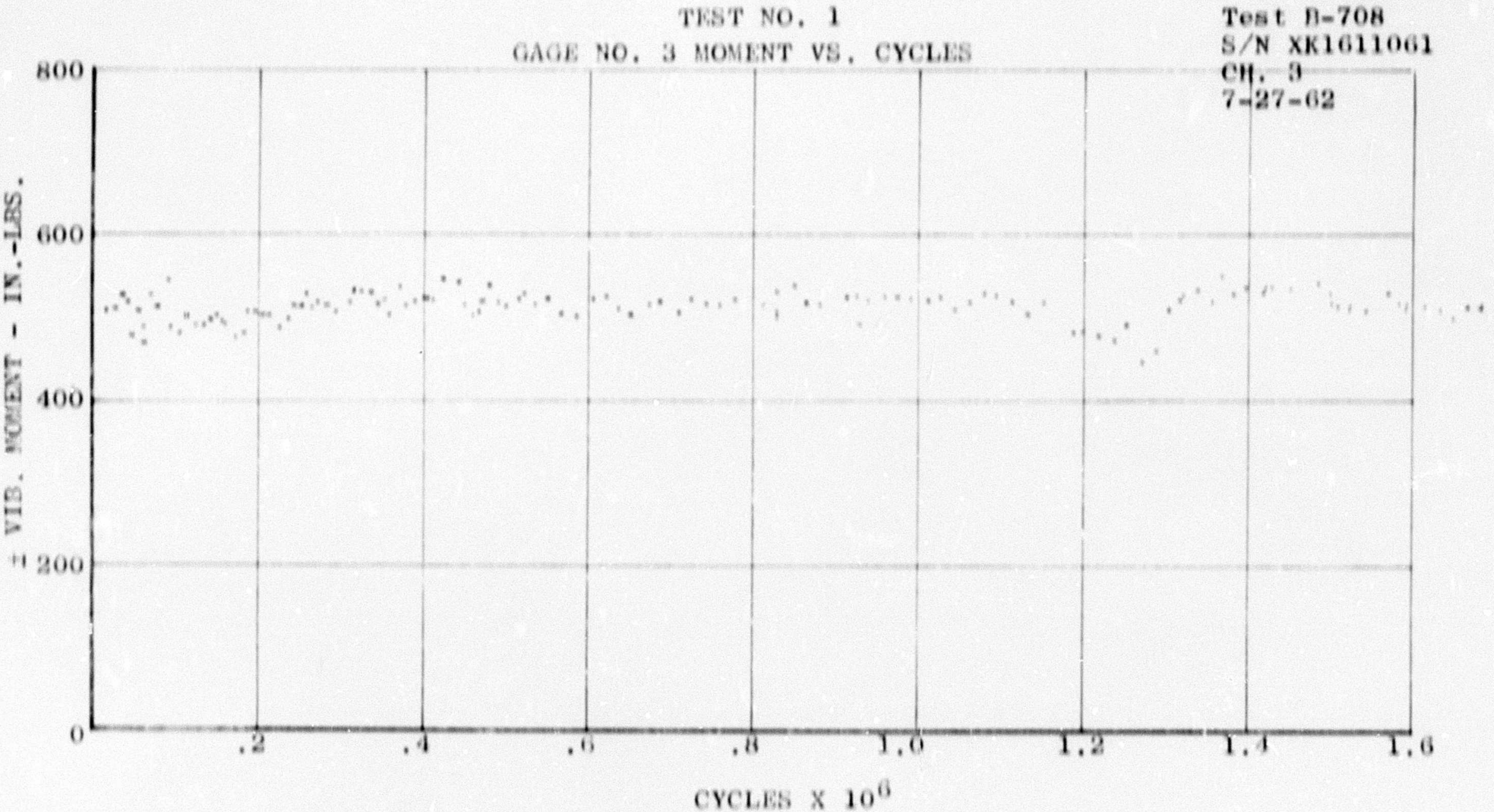

Figure VI-16. Flap Endurance

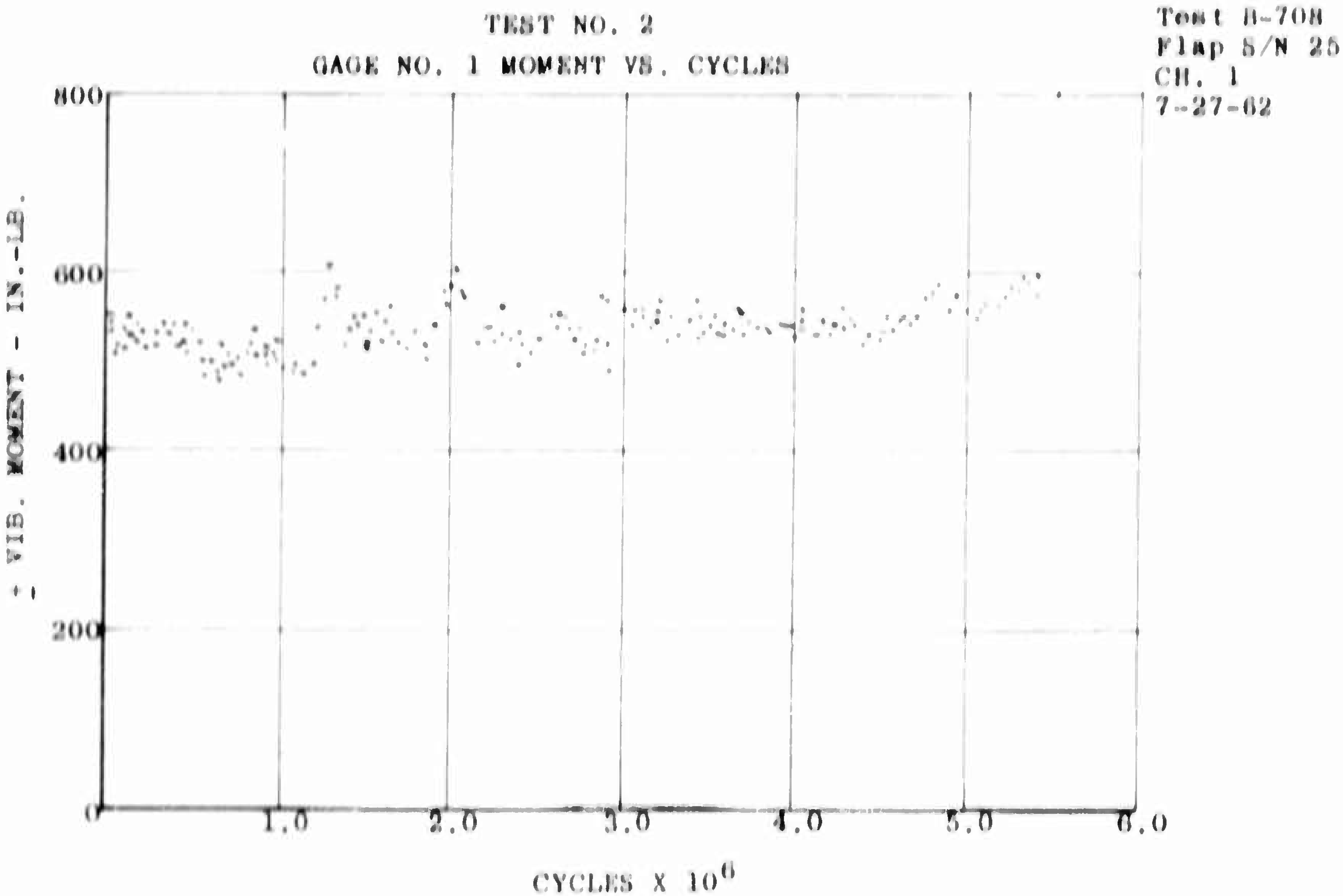

Figure VI-17. Flap Endurance

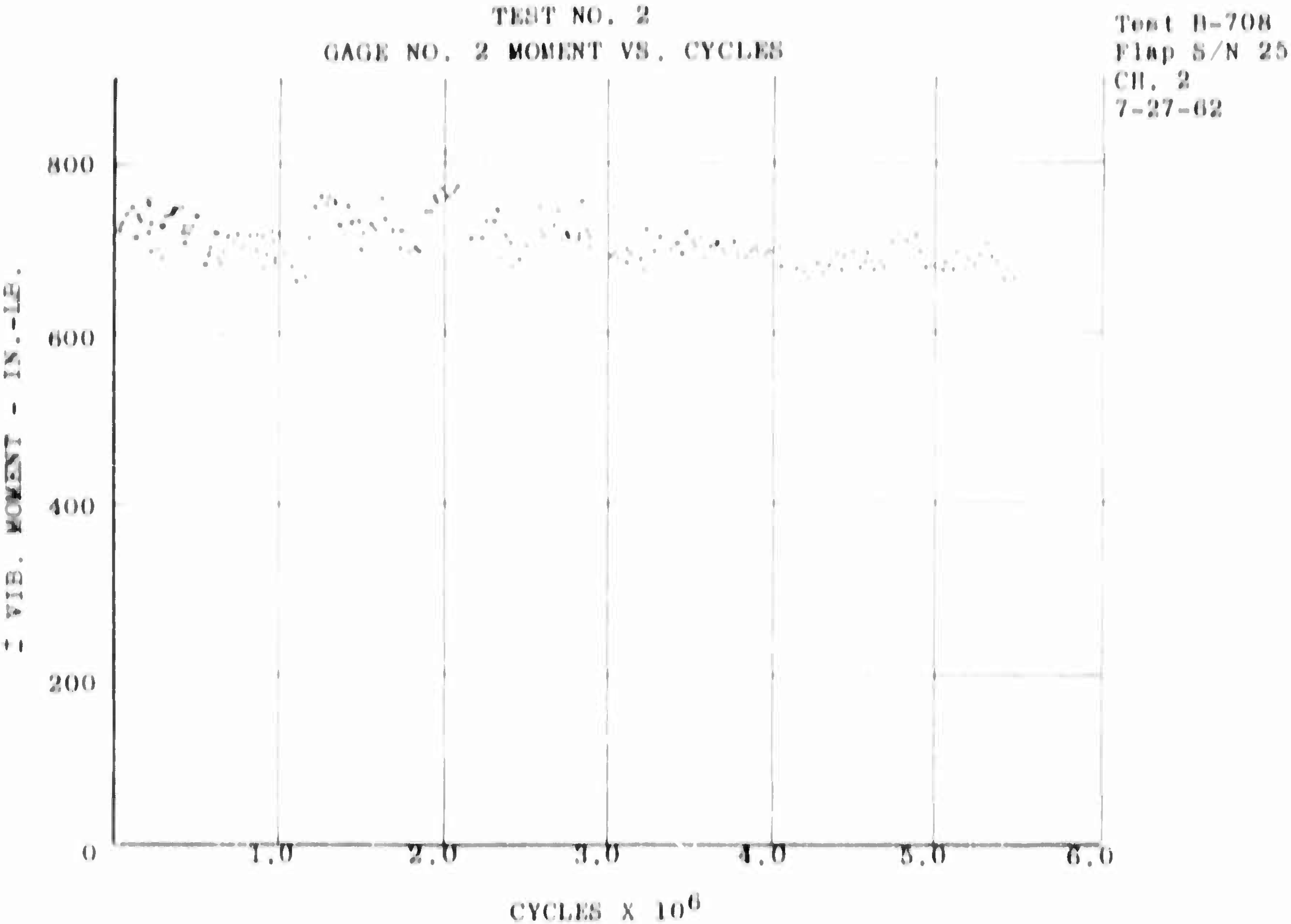

Figure VI-18. Flap Endurance

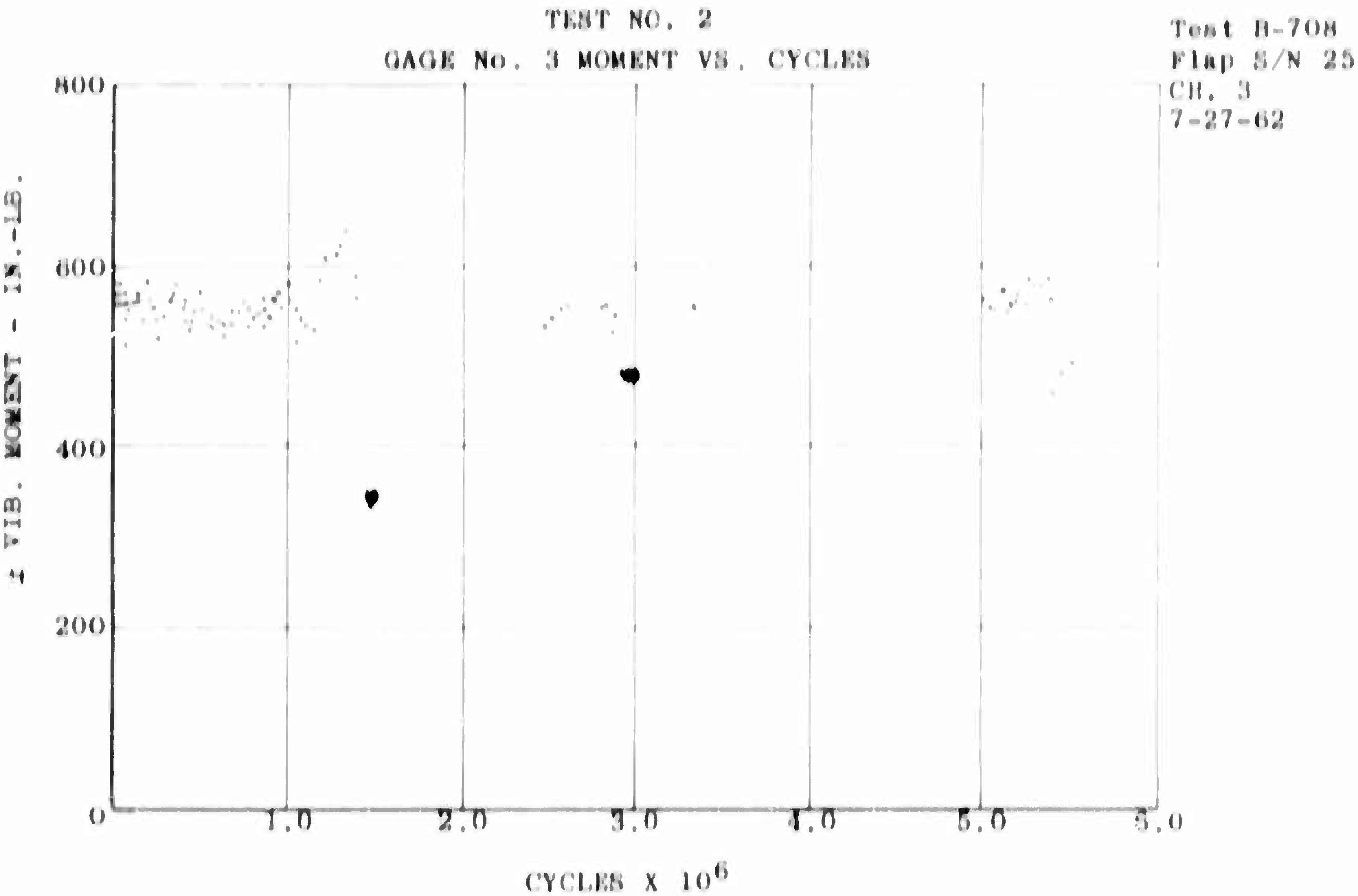

Figure VI-19. Flap Endurance

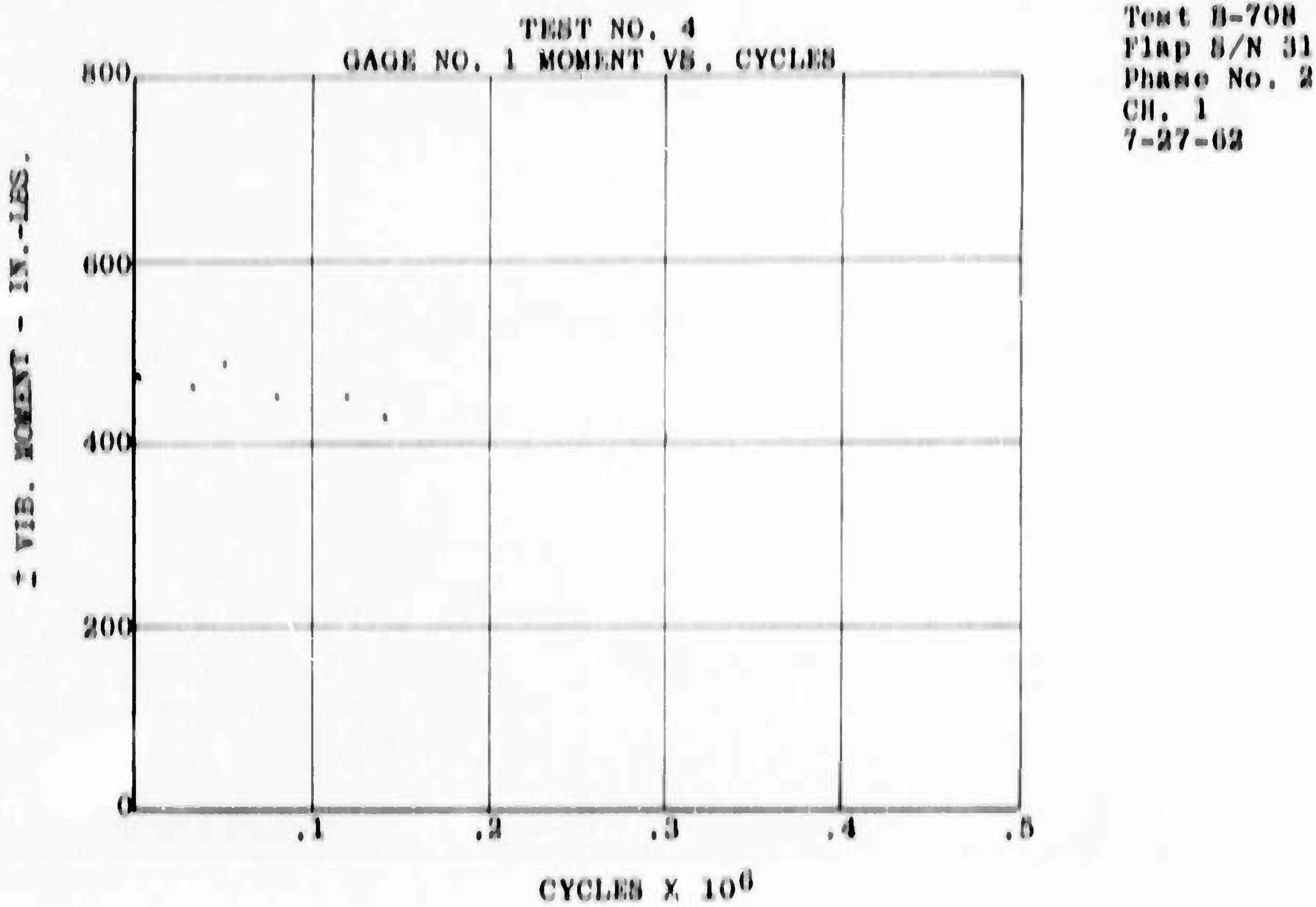

Figure VI-20. Flap Endurance

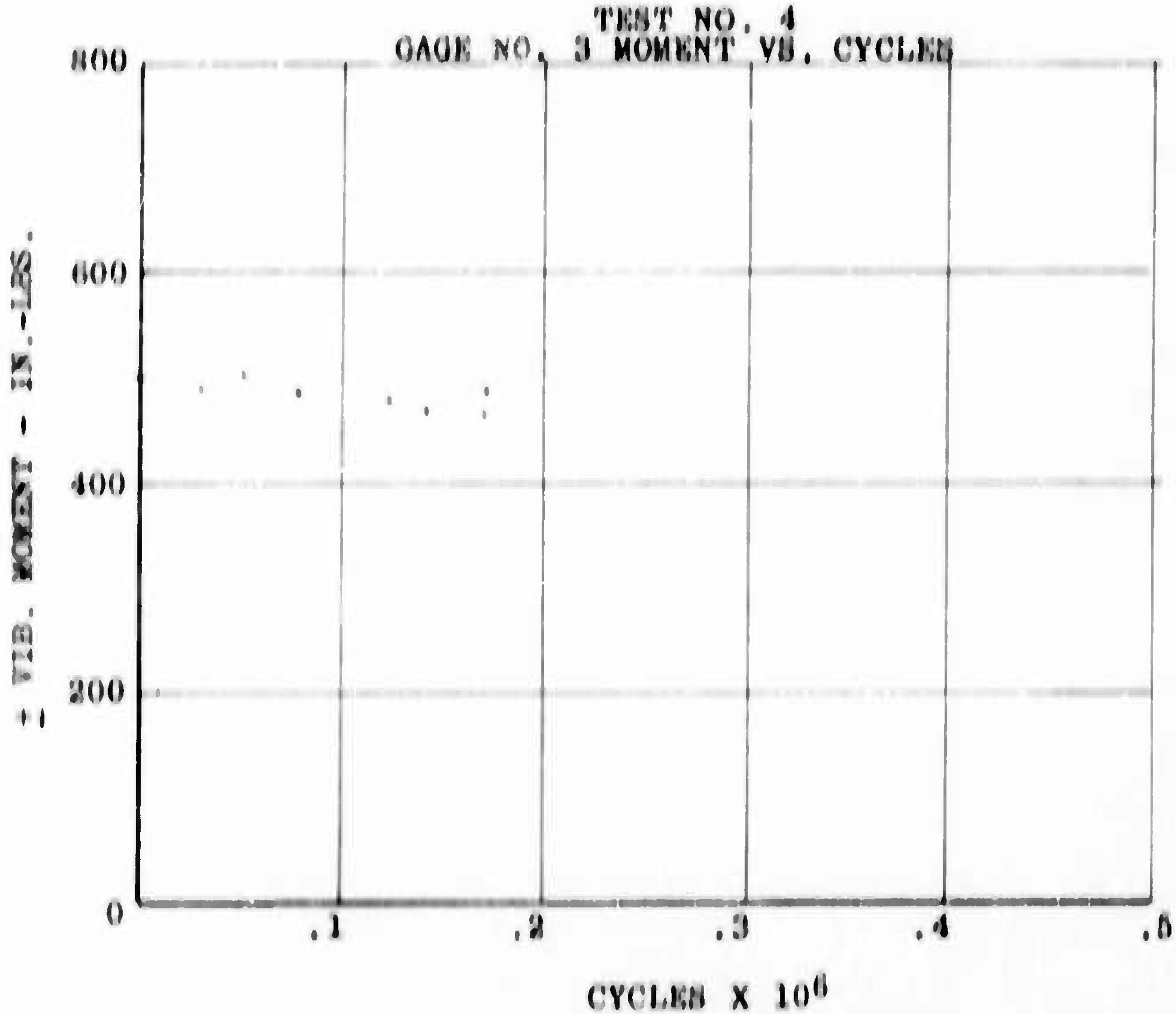

Test B-708
Flap S/N 31
Phase No. 2
CH. 3
7-27-62

Figure VI-21. Flap Endurance

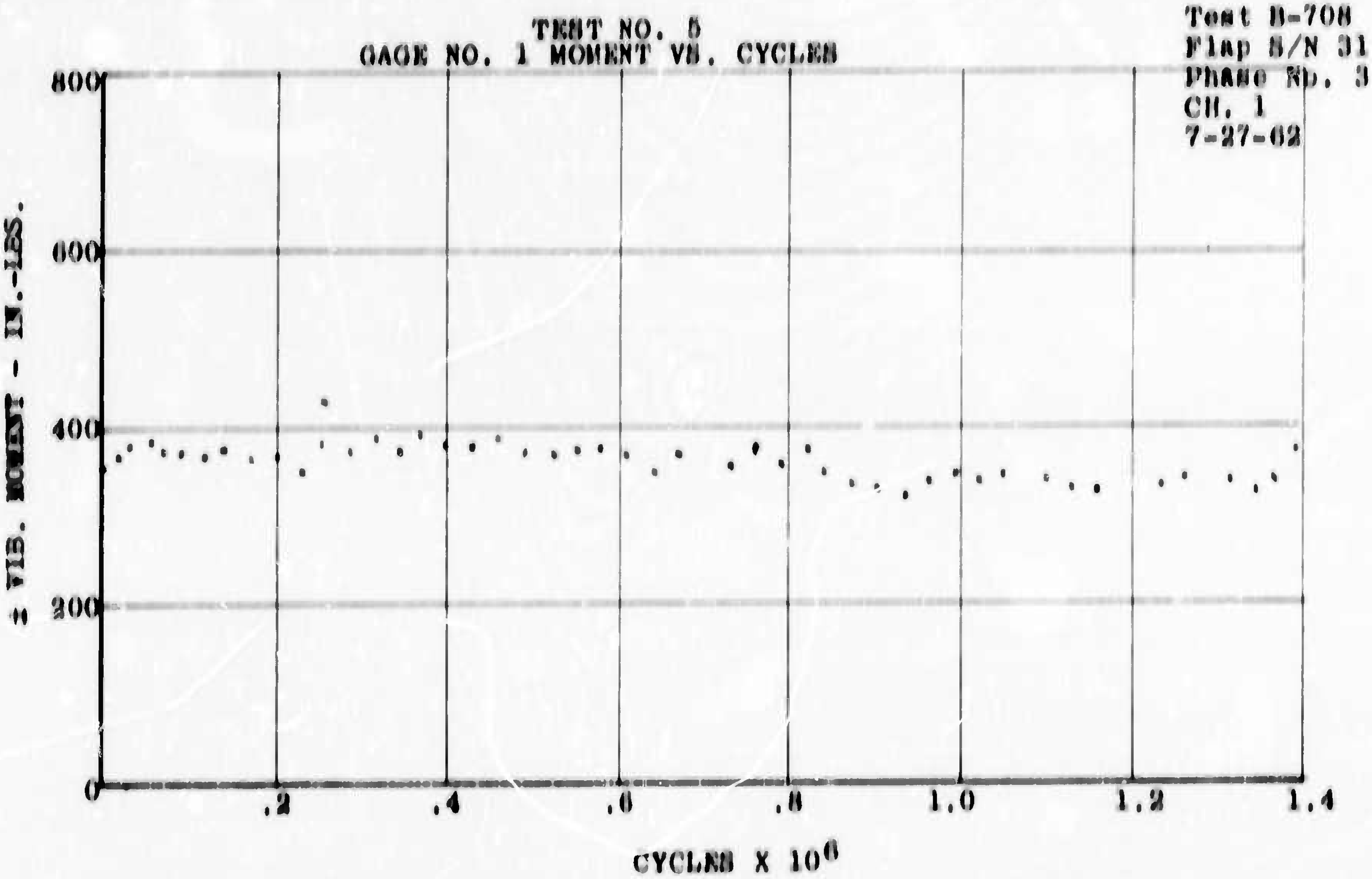

Figure VI-22. Flap Endurance

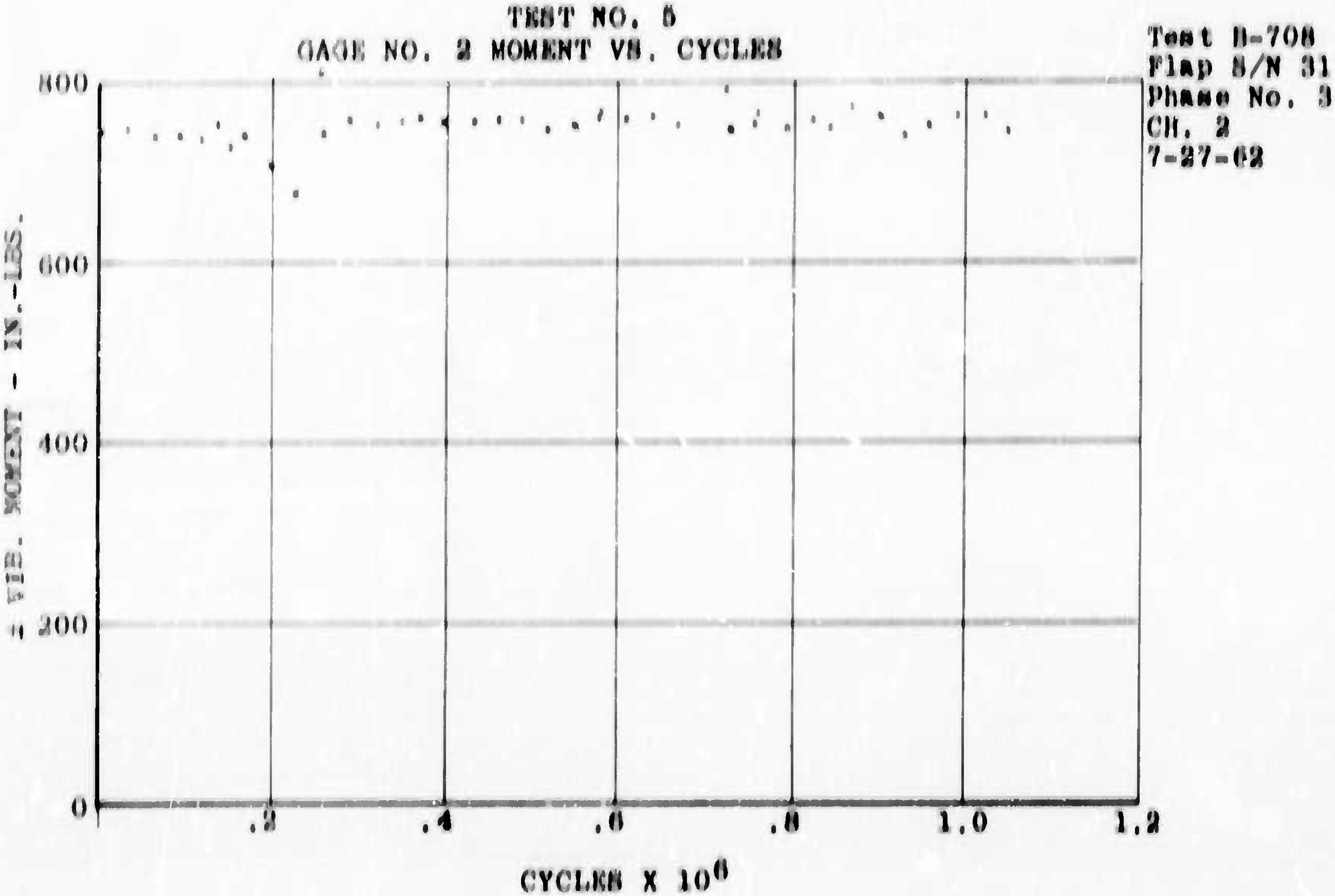

Figure VI-23. Flap Endurance

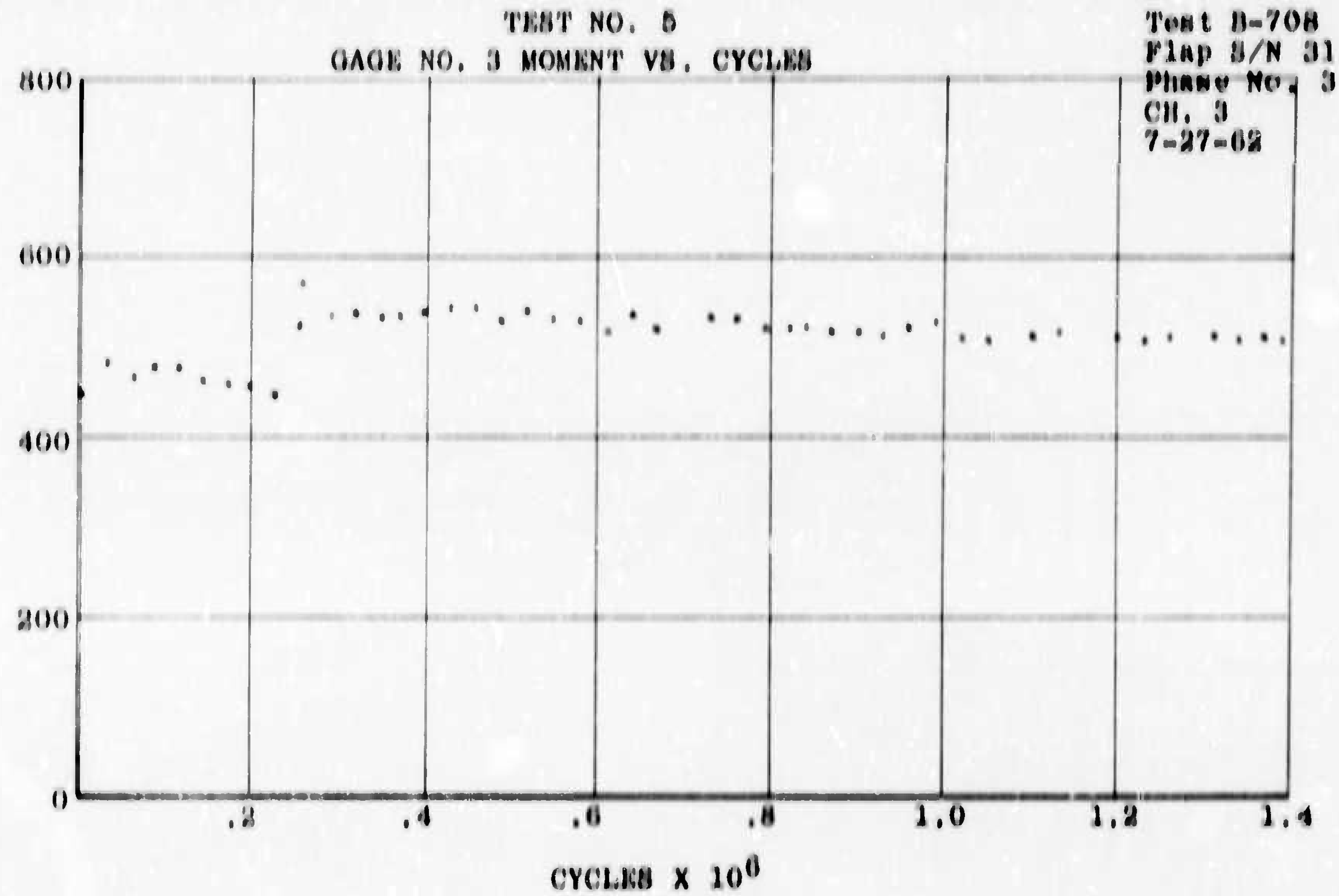

Figure VI-24. Flap Endurance

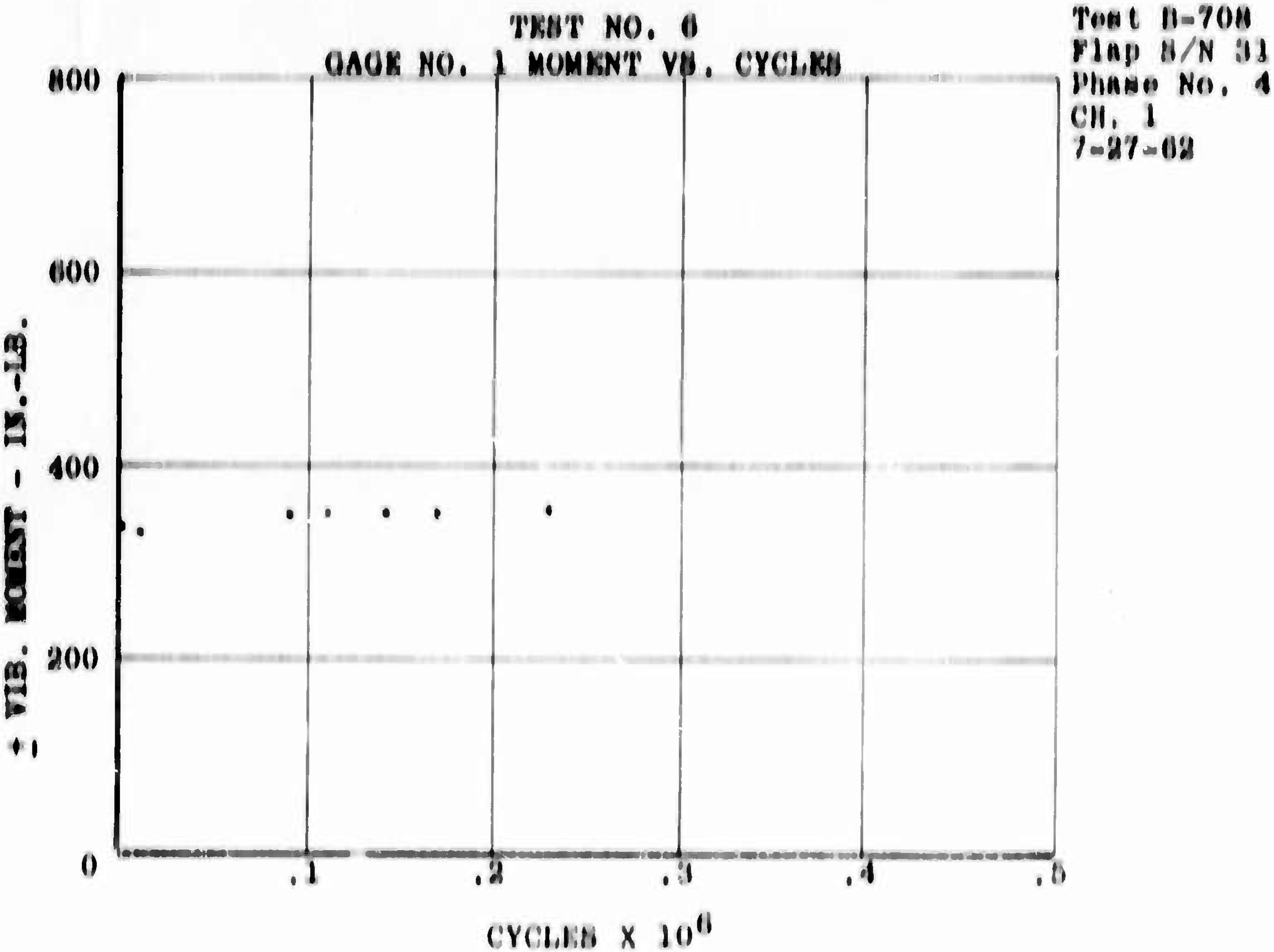

Figure VI-25. Flap Endurance

Test B-708
Flap S/N 31
Phase No. 4
CH. 2
7-27-62

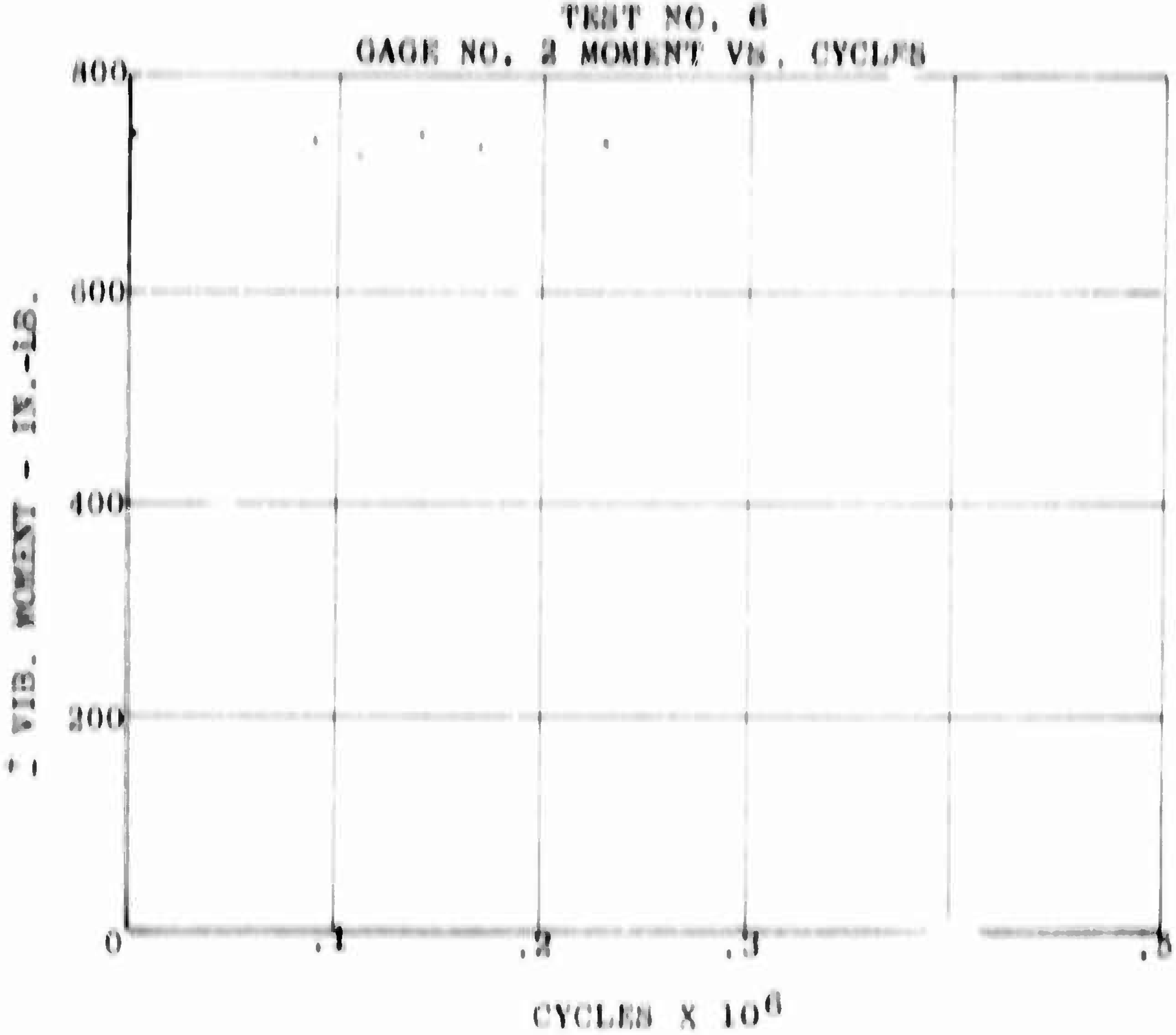

Figure VI-26. Flap Endurance

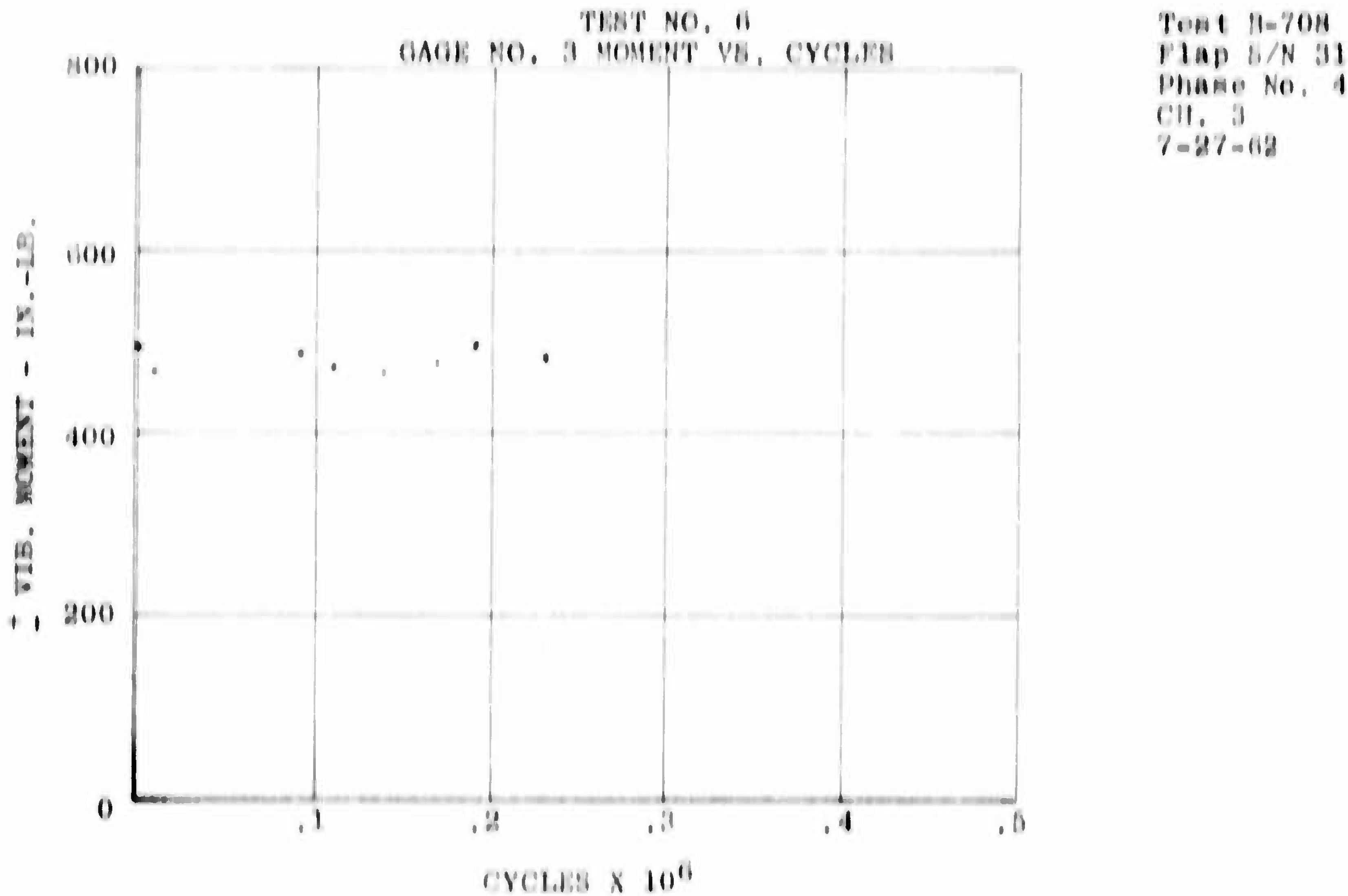

Figure VI-27. Flap Endurance

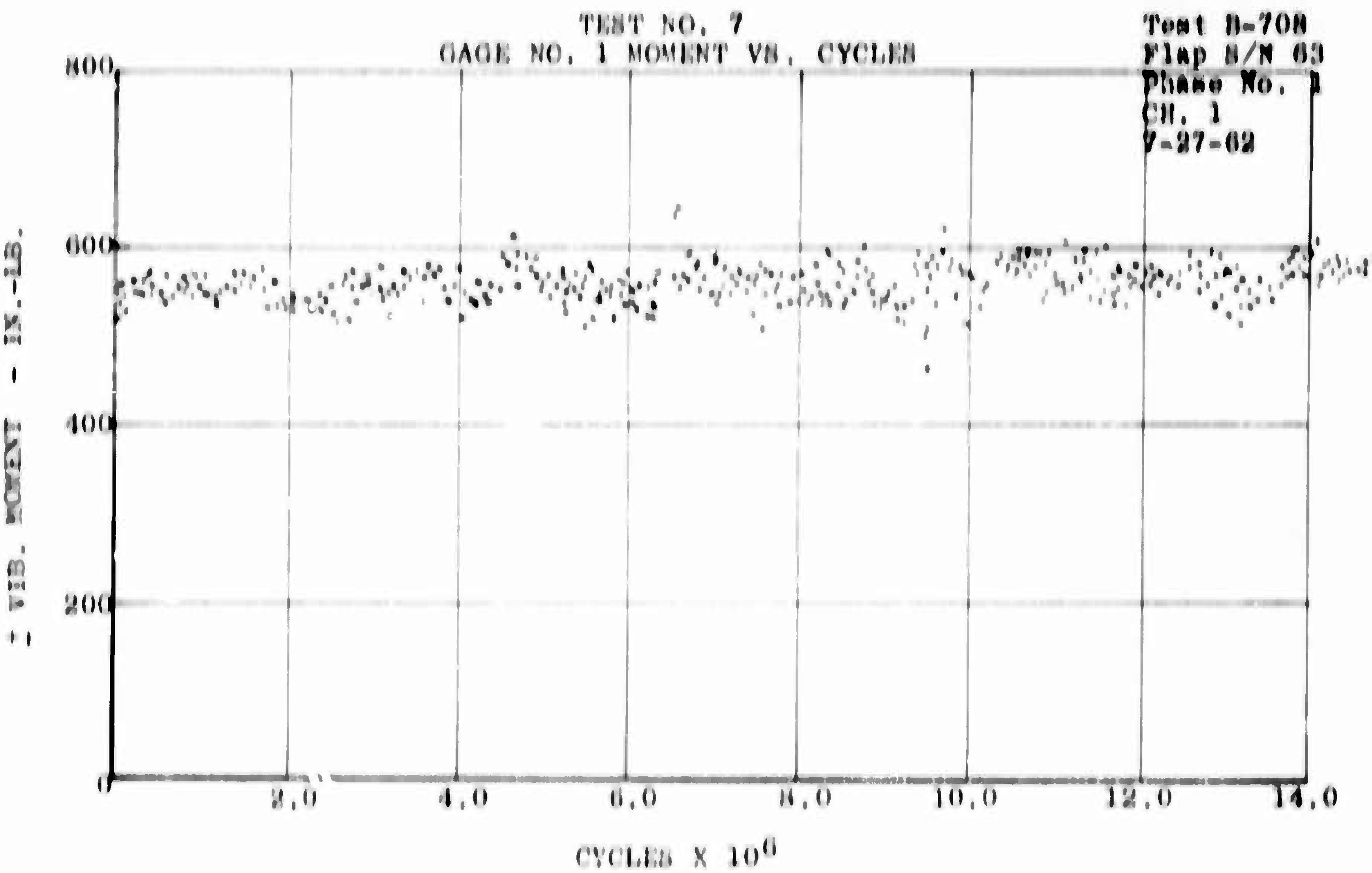

Figure VI-28. Flap Endurance

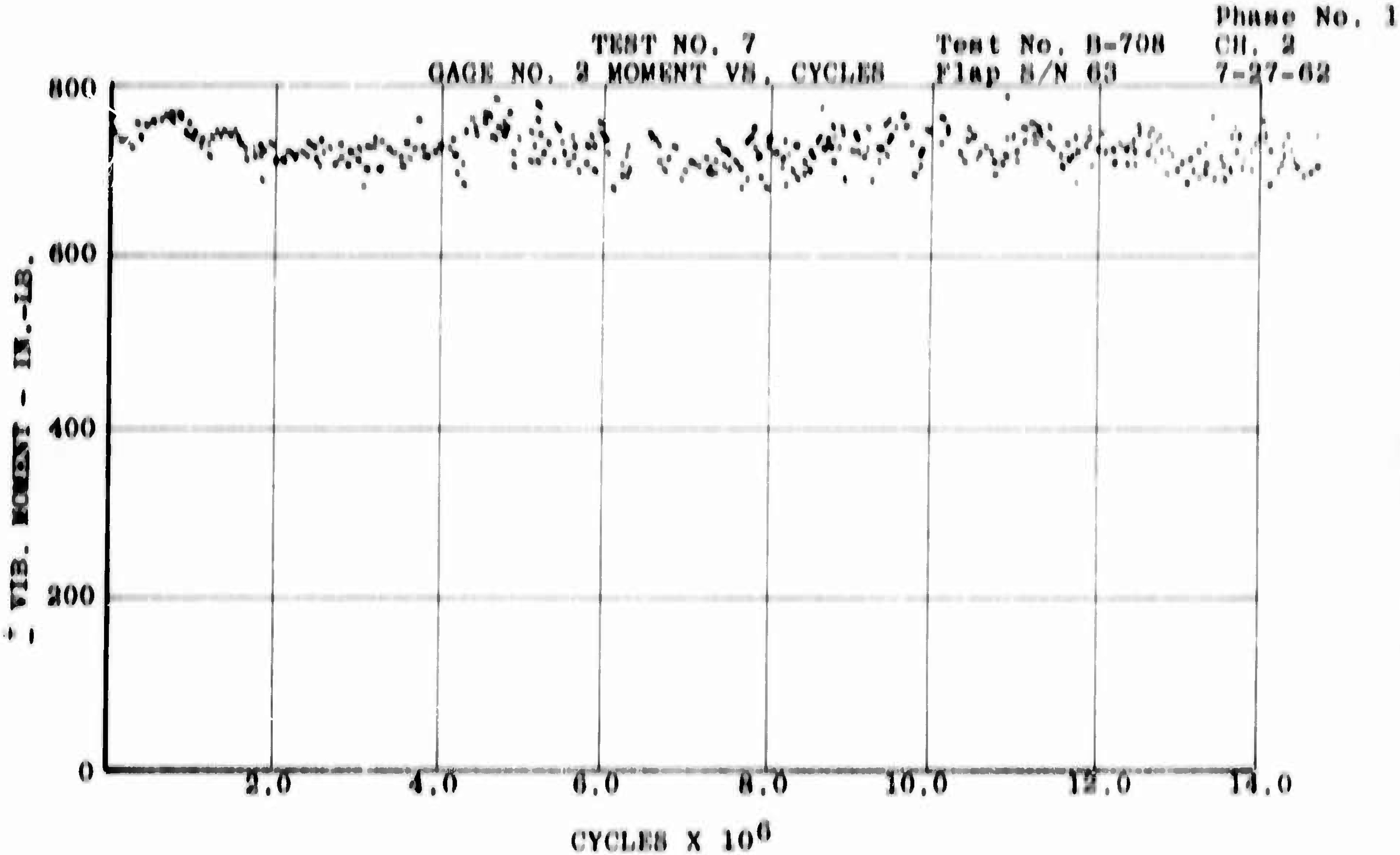

Figure VI-29. Flap Endurance

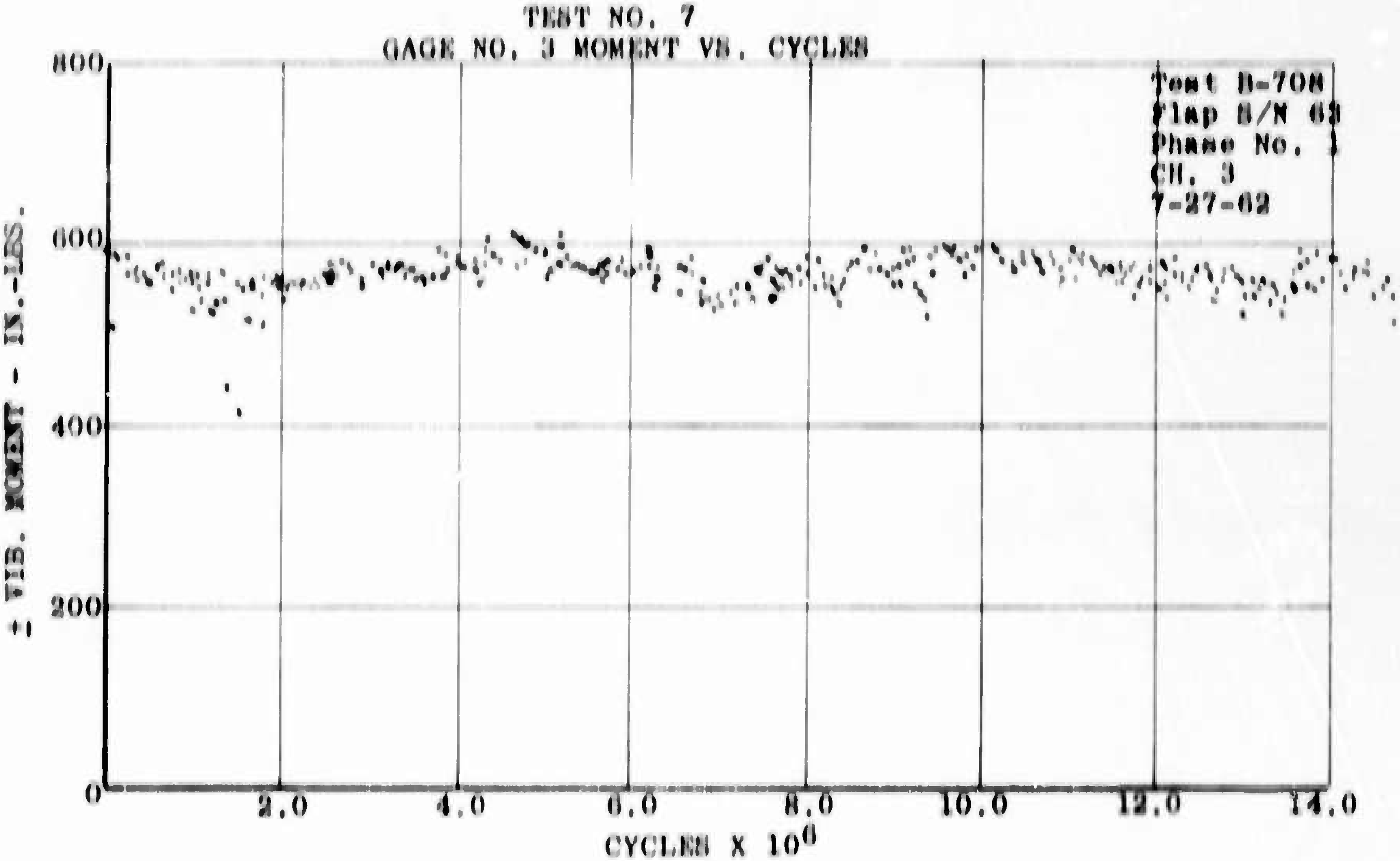

Figure VI-30. Flap Endurance

Figure VI-31. Tie-Down Test of K-16B Aircraft

CONCLUSION

Of the seven failures obtained during the discussed fatigue testing, two failures were due to the method of clamping the specimen to apply the loads and two failures were due to defective material. The three valid failures realized a flap and retention improvement of 2.136×10^6 to 14.7×10^6 cycles, which is equivalent to 48.8 and 337.9 aircraft hours respectively.

Although the most improved flap, as used on the test aircraft in the wind tunnel, was not tested to runout or failure, the final flap tested in the fatigue fixture showed a life of nearly seven times that of the nonreinforced flaps.

It is concluded that this improvement was attained by the inherent properties of fiberglass-reinforced plastics, combined with competent design analysis and quality controlled fabrication.